

Report No. UT-21.21

SIMPLIFIED CONE PENETRATION TEST PERFORMANCE-BASED ASSESSMENT OF LIQUEFACTION AND EFFECTS: PHASE 2, TASKS 5-10

Prepared For:

Utah Department of Transportation
Research & Innovation Division

Final Report – Phase 2 of 2

August 2021

DISCLAIMER

The authors alone are responsible for the preparation and accuracy of the information, data, analysis, discussions, recommendations, and conclusions presented herein. The contents do not necessarily reflect the views, opinions, endorsements, or policies of the Utah Department of Transportation or the U.S. Department of Transportation. The Utah Department of Transportation makes no representation or warranty of any kind, and assumes no liability therefore.

ACKNOWLEDGMENTS

The authors acknowledge the Utah, Oregon, South Carolina, and Connecticut Departments of Transportation for funding this research for pooled fund study TPF-5(338). The views and opinions presented in this report represent those of its authors, and may not represent those of the state agencies funding this research.

TECHNICAL REPORT ABSTRACT

1. Report No. UT-21.21		2. Government Accession No. NA		3. Recipient's Catalog No. NA	
4. Title and Subtitle SIMPLIFIED CONE PENETRATION TEST PERFORMANCE-BASED ASSESSMENT OF LIQUEFACTION AND EFFECTS: PHASE 2, TASKS 5-10				5. Report Date August 2021	
				6. Performing Organization Code NA	
7. Author(s) Kevin W. Franke, Jingwen He, Jenny L. Blonquist				8. Performing Organization Report No. NA	
9. Performing Organization Name and Address Brigham Young University Department of Civil and Environmental Engineering 368 Clyde Building Provo, UT 84602-4009				10. Work Unit No. 42074 15D	
				11. Contract or Grant No. 16-9826	
12. Sponsoring Agency Name and Address Utah Department of Transportation 4501 South 2700 West P.O. Box 148410 Salt Lake City, UT 84114-8410				13. Type of Report & Period Covered Final Report July 2017 – August 2021	
				14. Sponsoring Agency Code PIC No. UT15.402	
15. Supplementary Notes Prepared in cooperation with the Utah Department of Transportation and the U.S. Department of Transportation, Federal Highway Administration					
16. Abstract <p>The purpose of the research presented here is to provide the benefit of the full performance-based probabilistic earthquake hazard analysis using Cone Penetration Test (CPT) data without requiring special software, training, and experience. To do this, simplified models of liquefaction triggering, post-liquefaction settlement, and lateral spread displacement that approximate the results of the full probabilistic analysis were developed. The full project scope consisted of two phases: Phase 1) the development of a research tool to run full performance-based probabilistic calculations (Tasks 1 through 4), and Phase 2) the development of simplified performance-based methods (Tasks 5 through 10). This final report volume addresses the results of Phase 2 of the pooled fund study TPF-5(338) research contract.</p> <p>The goal of these simplified methods is to be user-friendly, requiring only simple calculations and a liquefaction parameter map. The simplified procedures are based on the Boulanger and Idriss (2014) probabilistic liquefaction triggering model, the Ku et al. (2012) (probabilistic version of Robertson and Wride (2009)) for liquefaction triggering; Juang et al. (2013) for post-liquefaction settlements; and lastly, Zhang et al (2004) for lateral spread displacement. This report details the development of the liquefaction parameter maps and provides a comparison of the simplified method, the pseudo-probabilistic method, and the deterministic method.</p> <p>To assist in implementing the simplified procedures, a tool was created to perform the simplified calculations, called <i>CPTLiq</i>. <i>CPTLiq</i> is available in spreadsheet format with a user's manual and provides an easily implemented procedure.</p>					
17. Key Words Lateral Spread Displacements, Liquefaction Triggering, Post-Liquefaction Settlements, Performance-based Engineering, Reference Maps, Simplified Models, Seismic Hazards, Cone Penetration Tests		18. Distribution Statement Not restricted. Available through: UDOT Research & Innovation Div. 4501 South 2700 West P.O. Box 148410 Salt Lake City, UT 84114-8410 www.udot.utah.gov/go/research		23. Registrant's Seal NA	
19. Security Classification (of this report) Unclassified	20. Security Classification (of this page) Unclassified	21. No. of Pages 183	22. Price NA		

TABLE OF CONTENTS

LIST OF TABLES	vi
LIST OF FIGURES	vii
UNIT CONVERSION FACTORS	x
LIST OF TERMS.....	xi
EXECUTIVE SUMMARY	1
1.0 INTRODUCTION	3
1.1 Problem Statement.....	3
1.2 Objectives	3
1.3 Scope.....	4
2.0 BACKGROUND OF SEISMIC HAZARD ANALYSIS	5
2.1 Deterministic Approach.....	5
2.2 Pseudo-Probabilistic Approach.....	5
2.3 Performance-Based Approach	6
2.4 Semi-Probabilistic Approach.....	6
3.0 DERIVATION OF THE SIMPLIFIED MODELS	7
3.1 Overview.....	7
3.2 Performance-based Liquefaction Triggering Evaluation.....	7
3.2.1 Empirical Liquefaction Triggering Models	7
3.2.2 Performance-based Liquefaction Triggering Assessment	9
3.3 Simplified Liquefaction Triggering Model.....	11
3.3.1 Liquefaction Parameter Maps & Reference Profile	12
3.3.2 Simplified Procedure Using the Boulanger and Idriss (2014) Probabilistic Liquefaction Triggering Model.....	15
3.3.3 Simplified Procedure Using the Ku et al. (2012) model [Probabilistic version of Robertson and Wride (2009)]	23
3.4 Performance-Based Post-liquefaction Free-field Settlement Models.....	29
3.4.1 Ishihara and Yoshimine (1992) Settlement Method	29
3.4.2 Juang et al. (2013) Procedure.....	30
3.5 Simplified Post-liquefaction Free-field Settlement Models	32

3.5.1 Site-Specific Correction for Reference Strain using Boulanger and Idriss (2014)	
Probabilistic Liquefaction Triggering Model	32
3.5.2 Site-Specific Correction for Reference Strain using the Ku et al. (2012) model.....	35
3.5.3 Summary	36
3.6 Empirical Lateral Spread Displacement Model.....	37
3.6.1 Zhang et al. (2004) Procedure.....	37
3.7 Simplified Performance-based Lateral Spread Model.....	39
3.7.1 Site-Specific Correction for Reference Strain using Boulanger and Idriss (2014)	
Probabilistic Liquefaction Triggering Model	40
3.7.2 Site-Specific Correction for Reference Strain using the Ku et al. (2012) model.....	41
3.7.3 Simplified Strain Summary.....	43
4.0 DEVELOPMENT OF LIQUEFACTION PARAMETER MAPS	44
4.1 Reference Profile	44
4.2 Development of Reference Parameter Maps	45
4.3 Grid Spacing Study	45
4.4 Create a List of Grid Points	50
4.5 Perform Full Performance-Based Analysis at the Grid Points	51
4.6 Create Contours Based on Interpolated Values	51
4.7 Summary.....	53
5.0 VALIDATION OF THE SIMPLIFIED MODELS	54
5.1 Overview.....	54
5.1.1 Sites used in the Analysis	54
5.2 Simplified Boulanger and Idriss (2014) Liquefaction Triggering Model Validation.....	56
5.3 Simplified Ku et al. (2012) Liquefaction Triggering Model Validation	57
5.4 Simplified Post-liquefaction Free-field Settlement Model Validation.....	60
5.5 Simplified Lateral Spread Displacement Model Validation.....	63
6.0 COMPARISON STUDY	67
6.1 Overview.....	67
6.2 Locations and Profiles	67
6.3 Comparison with the Pseudo-Probabilistic Procedure.....	68
6.4 Liquefaction Triggering Comparison	69

6.4.1 Ku et al. (2012) Comparison Results	69
6.4.2 Boulanger and Idriss (2014) Comparison Results	69
6.5 Post-Liquefaction Settlement Comparison	73
6.5.1 Post-Liquefaction Settlement Comparison Results using Boulanger and Idriss (2014)	73
6.5.2 Post-Liquefaction Settlement Comparison Results using Ku et al. (2012).....	75
6.6 Discussion.....	76
6.7 Lateral Spread Comparison Results.....	78
6.7.1 Lateral Spread Comparison Results using Zhang et al. (2004) with Boulanger and Idriss (2004)	78
6.7.2 Lateral Spread Comparison Results using Zhang et al. (2004) with Ku et al. (2012).	80
6.8 Comparison with the Deterministic Procedure	82
6.8.1 Locations and Profiles.....	83
6.9 Liquefaction Triggering Comparison	85
6.9.1 Robertson and Wride (2009) Comparison Results	86
6.9.2 Boulanger and Idriss (2014) Comparison Results	87
6.10 Post-Liquefaction Settlement Comparison (Ishihara and Yoshimine (1992)).....	88
6.11 Lateral Spread Comparison Results (Zhang et al. (2004))	89
6.12 Summary.....	90
7.0 CONCLUSIONS.....	91
7.1 Summary.....	91
7.2 Limitations and Challenges	92
REFERENCES	93
APPENDIX A: Liquefaction Reference Parameter Maps	97

LIST OF TABLES

Table 4-1. Proposed Optimum Grid Spacings within a <i>PGA</i> Range for a) <i>CSR%</i> , b) <i>q_{req}</i> , and c) ϵ_v and γ_{max}	50
Table 5-1. Locations of cities used in validation with corresponding <i>PGA</i> (g) values	55
Table 6-1. Sites Selected for Comparison Study	68
Table 6-2. NGA model weights used in the deterministic procedure.....	84
Table 6-3. Input variables used in the deterministic models (a_{max} calculated using F_{pga} from AASHTO code).	85

LIST OF FIGURES

Figure 3-1: Schematic illustration of: (a) definitions of FS_L and ΔN_L ; (b) relationship between FS_L and ΔN_L (after Mayfield et al. 2010).....	9
Figure 3-2. Reference soil profile used to develop liquefaction loading maps in the proposed simplified uniform hazard liquefaction procedure.....	13
Figure 3-3. Liquefaction loading map ($T_R = 1,033$ years) showing contours of $CSR_{ref}(\%)$ for a portion of the Salt Lake Valley in Utah (after Ulmer 2015).....	14
Figure 3-4. The relationship between FS_L , γ_{max} , and D_R (after Ishihara & Yoshimine, 1992). .	29
Figure 3-5. The relationship between maximum cyclic shear strain and factor of safety for.....	38
Figure 4-1. Reference Soil Profile	44
Figure 4-2. PGA Hazard Map ($T_R=2475$ years) after USGS 2014.....	46
Figure 4-3. Range of PGA Values for Cities Included in Grid Spacing Study.....	46
Figure 4-4. Layout of Grid Points Centered on a City’s Anchor Point (Ulmer, 2015)	47
Figure 4-5. Correlation between PGA and Optimum Grid Spacing for $CSR\%$ [Boulanger and Idriss (2014)].....	48
Figure 4-6. Correlation between PGA and Optimum Grid Spacing for q_{req} [Ku et al. (2012)]	48
Figure 4-7. Correlation between PGA and Optimum Grid Spacing for ϵ_v and γ_{max} [Boulanger and Idriss (2014)].....	49
Figure 4-8. Correlation between PGA and Optimum Grid Spacing for ϵ_v and γ_{max} [Ku et al. (2012)].....	49
Figure 4-9. Location of Grid Points for Oregon with PGA Color Zones in Background.....	51
Figure 4-10. Sample Kriging Raster for Oregon	52
Figure 4-11. Example contour map of Oregon	52
Figure 5-1. Site-specific soil profile used to validate the simplified performance-based model. .	56
Figure 5-2. Comparative Scatter Plots for Simplified and Full Performance-Based Procedures for (a) $CSR_{site}(\%)$, (b) FS_L , (c) P_L , and (d) Δq_L , (e) q_{req} for the Boulanger and Idriss(2014) model using the 2012 MSF.	58
Figure 5-3. Comparative Scatter Plots for Simplified and Full Performance-Based Procedures for (a) q_{req} , (b) FS_L , (c) P_L , (d) Δq_L , and (e) $CSR_{site}(\%)$ for the Ku et al. (2012) model.....	59

Figure 5-4. Boulanger and Idriss (2014) Full Performance-Based Settlement vs. Simplified Settlement Separated by Return Period (for <i>PGA</i> lower than 0.2g).	60
Figure 5-5. Boulanger and Idriss (2014) Full Performance-Based Settlement vs. Simplified Settlement Separated by Return Period (for <i>PGA</i> higher than 0.2g).	61
Figure 5-6. Ku et al. (2012) Performance-Based Total Settlement vs. Simplified Settlement Separated by Return Period (for <i>PGA</i> lower than 0.2g).	61
Figure 5-7. Ku et al. (2012) Performance-Based Total Settlement vs. Simplified Settlement Separated by Return Period (for <i>PGA</i> higher than 0.2g).	62
Figure 5-8. Boulanger and Idriss (2014) Performance-Based Lateral Spread Displacement vs. Simplified Lateral Spread Displacement (for <i>PGA</i> lower than 0.2g).	63
Figure 5-9. Boulanger and Idriss (2014) Performance-Based Lateral Spread Displacement vs. Simplified Lateral Spread Displacement (for <i>PGA</i> higher than 0.2g).	64
Figure 5-10. Ku et al. (2012) Performance-Based Lateral Spread Displacement vs. Simplified Lateral Spread Displacement (for <i>PGA</i> lower than 0.2g).	65
Figure 5-11. Ku et al. (2012) Performance-Based Lateral Spread Displacement vs. Simplified Lateral Spread Displacement (for <i>PGA</i> higher than 0.2g).	65
Figure 6-1. Comparison Results for the Ku et al. (2012) Triggering Model for (a) q_{req} , (b) FS_L , and (c) $CSR\%$	71
Figure 6-2. Comparison Results for the Boulanger and Idriss (2014) Triggering Model for (a) $CSR\%$, (b) FS_L , and (c) q_{req}	72
Figure 6-3. Settlement Comparison Results using the Boulanger and Idriss (2014) Triggering Model for Sites with $PGA < 0.2 g$ (for All Return Periods).	74
Figure 6-4. Settlement Comparison Results using the Boulanger and Idriss (2014) Triggering Model for Sites with $PGA \geq 0.2g$ (for All Return Periods)	74
Figure 6-5. Settlement Comparison Results using the Ku et al. (2012) Triggering Model for Sites with $PGA < 0.2 g$ (for All Return Periods).	75
Figure 6-6. Settlement Comparison Results using the Ku et al. (2012) Triggering Model for Sites with $PGA \geq 0.2g$ (for All Return Periods)	76
Figure 6-7. Ishihara and Yoshimine (1992) Method for Determining Volumetric Strain.	77
Figure 6-8. Lateral Spread Comparison Results using the Boulanger and Idriss (2014) Triggering Model for Sites with $PGA < 0.2g$ (for All Return Periods)	79

Figure 6-9. Lateral Spread Comparison Results using the Boulanger and Idriss (2014) Triggering Model for Sites with $PGA \geq 0.2g$ (for All Return Periods).	79
Figure 6-10. Lateral Spread Comparison Results using the Ku et al. (2012) Triggering Model for Sites with $PGA < 0.2g$ (for All Return Periods)	81
Figure 6-11. Lateral Spread Comparison Results using the Ku et al. (2012) Triggering Model for Sites with $PGA \geq 0.2g$ (for All Return Periods).....	82
Figure 6-12. Soil Profile used for the deterministic comparison study.	84
Figure 6-13. Comparison of deterministic and simplified performance-based values of q_{req}	86
Figure 6-14. Comparison of deterministic and simplified performance-based values of FS_L	86
Figure 6-15. Comparison of deterministic and simplified performance-based values of $CSR\%$. .	86
Figure 6-16. Comparison of deterministic and simplified performance-based values of q_{req}	87
Figure 6-17. Comparison of deterministic and simplified performance-based values of FS_L	87
Figure 6-18. Comparison of deterministic and simplified performance-based values of $CSR\%$..	87
Figure 6-19. Comparison of deterministic and simplified performance-based vertical strains using the Robertson and Wride (2009) model.	88
Figure 6-20. Comparison of deterministic and performance-based vertical strains using the Boulanger and Idriss (2014) model.....	88
Figure 6-21. Comparison of deterministic and simplified performance-based maximum strains using the Robertson and Wride (2009) model.	89
Figure 6-22. Comparison of deterministic and simplified performance-based maximum strains using the Boulanger and Idriss (2014) model.	89

UNIT CONVERSION FACTORS

Units used in this report and not conforming to the UDOT standard unit of measurement (U.S. Customary system) are given below with their U.S. Customary equivalents:

SI* (MODERN METRIC) CONVERSION FACTORS				
APPROXIMATE CONVERSIONS TO SI UNITS				
Symbol	When You Know	Multiply By	To Find	Symbol
LENGTH				
in	inches	25.4	millimeters	mm
ft	feet	0.305	meters	m
yd	yards	0.914	meters	m
mi	miles	1.61	kilometers	km
AREA				
in ²	square inches	645.2	square millimeters	mm ²
ft ²	square feet	0.093	square meters	m ²
yd ²	square yard	0.836	square meters	m ²
ac	acres	0.405	hectares	ha
mi ²	square miles	2.59	square kilometers	km ²
VOLUME				
fl oz	fluid ounces	29.57	milliliters	mL
gal	gallons	3.785	liters	L
ft ³	cubic feet	0.028	cubic meters	m ³
yd ³	cubic yards	0.765	cubic meters	m ³
NOTE: volumes greater than 1000 L shall be shown in m ³				
MASS				
oz	ounces	28.35	grams	g
lb	pounds	0.454	kilograms	kg
T	short tons (2000 lb)	0.907	megagrams (or "metric ton")	Mg (or "t")
TEMPERATURE (exact degrees)				
°F	Fahrenheit	5 (F-32)/9 or (F-32)/1.8	Celsius	°C
ILLUMINATION				
fc	foot-candles	10.76	lux	lx
fl	foot-Lamberts	3.426	candela/m ²	cd/m ²
FORCE and PRESSURE or STRESS				
lbf	poundforce	4.45	newtons	N
lbf/in ²	poundforce per square inch	6.89	kilopascals	kPa
APPROXIMATE CONVERSIONS FROM SI UNITS				
Symbol	When You Know	Multiply By	To Find	Symbol
LENGTH				
mm	millimeters	0.039	inches	in
m	meters	3.28	feet	ft
m	meters	1.09	yards	yd
km	kilometers	0.621	miles	mi
AREA				
mm ²	square millimeters	0.0016	square inches	in ²
m ²	square meters	10.764	square feet	ft ²
m ²	square meters	1.195	square yards	yd ²
ha	hectares	2.47	acres	ac
km ²	square kilometers	0.386	square miles	mi ²
VOLUME				
mL	milliliters	0.034	fluid ounces	fl oz
L	liters	0.264	gallons	gal
m ³	cubic meters	35.314	cubic feet	ft ³
m ³	cubic meters	1.307	cubic yards	yd ³
MASS				
g	grams	0.035	ounces	oz
kg	kilograms	2.202	pounds	lb
Mg (or "t")	megagrams (or "metric ton")	1.103	short tons (2000 lb)	T
TEMPERATURE (exact degrees)				
°C	Celsius	1.8C+32	Fahrenheit	°F
ILLUMINATION				
lx	lux	0.0929	foot-candles	fc
cd/m ²	candela/m ²	0.2919	foot-Lamberts	fl
FORCE and PRESSURE or STRESS				
N	newtons	0.225	poundforce	lbf
kPa	kilopascals	0.145	poundforce per square inch	lbf/in ²

*SI is the symbol for the International System of Units. (Adapted from FHWA report template, Revised March 2003)

LIST OF TERMS

Liquefaction Triggering Terms

a_{max}	peak ground surface acceleration
CRR	cyclic resistance ratio
$CRR_{PL=50\%}$	median CRR (CRR corresponding to a probability of liquefaction of 50%)
CSR	cyclic stress ratio
CSR^{ref}	uniform hazard estimate of CSR associated with the reference soil profile
CSR^{site}	site-specific uniform hazard estimate of CSR
ΔCSR_{σ}	correction factor for vertical stress
ΔCSR_{Fpga}	correction factor for soil amplification
ΔCSR_{rd}	correction factor for shear stress reduction
ΔCSR_{MSF}	correction factor for magnitude scaling factor
$\Delta CSR_{K\sigma}$	correction factor for overburden pressure
ΔCSR	difference between CSR^{site} and CSR^{ref} values
$CSR_{correction}$	correction function for CSR when using the 2014 MSF
$CSR_{corrected}^{site}$	CSR^{site} that is corrected when using the 2014 MSF
FC	finer content (%)
FS_L	factor of safety against liquefaction triggering
FS_L^{site}	site-specific uniform hazard estimate of FS_L
F_{PGA}	soil amplification factor
K_{σ}	overburden correction factor (Idriss and Boulanger model)
MSF	magnitude scaling factor
M_w	mean moment magnitude
q	CPT tip resistance
q_{c1Ncs}	normalized clean-sand equivalent, corrected CPT tip resistance
q_{req}	CPT resistance required to resist or prevent liquefaction
q_{req}^{ref}	uniform hazard estimate of q_{req} associated with the reference soil profile
q_{req}^{site}	site-specific uniform hazard estimate of q_{req}
Δq_L	difference between q_{site} and q_{req} values
P_a	atmospheric pressure (1 atm, 101.3 kPa, 0.2116 psf)
PGA	peak ground acceleration
P_L	probability of liquefaction
r_d	shear stress reduction coefficient
CPT	Cone Penetration Test
$V_{s,12}$	average shear wave velocity in upper 12 m (39.37 ft) of soil profile
z	depth to middle of soil profile layer
γ	unit weight of soil (i.e. pcf, kN/m ³ , etc.)
σ_{ϵ}	error term for either model + parametric uncertainty or parametric uncertainty

σ_T	error term for both model and parametric uncertainty
σ_v	total vertical stress in the soil
σ'_v	effective vertical stress in the soil
Λ_{FSL}^*	mean annual rate of not exceeding some given value of FS_L
$\lambda_{N_{req}}^*$	mean annual rate of not exceeding some given value of N_{req}
τ_{cyc}	equivalent uniform cyclic shear stress
Φ	standard normal cumulative distribution function

Post-Liquefaction Settlement Terms

D_R	relative density
IND_i	the probability of liquefaction occurring
M	model bias correction factor
N	number of layers
S_p	total ground surface settlement
$\Delta\varepsilon$	site-specific correction factor
ΔZ_i	the i^{th} layer's thickness
ε_v	vertical strain
$\varepsilon_{v,\text{calibrated}}^{\text{site}}$	site-specific strain calibrated for model non-linearity
$\varepsilon_v^{\text{ref}}$	vertical strain for the reference soil profile
$\varepsilon_v^{\text{site}}$	site-specific vertical strain
$\varepsilon_{v,\text{pseudo}}^{\text{ref}}$	vertical strain for the reference soil profile using pseudo-probabilistic approach
$\varepsilon_{v,\text{pseudo}}^{\text{site}}$	site-specific vertical strain using pseudo-probabilistic approach
$\sigma_{\ln(S)}$	model uncertainty
σ'_{vo}	effective vertical stress in the soil
Φ	standard normal cumulative distribution function

Lateral Spread Displacement Terms

DI	lateral displacement
H	height of the free face
L	distance to the free face
LDI	lateral displacement index
S	ground slope (%)
$\Delta\gamma$	site-specific correction factor
γ_{max}	maximum cyclic shear strain

$\gamma_{v, \text{simp}}^{\text{site}}$	final site-specific horizontal strain
$\gamma_{\text{max}}^{\text{ref}}$	horizontal strain for the reference soil profile
$\gamma_{\text{max}}^{\text{site}}$	site-specific horizontal strain
$\gamma_{v, \text{approx}}^{\text{ref}}$	horizontal strain for the reference soil profile using semi-probabilistic approach
$\gamma_{v, \text{approx}}^{\text{site}}$	site-specific horizontal strain using semi-probabilistic approach

EXECUTIVE SUMMARY

The purpose of the research presented is to provide the benefit of the full performance-based probabilistic earthquake hazard analysis using Cone Penetration Test (CPT) data without requiring special software, training, and experience. To do this, simplified models of liquefaction triggering, post-liquefaction settlement, and lateral spread displacements that approximate the results of the full probabilistic analysis were developed. These simplified methods are designed to require only a few simple equations and a liquefaction parameter map. This final report volume for Phase 2 of this research provides the derivation and validation of these simplified models, the development of the liquefaction reference parameter maps, and a comparison of the simplified, pseudo-probabilistic (i.e. conventional), and deterministic procedures to the full performance-based procedure, addressing Tasks 5 through 10 of the pooled fund study TPF-5(338) research contract. The Phase 1 final report volume was published separately and addressed Tasks 1 through 4 of the study, including development of a performance-based earthquake engineering (PBEE) liquefaction hazard analysis procedure for the CPT and of an analysis tool, *CPTLiquefY*, to simplify extensive probabilistic calculations.

In Phase 2 of the study, the simplified procedure using the Boulanger and Idriss (2014) probabilistic liquefaction triggering model is derived based on principles from the Mayfield et al. (2010) derivation of the simplified procedure for the Cetin et al. (2004) probabilistic liquefaction triggering model. The simplified Ku et al. (2012) procedure is a probabilistic version of the Robertson and Wride (2009) empirical liquefaction triggering model. The simplified procedure for predicting post-liquefaction settlement is derived based on the Juang et al. (2013) model. The simplified procedure for predicting lateral spread displacements is derived based on the Zhang et al. (2004) model. The procedures are based on retrieving a reference parameter value [i.e. CSR^{ref} (%), q_{req}^{ref} (%), ε_v^{ref} (%), and γ_{max}^{ref} (%)] from a hazard-targeted liquefaction parameter map, and calculating site-specific correction factors to adjust the reference value to represent the site-specific conditions. The simplified procedures were validated by comparing the results of the simplified analysis with a full performance-based analysis for 17 cities of varying seismicity using 20 different soil profiles.

A major component of the simplified procedure is the use of liquefaction reference parameter maps. A grid spacing study was conducted to understand how the spacing of points could potentially bias the predicted results from the procedure. Once the optimum grid spacing was identified, *CPTLiquefy* was used to perform full-probabilistic calculations for a reference soil profile at each grid point. The maps are developed in ArcMap. Using the completed reference maps, a comparison study between the simplified procedure, conventional pseudo-probabilistic procedure, and deterministic procedure was conducted for points throughout Utah, South Carolina, Connecticut, and Oregon.

To assist in implementing the simplified procedures, a tool was created to perform the simplified calculations, called *CPTLiq*. *CPTLiq* is available in spreadsheet format and provides an easily implemented procedure. A step-by-step process is provided in a user's manual additional to this report, and will assist in the use of the *CPTLiq* tool in those states for which liquefaction parameter maps have been developed.

1.0 INTRODUCTION

1.1 Problem Statement

The purpose of the research presented is to provide the benefit of the full performance-based probabilistic earthquake hazard analysis using Cone Penetration Test (CPT) data, without requiring special software, training, and experience. This research is comprised of two phases, with the results of Phase 2 being presented in this final report volume and Phase 1 being presented in a separate final report volume. The purpose of Phase 2 (Tasks 5-10) of this project is to develop a simplified performance-based method that closely approximates full-probabilistic analysis results for liquefaction triggering, post-liquefaction free-field settlement, and lateral spread. To do so, a simplified procedure was developed. A validation study was conducted to ensure the simplified models provide results that adequately approximate the results from full performance-based model at a given return period. Liquefaction reference parameter maps were also created for states involved in this study. The simplified performance-based procedures were also evaluated against conventional (i.e., pseudo-probabilistic, deterministic) and full performance-based procedures. Lastly, a tool, *CPTLiq*, was created to incorporate the simplified procedures.

It is noted that a related study was performed previously for Standard Penetration Test (SPT) data by some of the same authors of this study. More information on the SPT-based study is available under the TPF-5(296) pooled fund study on the pooledfund.org website, from the Utah Department of Transportation Research & Innovation Division, or from the current study authors.

1.2 Objectives

The objective of this report is to detail the development of the simplified performance-based method, the liquefaction parameter maps, and the *CPTLiq* tool. The main research steps addressed in this report include:

- Introduce the original models used to determine liquefaction hazards (i.e. liquefaction triggering, lateral spread displacement, and post-liquefaction settlement) and provide derivations and development of the simplified methods.
- Validate the simplified models by performing a site-specific analysis for several different sites using the simplified and full models.
- Describe the development of the reference parameter maps.
- Compare the simplified procedure, the pseudo-probabilistic procedure, and the deterministic procedure to the full performance-based procedure.
- Provide a recommended methodology for implementing the simplified procedure in practice.

These steps specifically address Tasks 5 through 10 of the pooled fund study TPF-5(338) research contract.

1.3 Scope

This report is organized to include the following topics:

- Background of Seismic Hazard Analysis
- Development of the Simplified Method for Liquefaction Triggering
- Development of the Simplified Method for Post-Liquefaction Settlement
- Development of the Simplified Method for Lateral Spread Displacement
- Development of Reference Parameter Maps
- Validation Results for Liquefaction Triggering
- Validation Results for Post-Liquefaction Settlement
- Validation Results for Lateral Spread Displacement
- Comparison of Simplified Procedure, Pseudo-Probabilistic Procedure, and Deterministic Procedure
- Conclusions
- References
- Appendix A: Liquefaction Reference Parameter Maps

2.0 BACKGROUND OF SEISMIC HAZARD ANALYSIS

The purpose of this section is to provide a brief background of different type of seismic hazard analysis that will be referred to throughout the report. Through the history of earthquake design, several types of analysis have been created to help engineers choose a representative earthquake to incorporate into design projects. This is important because this information dictates how infrastructures are designed to resist earthquakes. The following sections will describe how different seismic hazard analyses are used and referred to in this report.

2.1 Deterministic Approach

A deterministic seismic hazard analysis designs for the earthquake that generates the largest and most significant ground motion that may occur at the site. The corresponding ground motion (i.e., a_{\max}) and the moment magnitude (i.e., M_w) from this earthquake are used to calculate the factor of safety against liquefaction, FS_L , using either the Robertson and Wride (2009) model or the Boulanger and Idriss (2014) model. Then this FS_L is applied to a deterministic calculation of earthquake effects.

2.2 Pseudo-Probabilistic Approach

The pseudo-probabilistic seismic hazard analysis involves using a probabilistic seismic hazard analysis (PSHA) to decide the ground motion and moment magnitude. The selection of ground motion is usually done by the USGS deaggregation tool. The moment magnitude can be either the mean (i.e., average) magnitude or the modal (i.e., most occurring) magnitude. Then these values are applied to either the Robertson and Wride (2009) model or the Boulanger and Idriss (2014) model to calculate FS_L in a deterministic manner. This FS_L is also applied to a deterministic calculation of earthquake effects. The pseudo-probabilistic approach accounts for some uncertainty in ground motions, but ignores the inherent uncertainty within the triggering of liquefaction and the calculation of its effects.

2.3 Performance-Based Approach

The performance-based approach is a fully-probabilistic seismic analysis developed by the Pacific Earthquake Engineering Research (PEER) Center. To apply the PEER framework to liquefaction triggering, FS_L hazard curves are developed using the Kramer and Mayfield (2007) performance-based earthquake engineering (PBEE) approach. A detailed description of the performance-based liquefaction triggering procedure is described in the Section 3.2.2 of this report. The developed FS_L hazard curves will then be applied to a PBEE post-liquefaction analysis to obtain post-liquefaction settlement and lateral spread displacement.

2.4 Semi-Probabilistic Approach

The semi-probabilistic approach calculates FS_L using a performance-based liquefaction triggering procedure and then applies this FS_L to deterministic settlement and lateral spread calculation. This method accounts for the inherent uncertainty in predicting liquefaction triggering but fails to account for the uncertainty in calculating post-liquefaction settlement and lateral spread.

3.0 DERIVATION OF THE SIMPLIFIED MODELS

3.1 Overview

This section provides the derivation of the simplified liquefaction triggering, post-liquefaction settlement, and lateral spread displacement models. The original models will be discussed and the derivation process for the simplified models will be presented in detail.

3.2 Performance-based Liquefaction Triggering Evaluation

This section will provide the necessary background to understand the simplified performance-based liquefaction triggering procedure. The Boulanger and Idriss (2014) and Ku et al. (2012), (probabilistic version of Robertson and Wride [2009]) models will be introduced, followed by the derivation and validation of these models.

3.2.1 Empirical Liquefaction Triggering Models

In engineering practices today, the most commonly used approach to evaluate liquefaction triggering potential was first introduced by Seed and Idriss (Seed and Idriss 1971; Seed 1979; Seed and Idriss 1982; and Seed et al. 1985). This simplified empirical method compares the cyclic stress ratio (CSR) to the cyclic resistance ratio (CRR). The CSR represents the seismic demand or loading of a soil and the CRR represents the soil's resistance to seismic loading. The method proposed by Seed and Idriss to compute the cyclic stress ratio (CSR) can be expressed as:

$$CSR = 0.65 \frac{a_{\max}}{g} \frac{\sigma_v'}{\sigma_v} r_d \frac{1}{MSF} \quad (1)$$

where σ_v' is the effective vertical stress in the soil, a_{\max}/g is the peak ground surface acceleration as a fraction of gravity, σ_v is the total vertical stress in the soil, r_d is a shear stress reduction coefficient, and where MSF is the magnitude scaling factor.

The cyclic resistance ratio (CRR), or the cyclic stress required to initiate liquefaction, is more difficult to compute, but is typically interpreted from in-situ tests (i.e., SPT penetration tests,

CPT penetration tests, shear wave velocity, etc.). These results are then compared to databases and liquefaction case histories. Graphically, CRR is the dividing line between “liquefaction” and “non-liquefaction” cases. It also represents a combination of CSR values and in-situ soil test values at which liquefaction triggers.

Engineers and geologists commonly quantify liquefaction triggering using a factor of safety against liquefaction triggering, FS_L . This parameter is calculated as:

$$FS_L = \frac{\text{Resistance}}{\text{Loading}} = \frac{CRR}{CSR} \quad (2)$$

Kramer and Mayfield (2007) and Mayfield et al. (2010) introduced an alternative method to quantify liquefaction triggering. CRR is to be a function of soil resistance measured using in-situ test values. In this report, where the cone penetration test is used, CRR can be expressed as a function of q_{c1Ncs} , which is the clean-sand equivalent, corrected CPT tip resistance for the soil layer. From the CRR function, the CPT resistance required to resist or prevent liquefaction, q_{req} , can be obtained for a given seismic loading (i.e., CSR). This results in FS_L to be computed as:

$$FS_L = \frac{CRR}{CSR} = \frac{CRR(q_{c1Ncs})}{CRR(q_{req})} \quad (3)$$

where $CRR(q)$ denotes that CRR is a function of given value of CPT tip resistance, q .

Mayfield et al. (2010) defined the relationship between the actual SPT resistance for the given layer, N_{site} , and N_{req} :

$$\Delta N_L = N_{site} - N_{req} \quad (4)$$

This relationship can be adapted for CPT resistance for the given layer, q_{site} , and q_{req} as:

$$\Delta q_L = q_{site} - q_{req} \quad (5)$$

The relationship between CSR , CRR , N_{site} , and N_{req} (or q_{site} and q_{req}) is shown graphically in Figure 3-1, after Mayfield et al. (2010).

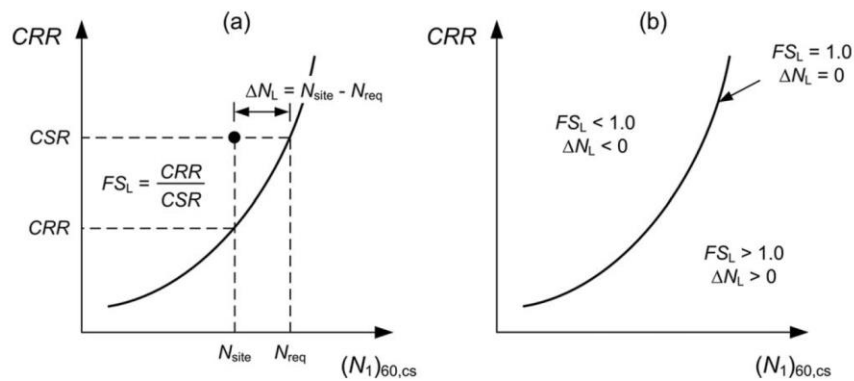


Figure 3-1: Schematic illustration of: (a) definitions of FS_L and ΔN_L ; (b) relationship between FS_L and ΔN_L (after Mayfield et al. 2010)

3.2.2 Performance-based Liquefaction Triggering Assessment

The simplified empirical liquefaction triggering models require engineers to select seismic loading parameters (i.e., peak ground surface acceleration a_{max} and moment magnitude M_w) to adequately represent an earthquake. This is a simple procedure when only a single seismic source contributes to the loading. However, this presents a problem when multiple seismic sources are present and contribute differently to the seismic hazard. In more complex cases, a probabilistic seismic hazard analysis (PSHA) is performed. The PSHA calculates the seismic hazard associated with a specified return period or likelihood of occurrence with the use of deaggregation tools. From the deaggregation results, a single magnitude (mean or modal) and peak ground acceleration are given for a targeted return period. Unfortunately, Kramer and Mayfield (2007) showed that these methods of assessment introduced bias into hazard calculations.

Potential biases introduced into the liquefaction triggering assessment through the improper and/or incomplete utilization of probabilistic ground motions and liquefaction triggering models could be reduced through the implementation of a performance-based approach (Franke et al. 2014a). Kramer and Mayfield (2007) presented such an approach, which utilized the probabilistic framework for performance-based earthquake engineering (PBEE) developed by the Pacific Earthquake Engineering Research Center (Cornell and Krawinkler 2000; Krawinkler 2002; Deierlein et al. 2003). This implementation of the PEER PBEE framework assigned the joint

occurrence of M_w and a_{max} as an intensity measure, and either FS_L or N_{req} as the engineering demand parameter. The Kramer and Mayfield (2007) approach produces liquefaction hazard curves for each layer in a soil profile while using ground motions in a probabilistic manner. This section will present a basic background of the Kramer and Mayfield performance-based approach, but further information can be found in Kramer and Mayfield (2007). Even though the approach is SPT-based (i.e. N_{req} , $(N_1)_{60}$), the same principles and ideas follow for performance-based approaches for CPT-based methods (i.e. q_{req} , q_{c1Ncs}).

Kramer and Mayfield (2007) demonstrated that a hazard curve for FS_L could be developed using the following relationship:

$$\Lambda_{FS_L^*} = \sum_{j=1}^{N_M} \sum_{i=1}^{N_{a_{max}}} P[FS_L > FS_L^* | a_{max_i}, m_j] \Delta\lambda_{a_{max_i}, m_j} \quad (6)$$

where $\Lambda_{FS_L^*}$ is the mean annual rate of *not* exceeding some given value of factor of safety, FS_L^* ; $P[FS_L < FS_L^* | a_{max_i}, m_j]$ is the conditional probability that the actual factor of safety is less than FS_L^* given peak ground surface acceleration a_{max} , and moment magnitude m_j ; $\Delta\lambda_{a_{max_i}, m_j}$ is the incremental joint mean annual rate of exceedance for a_{max} and m_j ; and N_M and $N_{a_{max}}$ are the number of magnitude and peak ground acceleration increments into which the intensity measure “hazard space” is subdivided.

The conditional probability component of Equation (6) can be solved with any selected probabilistic liquefaction triggering relationship, but that relationship must be manipulated to compute the desired probability.

Similar to the relationship for computing a hazard curve for FS_L , Kramer and Mayfield (2007) derived a relationship for computing a hazard curve for N_{req} as:

$$\lambda_{N_{req}^*} = \sum_{j=1}^{N_M} \sum_{i=1}^{N_{a_{max}}} P[N_{req} > N_{req}^* | a_{max_i}, m_j] \Delta\lambda_{a_{max_i}, m_j} \quad (7)$$

where $\lambda_{N_{req}^*}$ is the mean annual rate of exceeding some given clean sand-equivalent required SPT resistance, N_{req}^* , and $P[N_{req} < N_{req}^* | a_{max_i}, m_j]$ is the conditional probability that the actual N_{req} is greater than N_{req}^* given peak ground surface acceleration a_{max} and moment magnitude m_j .

3.3 Simplified Liquefaction Triggering Model

The Kramer and Mayfield (2007) performance-based liquefaction triggering procedure summarized in Section 3.2.2 is an effective solution to mitigating the deficiencies introduced by the conventional liquefaction triggering approach. Unlike conventional approaches where seismic contributions are only considered at a given return period, this probabilistic performance-based approach considers seismic contributions from *all* hazard levels and *all* earthquake magnitudes (Kramer and Mayfield 2007). However, the Kramer and Mayfield (2007) performance-based procedure considers *all* the seismic loading contributions from *all* return periods, not just return periods given by design. Unfortunately, the Kramer and Mayfield procedure is relatively sophisticated and difficult for many engineers and geologists to apply in a practical manner. Specialized computational tools such as *WSliq* (Kramer 2008), *PBliquefY* (Franke et al. 2014c), and *CPTLiquefY* (Franke et al. 2018) have been developed to assist these professionals in implementing the performance-based procedure. However, even the availability of computational tools is not sufficient for many professionals, who routinely need to perform and/or validate liquefaction triggering hazard calculations in a rapid and efficient manner.

An ideal solution to this dilemma would be the introduction of a new liquefaction analysis procedure that combined the simplicity and user-friendliness of traditional liquefaction hazard maps with the flexibility and power of a site-specific performance-based liquefaction triggering analysis. Mayfield et al. (2010) introduced such a procedure, which was patterned after the map-based procedure used in most seismic codes and provisions for developing probabilistic ground motions for engineering design. Franke et al. (2014d) later refined the Mayfield et al. (2010) simplified procedure for easier implementation in seismic codes and provisions.

Mayfield et al. (2010) demonstrated with the Cetin et al. (2004) liquefaction model that probabilistic estimates of liquefaction resistance (i.e. N_{req} or q_{req}) can be computed for a reference soil profile across a grid of locations to develop contour plots called liquefaction parameter maps. A liquefaction parameter map incorporating N_{req} or q_{req} can be a useful tool to evaluate the seismic demand for liquefaction at a given return period because N_{req} or q_{req} is directly related to *CSR* (i.e. Figure 3-1). Mayfield et al. (2010) demonstrated how these mapped “reference” values of N_{req} could be adjusted for site-specific conditions and used to develop site-specific uniform hazard

estimates of N_{req} (i.e., N_{req}^{site}) and/or FS_L (i.e., FS_L^{site}) at the targeted return period or hazard level. The derivation of the simplified method for the Cetin et al. (2004) liquefaction triggering model will not be included in this report but is presented in detail in Mayfield et al. (2010).

The most widely used CPT-based methods for liquefaction initiation evaluation are the Boulanger and Idriss (2014) model and the Robertson and Wride (2009) model. The Ku et al. (2012) probabilistic version of the Robertson and Wride (2009) liquefaction triggering model will also be used in this study. This report will show the derivation of the simplified probabilistic method incorporating these models by using the framework introduced by Mayfield et al. (2010).

3.3.1 Liquefaction Parameter Maps & Reference Profile

As previously discussed, liquefaction loading maps are an important part to the simplified method as it provides the benefits of site-specific performance-based analysis while being user-friendly. While liquefaction parameter maps will be discussed later in this report, the purpose of this section is to give a brief introduction to what role these maps play in the simplified method and briefly discuss the use of the reference profile. Figure 3-2 presents a generic soil profile representing a reference site that was applied in this study. This profile is similar to the one originally introduced by Mayfield et al. (2010) and used for the simplified Cetin et al. (2004) procedure and simplified Boulanger and Idriss (2012) procedure derived by Ulmer (2015). This reference soil profile is used to find reference values at a depth of 6 meters for the targeted return period (T_R) or hazard level for all the models (triggering, settlement, and lateral spread) in this report. The goal of the liquefaction loading maps is to allow users to easily interpret reference values from the liquefaction loading maps to be used in simplified method calculations. For the simplified Boulanger and Idriss (2014) and simplified Ku et al (2012) triggering procedures, reference values for q_{req} and CSR will be mapped, respectively. For the simplified settlement and lateral spread procedures, reference values for ε_v (%) and γ_{max} (%) will be mapped separately. Because these values associated with the reference soil profile do not represent any actual soil profile, reference values are distinguished using the terms q_{req}^{ref} , CSR^{ref} , ε_v (%), and γ_{max} (%). By computing these hazard-targeted values at different locations across a geographic area, contoured maps can be created. Detailed steps on how these values are used in the simplified methods will

be discussed in each corresponding section. Because CSR , $\varepsilon_v(\%)$ and $\gamma_{max}(\%)$ are often a decimal, mapping these values in percent allows for more precise contour mapping, as well as easier interpretation and interpolation for design engineers. The liquefaction reference parameter maps from this current study are provided in the Appendix of this final report. However, Figure 3-3 shows an example of a liquefaction loading map of $CSR^{ref}(\%)$ at a return period of 1,033 years for a portion of the Salt Lake Valley in Utah from a previous study. The development of these maps will be presented in a later section.

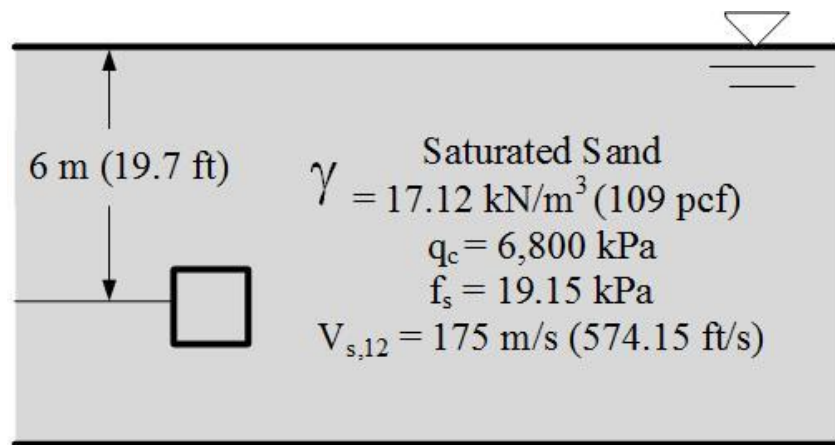


Figure 3-2. Reference soil profile used to develop liquefaction loading maps in the proposed simplified uniform hazard liquefaction procedure



Figure 3-3. Liquefaction loading map ($T_R = 1,033$ years) showing contours of $CSR^{ref}(\%)$ for a portion of the Salt Lake Valley in Utah (after Ulmer 2015)

To account for site-specific conditions, the equations developed in the simplified procedures will correct the mapped liquefaction loading values to site-specific liquefaction loading values. These can then be used to compute site-specific performance-based estimates of liquefaction triggering, settlement, and lateral spread at a targeted return period. The following sections will show the simplified method derivations for the Boulanger and Idriss (2014) liquefaction triggering model and the Ku et al. (2012) model (probabilistic version of the Robertson and Wride (2009) model). The derivations for the simplified settlement and lateral spread procedures will follow.

3.3.2 Simplified Procedure Using the Boulanger and Idriss (2014) Probabilistic Liquefaction Triggering Model

According to the probabilistic liquefaction triggering relationship developed by Boulanger and Idriss (2012), the probability of liquefaction P_L is given as:

$$P_L = \Phi \left[-\frac{\ln(CRR_{P_L=50\%}) - \ln(CSR)}{\sigma_T} \right] \quad (8)$$

where Φ represents the standard normal cumulative distribution function, σ_T is the total uncertainty of the liquefaction model, and $CRR_{P_L=50\%}$ is the cyclic resistance ratio corresponding to a probability of liquefaction of 50% (i.e. median CRR), which is computed as:

$$CRR_{P_L=50\%} = \exp \left[\frac{q_{c1Ncs}}{113} + \left(\frac{q_{c1Ncs}}{1000} \right)^2 - \left(\frac{q_{c1Ncs}}{140} \right)^3 + \left(\frac{q_{c1Ncs}}{137} \right)^4 - 2.60 \right] \quad (9)$$

Unlike the Mayfield et al. (2010) simplified liquefaction procedure, which incorporates the Cetin et al. (2004) liquefaction model, the simplified uniform hazard liquefaction procedure for the Boulanger and Idriss (2014) liquefaction model cannot be derived to solve for q_{req}^{site} in a convenient manner because of the 4th-order polynomial equation in CRR (i.e. Equation (9)). Fortunately, this simplified procedure can be modified to incorporate CRR and CSR instead of q_{req} , which greatly simplifies the derivation of the new procedure, and makes it somewhat more intuitive.

By substituting q_{req}^{ref} into Equation (9), the median CSR associated with the reference site (i.e. CSR^{ref}) at the targeted return period can be computed. CSR^{ref} represents a uniform hazard estimate of the seismic loading that must be overcome to prevent liquefaction triggering if the reference soil profile existed at the site of interest.

3.3.2.1 Site-Specific Correction for CSR^{ref}

Because CSR^{ref} was developed using the reference soil profile, it must be corrected for site-specific soil conditions and depths to be used in computing site-specific uniform hazard values of

FS_L , P_L , and q_{req} . If CSR^{site} represents the site-specific uniform hazard value of CSR , then CSR^{ref} and CSR^{site} can be related as:

$$\ln(CSR^{site}) = \ln(CSR^{ref}) + \Delta CSR \quad (10)$$

where ΔCSR is a site-specific correction factor. By rearranging Equation (10), we can solve for ΔCSR as:

$$\Delta CSR = \ln(CSR^{site}) - \ln(CSR^{ref}) = \ln \left[\frac{CSR^{site}}{CSR^{ref}} \right] \quad (11)$$

Similar to Equation (1), the magnitude- and stress-corrected CSR for level or near-level ground according to Boulanger and Idriss (2014) is computed as:

$$CSR_{M=7.5, \sigma'_v=1atm} = 0.65 \frac{a_{max,i}}{g} \frac{\sigma'_v}{\sigma'_v} (r_d)_j \frac{1}{(MSF)_j} \frac{1}{K_\sigma} = 0.65 \frac{\sigma'_v}{\sigma'_v} \frac{(F_{pga} \cdot PGA_{rock})}{g} r_d \frac{1}{MSF} \frac{1}{K_\sigma} \quad (12)$$

where F_{pga} is the soil amplification factor corresponding to the peak ground acceleration (PGA), and PGA_{rock} is the PGA corresponding to bedrock (i.e. $V_s=760$ m/s). Equations for r_d , MSF , and K_σ are provided in later sections of this report. If Equation (12) is substituted into Equation (11) then Equation (11) can be rewritten as:

$$\Delta CSR = \ln \left[\frac{0.65 \left(\frac{\sigma'_v}{\sigma'_v} \right)^{site} \left(\frac{F_{pga}^{site} \cdot PGA_{rock}^{site}}{g} \right) \cdot r_d^{site} \cdot \left(\frac{1}{MSF^{site}} \right) \cdot \left(\frac{1}{K_\sigma^{site}} \right)}{0.65 \left(\frac{\sigma'_v}{\sigma'_v} \right)^{ref} \left(\frac{F_{pga}^{ref} \cdot PGA_{rock}^{ref}}{g} \right) \cdot r_d^{ref} \cdot \left(\frac{1}{MSF^{ref}} \right) \cdot \left(\frac{1}{K_\sigma^{ref}} \right)} \right] \quad (13)$$

Because there should be no difference in the ground motions between the reference soil profile and the actual soil profile, $PGA_{rock}^{site} = PGA_{rock}^{ref}$. Therefore, Equation (13) can be simplified as:

$$\begin{aligned}\Delta CSR &= \ln \left(\frac{\left(\frac{\sigma_v}{\sigma'_v} \right)^{site}}{\left(\frac{\sigma_v}{\sigma'_v} \right)^{ref}} \right) + \ln \left(\frac{F_{pga}^{site}}{F_{pga}^{ref}} \right) + \ln \left(\frac{r_d^{site}}{r_d^{ref}} \right) - \ln \left(\frac{MSF^{site}}{MSF^{ref}} \right) - \ln \left(\frac{K_\sigma^{site}}{K_\sigma^{ref}} \right) \\ &= \Delta CSR_\sigma + \Delta CSR_{F_{pga}} + \Delta CSR_{r_d} + \Delta CSR_{MSF} + \Delta CSR_{K_\sigma}\end{aligned}\quad (14)$$

where ΔCSR_σ , $\Delta CSR_{F_{pga}}$, ΔCSR_{r_d} , ΔCSR_{MSF} , and ΔCSR_{K_σ} are site-specific correction factors for stress, soil amplification, shear stress reduction, earthquake magnitude, and overburden pressure, respectively.

3.3.2.2 Correction for Vertical Stress, ΔCSR_σ

The relationship for the stress correction factor, ΔCSR_σ is defined as:

$$\Delta CSR_\sigma = \ln \left[\frac{\left(\frac{\sigma_v}{\sigma'_v} \right)^{site}}{\left(\frac{\sigma_v}{\sigma'_v} \right)^{ref}} \right] \quad (15)$$

If the liquefaction parameter map for CSR^{ref} (%) was developed using the reference soil profile shown in Figure 3-2, then Equation (15) can be simplified as:

$$\Delta CSR_\sigma = \left[\frac{\left(\frac{\sigma_v}{\sigma'_v} \right)^{site}}{2.34} \right] \quad (16)$$

3.3.2.3 Correction for Soil Amplification, $\Delta CSR_{F_{pga}}$

The relationship for the soil amplification factor, $\Delta CSR_{F_{pga}}$ is defined as:

$$\Delta CSR_{F_{pga}} = \ln \left(\frac{F_{pga}^{site}}{F_{pga}^{ref}} \right) \quad (17)$$

If the value of F_{pga}^{ref} for the reference soil profile is fixed at 1, then the correction factor for soil amplification can be written as:

$$\Delta CSR_{F_{pga}} = \ln\left(\frac{F_{pga}^{site}}{1}\right) = \ln(F_{pga}^{site}) \quad (18)$$

Thus, the only parameter required to calculate the soil amplification factor is the F_{pga}^{site} value from AASHTO 2012 Table 3.10.3.2-1 corresponding to the site of interest. The *PGA* value used to determine F_{pga}^{site} from the table should be calculated from the USGS 2014 interactive deaggregation website for the return period of interest (e.g., 2% probability of exceedance in 21 years, $T_R = 1039$).

3.3.2.4 Correction for Shear Stress Reduction, ΔCSR_{rd}

The shear stress reduction factor, r_d , was defined by Boulanger and Idriss (2012, 2014) as:

$$r_d = \exp[\alpha + \beta \cdot M_w] \quad (19)$$

$$\alpha = -1.012 - 1.126 \sin\left(\frac{z}{11.73} + 5.133\right) \quad (20)$$

$$\beta = 0.106 - 0.118 \sin\left(\frac{z}{11.28} + 5.142\right) \quad (21)$$

where z represents sample depth in meters and M_w is the mean moment magnitude. Thus, the equation for ΔCSR_{rd} becomes:

$$\Delta CSR_{rd} = \ln\left(\frac{r_d^{site}}{r_d^{ref}}\right) = \ln\left(\frac{\exp(\alpha^{site} + \beta^{site} \cdot M_w^{site})}{\exp(\alpha^{ref} + \beta^{ref} \cdot M_w^{ref})}\right) \quad (22)$$

Both the site soil profile and the reference soil profile experience the same ground motions, so $M_w^{site} = M_w^{ref}$. Therefore, Equation (22) can be written as:

$$\Delta CSR_{r_d} = (\alpha^{site} - \alpha^{ref}) + M_w^{site} (\beta^{site} - \beta^{ref}) \quad (23)$$

For the reference soil profile used in this study (Figure 3-2), $\alpha^{ref} = -0.3408$ and $\beta^{ref} = 0.0385$. Thus, Equation (23) becomes:

$$\Delta CSR_{r_d} = (a^{site} - 0.341) + M_w^{site} (\beta^{site} - 0.0385) \quad (24)$$

Equation (24) can also be written in terms of depth to the site-specific soil layer (in meters) from the ground surface, z^{site} as:

$$\begin{aligned} \Delta CSR_{r_d} = & \left(-0.6712 - 1.126 \sin \left(\frac{z^{site}}{11.73} + 5.133 \right) \right) \\ & + M_w^{site} (0.0675 + 0.118 \sin \left(\frac{z^{site}}{11.28} + 5.142 \right)) \end{aligned} \quad (25)$$

3.3.2.5 Correction for Magnitude Scaling Factor, ΔCSR_{MSF}

Boulangier and Idriss have introduced two methods to calculate the Magnitude Scaling Factor, MSF (Boulangier and Idriss models (2012 and 2014)). Instead of using the 2014 MSF for this simplified procedure, the 2012 MSF was used. The explanation for this decision will be discussed later.

Similar to previous sections, we compute the site-specific correction for the magnitude scaling factor, ΔCSR_{MSF} , as:

$$\Delta CSR_{MSF} = -\ln \left[\frac{MSF^{site}}{MSF^{ref}} \right] \quad (26)$$

Since the 2012 MSF is a function of magnitude, $MSF^{site} = MSF^{ref}$ because there should be no difference in the earthquake magnitude between the reference soil profile and the actual soil profile. Therefore, $\Delta CSR_{MSF} = 0$ and can be excluded from Equation (14).

During this research process, we observed that the 2014 MSF produced inconsistent results and biased trends in the simplified procedure that could not be resolved with a calibration or correction equation. Because the 2012 MSF produced more consistent results, we chose to

implement the 2012 MSF in the simplified procedure. At the time of this report, ongoing research by others is underway that will highlight additional problems/concerns involving the 2014 MSF.

3.3.2.6 Correction for Overburden Pressure, $\Delta CSR_{K\sigma}$

Both the 2010 and 2014 versions of the Boulanger and Idriss model use the same overburden correction factor, K_σ :

$$K_\sigma = 1 - C_\sigma \ln \left(\frac{\sigma'_v}{P_a} \right) \leq 1.1 \quad (27)$$

$$C_\sigma = \frac{1}{37.3 - 8.27 (q_{c1Ncs})^{0.264}} \leq 0.3 \quad (28)$$

where P_a is 1 atmosphere of pressure (i.e. 1 atm, 101.3 kPa, 0.2116 psf). Note that the value q_{c1Ncs} must be computed using the equations found in Idriss and Boulanger (2008, 2010). Idriss and Boulanger (2010) commented that the K_σ limit of 1.1 has a somewhat negligible effect. Therefore, the simplified method derived here will not use the restriction on K_σ . However, the limit of 0.3 for values of C_σ will be incorporated. Now the correction term $\Delta CSR_{K\sigma}$ can be written as:

$$\Delta CSR_{K_\sigma} = -\ln \left(\frac{K_\sigma^{site}}{K_\sigma^{ref}} \right) = -\ln \left(\frac{1 - C_\sigma^{site} \ln \left(\frac{(\sigma'_v)^{site}}{P_a} \right)}{1 - C_\sigma^{ref} \ln \left(\frac{(\sigma'_v)^{ref}}{P_a} \right)} \right) \quad (29)$$

If the liquefaction parameter map for CSR^{ref} (%) was developed using the reference soil profile shown in Figure 3-2, then $C_\sigma^{ref} = 0.108$, $K_\sigma^{ref} = 1.09$, and Equation (29) would become:

$$\Delta CSR_{K_\sigma} = -\ln \left(\frac{1 - \left(\text{MIN} \left\{ \begin{array}{l} 0.3 \\ \frac{1}{37.3 - 8.27 (q_{c1Ncs})^{0.264}} \end{array} \right\} \right) \cdot \ln \left(\frac{(\sigma'_v)^{site}}{P_a} \right)}{1.09} \right) \quad (30)$$

3.3.2.7 Equations for CSR^{site} , q_{req}^{site} , FS_L , and P_L

The following section will summarize the equations we derived for the simplified Boulanger and Idriss (2014) liquefaction triggering model and how to use them.

3.3.2.8 Simplified CSR, CSR^{site}

Once the CSR^{ref} (%) is obtained from the appropriate (i.e. hazard-targeted) map and the appropriate correction factors are computed using Equations (16), (18), (25), and (30) the site-specific hazard-targeted CSR^{site} can be computed for site-specific soil layer i using the following equation (from Equation (10)):

$$(CSR^{site})_i = \exp \left[\ln \left(\frac{CSR^{ref}(\%)}{100} \right) + (\Delta CSR_{\sigma})_i + (\Delta CSR_{F_{pga}})_i + (\Delta CSR_{r_d})_i + (\Delta CSR_{MSF})_i + (\Delta CSR_{K_{\sigma}})_i \right] \quad (31)$$

During the research process, we observed that a calibration equation was needed to correct a non-linear bias based on PGA . The corrected (calibrated) simplified CSR, $CSR_{calibrated}^{site}$ can be calculated as:

$$CSR_{calibrated}^{site} = \left\{ \begin{array}{ll} PGA \leq 0.05g & MAX \left(\left(\frac{(CSR^{site} + 15)}{3.3661} \right), 0 \right) \\ 0.05 > PGA > 0.2g & MAX \left(\left(\frac{(CSR^{site} - 2.1362)}{0.957} \right), 0 \right) \\ PGA > 0.2g & CSR^{site} \text{ (no correction needed)} \end{array} \right\} \quad (32)$$

3.3.2.9 Simplified Factor of Safety Against Liquefaction, FS_L

To calculate the simplified FS_L for site-specific soil layer i , the Boulanger and Idriss (2014) equation for FS_L is slightly modified by inserting $CSR_{calibrated}^{site}$ into the following equation:

$$(FS_L)_i = \frac{(CRR^{site})_i}{(CSR^{site})_i} = \frac{\exp \left[\frac{(q_{c1Ncs})_i}{113} + \left(\frac{(q_{c1Ncs})_i}{1000} \right)^2 - \left(\frac{(q_{c1Ncs})_i}{140} \right)^3 + \left(\frac{(q_{c1Ncs})_i}{137} \right)^4 - 2.60 \right]}{(CSR_{calibrated}^{site})_i} \quad (33)$$

where q_{c1Ncs} is the clean sand corrected CPT resistance computed using the Boulanger and Idriss method and $CSR_{calibrated}^{site}$ is the value computed in equation (32).

3.3.2.10 Simplified Probability of Liquefaction, P_L

To solve for the uniform hazard P_L for the soil layer i , insert $CSR_{calibrated}^{site}$ into the following Boulanger and Idriss relationship:

$$(P_L)_i = F \left[\frac{\left(\frac{q_{c1Ncs}}{113} \right)_i + \left(\frac{q_{c1Ncs}}{1000} \right)_i^2 - \left(\frac{q_{c1Ncs}}{140} \right)_i^3 + \left(\frac{q_{c1Ncs}}{137} \right)_i^4 - 2.60 - \ln \left[\left(CSR_{calibrated}^{site} \right)_i \right]}{S_e} \right] \quad (34)$$

where q_{c1Ncs} is the clean sand corrected CPT resistance computed using the Boulanger and Idriss method, and $CSR_{calibrated}^{site}$ is the value computed in equation (32), σ_ε is 0.276 if parametric uncertainty (i.e., uncertainty in measuring q_{c1Ncs} and estimating seismic loading) is neglected, and σ_ε is 0.506 if parametric uncertainty is considered.

3.3.2.11 Simplified q_{req}^{site}

To compute Δq_L (or the difference between the soil resistance of the site and the resistance required to resist liquefaction) for soil sublayer i , we adapted the Mayfield et al (2010) equation for CPT methods. The resulting equation to compute Δq_L is:

$$\Delta q_L = [q_{c1Ncs}]_i - (q_{req}^{site})_i \quad (35)$$

where q_{c1Ncs} is the clean sand corrected CPT resistance computed using the Boulanger and Idriss method and $(q_{req}^{site})_i$ can be closely approximated as:

$$\begin{aligned}
q_{req}^{site} = & -0.4021 \cdot \left(\ln \left(\frac{1}{(CSR_{calibrated}^{site})_i} \right) \right)^4 - 3.367 \cdot \left(\ln \left(\frac{1}{(CSR_{calibrated}^{site})_i} \right) \right)^3 \\
& - 8.761 \cdot \left(\ln \left(\frac{1}{(CSR_{calibrated}^{site})_i} \right) \right)^2 - 21.38 \cdot \left(\ln \left(\frac{1}{(CSR_{calibrated}^{site})_i} \right) \right) + 186.3
\end{aligned} \tag{36}$$

where $CSR_{calibrated}^{site}$ is the value computed in equation (32). We derived equation (36) plotting the Boulanger and Idriss CRR curve (equation (9)) for different values of resistance, q_{req} . Recalling the relationship between CRR , CSR , and q_{req} (equation (3)), plotting $CRR(q_{req})$ is also equivalent to CSR . Once plotted, we fit a polynomial equation to the curve with q_{req} as the dependent variable and CSR as the independent variable.

3.3.3 Simplified Procedure Using the Ku et al. (2012) model [Probabilistic version of Robertson and Wride (2009)]

The deterministic Robertson and Wride (2009) model is one of the most widely-used methods for CPT-based liquefaction triggering evaluation. With the increasing popularity of performance-based procedures, Ku et al. (2012) developed a probabilistic version of the Robertson and Wride (2009) model. From this point on in the report, the simplified procedure will be referred to as the simplified Ku et al. (2012) method.

The simplified procedure follows a similar setup (Equation (10)) for the simplified Boulanger and Idriss (2014) method. Unlike the Boulanger and Idriss method, it is easier to isolate q_{req} in the Robertson and Wride (2009) equations. Thus, the framework of the simplified procedure can be expressed as:

$$q_{req}^{site} = q_{req}^{ref} + \Delta q_{req} \tag{37}$$

where q_{req}^{site} is the simplified method approximation of q_{req} , q_{req}^{ref} is the reference value provided by the liquefaction parameter maps, and Δq_{req} is the site-specific correction factor. Δq_{req} is expressed as:

$$\Delta q_{req} = \left[q_{req}^{site} \right]_{pseudo} - \left[q_{req}^{ref} \right]_{pseudo} \tag{38}$$

where $\left[q_{req}^{site} \right]_{pseudo}$ is the q_{req} computed for the site using information from a pseudo analysis, and $\left[q_{req}^{ref} \right]_{pseudo}$ is the q_{req}^{ref} computed for the reference soil profile using information from a pseudo-probabilistic analysis. This simplified procedure only requires the engineer to compute the Δq_{req} factor. The remaining section will derive the equations needed to compute Δq_{req} .

First, the Ku et al. (2010) probability of liquefaction, P_L is expressed as:

$$P_L = 1 - \Phi \left[\frac{0.102 + FS_L}{\sigma} \right] \quad (39)$$

where Φ represents the standard normal cumulative distribution function, FS_L is the factor of safety against liquefaction computed using the Robertson and Wride (2009) method, and σ is equal to 0.276 for model uncertainty or 0.3537 total uncertainty.

Recalling that $FS_L = CRR/CSR$, Equation (39) becomes:

$$P_L = 1 - \Phi \left[\frac{0.102 + \ln(CRR) - \ln(CSR)}{\sigma} \right] \quad (40)$$

where CSR and CRR are expressed as:

$$CSR = 0.65 \left(\frac{S_v}{S_v'} \right) \left(\frac{a_{max}}{g} \right) r_d \quad (41)$$

$$CRR = \begin{cases} 93 \left[\frac{q_{req}^*}{1000} \right]^3 + 0.08 & \text{for } 50 \leq q_{req}^* < 165 \\ 0.833 \left[\frac{q_{req}^*}{1000} \right] + 0.05 & \text{for } q_{req}^* < 50 \end{cases} \quad (42)$$

where q_{req}^* is the q_{req} that corresponds to a $P_L=50\%$ (the CRR curve is the dividing line between liquefiable and non-liquefiable soils which is equivalent to a probability of liquefaction, $P_L=50\%$).

Equation (40) is then re-arranged to solve for CRR as:

$$\ln(CRR) = \ln(CSR) + \sigma \cdot \Phi^{-1} [1 - P_L] - 0.102 \quad (43)$$

$$CRR = \exp\left[CSR + \sigma \cdot \Phi^{-1}\left[1 - P_L\right] - 0.102\right] \quad (44)$$

For a CRR corresponding to a probability of liquefaction of 50%, the standard normal cumulative distribution function, Φ , is equal to 0. By setting Equation (42) equal to Equation (44), q_{req}^* can be isolated and expressed as:

$$\text{For } q_{req}^* < 50, \quad q_{req}^* = \left[\frac{\exp[\ln(CSR) - 0.102] - 0.05}{0.833} \right] \cdot 1000 \quad (45)$$

$$\text{For } 50 \leq q_{req}^* < 165, \quad q_{req}^* = \left[\frac{\exp[\ln(CSR) - 0.102] - 0.08}{93} \right]^{\frac{1}{3}} \cdot 1000 \quad (46)$$

$$\text{For } q_{req}^* > 165, \quad q_{req}^* = -91.63(CSR)^{-0.2524} + 273.8 \quad (47)$$

For Robertson and Wride (2009), q_{req} values greater than 165 are not defined by an equation and are considered “non-susceptible” to liquefaction (personal communication, P. Robertson, 2017). However, in a probabilistic analysis, a possibility of liquefaction triggering must be defined and quantified for all soil penetration resistances. Therefore, for this study, Boulanger and Idriss (2014) triggering relationships were assumed for $q_{req} > 165$. An equation was fit to the Boulanger and Idriss (2014) CRR curve for q_{req} values greater than 165 and solved for q_{req} . Therefore $q_{req}^* > 165$ is expressed as shown in Equation (47).

To compute q_{req}^* , Equations (45), (46), and (47) are used iteratively. Given CSR , the user enters Equation (45) and computes q_{req}^* . If the resulting q_{req}^* is less than 50, the q_{req}^* for that soil layer is computed using Equation (45). If the resulting q_{req}^* is not less than 50, the user continues to Equation (46) and computes q_{req}^* . If the resulting q_{req}^* falls within the range of 50 and 165, q_{req}^* is computed using Equation (46). If the resulting q_{req}^* does not fall within the range, q_{req}^* for that soil layer is computed using Equation (47).

3.3.3.1 Equations for q_{req}^{site} , FS_L , P_L , Δq_L , and CSR^{site}

Once the q_{req}^{ref} has been computed, other liquefaction hazard parameters (i.e. FS_L , P_L , Δq_L , and CSR) can be quickly calculated using the equations in the following sections. This section summarizes the derived equations and the procedure for the simplified Ku et al. (2012) liquefaction triggering model.

3.3.3.2 Simplified q_{req}^{site}

The following steps are used to compute the simplified q_{req}^{site} :

1. Compute Δq_{req} as:

$$\Delta q_{req} = \left[q_{req}^{site} \right]_{pseudo} - \left[q_{req}^{ref} \right]_{pseudo} \quad (48)$$

- $\left[q_{req}^{site} \right]_{pseudo}$ is computed using the steps outlined above [iterative process using equations (45) through (47)] by using *site-specific* information at the location of interest obtained from a pseudo-probabilistic analysis (i.e., CSR is computed using a pseudo-probabilistic analysis given the site-specific information).
- $\left[q_{req}^{ref} \right]_{pseudo}$ is also computed using equations as outlined above by using *reference profile* information at the location of interest obtained from a pseudo-probabilistic analysis. If the reference profile previously introduced is being used, $\left(\frac{S_v}{S_v^r} \right) = 2.34$ and $r_d = 0.892$.

2. Obtain q_{req}^{ref} from liquefaction parameter maps.
3. Compute q_{req}^{site} as:

$$q_{req}^{site} = q_{req}^{ref} + \Delta q_{req} \quad (49)$$

Similar to the simplified Boulanger and Idriss (2014) procedure, we applied a calibration equation to correct a PGA bias. The corrected q_{req}^{site} is distinguished as $q_{req,calibrated}^{site}$ and is computed as follows:

$$q_{req,calibrated}^{site} = \left\{ \begin{array}{ll} PGA \leq 0.05g & MAX(q_{req}^{site} - 45, 0) \\ 0.05 > PGA < 0.2g & MAX\left(\left(\frac{q_{req}^{site} - 10.025}{0.879}\right), 0\right) \\ PGA > 0.2g & q_{req}^{site} \text{ (no correction needed)} \end{array} \right\} \quad (50)$$

3.3.3.3 Simplified FS_L

Once q_{req}^{site} or $q_{req,calibrated}^{site}$ is computed, FS_L can be obtained for the soil layer i , using the following relationship:

$$(FS_L)_i = \frac{(CRR)_i}{(CSR)_i} = \frac{CRR(q_{site})}{CRR(q_{req}^{site})} = \frac{(CRR(Q_{mcs}))_i}{(CRR(q_{req}^{site}))_i} \quad (51)$$

where q_{req}^{site} can be the calibrated $q_{req,calibrated}^{site}$ (if the correction is applied) and Q_{mcs} is the corrected cone tip resistance calculated using the Robertson and Wride (2009) procedure.

3.3.3.4 Simplified P_L

To solve for the uniform hazard probability of liquefaction, P_L , for the soil layer i , insert the simplified FS_L into the following equation (from Ku et al. (2012):

$$(P_L)_i = 1 - \Phi \left[\frac{0.102 + \ln((FS_L)_i)}{\sigma_\varepsilon} \right] \quad (52)$$

where Φ represents the standard normal cumulative distribution function and σ_ε is the standard deviation for model ($\sigma_\varepsilon = 0.276$) or total ($\sigma_\varepsilon = 0.3537$) uncertainty. The standard normal

cumulative distribution function can be evaluated using the built-in *Excel* function NORM.S.DIST().

3.3.3.5 Simplified Δq_L

After the Mayfield et al. (2010) procedure, Δq_L for soil sublayer i is computed as the difference between the soil's ability to resist liquefaction (Q_{mcs}) and the required resistance to resist liquefaction (q_{req}^{site} or $q_{req,calibrated}^{site}$). This is expressed as:

$$\Delta(q_L)_i = [q_{c1Ncs}]_i - [q_{req}^{site}]_i \quad (53)$$

3.3.3.6 Simplified CSR_{Ku}^{site}

To develop an equation to compute CSR , we re-arranged the probability of liquefaction equation, P_L (Equation (52)), and solved for CSR . Therefore, the simplified Ku et al. (2012) cyclic stress ratio, CSR_{Ku}^{site} , (Ku subscript added to distinguish from the Boulanger and Idriss CSR^{site}) is computed as:

$$CSR_{Ku}^{site} (\%) = \exp\left(0.102 + \ln\left(CRR(q_{req}^{site})\right)\right) * 100 \quad (54)$$

Recalling from the previous section, for values of $q_{req} > 165$, the Boulanger and Idriss (2014) relationship takes over. When computing CSR_{Ku}^{site} , the q_{req}^{site} that is to be used needs to be checked. For values of $q_{req}^{site} > 165$, the CSR_{Ku}^{site} procedure uses the CSR^{site} from the simplified Boulanger and Idriss (2014) method (i.e., Equation (31)). For $q_{req}^{site} < 165$, values, CSR_{Ku}^{site} can be computed following Equation (54) using the Robertson and Wride (2009) CRR equations.

3.4 Performance-Based Post-liquefaction Free-field Settlement Models

This section will provide a brief overview of the Ishihara and Yoshimine (1992) and Juang et al. (2013) post-liquefaction free-field settlement models and how the Juang et al. (2013) model fits into the performance-based settlement calculation.

3.4.1 Ishihara and Yoshimine (1992) Settlement Method

Ishihara and Yoshimine (1992) produced a deterministic procedure to calculate post-liquefaction ground settlement based on volumetric strains in liquefiable soils. This volumetric strain is a function of the factor of safety against liquefaction, FS_L . Ishihara and Yoshimine summarized the relationship between FS_L , γ_{max} , and D_R using the curves presented in Figure 3-4. In this Figure, volumetric strain is referred to as γ_{max} . For the rest of the report, volumetric strain will be denoted as ϵ_v , to be distinguished from the horizontal strain in the lateral spread section.

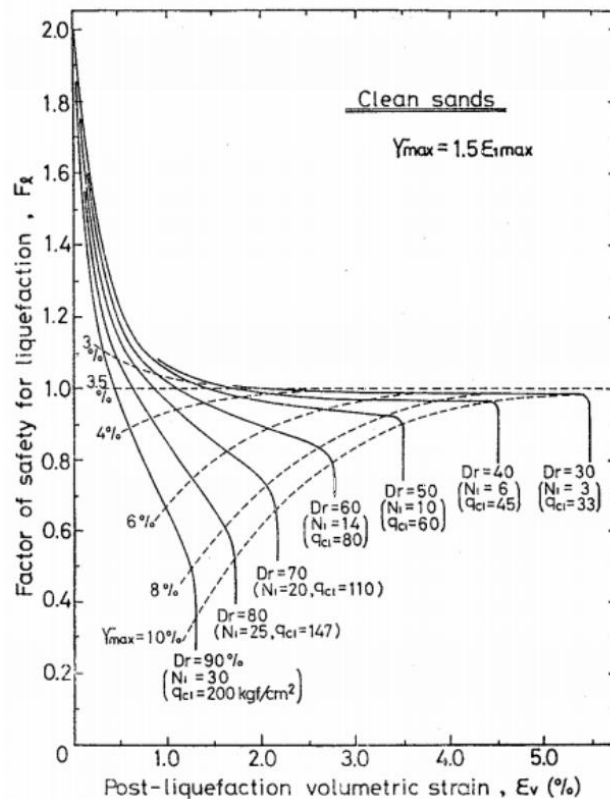


Figure 3-4. The relationship between FS_L , γ_{max} , and D_R (after Ishihara & Yoshimine, 1992).

The procedure for applying the Ishihara and Yoshimine (1992) method is given as follows: first, FS_L for each layer of the soil profile is calculated using a liquefaction triggering procedure (e.g., Robertson and Wride, 2009; Boulanger and Idriss, 2014). Second, a relative density is obtained for each layer using Tatsuoka et al. (1990):

$$D_R = -85 + 76 \log \frac{q_c}{\sqrt{\sigma'_v}} \quad (55)$$

where q_c is the cone tip resistance and σ'_v is the vertical effective stress. Third, volumetric strain, ε_v , is obtained using the FS_L , and D_R calculated previously for each layer from the Ishihara and Yoshimine strain curves (Figure 3-4). Fourth, the settlement of each layer is the product of each layer's strain and thickness. Finally, the predicted total ground surface settlement (S_p) is computed by summing each layer's settlement as:

$$S_p = \sum_{i=1}^N \varepsilon_v \Delta Z_i \quad (56)$$

where ε_v is volumetric strain for the i^{th} layer, N is number of layers, and ΔZ_i is the i^{th} layer's thickness.

3.4.2 Juang et al. (2013) Procedure

Juang et al. (2013) calculated post-liquefaction settlements by applying the Ishihara and Yoshimine (1992) method probabilistically for the CPT. The method adds probabilistic parameters to equation (56) to account for the probability of liquefaction triggering by using the following equation:

$$S_p = M \sum_{i=1}^N \varepsilon_v \Delta Z_i IND_i \quad (57)$$

where ε_v is volumetric strain for the i^{th} layer, N is number of layers, M represents a modal bias correction factor equal to 1.0451, IND_i represents the probability of liquefaction occurring, which is defined in equation (58), and ΔZ_i is the i^{th} layer's thickness.

The model bias correction factor M was calculated by Juang et al. (2013) by calibrating their model against settlement case histories from the field. Juang et al. (2013) present the IND_i as probability of liquefaction (P_L), which is calculated as:

$$IND_i = P_L = 1 - \Phi \left\{ \frac{0.102 + \ln(FS_L)}{\sigma_{\ln(S)}} \right\} \quad (58)$$

where Φ represents the standard normal cumulative distribution function, and $\sigma_{\ln(S)}$ represents the model uncertainty and is 0.276.

One significant disadvantage associated with the Juang et al. (2013) model is that the model was based on the binomial assumption that both liquefied and non-liquefied soils can cause liquefaction settlement. Hatch (2017) re-solved the maximum likelihood equation developed by Juang et al. (2013) to neglect the possibility of non-liquefied layers contributing to post-liquefaction settlement. The resulting values of M and $\sigma_{\ln(S)}$ are 1.014 and 0.3313, respectively. Any potential error introduced by this simplification is accounted for in the larger value of model uncertainty, $\sigma_{\ln(S)}$. These re-solved values are used in the computational tool *CPTLiquefY*.

For the Juang et al. (2013) procedure, ε_v is calculated by using a curve-fitted equation based on the Ishihara and Yoshimine (1992) curves (Figure 3-4), given as:

$$\varepsilon_v(\%) = \left\{ \begin{array}{ll} 0 & \text{for } FS \geq 2 \\ \min \left\{ \begin{array}{l} \frac{a_0 + a_1 \ln(q)}{(2 - FS) - [a_2 + a_3 \ln(q)]} \\ b_0 + b_1 \ln(q) + b_2 \ln(q)^2 \end{array} \right\} & \text{for } 2 - \frac{1}{a_2 + a_3 \ln(q)} < FS < 2 \\ b_0 + b_1 \ln(q) + b_2 \ln(q)^2 & \text{for } FS \leq 2 - \frac{1}{a_2 + a_3 \ln(q)} \end{array} \right\} \quad (59)$$

where $a_0 = 0.3773$, $a_1 = -0.0337$, $a_2 = 1.5672$, $a_3 = -0.1833$, $b_0 = 28.45$, $b_1 = -9.3372$, $b_2 = 0.7975$ and $q = q_{1Ncs}$.

3.5 Simplified Post-liquefaction Free-field Settlement Models

The performance-based method of calculating post-liquefaction settlement in Section 3.4 is an effective solution to mitigate the deficiencies introduced by the conventional (i.e. “pseudo-probabilistic”) method. However, the performance-based approach is complex and difficult to use. Performing a performance-based analysis may not be practical for professionals who need to routinely perform settlement calculations in a rapid and efficient manner.

An ideal solution to this dilemma is the introduction of a new procedure that combines the simplicity of traditional liquefaction hazard maps with the accuracy of a site-specific performance-based liquefaction hazard analysis. Section 3.3 of this report presents such a simplified procedure that has been developed for calculating liquefaction triggering.

In a manner similar to that developed for simplified liquefaction triggering, vertical strains for a reference profile, ε_v^{ref} , can be probabilistically computed across a grid of geographic locations. These results can be used to develop contours for the vertical strains that correspond to various return periods. These maps are called the volumetric strain reference parameter maps. ε_v^{ref} is a proxy for the seismic loading that impacts post-liquefaction settlement, and it needs to be adjusted for site-specific conditions. A detailed derivation for the correction equations, using both the Boulanger and Idriss (2014) and the Ku et al. (2012) probabilistic liquefaction triggering models will be given. For consistency, all vertical strains will be in percent in the simplified performance-based method.

3.5.1 Site-Specific Correction for Reference Strain using Boulanger and Idriss (2014)

Probabilistic Liquefaction Triggering Model

Because ε_v^{ref} was calculated using the reference soil profile, it must be corrected for site-specific soil conditions and depths before obtaining ε_v^{site} . A variety of relationships have been tested to relate ε_v^{ref} and ε_v^{site} . These relationships include:

$$\varepsilon_v^{site} = \varepsilon_v^{ref} - \Delta\varepsilon \quad (60)$$

$$\ln(\varepsilon_v^{site} + a)^b = \ln(\varepsilon_v^{ref} + a)^b + \Delta\varepsilon \quad (61)$$

$$\ln(\varepsilon_v^{site} + a)^b = \ln(\varepsilon_v^{ref} + a)^b \cdot \Delta\varepsilon \quad (62)$$

where a and b are constants ranging from 0.001 to 1000. A constant a was added to both ε_v^{site} and ε_v^{ref} to prevent a value of zero from occurring in the natural log operators.

After performing preliminary assessment, Equation (63) is found to best predict the volumetric strain calculated by the performance-based method.

$$\ln(\varepsilon_v^{site} + 1000) = \left(\ln(\varepsilon_v^{ref} + 1000) \right)^{\frac{1}{3}} \cdot \Delta\varepsilon \quad (63)$$

where $\Delta\varepsilon$ is a site-specific correction factor. Rearranging Equation (63), we can solve for the correction factor $\Delta\varepsilon$ as:

$$\Delta\varepsilon = \frac{\ln(\varepsilon_v^{site} + 1000)}{(\ln(\varepsilon_v^{ref} + 1000))^{1/3}} \quad (64)$$

ε_v^{site} in Equation (66) represents the probabilistic strain in the sublayer of interest and is unknown. To simplify the analysis, both ε_v^{ref} and ε_v^{site} can be approximated using the pseudo-probabilistic approach. This is an appropriate simplification because the same errors introduced by using the pseudo-probabilistic method should occur in both ε_v^{ref} and ε_v^{site} . These errors are minimized when performing the division in Equation (64). Thus, the equation for the correction factor may be approximated as:

$$\Delta\varepsilon \cong \frac{\ln(\varepsilon_{v,pseudo}^{site} + 1000)}{\left(\ln(\varepsilon_{v,pseudo}^{ref} + 1000) \right)^{\frac{1}{3}}} \quad (65)$$

where ε_v^{ref} and ε_v^{site} are volumetric strains calculated using pseudo-probabilistic method with FSL computed using the mean magnitude from the deaggregation of *PGA* at the return period of interest.

Once the correction factor for a given soil sublayer is computed, site-specific strains are computed as:

$$\varepsilon_v^{site} = \exp\left(\ln\left(\varepsilon_v^{ref} + 1000\right)^{\frac{1}{3}} \cdot \Delta\varepsilon\right) - 1000 \quad (66)$$

where ε_v^{ref} is the volumetric strain obtained from the reference volumetric strain parameter map. Preliminary assessments showed that different sets of correction equations are needed for sites with PGA lower than 0.2g and sites with PGA larger than or equal to 0.2g. A calibration equation was developed to correct this non-linear bias. The following equations are used to calculate the simplified site strain based on seismicity levels as:

For $PGA < 0.2g$

$$\varepsilon_{v,calibrated}^{site} (\%) = \left\{ \begin{array}{ll} 0 & \text{for } \varepsilon_v^{site} \leq 0 \\ 0.7 \cdot \varepsilon_v^{site} & \text{for } 0 < \varepsilon_v^{site} \leq 1.7 \\ (\varepsilon_v^{site} + 1.7)^{0.6} & \text{for } \varepsilon_v^{site} > 1.7 \end{array} \right\} \quad (67)$$

For $PGA \geq 0.2g$:

$$\varepsilon_{v,calibrated}^{site} (\%) = \left\{ \begin{array}{ll} 0 & \text{for } \varepsilon_v^{site} \leq 0 \\ 0.05 \cdot \varepsilon_v^{site} & \text{for } 0 < \varepsilon_v^{site} \leq 1.7 \\ 0.975 \cdot \sqrt{2.5 \cdot \left[\frac{(\varepsilon_v^{site})^3}{3.25} - 1.5 \right]} & \text{for } \varepsilon_v^{site} > 1.7 \end{array} \right\} \quad (68)$$

where ε_v^{site} is the site strain as calculated in Equation (66). Once $\varepsilon_{v,calibrated}^{site}$ has been computed, the following equation may be applied to obtain the simplified performance-based settlement for the entire profile.

$$S_p = M \sum_{i=1}^N \varepsilon_{v,calibrated}^{site} \Delta Z_i \quad (69)$$

where M represents the re-solved modal bias correction factor equal to 1.014, $\varepsilon_{v,calibrated}^{site}$ is the simplified site strain calculated from Equations (67) or (68), and ΔZ_i is the i^{th} layer's thickness.

3.5.2 Site-Specific Correction for Reference Strain using the Ku et al. (2012) model

The framework presented in Section 3.5.1 can also be applied to the Ku et al. (2012) model. A preliminary assessment was also performed to relate ε_v^{ref} and ε_v^{site} . Equation (70) was found to minimize the difference between the full-performance based method and the simplified method.

$$\ln(\varepsilon_{v,pseudo}^{site} + 100) = \left(\ln(\varepsilon_{v,pseudo}^{ref} + 100) \right)^{\frac{1}{3}} \cdot \Delta\varepsilon \quad (70)$$

As explained in Section 3.5.1, the correction factor, $\Delta\varepsilon$, can be approximated using pseudo-probabilistic estimates of ε_v^{ref} and ε_v^{site} . $\Delta\varepsilon$ for a given soil sublayer using the Ku et al. (2012) model can then be estimated as:

$$\Delta\varepsilon \cong \frac{\ln(\varepsilon_{v,pseudo}^{site} + 100)}{\left(\ln(\varepsilon_{v,pseudo}^{ref} + 100) \right)^{\frac{1}{3}}} \quad (71)$$

where ε_v^{ref} and ε_v^{site} are volumetric strains calculated using pseudo probabilistic method.

The site-specific strain for the soil sublayer can be computed as:

$$\varepsilon_v^{site} = \exp\left(\ln(\varepsilon_v^{ref} + 100)^{\frac{1}{3}} \cdot \Delta\varepsilon \right) - 100 \quad (72)$$

where ε_v^{ref} is the volumetric strain obtained from the reference volumetric strain parameter map.

Again, due to the non-linearity of the model, a calibration equation was developed to obtain the final site-specific strains for different seismicity levels as:

For $PGA < 0.2g$:

$$\varepsilon_{v,calibrated}^{site} (\%) = \left\{ \begin{array}{ll} 0 & \varepsilon_v^{site} \leq 0 \\ 0.8 \cdot \varepsilon_v^{site} & 0 < \varepsilon_v^{site} \leq 2 \\ \sqrt{\frac{\varepsilon_v^{site} - 0.86}{0.38}} & \varepsilon_v^{site} > 2 \end{array} \right\} \quad (73)$$

For $PGA \geq 0.2g$:

$$\varepsilon_{v,calibrated}^{site} (\%) = \left\{ \begin{array}{ll} 0 & \varepsilon_v^{site} \leq 0 \\ 0.322 \cdot \varepsilon_v^{site} & 0 < \varepsilon_v^{site} \leq 1.8 \\ 0.805 \cdot \sqrt{8 \cdot \left[\frac{(\varepsilon_v^{site})^2}{3} - 1 \right]} & \varepsilon_v^{site} > 1.8 \end{array} \right\} \quad (74)$$

$\varepsilon_{v,calibrated}^{site}$ can then be applied to Equation (69) to obtain the total settlement using the Ku et al. (2012) model for FS_L .

3.5.3 Summary

The simplified method for calculating site-specific settlement consists of the following steps:

1. Obtain a reference strain, ε_v^{ref} , from a liquefaction parameter map. These values are calculated using the full performance-based method.
2. Calculate the correction factor, $\Delta\varepsilon$, with $\varepsilon_{v,pseudo}^{site}$ and $\varepsilon_{v,pseudo}^{ref}$.
3. Compute site-specific strains, $\varepsilon_{v,calibrated}^{site}$.
4. Compute total settlement for the whole soil profile.

3.6 Empirical Lateral Spread Displacement Model

Empirical methods use large databases of earthquake case histories to create a predictive relationship. These relationships are developed using a statistical procedure known as a multilinear regression. They should be used only within the recommended range because extrapolation of an empirical model can lead to large amounts of error.

Empirical models for predicting lateral spread displacements are widely used because they are reliable, easy to understand, and easy to incorporate into engineering software. Multiple empirical predictive relationships have been created over the years; some common relationships recognized in industry today are Youd et al. (2002) and Zhang et al. (2004). The simplified performance-based method developed in this study will be using the Zhang et al. (2004) procedure, as it is the most common procedure for predicting lateral spread displacements using the CPT.

3.6.1 Zhang et al. (2004) Procedure

The predictive relationships for lateral spread displacements as laid out by Zhang et al. (2004) are the first that incorporate both SPT and CPT case histories, with 150 SPT results and 41 CPT results. With far fewer case histories for the CPT, caution must be taken to not extrapolate outside the bounds of the data. An estimate of lateral spread displacement can be made with a CPT sounding of tip resistance, sleeve friction and pore pressure with depth.

The following are the steps for the Zhang et al. (2004) procedure. To begin the calculation, an estimate of D_R must be made for every soil layer as shown, using Tatsuoka et al. (1990):

$$D_R = -85 + 76 \log(q_{c1N}) \quad (75)$$

where q_{c1N} is the corrected cone tip resistance. In the Robertson and Wride (1998) liquefaction triggering procedure, this value is referred to as Q_m , while in the Boulanger and Idriss (2016) liquefaction triggering procedure this value is simply q_{c1N} .

The maximum cyclic shear strain (γ_{\max}) can then be determined using the known value of D_R and the FS_L from the liquefaction triggering procedure. Figure 3-5 represents the relationship

between maximum cyclic shear strain and factor of safety for different relative densities. These curves are based on data from Ishihara and Yoshimine (1992) and Seed (1979).

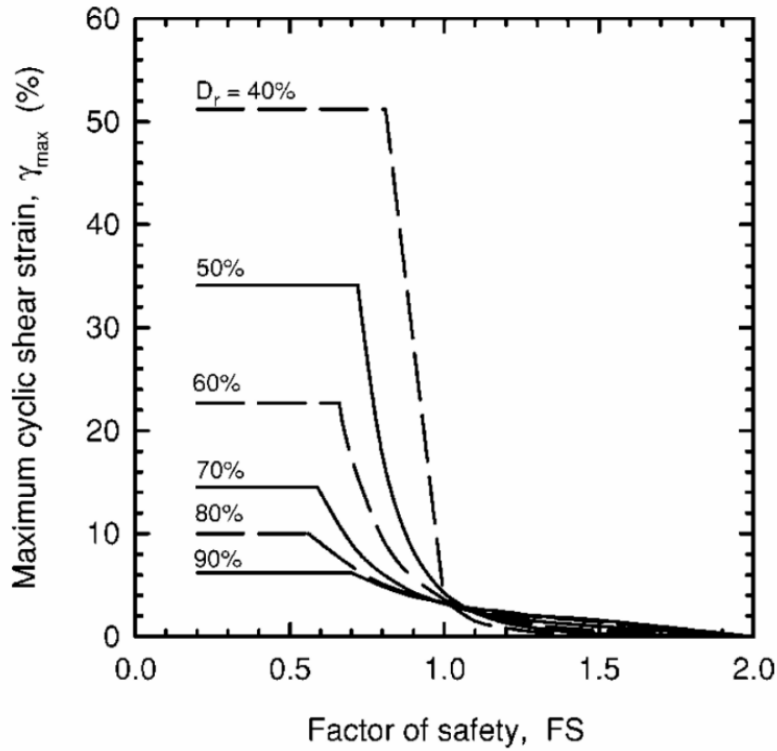


Figure 3-5. The relationship between maximum cyclic shear strain and factor of safety for different relative densities (after Zhang et al. (2004)).

With values of γ_{max} known for each soil layer, the lateral displacement index (LDI) can be calculated by integrating γ_{max} with depth, as presented in Equation (76):

$$LDI = \int_0^{Z_{max}} \gamma_{max} dz \quad (76)$$

where Z_{max} is the maximum depth below all the potential liquefiable layers with an FS_L less than 2.0.

The actual value of the lateral displacement (LD) is a function of LDI and the site geometry. There are three types of site geometries considered: (1) gently sloping ground, (2) level

ground near a free face, and (3) gently sloping ground near a free face. For sites with gently sloping ground, LD is calculated using Equation (77).

$$LD = (S + 0.2) \cdot LDI \quad \text{for } 0.2\% < S < 3.5\% \quad (77)$$

where S is the ground slope measured in percent.

For sites with level ground near a free face, LD is calculated using Equation (78).

$$LD = 6 \cdot \left(\frac{L}{H} \right)^{-0.8} \cdot LDI \quad \text{for } 4 < \frac{L}{H} < 40 \quad (78)$$

where L is the distance to the free face and H is the height of the free face. The same units must be used for L and H . For sites with gently sloping ground near a free face, Equation (78) is also used because the data points for gently sloping ground with a free face lie generally within the scatter of the results for nearly level ground with a free face (Zhang et al, 2004).

3.7 Simplified Performance-based Lateral Spread Model

Similar to the simplified post-liquefaction settlement method, a generic reference site is used to compute lateral spread. A series of performance-based lateral spread analyses are performed across a grid to develop contour maps of horizontal strains corresponding to return periods of interest. These maps are called reference horizontal strain maps.

The simplified performance-based post-liquefaction lateral spread procedure builds upon the recently developed simplified performance-based liquefaction triggering models, the Boulanger and Idriss (2014) probabilistic liquefaction triggering model and the Ku et al. (2012) model. The procedure requires FS_L calculated from one of these two triggering models. A detailed derivation of the correction equations using both of these triggering models will be given. For consistency, all horizontal strains will be in percent in the simplified performance-based method.

3.7.1 Site-Specific Correction for Reference Strain using Boulanger and Idriss (2014) Probabilistic Liquefaction Triggering Model

The framework in Section 3.5 may also be applied to develop the simplified lateral spread method. A preliminary assessment was performed to find the best-fit relationship between γ_{\max}^{ref} and γ_{\max}^{site} . Some of the tested relationships include:

$$\gamma_{\max}^{site} = \gamma_{\max}^{ref} \cdot \Delta\gamma \quad (79)$$

$$\ln(\gamma_{\max}^{site} + a)^b = \ln(\gamma_{\max}^{ref} + a)^b + \Delta\gamma \quad (80)$$

$$\ln(\gamma_{\max}^{site} + a)^b = \ln(\gamma_{\max}^{ref} + a)^b \cdot \Delta\gamma \quad (81)$$

where a and b are constants ranging from 0.001 to 1000. A constant a was added to both between γ_{\max}^{ref} and γ_{\max}^{site} to prevent a value of zero from occurring in the natural log operators.

For the Boulanger and Idriss (2014) triggering model, the correction factor is calculated as:

$$\Delta\gamma_{\max} \cong \frac{\ln(\gamma_{\max, pseudo}^{site} + 10000)}{(\ln(\gamma_{\max, pseudo}^{ref} + 10000))^{\frac{1}{3}}} \quad (82)$$

where γ_{\max}^{ref} and γ_{\max}^{site} are horizontal strains calculated using pseudo probabilistic method. By rearranging Equation (82), the simplified horizontal strain may be estimated as:

$$\gamma_{\max}^{site} = \exp\left(\ln(\gamma_{\max, pseudo}^{ref} + 10000)^{\frac{1}{3}} \cdot \Delta\gamma\right) - 10000 \quad (83)$$

For the simplified method, both γ_{\max}^{ref} and γ_{\max}^{site} are computed using a semi-probabilistic method. The semi-probabilistic method is applied as follows: first, obtain D_R for the reference profile using the q_{c1N} value from the liquefaction triggering section. Second, with D_R and FS_L calculated from the simplified triggering models, γ_{\max} is found using Figure 3-5. This is called the

semi-probabilistic method because FS_L is obtained using the simplified performance-based method and then applied to Figure 3-5 in a deterministic manner in the semi-probabilistic method.

As with the triggering and settlement procedures, a correction based on different seismicity levels is needed:

For $PGA < 0.2g$

$$\gamma_{\max,calibrated}^{site}(\%) = \begin{cases} 0.2 * \gamma_{\max}^{site} & \text{for } \gamma_{\max}^{site} < 10 \\ 1.19 * \gamma_{\max}^{site} & \text{for } \gamma_{\max}^{site} \geq 10 \end{cases} \quad (84)$$

For $PGA \geq 0.2g$

$$\gamma_{\max,calibrated}^{site}(\%) = \begin{cases} 0.1 * \gamma_{\max}^{site} & \text{for } \gamma_{\max}^{site} < 10 \\ 0.9 * \gamma_{\max}^{site} & \text{for } \gamma_{\max}^{site} \geq 10 \end{cases} \quad (85)$$

where γ_{\max}^{site} is the calculated site horizontal strain and $\gamma_{\max,calibrated}^{site}$ is between 0% and 51.2%. Once $\gamma_{\max,calibrated}^{site}$ has been computed, the simplified performance-based lateral displacement may be calculated for the entire profile. Sometimes γ_{\max}^{site} may result in values that are negative or larger than 51.2%. The following conditions are applied to obtain the final simplified performance-based horizontal strains:

$$\gamma_{\max,simp}^{site}(\%) = \begin{cases} 0 & \text{for } \gamma_{\max}^{site} \leq 0 \\ \gamma_{\max}^{site} & \text{for } 0 < \gamma_{\max}^{site} < 51.2 \\ 51.2 & \text{for } \gamma_{\max}^{site} \geq 51.2 \end{cases} \quad (86)$$

Once $\gamma_{\max,simp}^{ref}$ has been computed, Equations (76) thru (78) from Section 3.6.1 may be applied to obtain the overall lateral displacement for the entire soil profile.

3.7.2 Site-Specific Correction for Reference Strain using the Ku et al. (2012) model

The procedure presented in Section 3.7.1 can also be applied to the Ku et al. (2012) triggering model. For different seismicity levels, these equations can be used to define the horizontal correction factor, $\Delta\gamma$.

For $PGA < 0.2g$,

$$\Delta\gamma_{\max} \cong \frac{\ln(\gamma_{\max,pseudo}^{site} + 1000)}{\left(\ln(\gamma_{\max,pseudo}^{ref} + 1000)\right)^{\frac{1}{3}}} \quad (87)$$

For $PGA \geq 0.2g$,

$$\Delta\gamma_{\max} \cong \frac{\ln(\gamma_{\max,pseudo}^{site} + 0.1)}{\left(\ln(\gamma_{\max,pseudo}^{ref} + 0.1)\right)^{\frac{1}{3}}} \quad (88)$$

For the Ku et al. (2012) triggering model, Q_m is used to obtain D_R as shown in Equation (75). Then FS_L needs to be obtained from the simplified triggering model. With D_R , FS_L and Figure 3-5, the approximated horizontal strains are computed as:

For $PGA < 0.2g$,

$$\gamma_{\max}^{site} = \exp\left(\ln(\gamma_{\max,pseudo}^{ref} + 1000)^{\frac{1}{3}} \cdot \Delta\gamma\right) - 1000 \quad (89)$$

For $PGA \geq 0.2g$,

$$\gamma_{\max}^{site} = \exp\left(\ln(\gamma_{\max,pseudo}^{ref} + 0.1)^{\frac{1}{3}} \cdot \Delta\gamma\right) - 0.1 \quad (90)$$

Finally, the final calibrated simplified performance-based horizontal strain is computed as:

$$\gamma_{\max,calibrated}^{site} (\%) = \left\{ \begin{array}{ll} \frac{\gamma_{\max}^{site}}{1.4} & \text{for } PGA < 0.2g \\ \gamma_{\max}^{site} & \text{for } PGA \geq 0.2g \end{array} \right\} \quad (91)$$

where γ_{\max}^{site} is the site horizontal strain, and $\gamma_{\max,calibrated}^{site}$ is between 0% and 51.2%. Once $\gamma_{\max,calibrated}^{site}$ has been computed, the simplified performance-based settlement may be calculated for the entire profile.

Conditions are also applied to obtain the final simplified performance-based horizontal strains:

$$\gamma_{\max, \text{simp}}^{\text{site}} (\%) = \begin{cases} \gamma_{\max}^{\text{site}} & \text{for } \gamma_{\max}^{\text{site}} < 51.2 \\ 51.2 & \text{for } \gamma_{\max}^{\text{site}} \geq 51.2 \end{cases} \quad (92)$$

$\gamma_{\max, \text{simp}}^{\text{ref}}$ can then be applied to Equations (76) thru (78) to obtain the overall lateral spread for the site-specific soil profile.

3.7.3 Simplified Strain Summary

The simplified method for calculating site-specific lateral spread consists of the following steps:

1. Obtain a reference horizontal strain, $\gamma_{\max}^{\text{ref}}$, from a liquefaction parameter map.
These values are calculated using the full performance-based method.
2. Calculate the correction factor, $\Delta\gamma$, with $\gamma_{\max, c \text{pseudo}}^{\text{ref}}$ and $\gamma_{\max, a \text{pseudo}}^{\text{site}}$.
3. Compute site-specific strains, $\gamma_{\max, \text{simp}}^{\text{ref}}$.
4. Compute total lateral spread for the whole soil profile.

4.0 DEVELOPMENT OF LIQUEFACTION PARAMETER MAPS

The purpose of this Section is to detail the steps to develop the reference parameter maps. These maps provide values for a reference soil profile at a set of grid points for a return period of interest.

4.1 Reference Profile

Liquefaction parameter maps are an important part of the simplified procedure because they provide the same benefits of a site-specific, full performance-based analysis, but do not require the user to perform the associated probabilistic calculations. The maps are based on a reference soil profile that is presented in Figure 4-1. This soil profile was used for the simplified procedure and is similar to the one originally introduced by Mayfield et al. (2010). The goal of the liquefaction parameter maps is to allow users to interpolate reference values for use in the simplified performance-based procedures developed through this research. For the simplified liquefaction triggering procedures using Boulanger and Idriss (2014) and Ku et al (2012), respective reference values for q_{req} and CSR are mapped in this study. For the simplified settlement and lateral spread procedures using Juang et al. (2013) and Zhang et al. (2004), respectively, respective reference values of ε_v (%) and γ_{max} (%) are mapped in this study. These computed reference parameter values are distinguished using the terms q_{req}^{ref} , CSR^{ref} , ε_v^{ref} (%), and γ_{max}^{ref} (%).

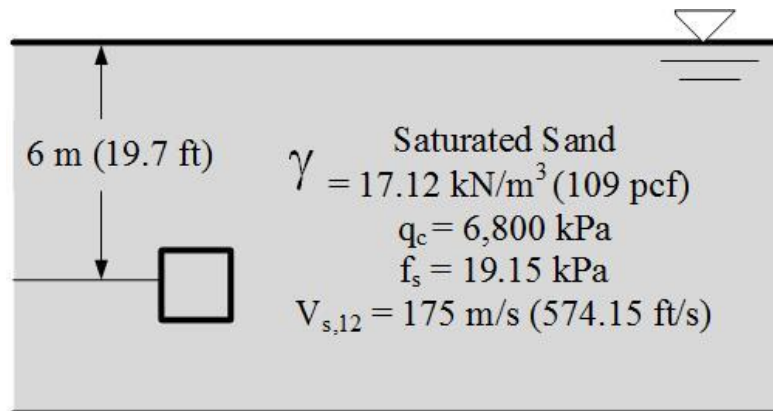


Figure 4-1. Reference Soil Profile

4.2 Development of Reference Parameter Maps

The reference parameter maps are created following these steps:

1. Perform a grid spacing study
2. Create a list of grid points
3. Run a full performance-based analysis on grid points using *CPTLiquefY*
4. Create contours based on interpolated values

Steps 2 and 4 are accomplished using software developed by ESRI, ArcMap. The following Sections will describe each step. The liquefaction reference parameter maps from this current study are provided in the Appendix of this final report.

4.3 Grid Spacing Study

The distance between grid points is important in determining the accuracy of the parameter maps. From the grid points, contours are developed by interpolating the values between grid points. If the grid points are too far apart, the maps may not be able to capture potential seismic gradients over areas with complex seismic sources. If the grid points are too close, the maps become computationally expensive to develop. Therefore, a study to optimize the grid spacing to an acceptable maximum interpolative error through correlation with mapped probabilistic seismic hazard (i.e., ground motions) is warranted.

Based on previous research involving simplified procedures for the SPT (Ulmer, 2015; Ekstrom, 2015; Error, 2017), researchers observed that areas of high mapped *PGA* hazard would require smaller grid spacing, and areas of low mapped *PGA* hazard would allow larger grid spacing. We also evaluated if this observation was true for the CPT. The USGS 2014 *PGA* hazard map (Figure 4-2) is chosen for this study. The map divides the United States into areas of different *PGA* ranges that are represented by different color bins. Thirty-six cities representing different *PGA* ranges are chosen from various locations across the United States as part of the study and are presented in Figure 4-3 with their corresponding *PGA* values corresponding to a return period of 2475 years. The goal of the grid spacing study is to find an optimal grid spacing for each *PGA* color bin on the map.

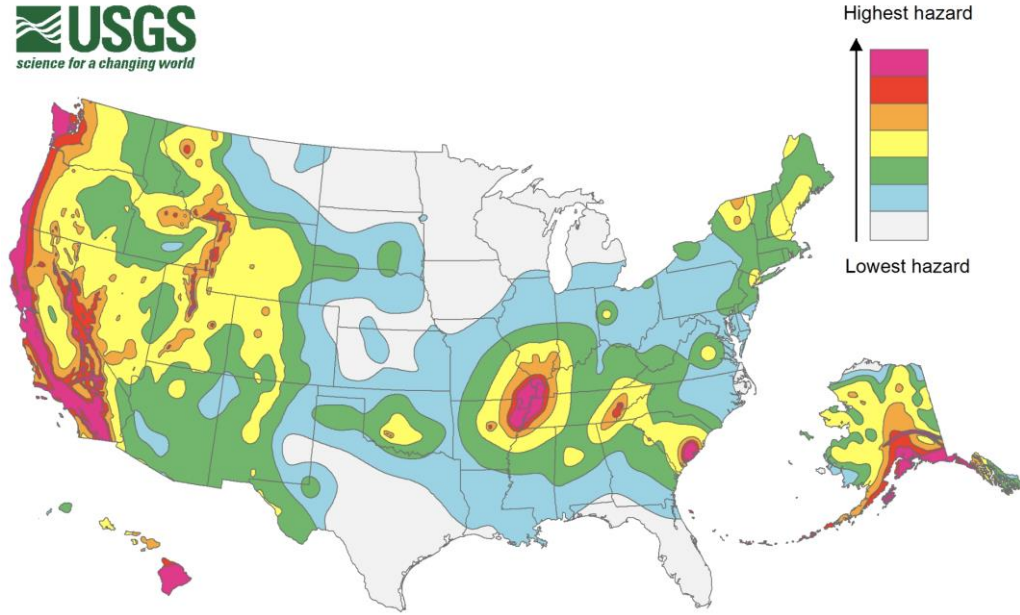


Figure 4-2. PGA Hazard Map ($T_R=2475$ years) after USGS 2014

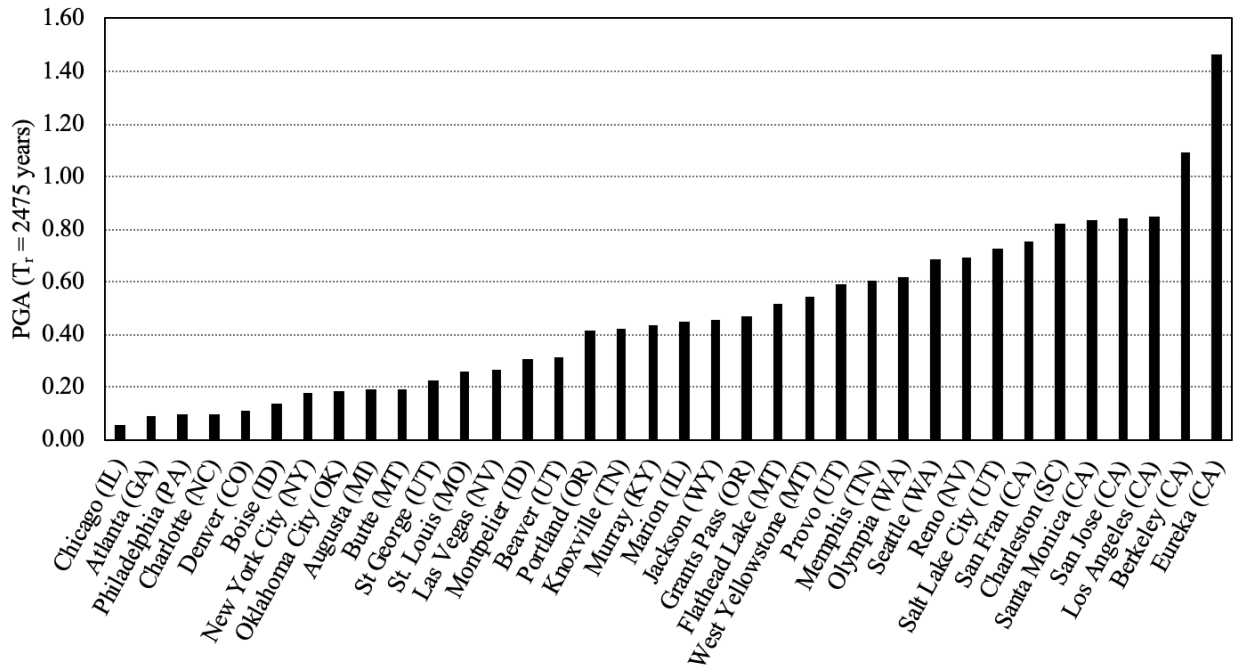


Figure 4-3. Range of PGA Values for Cities Included in Grid Spacing Study

Following the framework and methodology described by Ulmer (2015), the grid spacing study is performed using square grids with the site of interest as the anchor (or center) point in the center, as shown in Figure 4-4. To determine the maximum grid spacing, corner points are created with spacings of 1, 2, 4, 8, 16, 25, and 50 km.

Full performance-based analyses are performed at the center point and four corner points using *CPTLiquefY*. The average of the four corner points are then compared to the center point. An error is then calculated as the absolute difference between the interpolated and the anchor value. For this study, the optimum grid spacing is defined as the smallest grid spacing that yields a selected maximum percent error. The maximum percent error is selected as 5% (for *CSR%* and q_{req}) and 0.1% (for e_v and γ_{max}) based on engineering judgment.

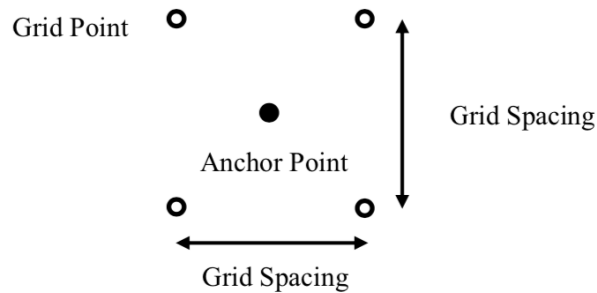


Figure 4-4. Layout of Grid Points Centered on a City’s Anchor Point (Ulmer, 2015)

The resulting correlations between optimum grid spacing and *PGA* for all the evaluated cities are shown for the Boulanger and Idriss (2014) and Ku et al. (2012) triggering models in Figure 4-5 through Figure 4-8. The vertical dashed lines indicate different *PGA* ranges (or color bins) from the USGS 2014 *PGA* hazard map. The horizontal blue lines are chosen to define the apparent lower bound of the grid spacing for each range. Table 4-1a, b, and c summarize the optimum grid spacing of each *PGA* range for *CSR%*, q_{req} , e_v , and γ_{max} , respectively.

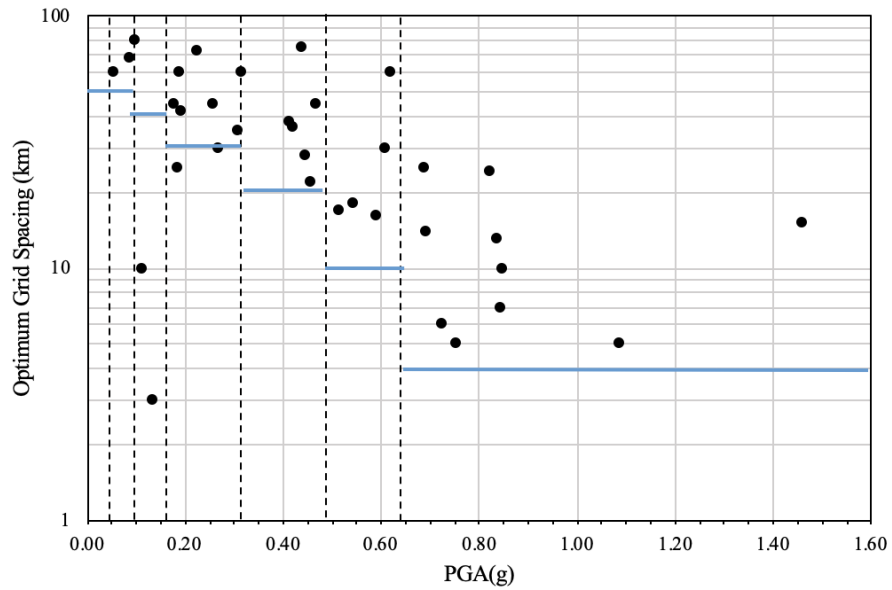


Figure 4-5. Correlation between *PGA* and Optimum Grid Spacing for CSR% [Boulanger and Idriss (2014)]

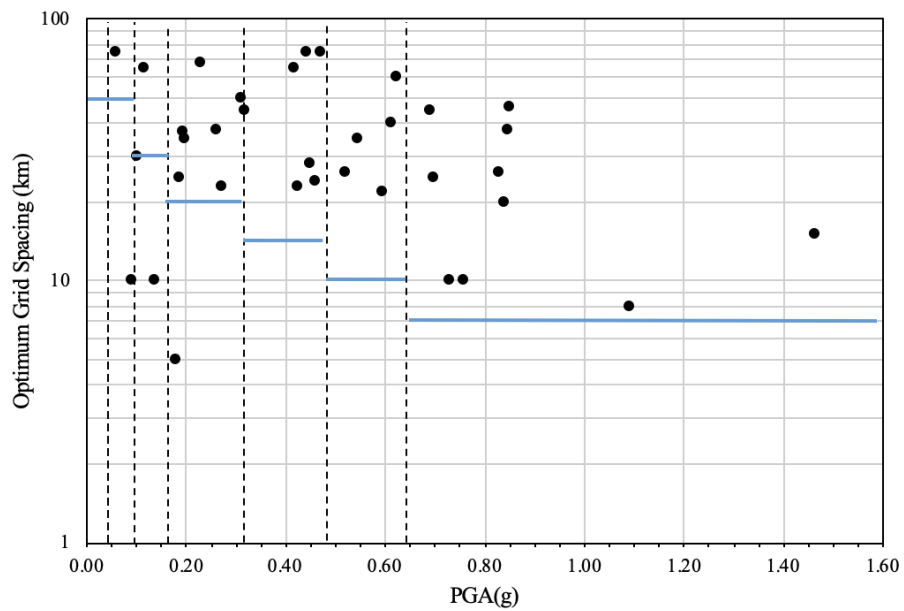


Figure 4-6. Correlation between *PGA* and Optimum Grid Spacing for q_{req} [Ku et al. (2012)]

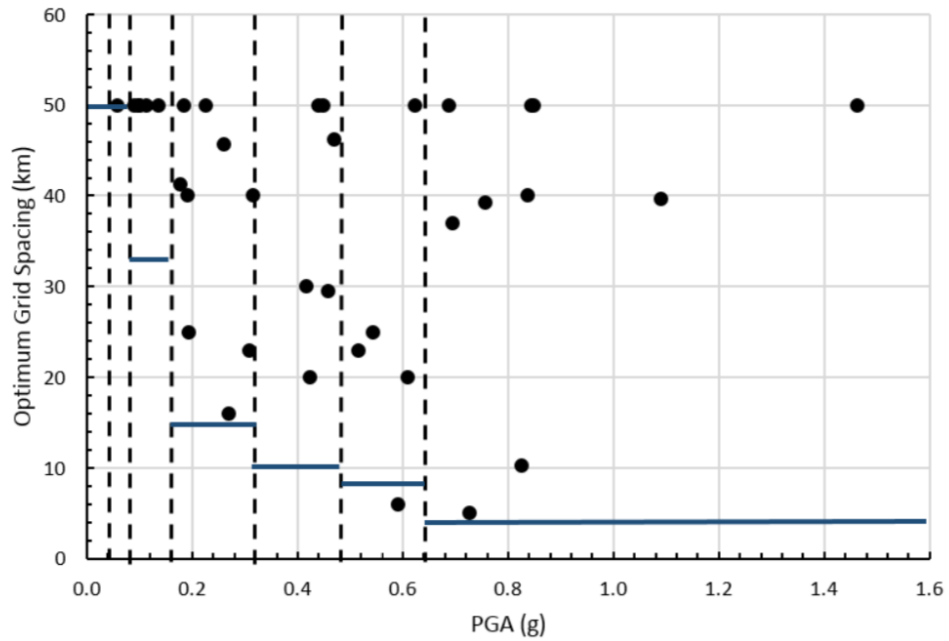


Figure 4-7. Correlation between PGA and Optimum Grid Spacing for ϵ_v and γ_{max} [Boulanger and Idriss (2014)]

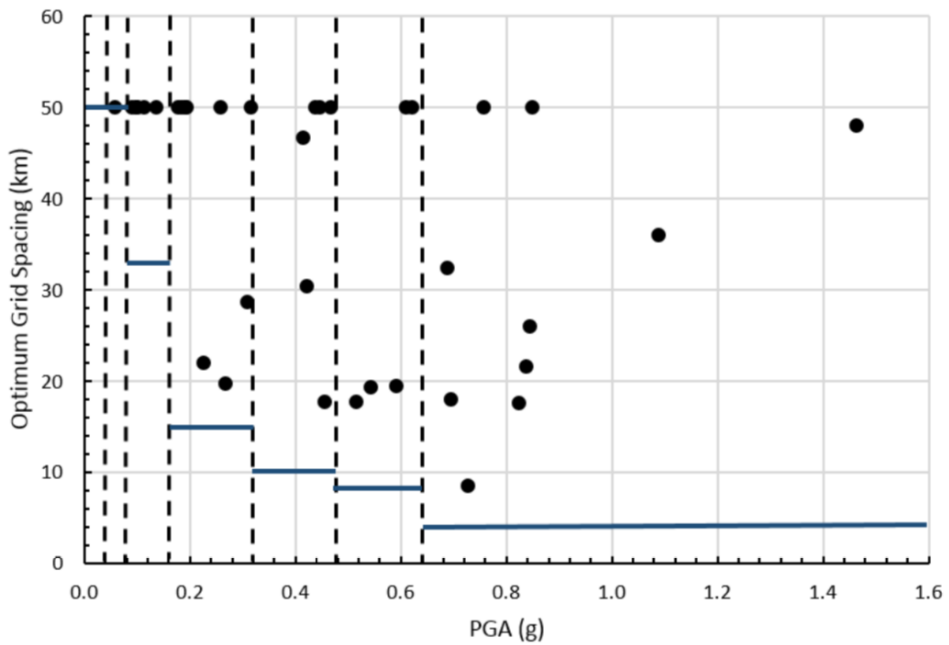


Figure 4-8. Correlation between PGA and Optimum Grid Spacing for ϵ_v and γ_{max} [Ku et al. (2012)]

Table 4-1. Proposed Optimum Grid Spacings within a *PGA* Range for a) *CSR%*, b) q_{req} , and c) ε_v and γ_{max}

a) <i>CSR%</i>				b) q_{req}			
PGA	Color	Spacing (km)	Spacing (mi)	PGA	Color	Spacing (km)	Spacing (mi)
0-0.04	Gray	50	31.1	0-0.04	Gray	50	31.1
0.04-0.08	Blue	50	31.1	0.04-0.08	Blue	50	31.1
0.06-0.16	Green	40	24.9	0.06-0.16	Green	30	18.6
0.16-0.32	Yellow	30	18.6	0.16-0.32	Yellow	20	12.4
0.32-0.48	Orange	20	12.4	0.32-0.48	Orange	15	9.3
0.48-0.64	Red	10	6.2	0.48-0.64	Red	10	6.2
0.64+	Pink	4	2.5	0.64+	Pink	8	5.0

c) ε_v and γ_{max}			
PGA	Color	Spacing (km)	Spacing (mi)
0-0.04	Gray	50	31.1
0.04-0.08	Blue	50	31.1
0.06-0.16	Green	33	20.5
0.16-0.32	Yellow	15	9.3
0.32-0.48	Orange	10	6.2
0.48-0.64	Red	8	5
0.64+	Pink	4	2.5

4.4 Create a List of Grid Points

In ArcMap, polygons are created to represent each *PGA* range or color bin presented in Figure 4-2. Within each polygon, the *Fishnet* tool is used to create the grid points based on the determined grid spacing. The latitude and longitude of each of these grid points are combined into one text file to be analyzed. Figure 4-9 shows an example of Oregon with optimally spaced grid points and the corresponding USGS *PGA* color zones.

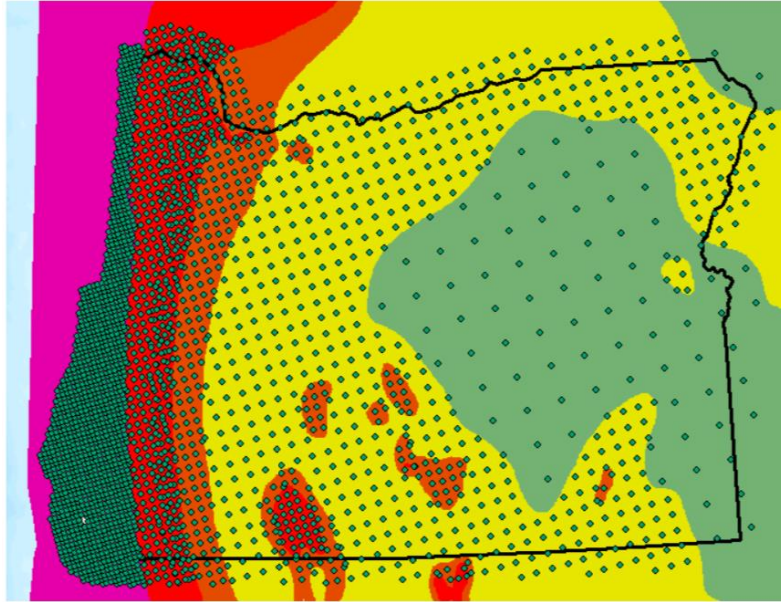


Figure 4-9. Location of Grid Points for Oregon with *PGA* Color Zones in Background

4.5 Perform Full Performance-Based Analysis at the Grid Points

Using *CPTLiquefY* (Franke et al., 2017), full performance-based liquefaction hazard analysis calculations are performed at each of the mapped grid points using the reference soil profile presented in Figure 4-1. These analyses are performed at return periods of 475, 1039, and 2475 years for both the Boulanger and Idriss (2014) and Ku et al. (2012) triggering models. Resulting liquefaction hazard curves computed at the grid points are then compiled and formatted in preparation for map creation.

4.6 Create Contours Based on Interpolated Values

Before creating the contours, the values from Section 4.5 must be interpolated. Using the *Kriging* tool in ArcMap, values between the grid points are interpolated to generate a raster that can be used to create contours. An example of a raster for Oregon is shown in Figure 4-10 where varying shades of grey represent higher or lower values. Darker shades represent lower relative reference parameter values.

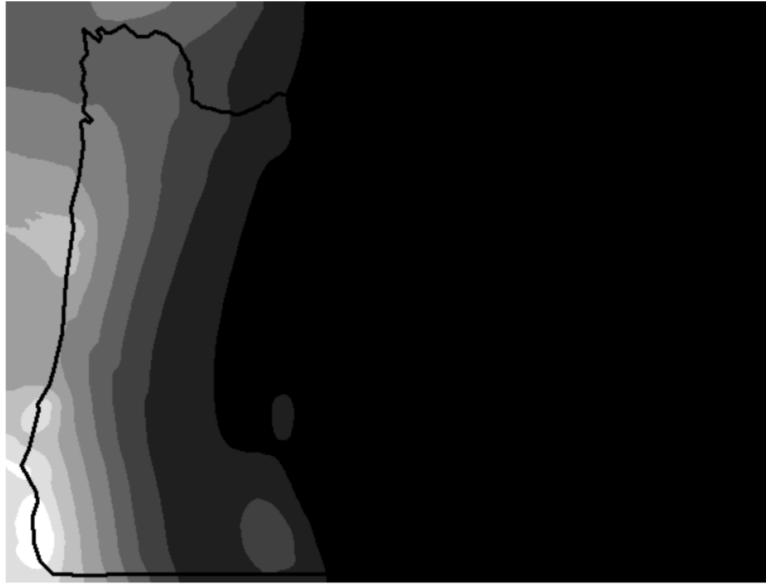


Figure 4-10. Sample Kriging Raster for Oregon

Once the raster is created, the *Contour* tool is used to create contour lines at any specified interval. For higher seismicity areas, smaller contour intervals are used to show the detailed changes, while lower seismicity areas used larger contour intervals. Figure 4-11 shows an example contour map for Oregon.

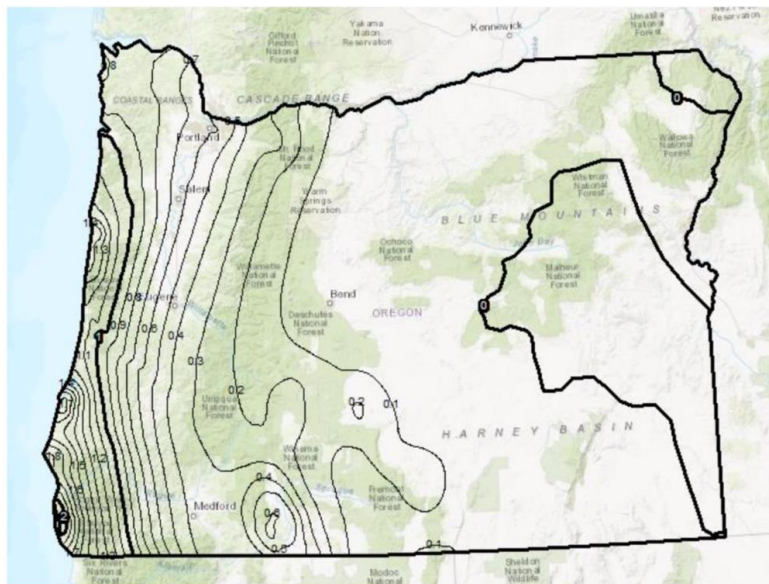


Figure 4-11. Example contour map of Oregon

4.7 Summary

This section outlined the steps to develop the reference parameter maps for Utah, South Carolina, Oregon, and Connecticut for the return periods of 475, 1039, and 2475 years. These maps are a crucial part of the simplified liquefaction hazard analysis procedure for the CPT because they provide a user-friendly process to quantify seismic loading at a targeted return period and they allow for the close approximation of values computed using the sophisticated full performance-based liquefaction hazard analysis.

5.0 VALIDATION OF THE SIMPLIFIED MODELS

5.1 Overview

The effectiveness of the simplified performance-based procedure introduced in this report depends on how closely they approximate the results of a complete site-specific probabilistic seismic hazard analysis. To evaluate the accuracy of the derived simplified procedure, we conducted a validation study that compared the results of the simplified method to the full performance-based method. We performed the validation study at 17 sites throughout the United States of varying soil profiles and seismicity for the 475, 1033, and 2475 return periods. The following sections will show the plotted results with the full performance-based results plotted on the x-axis and the simplified procedure results plotted on the y-axis. The analysis of the validation results is based on two main criteria: the slopes of the trend line and the R^2 values. The data with a trend line slope closer to 1.0 is considered to better approximate the full-performance based procedure on average, and the data with the larger R^2 value is more consistent in its predictions.

5.1.1 Sites used in the Analysis

For this study, we chose selected sites based on their seismicity and distribution across the United States. Table 5-1 lists the location of these sites as well as their latitudes, longitudes, and *PGA* (at the return period of 2475 years). These *PGA* values were retrieved from the 2014 USGS interactive deaggregation tool. To represent a variety of soil types and stiffnesses, this validation study used 20 CPT soundings obtained from the USGS CPT data database. The corrected cone tip resistance (q_{c1Ncs}) with depth for each CPT sounding is plotted in Figure 5-1. For all analyses, the ground water table was assumed at the ground surface.

Table 5-1. Locations of cities used in validation with corresponding *PGA*(g) values

Site	Latitude	Longitude	PGA (g)
Charleston, SC	32.726	79.931	0.73
Eureka, CA	40.802	-124.162	1.462
Memphis, TN	35.149	-90.048	0.609
Portland, OR	45.523	-122.675	0.415
Salt Lake City, UT	40.755	-111.898	0.726
San Francisco, CA	37.775	-122.418	0.757
San Jose, CA	37.339	-121.893	0.845
Santa Monica, CA	34.015	-118.492	0.838
Seattle, WA	47.53	-122.3	0.689
Louisville, KY	38.367	-83.828	0.099
Battleground, AL	34.316	-87.051	0.135
Leland, IL	41.577	-88.791	0.076
Quality, KY	37.115	-86.861	0.153
Boeli Landing, AZ	35.995	-114.569	0.179
Grand View, ID	42.695	-116.171	0.112
Spokane, WA	47.768	-117.652	0.136
Butte, MT	46.003	-112.533	0.193

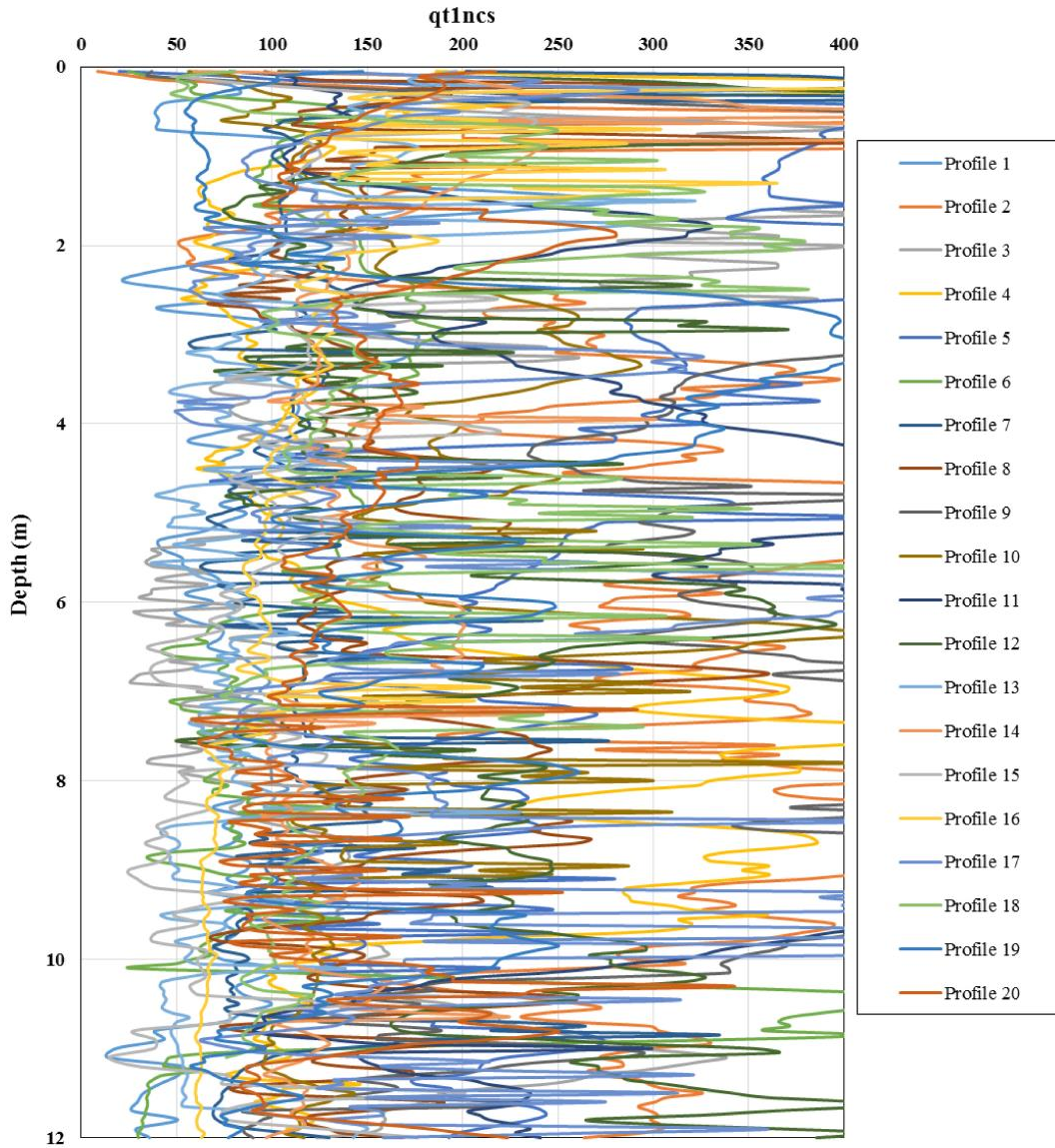


Figure 5-1. Site-specific soil profile used to validate the simplified performance-based model.

5.2 Simplified Boulanger and Idriss (2014) Liquefaction Triggering Model Validation

Figure 5-2 (a) through (e) show the validation scatter plot results of the simplified performance-based procedure using the Boulanger and Idriss (2014) triggering model for parameters (a) $CSR^{site}(\%)$, (b) FS_L , (c) P_L , (d) Δq_t , and (e) q_{req} . From a visual standpoint, the results

of the simplified procedure fall on or near the 1:1 line, meaning the simplified procedure closely approximates the full performance-based results.

In addition, all the triggering parameters have R^2 values higher than 0.980 and trendlines with slopes between 0.9931 and 1.0139, indicating the simplified procedure is consistent in estimating the full performance-based procedure.

These results demonstrate that the Boulanger and Idriss (2014) simplified performance-based procedure is able to closely approximate full performance-based results.

5.3 Simplified Ku et al. (2012) Liquefaction Triggering Model Validation

Figure 5-3 (a) through (e) show the validation scatter plots of the simplified performance-based procedure using the Ku et al. (2012) triggering model for parameters (a) q_{req} , (b) FS_L , (c) P_L , (d) Δq_L , and (e) $CSR^{site}(\%)$. All of the triggering parameters have R^2 values higher than 0.984, meaning the simplified Ku et al. (2012) procedure consistently approximates the full performance-based procedure. The slope of the trendlines range between 0.943 and 1.009, indicating that the simplified method accurately estimates the full performance-based method. These results suggest that the Ku et al. (2012) simplified performance-based procedure is able to closely approximate full performance-based results.

When compared to the Boulanger and Idriss (2014) simplified method, the Ku et al. (2012) method appears to have more spread in the data, especially for P_L and Δq_L . We observed that some of this scatter occurred for areas of very low PGA (less than 0.2g). Despite this observation, the Ku et al. (2012) method still closely approximates the full performance-based method.

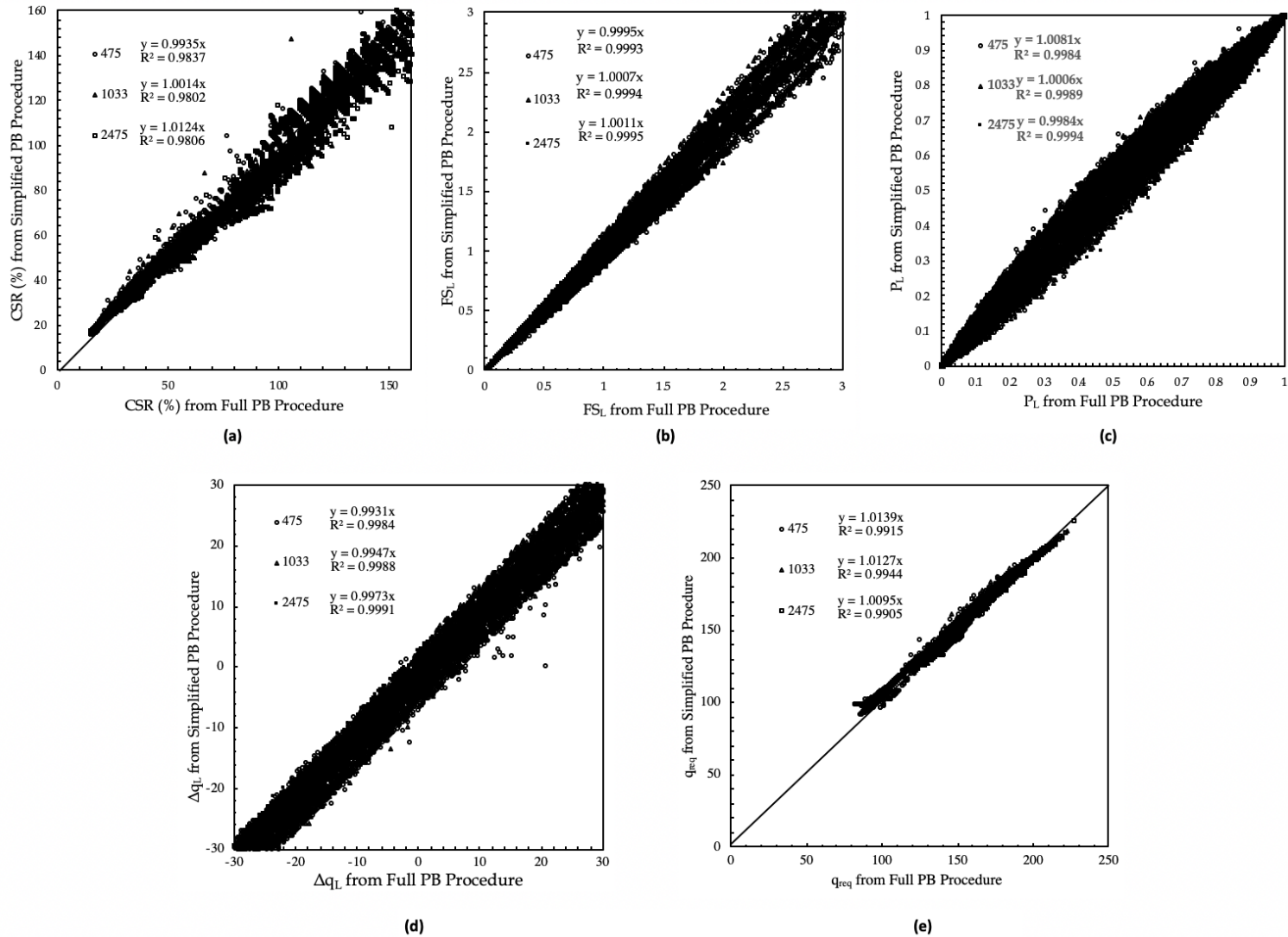


Figure 5-2. Comparative Scatter Plots for Simplified and Full Performance-Based Procedures for (a) CSR^{site}(%), (b) FS_L, (c) P_L, and (d) Δq_L, (e) q_{req} for the Boulanger and Idriss(2014) model using the 2012 MSF.

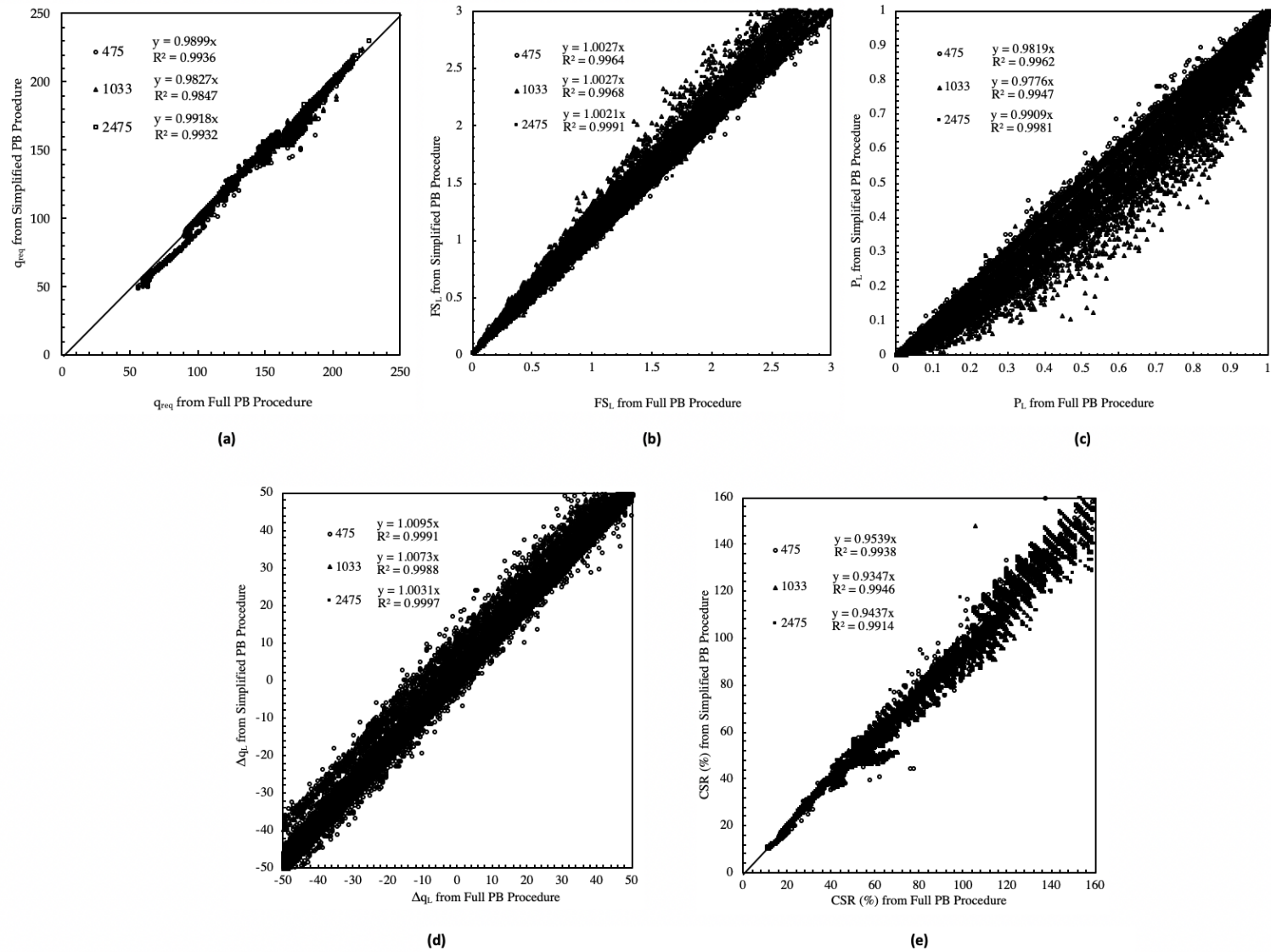


Figure 5-3. Comparative Scatter Plots for Simplified and Full Performance-Based Procedures for (a) q_{req} , (b) FS_L , (c) P_L , (d) Δq_L , and (e) $CSR^{site}(\%)$ for the Ku et al. (2012) model.

5.4 Simplified Post-liquefaction Free-field Settlement Model Validation

Figure 5-4 and Figure 5-5 show the validations of the simplified performance-based procedure using the Boulanger and Idriss (2014) triggering model for cities with *PGA* lower and greater than 0.2g.

Overall, the simplified performance-based procedure is able to closely estimate the settlements calculated using the full performance-based procedure, but involves more scatter for cities with lower *PGA*. As shown in Figure 5-4, the trend lines have slopes between 0.9292 and 1.19 and R^2 values higher than 0.891. In Figure 5-5, the trend lines have slopes between 0.9755 and 1.0162 and R^2 higher than 0.9873. The high R^2 values indicates a strong relationship between the simplified and full performance-based results.

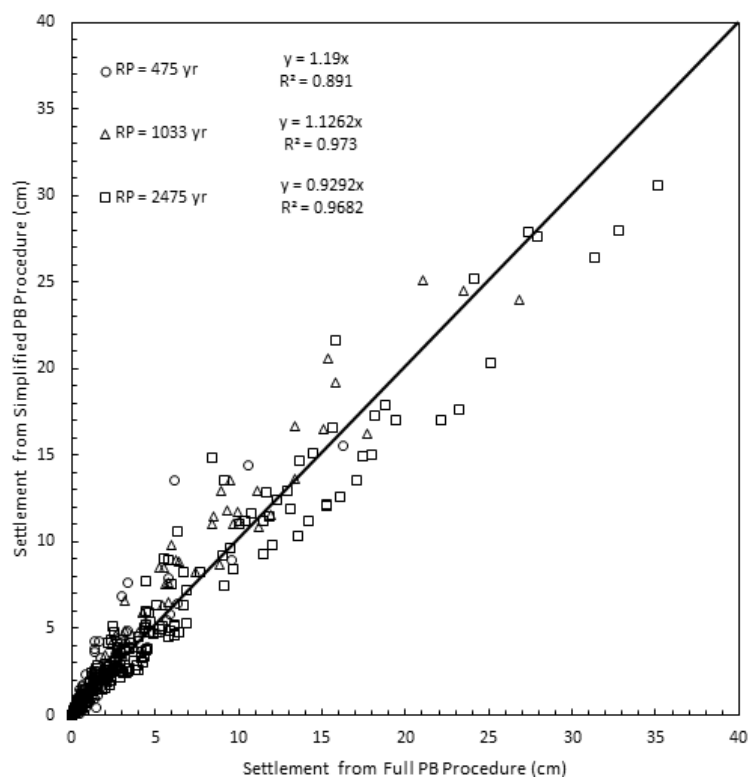


Figure 5-4. Boulanger and Idriss (2014) Full Performance-Based Settlement vs. Simplified Settlement Separated by Return Period (for *PGA* lower than 0.2g).

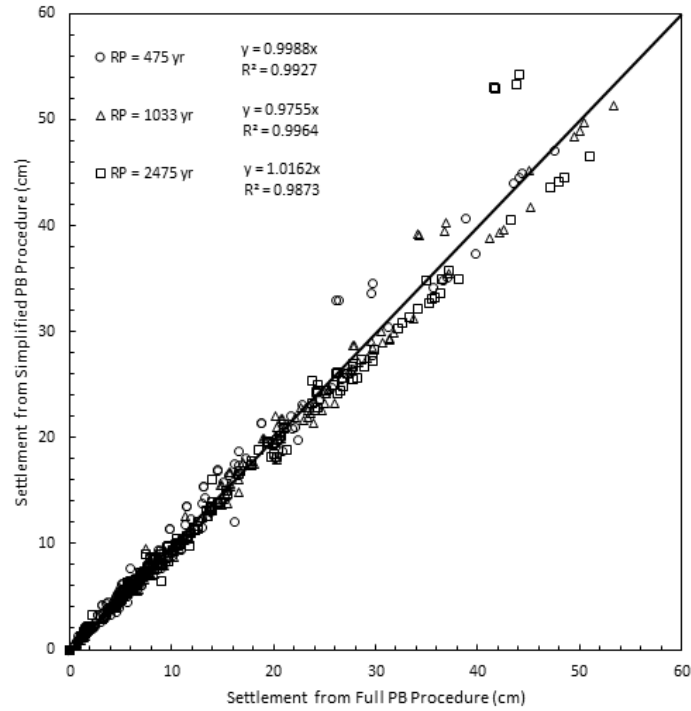


Figure 5-5. Boulanger and Idriss (2014) Full Performance-Based Settlement vs. Simplified Settlement Separated by Return Period (for *PGA* higher than 0.2g).

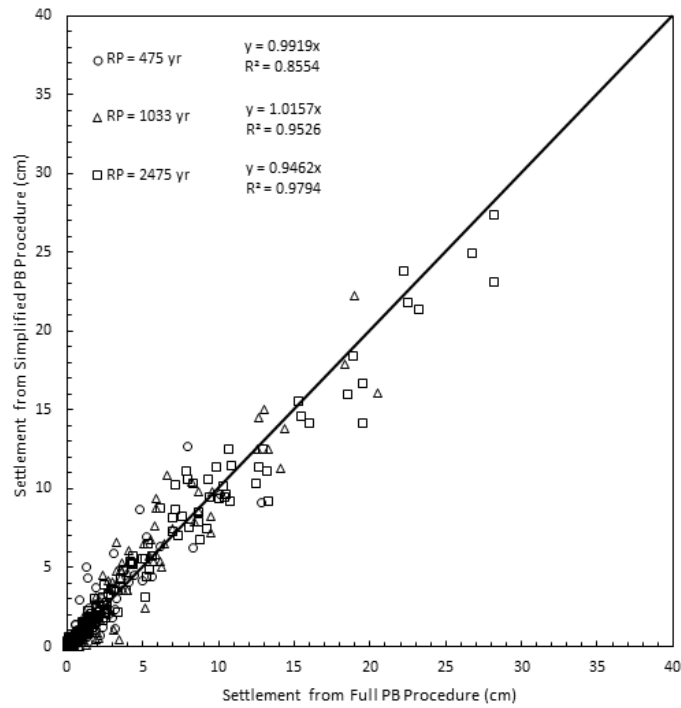


Figure 5-6. Ku et al. (2012) Performance-Based Total Settlement vs. Simplified Settlement Separated by Return Period (for *PGA* lower than 0.2g).

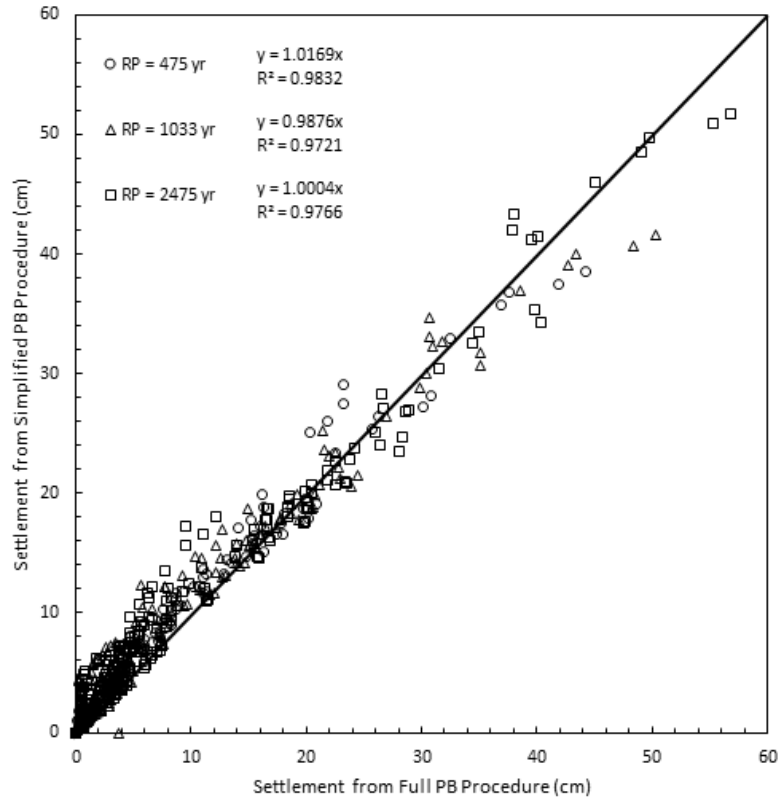


Figure 5-7. Ku et al. (2012) Performance-Based Total Settlement vs. Simplified Settlement Separated by Return Period (for *PGA* higher than 0.2g).

The validation plots for the Ku et. al (2012) triggering model are shown in Figure 5-6 and Figure 5-7, which present data from sites that have *PGA* < 0.2g and *PGA* > 0.2g , respectively.

For cities with *PGA* lower than 0.2g, the simplified procedure was able to approximate the full performance-based procedure with less than 7 cm of difference for all return periods and settlement ranges. For cities with *PGA* higher than 0.2g, the simplified procedure estimated the total ground surface settlements within 4 cm of error when no more than 30 cm of total settlement was predicted. Larger errors (i.e., 10 cm) were observed in predicted total settlements larger than 30 cm.

5.5 Simplified Lateral Spread Displacement Model Validation

As with the settlement validation, a full performance-based lateral spread analysis and a simplified performance-based lateral spread analysis were performed for the 20 different soil profiles in 10 different cities across the United States. The same reference profile was used. A ground slope of 1% was used in the analysis.

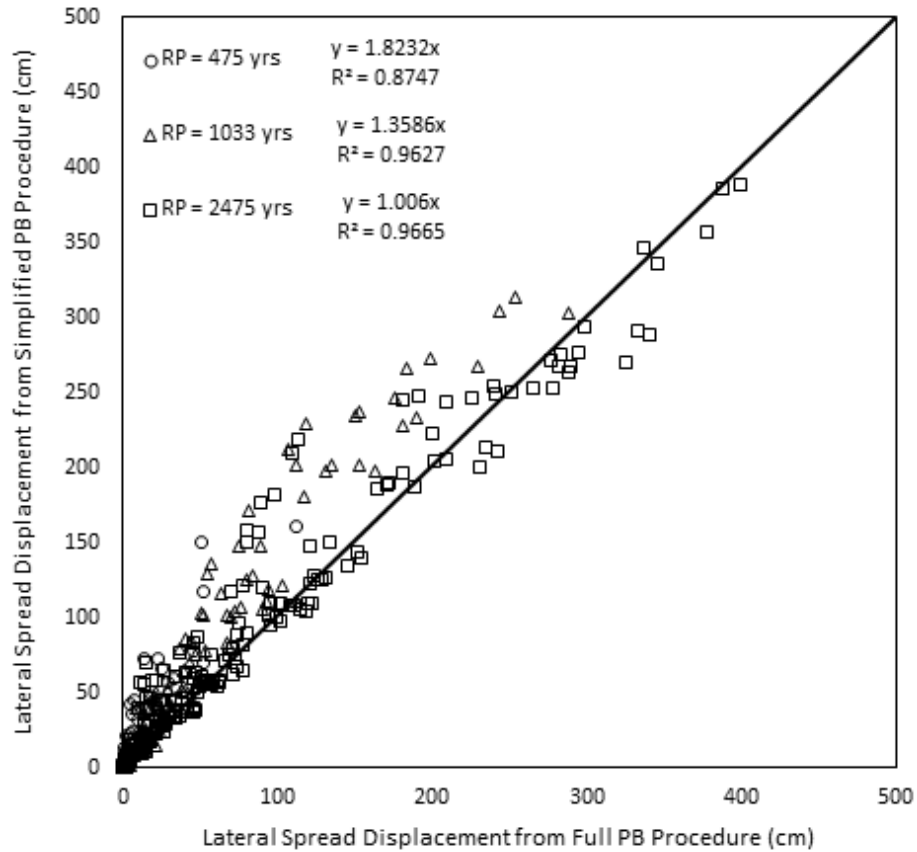


Figure 5-8. Boulanger and Idriss (2014) Performance-Based Lateral Spread Displacement vs. Simplified Lateral Spread Displacement (for *PGA* lower than 0.2g).

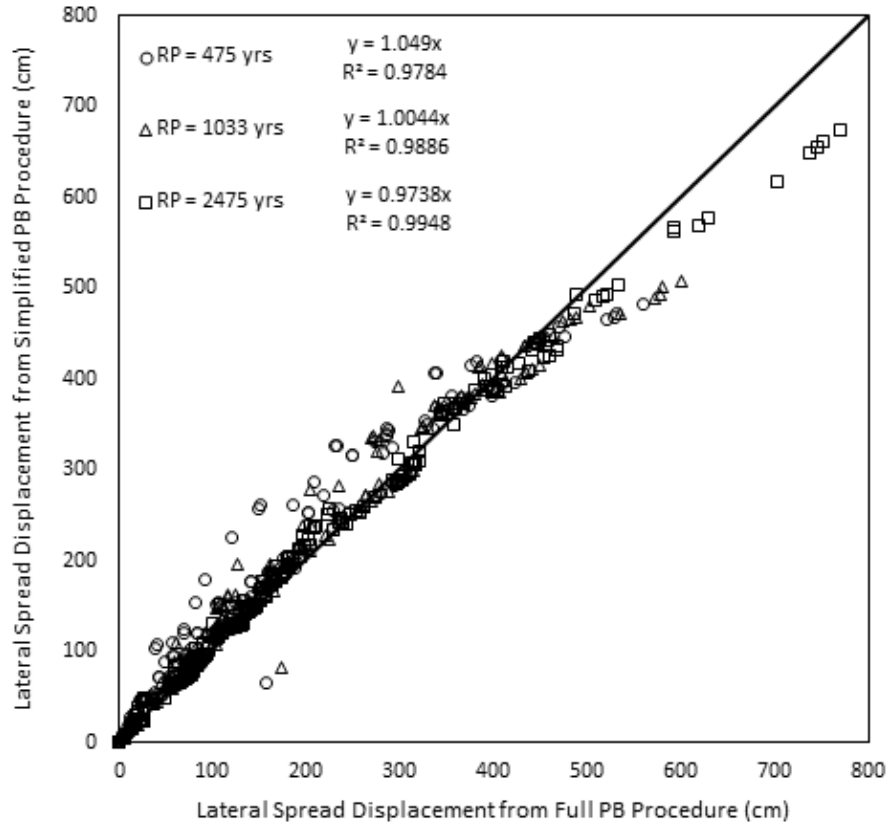


Figure 5-9. Boulanger and Idriss (2014) Performance-Based Lateral Spread Displacement vs. Simplified Lateral Spread Displacement (for *PGA* higher than 0.2g).

Overall, the simplified performance-based procedure is able to estimate the lateral spread displacements calculated using the full performance-based procedure, but involves more scatter for cities with lower *PGA*. As shown in Figure 5-8 the trend lines have slopes between 1.006 and 1.823 and R^2 values higher than 0.8747. In Figure 5-9, the trend lines have slopes between 0.9738 and 1.049 and R^2 higher than 0.9784.

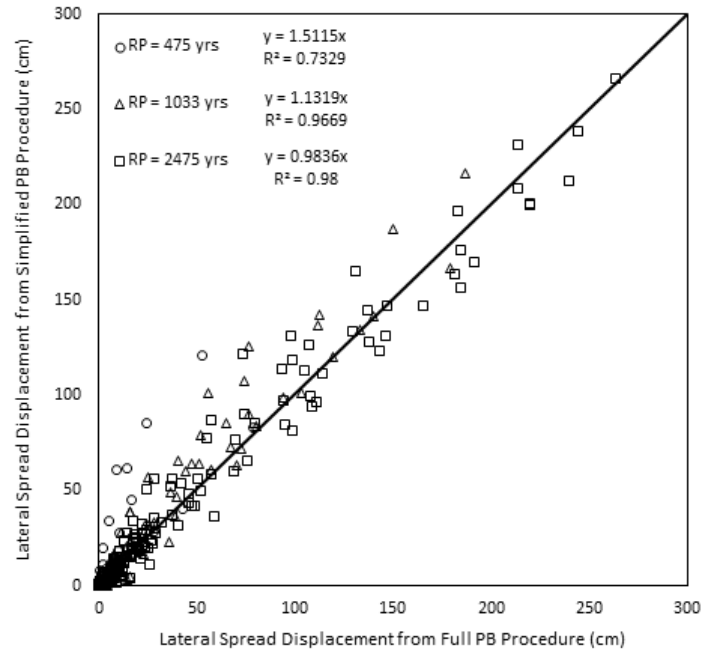


Figure 5-10. Ku et al. (2012) Performance-Based Lateral Spread Displacement vs. Simplified Lateral Spread Displacement (for *PGA* lower than 0.2g).

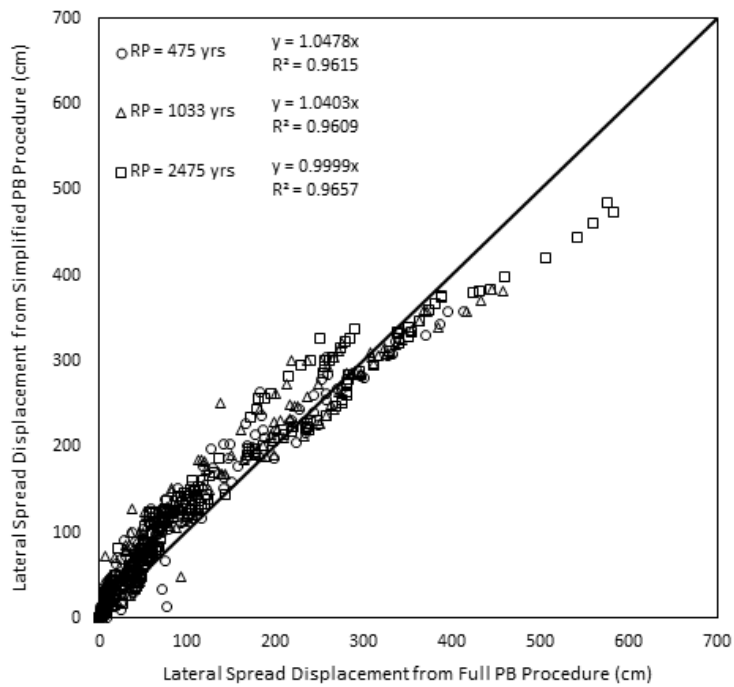


Figure 5-11. Ku et al. (2012) Performance-Based Lateral Spread Displacement vs. Simplified Lateral Spread Displacement (for *PGA* higher than 0.2g).

Similar to the Idriss and Boulanger (2014) triggering procedure, the simplified performance-based procedure is able to estimate the lateral spread displacements calculated using the full performance-based procedure, but involves more scatter for cities with lower *PGA*. As shown in Figure 5-10, the trend lines have slopes between 0.9836 and 1.5115. For return period of 475 years, the R^2 value is 0.7329, which indicates that the simplified performance-based procedure has lower precision and consistency in predicting the full performance-based procedure at this return period. In Figure 5-11, the trend lines have slopes between 0.9999 and 1.0478 and R^2 higher than 0.9609.

6.0 COMPARISON STUDY

6.1 Overview

This section presents the comparison between the simplified performance-based liquefaction hazard analysis developed through this research, the deterministic, and conventional pseudo-probabilistic liquefaction hazard analysis routinely applied in engineering practice and currently prescribed by AASHTO code. The ultimate goal of these comparisons is to demonstrate that the simplified performance-based analysis is a much more reliable and accurate approximation of the full performance-based analysis than the conventional deterministic and pseudo-probabilistic analyses. This section compares the accuracy between the simplified performance-based analysis results and the conventional pseudo-probabilistic analysis results.

6.2 Locations and Profiles

Twelve locations were chosen at random from among cities in the four participating states (Utah, South Carolina, Connecticut, and Oregon), resulting in three selected sites in each state. Out of the 12 sites, 8 sites have a *PGA* less than 0.2g, with the remaining sites having *PGA* values greater than 0.2g. We have defined low seismicity areas as cities with a *PGA* less than 0.2g and areas of moderate to high seismicity as cities with a *PGA* greater than or equal to 0.2g. Table 6-1 presents a list of the 12 sites and their corresponding latitudes and longitudes, *PGA*, and mean magnitude at the 2475-year return period (from the deaggregation results of the 2014 USGS seismic hazard maps). For the simplified performance-based analyses in this study, the developed reference parameter maps are used to interpolate reference parameter values rather than calculate them directly at each of the selected sites. Such interpolation allows for evaluation of the potential bias that could be introduced through interpolation with the reference parameter maps.

Table 6-1. Sites Selected for Comparison Study

State	City	Latitude	Longitude	PGA	Mw
Utah	Salt Lake City	40.755	-111.898	0.726	6.8
	Fillmore	38.964	-112.339	0.178	6.31
	Moab	38.598	-109.547	0.1	5.74
Oregon	Eugene	44.075	-123.132	0.398	8.68
	Bend	44.079	-121.306	0.175	7.13
	Mt. Vernon	44.405	-119.113	0.139	6.24
Connecticut	Hartford	41.779	-72.666	0.099	5.64
	Stamford	41.077	-73.565	0.161	5.49
	New Haven	41.317	-72.963	0.111	5.58
South Carolina	Charleston	32.821	-79.943	0.945	6.77
	Columbia	34.037	-81.038	0.189	6.14
	Florence	34.222	-79.754	0.161	6.81

6.3 Comparison with the Pseudo-Probabilistic Procedure

This section will present the results of the comparison study for the Boulanger and Idriss (2014) and Ku et al. (2012) models. For each plot, computed results for the full performance-based procedure that we are attempting to approximate are plotted on the x-axis. Computed results for the pseudo-probabilistic and simplified performance-based procedures are plotted on the y-axis. The comparison between the simplified performance-based procedure and the pseudo-probabilistic procedure is based on two main criteria: the slopes of the trend line and the R^2 values. The data with a trend line slope closer to 1.0 is considered to better approximate the full-performance based procedure on average, and the data with the larger R^2 value is more consistent in its predictions. Sections 6.4 through 6.7 will present the comparison plots for liquefaction triggering, settlement, and lateral spread.

6.4 Liquefaction Triggering Comparison

6.4.1 Ku et al. (2012) Comparison Results

The comparison results for the Ku et al. (2012) triggering model are presented in Figure 6-1 using different representations of liquefaction triggering hazard: q_{req} (a), FS_L (b), and $CSR\%$ (c). Each plot contains the results of all three analyzed return periods. An initial observation of the comparison plots shows that the pseudo-probabilistic procedure exhibits much greater scatter than the simplified procedure. For all three parameters shown, the simplified procedure achieved a much higher R^2 value than the pseudo-probabilistic procedure.

The average R^2 values are 0.7 (pseudo-probabilistic) and 0.975 (simplified), suggesting that, on average, the simplified performance-based procedure is a better overall approximation of the full performance-based procedure. For the slope of the trend lines, the average slopes are 1.04 (pseudo-probabilistic) and 0.981 (simplified). This means, on average, the pseudo-probabilistic procedure over-predicts the full performance-based procedure by 4% (with the exception of the FS_L) and the simplified procedure is underpredicting by 1.9%. Based on the results, the proposed simplified performance-based procedure incorporating the Ku et al (2012) triggering model provides a more consistent and precise approximation of the full performance-based procedure than the conventional pseudo-probabilistic procedure.

6.4.2 Boulanger and Idriss (2014) Comparison Results

The comparison results for the Boulanger and Idriss (2014) triggering model are presented in Figure 6-2 for $CSR\%$ (a), FS_L (b), and q_{req} (c), also showing all three return periods. Similar to the Ku et al. (2012) comparison results, the pseudo-probabilistic procedure also visually exhibits much greater scatter than the simplified procedure. By comparing average R^2 values, the simplified procedure had a higher average R^2 value (0.987) than the pseudo-probabilistic procedure (0.921). In the case of q_{req} , the pseudo-probabilistic has a slightly greater R^2 value (0.977) than the simplified procedure (0.975), however such small differences are negligible. The average slopes of the trendlines are 1.016 (pseudo-probabilistic) and 0.996 (simplified), meaning the pseudo-probabilistic procedure overestimates the full performance-based method by 1.62% and the simplified procedure underpredicts by 0.42%. Overall, a similar conclusion can be made that the

proposed simplified performance-based procedure incorporating the Boulanger and Idriss (2014) triggering model also provides a more consistent and equally precise approximation of the full performance-based procedure as the conventional pseudo-probabilistic procedure.

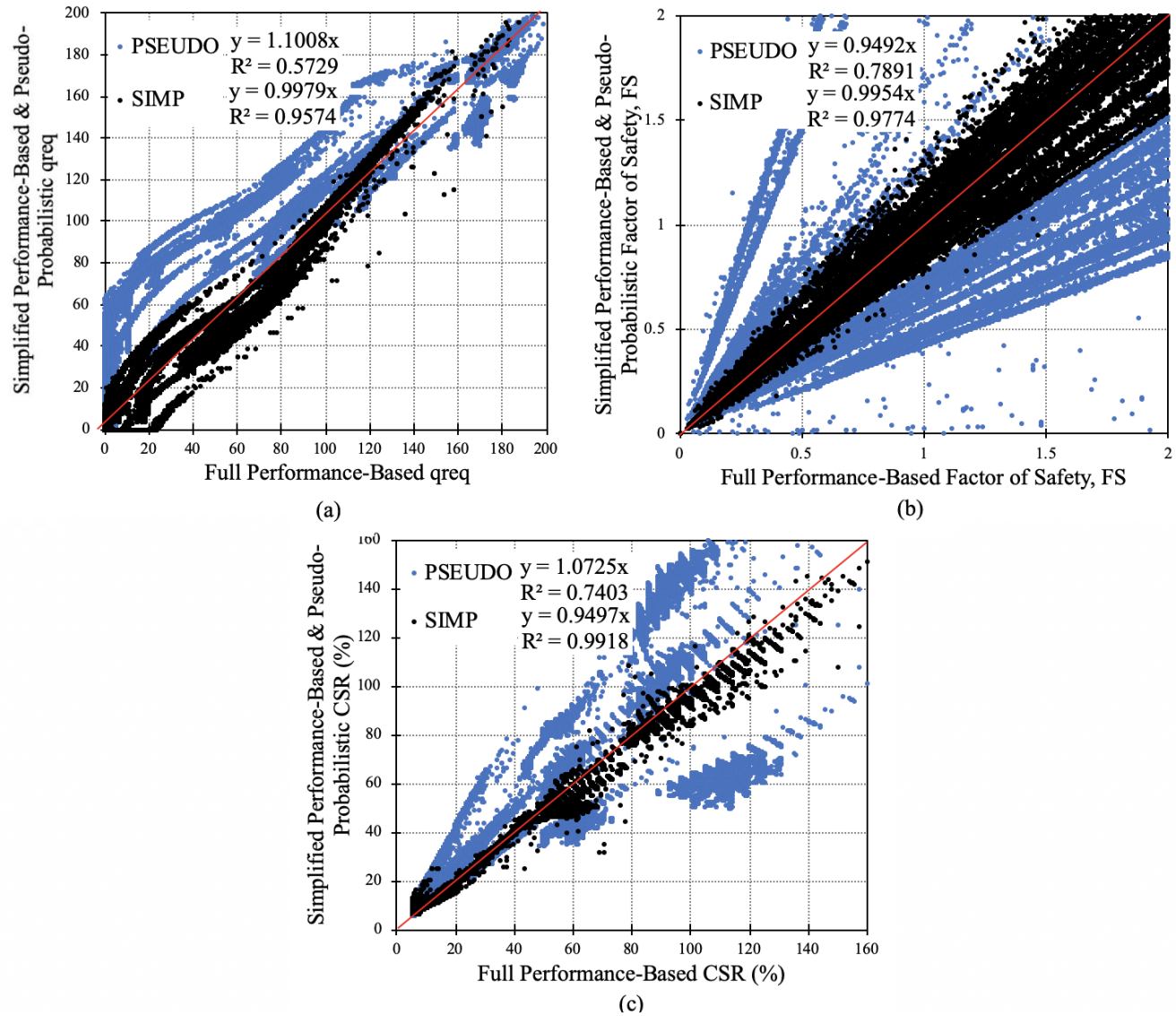


Figure 6-1. Comparison Results for the Ku et al. (2012) Triggering Model for (a) q_{req} , (b) FS_L , and (c) $CSR\%$

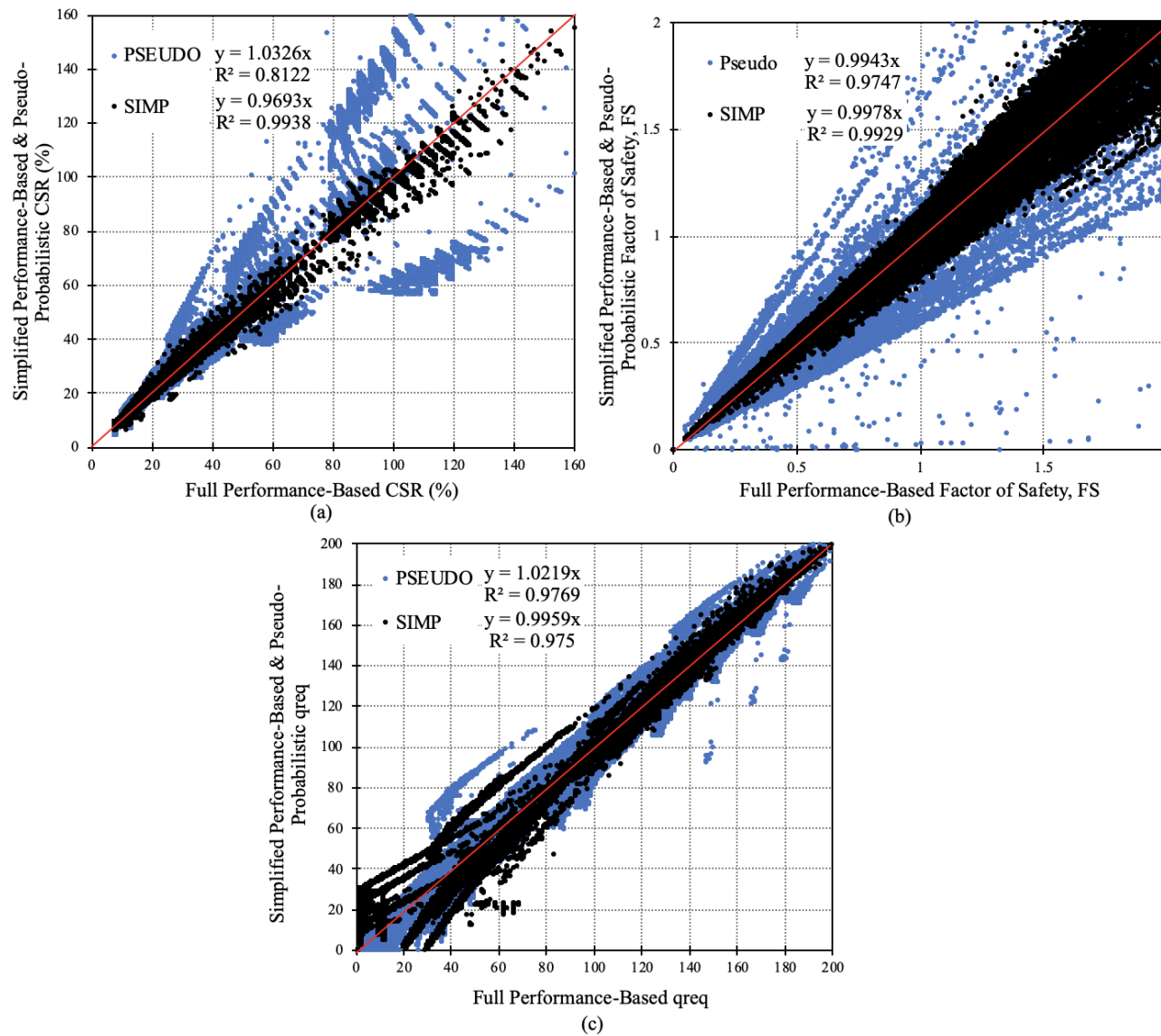


Figure 6-2. Comparison Results for the Boulanger and Idriss (2014) Triggering Model for (a) $CSR\%$, (b) FS_L , and (c) q_{req}

6.5 Post-Liquefaction Settlement Comparison

6.5.1 Post-Liquefaction Settlement Comparison Results using Boulanger and Idriss (2014)

The comparison results of all three return periods for the Boulanger and Idriss (2014) triggering model are shown in Figure 6-3 and Figure 6-4. Figure 6-3 contains sites with PGA less than $0.2g$ and Figure 6-4 contains sites with PGA higher than $0.2g$.

For all return periods and for both the simplified performance-based and the pseudo-probabilistic procedures, more scatter is observed for sites with PGA less than $0.2g$ (Figure 6-3). At sites with $PGA < 0.2g$, the slopes of the trend lines are 1.0545 and 1.2398 for the simplified performance-based procedure and the pseudo-probabilistic procedure, respectively, meaning that the simplified procedure overestimates the full performance-based procedure by 5.5% and the pseudo-probabilistic procedure overestimates by 24% on average. As for the R^2 values, both the simplified performance-based procedure and the probabilistic procedure have R^2 values near 0.925 , suggesting comparable consistencies between the two procedures. For sites with $PGA \geq 0.2g$ (Figure 6-4), the plot shows that the simplified performance-based procedure underestimates the full performance-based procedure by 3.2% on average, and the pseudo-probabilistic procedure overestimates the full performance-based procedure by 10.3% on average. Additionally, the simplified performance-based procedure has a slightly higher R^2 value of 0.9729 , which is greater than the value of the pseudo-probabilistic procedure at $R^2 = 0.9515$, though such small differences in R^2 are likely insignificant.

Overall, both the simplified performance-based procedure and the pseudo-probabilistic procedure overestimate the full performance-based procedure for sites with $PGA < 0.2g$ (i.e., low seismicity areas), and underestimate for $PGA \geq 0.2g$ (i.e., moderate to high seismicity areas). However, the simplified performance-based procedure more accurately approximates the full performance-based procedure on average and is slightly more consistent and precise than the pseudo-probabilistic procedure based on the comparisons performed in this study.

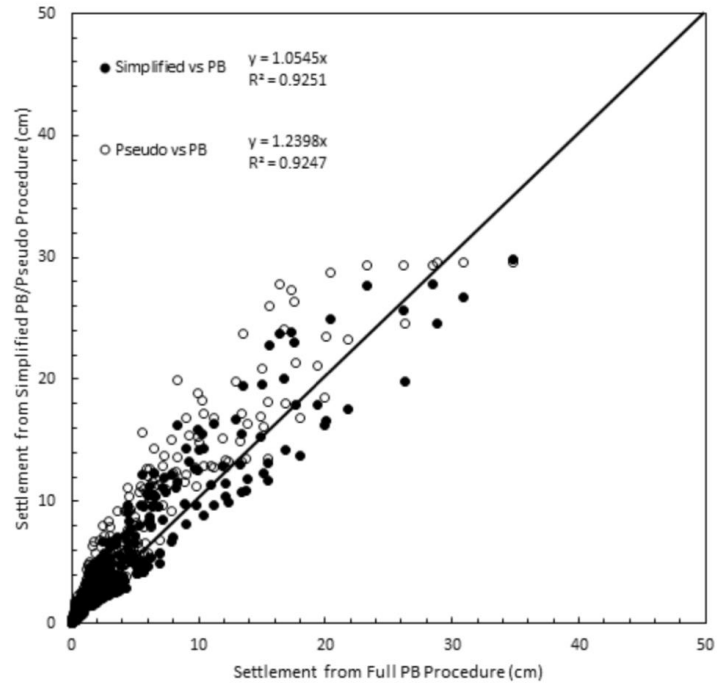


Figure 6-3. Settlement Comparison Results using the Boulanger and Idriss (2014) Triggering Model for Sites with $PGA < 0.2 g$ (for All Return Periods)

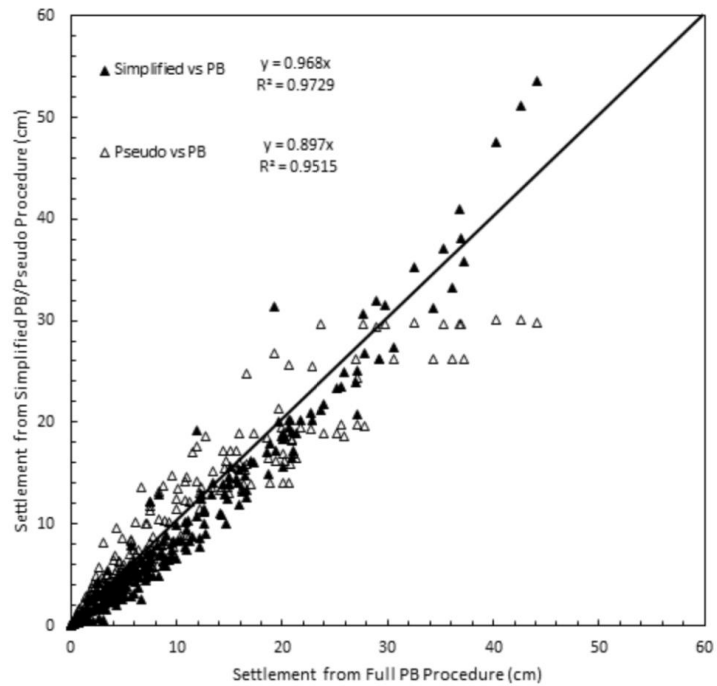


Figure 6-4. Settlement Comparison Results using the Boulanger and Idriss (2014) Triggering Model for Sites with $PGA \geq 0.2 g$ (for All Return Periods)

6.5.2 Post-Liquefaction Settlement Comparison Results using Ku et al. (2012)

The comparison plots based on the Ku et al. (2012) triggering model are shown in Figure 6-5 and Figure 6-6, with Figure 6-5 containing sites with $PGA < 0.2g$ and Figure 6-6 containing sites with $PGA \geq 0.2g$.

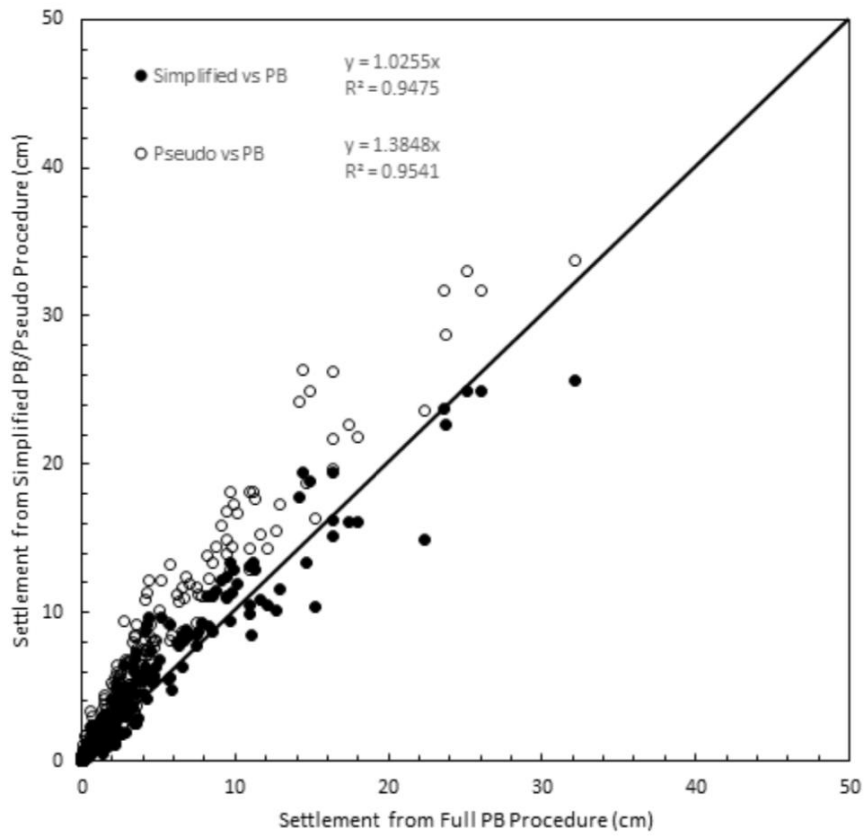


Figure 6-5. Settlement Comparison Results using the Ku et al. (2012) Triggering Model for Sites with $PGA < 0.2 g$ (for All Return Periods)

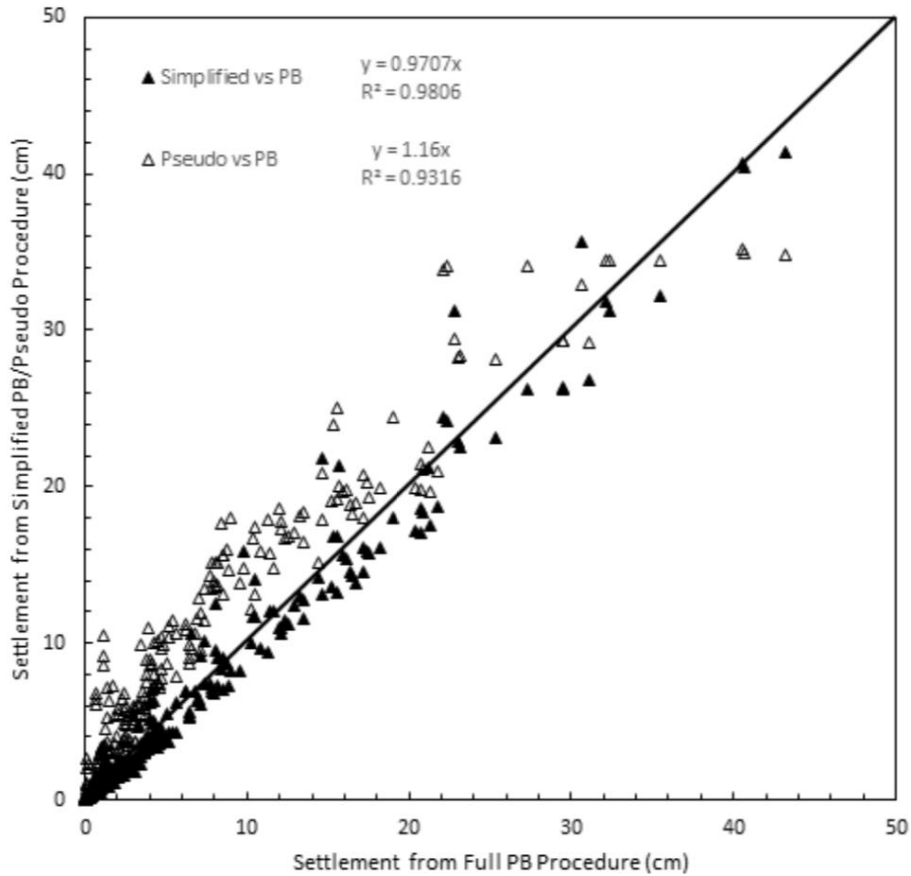


Figure 6-6. Settlement Comparison Results using the Ku et al. (2012) Triggering Model for Sites with $PGA \geq 0.2g$ (for All Return Periods)

As observed with the Boulanger and Idriss (2014) model, the simplified performance-based procedure with the Ku et al (2012) model produced better approximations of the full performance-based procedure and was slightly more consistent and precise than the pseudo-probabilistic procedure.

6.6 Discussion

From a visual observation of the comparison plots, the plots do not show an obvious visual difference between the simplified procedure and the pseudo-probabilistic procedure. However, the trend line slopes and R^2 values presented suggest that the simplified performance-based procedure

can consistently provide better approximations of the full performance-based procedure than the pseudo-probabilistic procedure.

The apparent similarities between the simplified performance-based and pseudo-probabilistic procedures for post-liquefaction settlement can be explained. Studies have shown that the performance-based procedure generally deviates significantly from the pseudo-probabilistic procedure in liquefaction triggering (Kramer and Mayfield, 2007; Franke et al., 2013). However, these significant differences in computed FS_L are not fully transferred to the resulting volumetric strains, which are computed using the Ishihara and Yoshimine (1992) method.

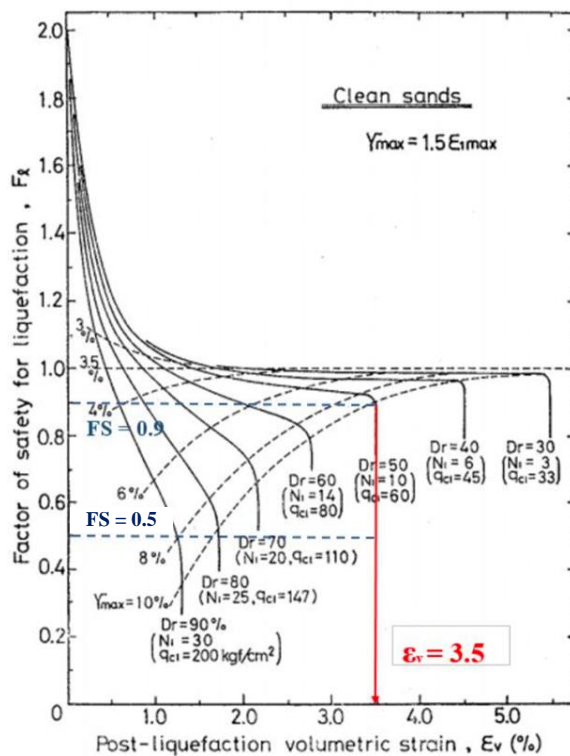


Figure 6-7. Ishihara and Yoshimine (1992) Method for Determining Volumetric Strain

Consider, for example, two different values of FS_L (0.9 and 0.5) and the resulting volumetric strains from Ishihara and Yoshimine (1992) presented in Figure 6-7. Each of the FS_L values, although significantly different, is predicted to result in approximately the same amount of volumetric strain: 3.5%. As such, significant differences in the computed FS_L between the simplified performance-based procedure and the pseudo-probabilistic procedure may not translate

directly to significant differences in volumetric strain when using the Ishihara and Yoshimine (1992) volumetric strain curves. Consequently, the resulting post-liquefaction settlements computed using the two different procedures can appear quite similar.

Regardless, engineers in practice may question why the simplified procedure should be used over the pseudo-probabilistic procedure when no visually obvious improvements have been achieved. In response to this question, the simplified performance-based procedure clearly demonstrates trend line slopes that are closer to 1.0 and larger R^2 values than the conventional pseudo-probabilistic approach. This indicates that the simplified approach is better at approximating the full performance-based approach. However, engineers may choose if they would like to benefit from the increased accuracy, consistency, and precision of the simplified performance-based approach or continue using the approach they are already familiar with. Continued use of the pseudo-probabilistic approach in computing post-liquefaction settlements will not produce substantially inaccurate estimates of the full performance-based post-liquefaction settlements.

6.7 Lateral Spread Comparison Results

6.7.1 Lateral Spread Comparison Results using Zhang et al. (2004) with Boulanger and Idriss (2004)

The comparison of predicted lateral spread displacements using Zhang et al. (2004) for all three return periods using the Boulanger and Idriss (2014) triggering model are presented in Figure 6-8 and Figure 6-9, which contain sites with $PGA < 0.2g$ and $PGA \geq 0.2g$.

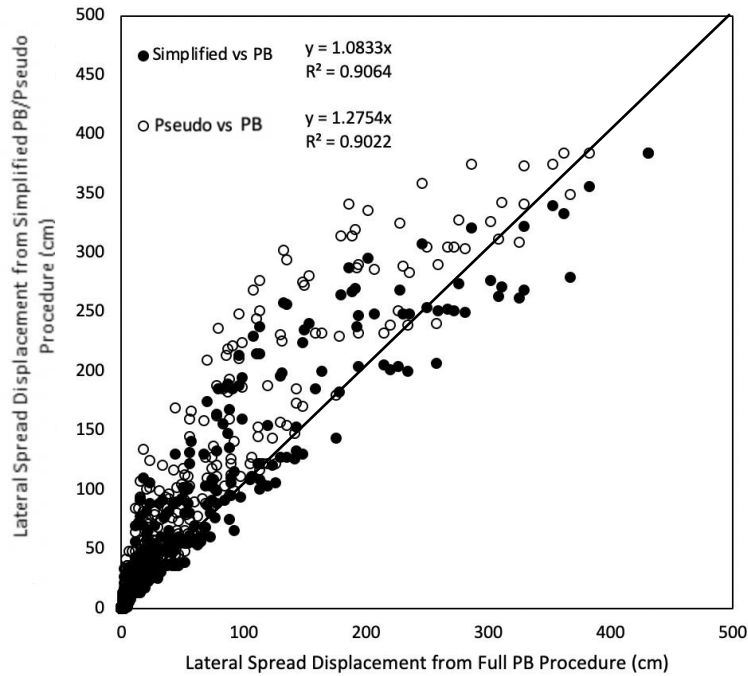


Figure 6-8. Lateral Spread Comparison Results using the Boulanger and Idriss (2014) Triggering Model for Sites with $PGA < 0.2g$ (for All Return Periods)

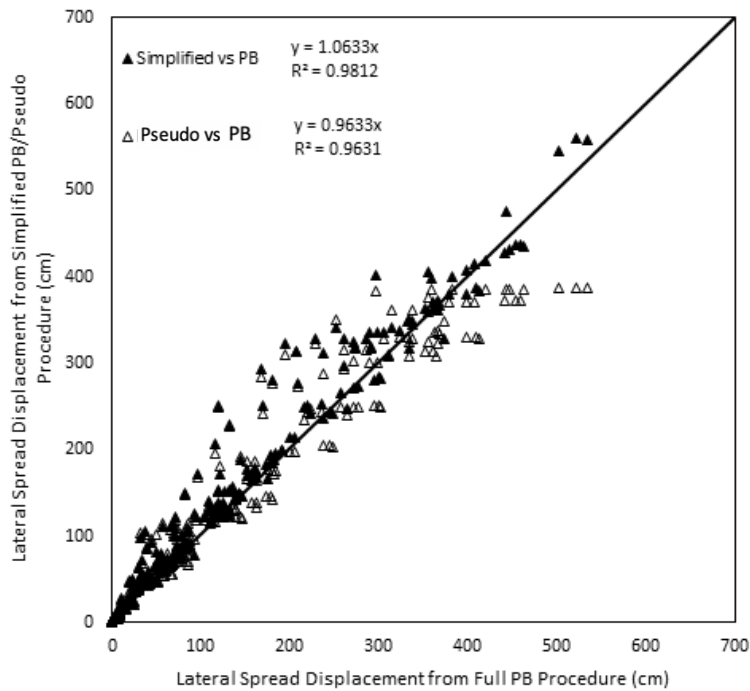


Figure 6-9. Lateral Spread Comparison Results using the Boulanger and Idriss (2014) Triggering Model for Sites with $PGA \geq 0.2g$ (for All Return Periods).

For both the simplified performance-based procedure and the pseudo-probabilistic procedure, more scatter is observed for sites with $PGA < 0.2g$ (Figure 6-8). At sites with $PGA < 0.2g$ (Figure 6-8), slopes of the trend lines are 1.0833 and 1.2754 for the simplified procedure and the pseudo-probabilistic procedure, respectively, suggesting that, on average, the simplified performance-based procedure is over-predicting the full performance-based procedure by 8.3% and the pseudo-probabilistic method is over-predicting by 27.5%. Considering the R^2 values, both the simplified performance-based procedure and the pseudo-probabilistic method produce R^2 values around 0.90. Similarly, results at sites with $PGA \geq 0.2g$ (Figure 6-9) show that the simplified procedure overestimates the full performance-based procedure by 6.3% and the pseudo-probabilistic underestimates by 3.7% on average. The simplified performance-based procedure also has a slightly higher R^2 value (0.9812) than the pseudo-probabilistic procedure (0.9631).

Overall, the simplified procedure produces a slightly better approximation of the full performance-based procedure. While a visual inspection of the comparison plots may make them appear similar, the simplified procedure does indeed provide more consistent and accurate approximations of the full performance-based procedure than the pseudo-probabilistic approach on average.

6.7.2 Lateral Spread Comparison Results using Zhang et al. (2004) with Ku et al. (2012)

The comparison of predicted lateral spread displacements using Zhang et al. (2004) procedure with the Ku et al. (2012) triggering model are shown in Figure 6-10 and Figure 6-11 with Figure 6-10 presenting the results for sites with $PGA < 0.2g$ and Figure 6-11 presenting the results for sites with $PGA \geq 0.2g$.

For both the simplified performance-based procedure and the pseudo-probabilistic procedure, more scatter is observed for sites with $PGA < 0.2g$ (Figure 6-10). At sites with $PGA < 0.2g$ (Figure 6-10), slopes of the trend lines are 1.055 and 1.4925 for the simplified procedure and the pseudo-probabilistic procedure, respectively, suggesting that, on average, the simplified performance-based procedure is over-predicting the full performance-based procedure by 5.5% and the pseudo-probabilistic method is over-predicting by 49.25%. Considering the R^2 values, both the simplified performance-based procedure and the pseudo-probabilistic procedure produce an R^2 value around 0.94. Similarly, results at sites with $PGA \geq 0.2g$ (Figure 6-11) show that the

simplified procedure overestimates the full performance-based procedure by 1.25% and the pseudo-probabilistic overestimates by 24.38%. At approximately 150 cm of lateral spread displacement, the pseudo-probabilistic procedure overestimates the full performance-based procedure while the simplified procedure underestimates the full performance-based procedure. The simplified performance-based procedure also has a slightly higher R^2 value (0.9628) than the pseudo-probabilistic procedure (0.9396).

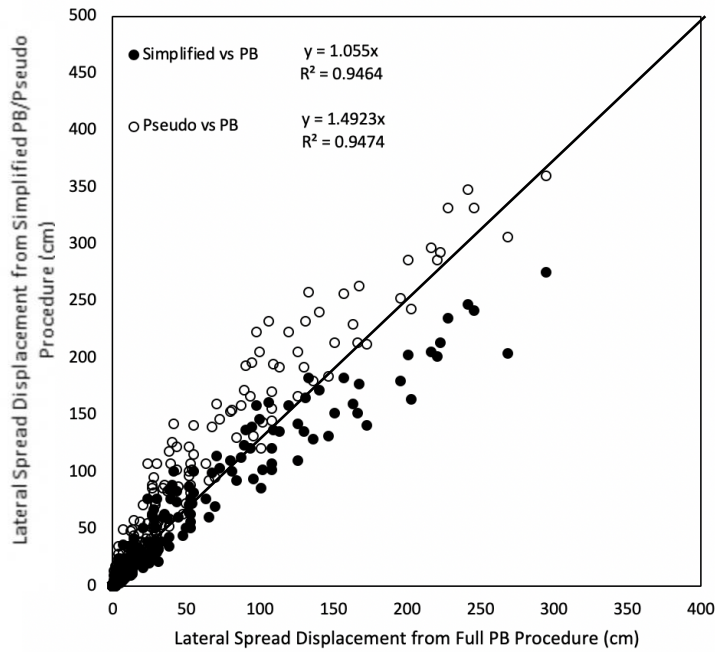


Figure 6-10. Lateral Spread Comparison Results using the Ku et al. (2012) Triggering Model for Sites with $PGA < 0.2g$ (for All Return Periods)

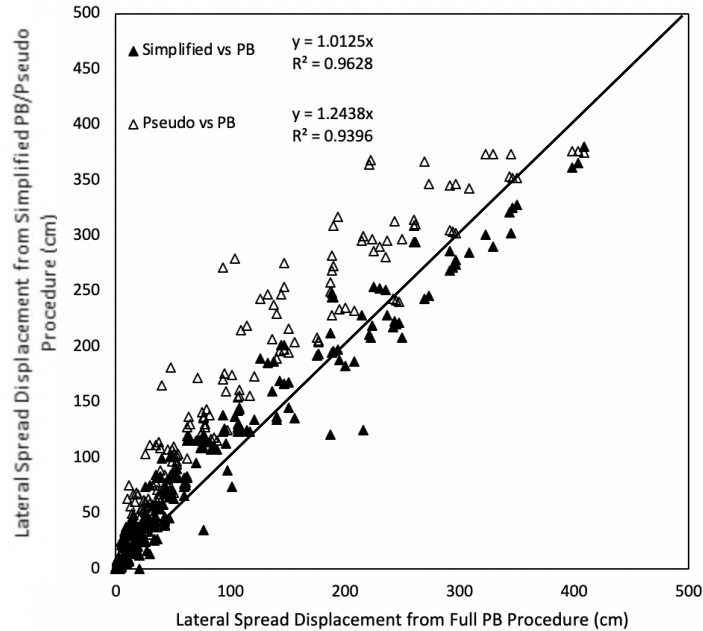


Figure 6-11. Lateral Spread Comparison Results using the Ku et al. (2012) Triggering Model for Sites with $PGA \geq 0.2g$ (for All Return Periods)

The results of the simplified and pseudo-probabilistic lateral spread procedures using Ku et al. (2012) are, fairly similar up to a displacement of 150 cm. However, based on the R^2 values and the trendlines, the simplified procedure produces an overall slightly better approximation of the full performance-based procedure.

6.8 Comparison with the Deterministic Procedure

This section will present the results of the deterministic comparison study for the Boulanger and Idriss (2014) and Ku et al. (2012) models. For each plot, computed results for the simplified performance-based procedure are plotted on the x-axis and the deterministic procedure results are plotted on the y-axis. Sections 6.9 through 6.11 will present the comparison plots for liquefaction triggering, settlement, and lateral spread.

6.8.1 Locations and Profiles

Three locations were chosen across the United States: Butte, Salt Lake City, and San Francisco. For the deterministic procedure, ground motions are obtained through a Deterministic Seismic Hazard Analysis (DSHA). A DSHA involves deterministically assessing the seismic sources in the nearby region of the site of interest and identifying the source which produces the highest hazard in the area. The software EZ-FRISK was used to identify the top five seismic sources within 200 km for San Francisco, Butte, and Salt Lake City. The 2008 USGS Seismic Source Model within EZ-FRISK does not include some smaller faults in low seismic regions, such as Butte. Thus, the governing fault for Butte (Rocker Fault) was identified using the USGS quaternary fault database (USGS et al., 2006). In the case of Salt Lake City and San Francisco, EZ-FRISK provided values of M_w , PGA , and R for both the 50th (i.e. median) and 84th (i.e. median + σ) percentiles using the Next Generation Attenuation (NGA) models for the Western United States (Boore and Atkinson, 2008; Campbell and Bozorgnia, 2008; and Chiou and Youngs, 2008) and weighting schemes shown in Table 6-2. For Butte, the 50th and 84th percentile M_w values were estimated using a correlation with surface rupture length developed by Wells and Coppersmith (1994), and PGA was calculated using the same three (NGA) models based on measured dimensions and assumed characteristics of the Rocker Fault. Once the model inputs have been determined through the DSHA they are entered into the respective empirical liquefaction hazard models. A summary of the input variables utilized in the deterministic analyses are provided in Table 6-3. One single CPT soil profile, shown in Figure 6-12, was used in this comparison.

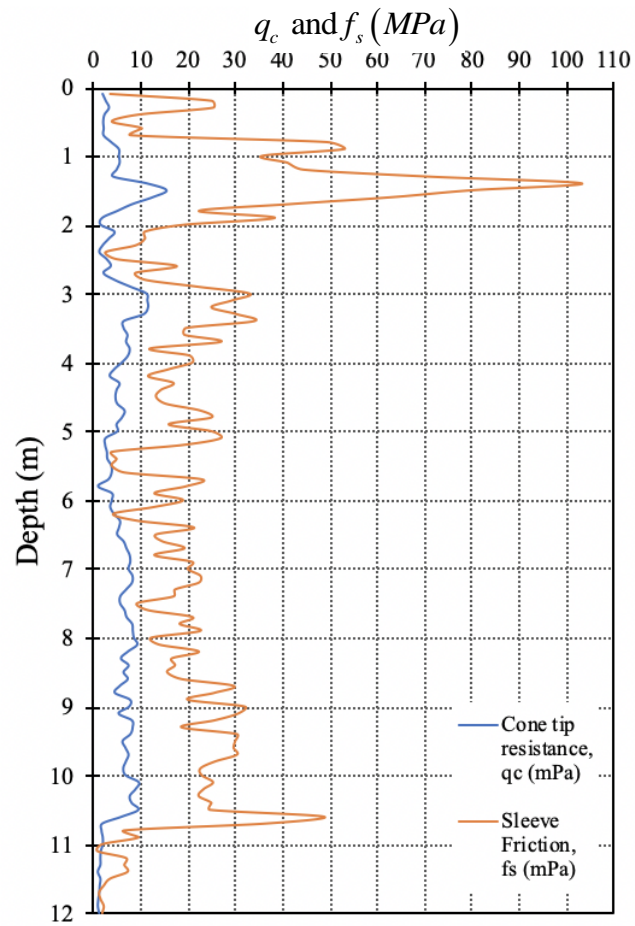


Figure 6-12. Soil Profile used for the deterministic comparison study.

Table 6-2. NGA model weights used in the deterministic procedure.

Attenuation Model	Weight
Boore & Atkinson (2008)	0.333
Campbell & Bozorgnia (2008)	0.333
Chiou & Youngs (2008)	0.333

Table 6-3. Input variables used in the deterministic models (a_{max} calculated using F_{pga} from AASHTO code).

Location	Latitude	Longitude	Distance [km]	Mean M_w	Median (50%)		Median + σ (84%)	
					PGA	a_{max}	PGA	a_{max}
Butte	46.003	-112.533	4.92	6.97	0.539	0.539	0.9202	0.9202
Salt Lake City	40.755	-111.898	1.02	7.0	0.5911	0.5911	1.005	1.005
San Francisco	37.775	-122.418	12.4	8.05	0.3175	0.3754	0.5426	0.5426

6.9 Liquefaction Triggering Comparison

The comparison results for the Robertson and Wride (2009) triggering model are presented in Figure 6-13, Figure 6-14, and Figure 6-15 for different representations of liquefaction triggering hazards: q_{req} , FS_L , and $CSR\%$, respectively. Each figure shows plots for the 475, 1039, and 2475-year return period. A comparison of the plots show that the deterministic analyses frequently over-predicts the simplified performance-based method for q_{req} and $CSR\%$ and under-predicts FS_L . However, in the case of San Francisco, the deterministic analyses often under-predicted the simplified performance-based method for q_{req} and $CSR\%$. The comparison plots also highlights the differences between the 50th and 84th percentile ground motion results. For example, in the case of San Francisco, the 84th percentile ground motions over-predicted values of q_{req} while the 50th percentile ground motions under-predicted q_{req} . However, in the case of Salt Lake City ($T_r= 1039$), both the 50th and 84th percentile ground motions over-predicted the simplified method. In addition, the 50th percentile ground motions more closely approximated the simplified performance-based method than the 84th percentile ground motions. In other cases, the 84th percentile ground motions produced closer approximations of the simplified method than the 50th percentile ground motions. These discrepancies and inconsistencies can be confusing for the engineer who has to decide which ground motions appropriately characterize the liquefaction hazard for the given site.

The comparison results for the Boulanger and Idriss (2014) triggering model are presented in Figure 6-16, Figure 6-17, and Figure 6-18 for q_{req} , FS_L , and $CSR\%$, respectively. Similar to the Robertson and Wride results, these plots also show that the deterministic analyses frequently over-predicted the simplified-based method for q_{req} and $CSR\%$ and under-predicted the FS_L . These plots also highlight the inconsistencies of the 50th and 84th percentile ground motions.

6.9.1 Robertson and Wride (2009) Comparison Results

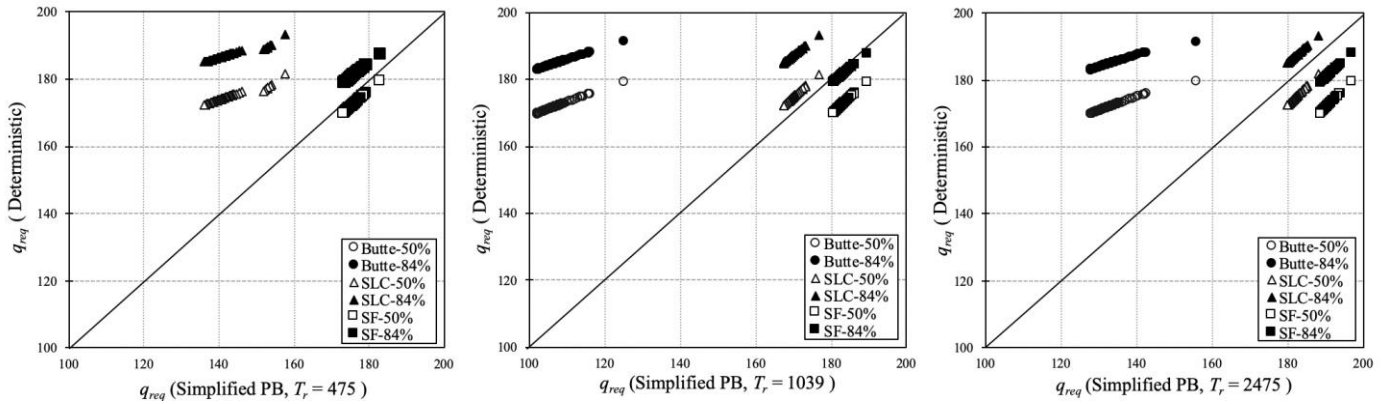


Figure 6-13. Comparison of deterministic and simplified performance-based values of q_{req} .

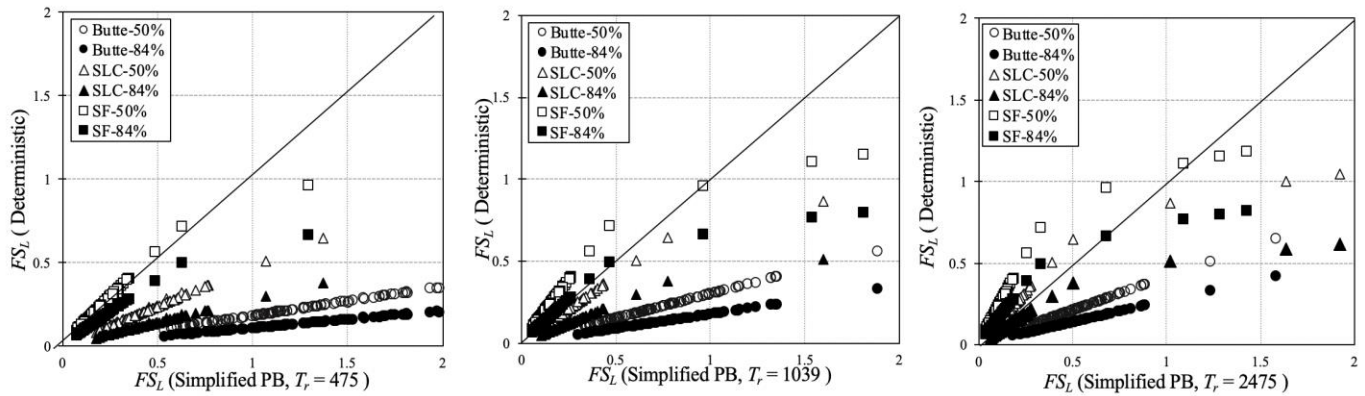


Figure 6-14. Comparison of deterministic and simplified performance-based values of FS_L .

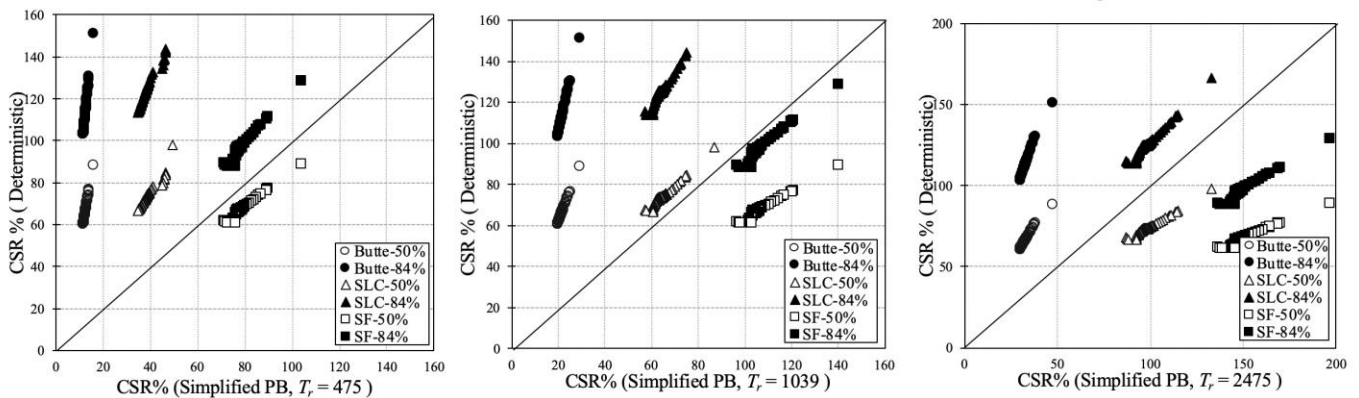


Figure 6-15. Comparison of deterministic and simplified performance-based values of $CSR\%$.

6.9.2 Boulanger and Idriss (2014) Comparison Results

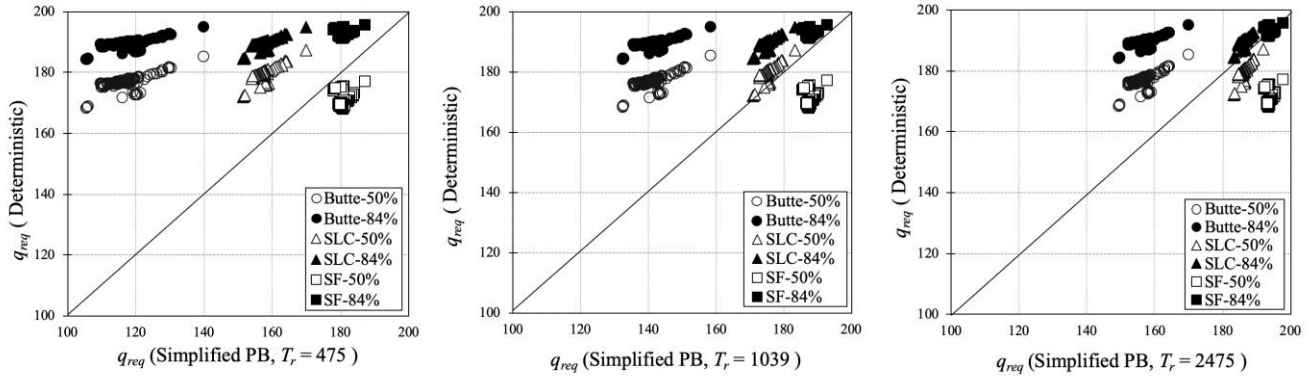


Figure 6-16. Comparison of deterministic and simplified performance-based values of q_{req} .

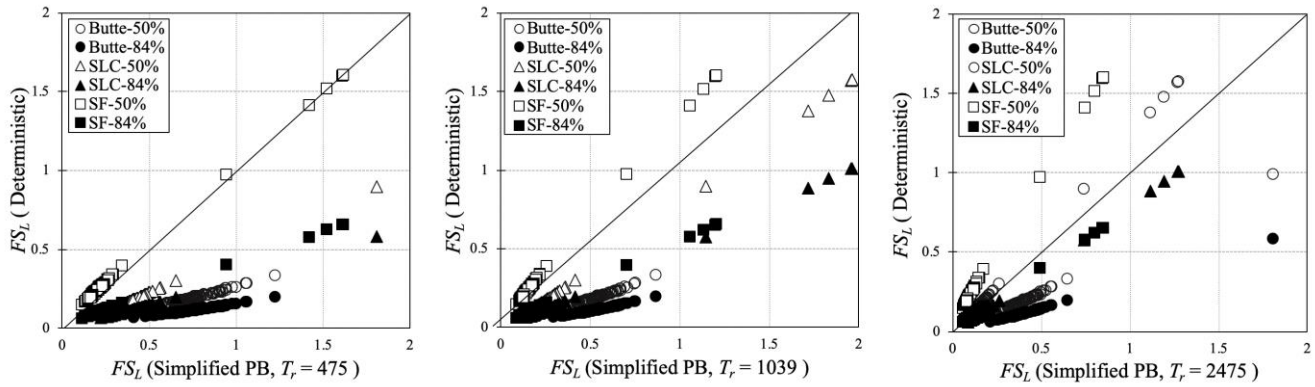


Figure 6-17. Comparison of deterministic and simplified performance-based values of FS_L .

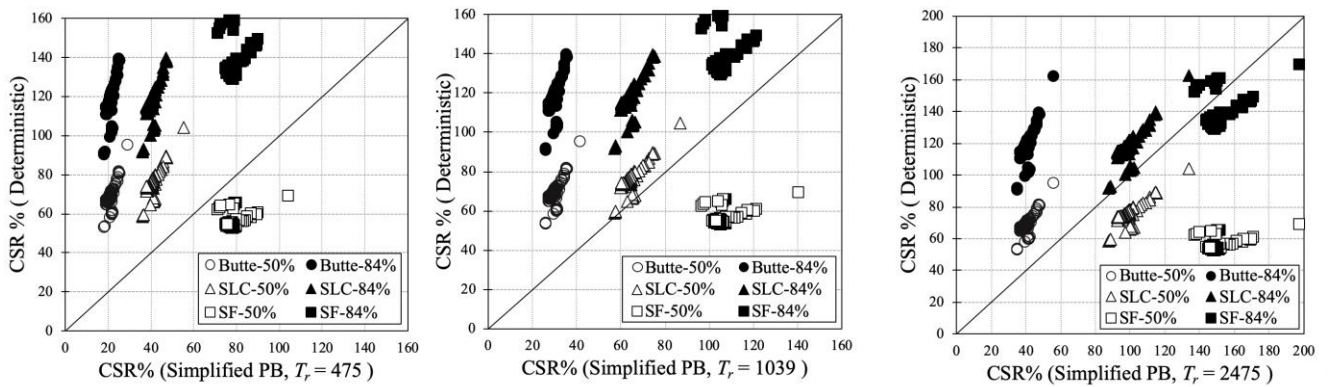


Figure 6-18. Comparison of deterministic and simplified performance-based values of CSR%

6.10 Post-Liquefaction Settlement Comparison (Ishihara and Yoshimine (1992))

The comparison plots in this section show the results of the Ishihara and Yoshimine (1992) deterministic analyses using the Robertson and Wride (2009) (Figure 6-19) and Boulanger and Idriss (2014) (Figure 6-20) models. These comparison plots show that the deterministic analyses often over-predicted simplified performance-based vertical strains for cities of low to medium seismicity (Butte and Salt Lake City), and under-predicted vertical strains for cities of medium to high seismicity (San Francisco). In many cases, the 50th and 84th percentile ground motions produced similar results.

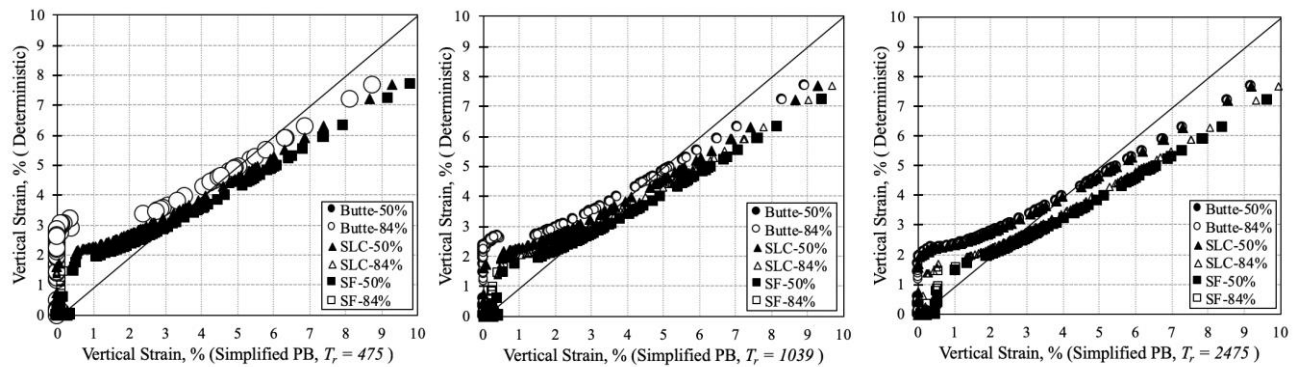


Figure 6-19. Comparison of deterministic and simplified performance-based vertical strains using the Robertson and Wride (2009) model.

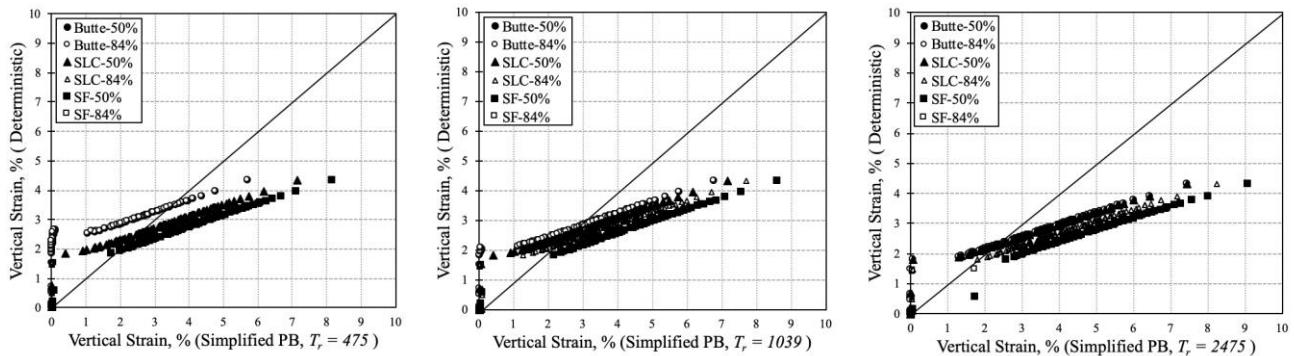


Figure 6-20. Comparison of deterministic and performance-based vertical strains using the Boulanger and Idriss (2014) model.

6.11 Lateral Spread Comparison Results (Zhang et al. (2004))

The comparison plots show the results of the Zhang et al. (2004) deterministic analyses using the Robertson and Wride (2009) (Figure 6-21) and Boulanger and Idriss (2014) (Figure 6-22) models. Based on these plots, the deterministic analyses greatly over-predicted the simplified performance-based method for low seismicity areas (Butte) for both models. When using the Robertson and Wride model, the deterministic analyses provided closer approximations of the simplified performance-based method for medium to high seismicity areas (Salt Lake City and San Francisco) at higher return periods. When using the Boulanger and Idriss model, the deterministic approach generally under-predicted the simplified method, with the exception of the 475-year return period. Similar to the settlement comparison plots, the 50th and 84th percentile ground motions also produced similar results.

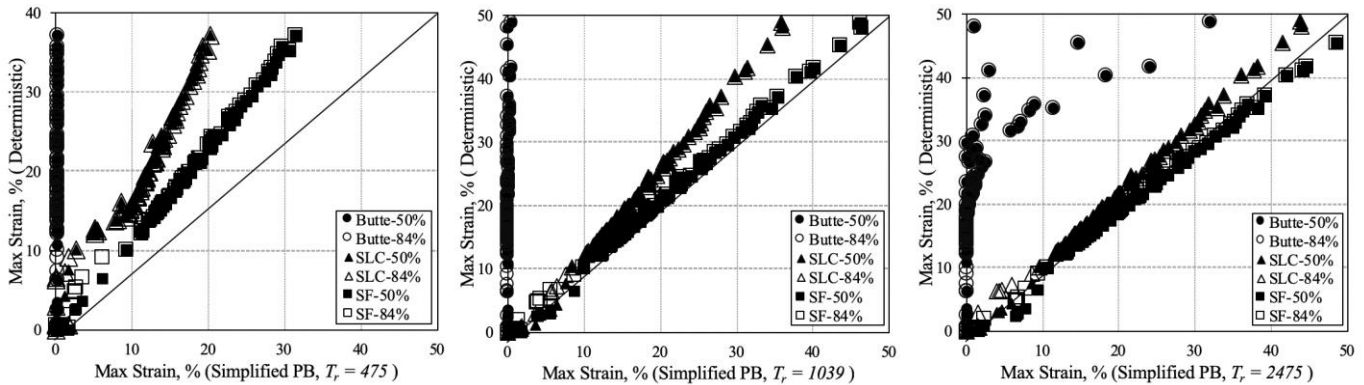


Figure 6-21. Comparison of deterministic and simplified performance-based maximum strains using the Robertson and Wride (2009) model.

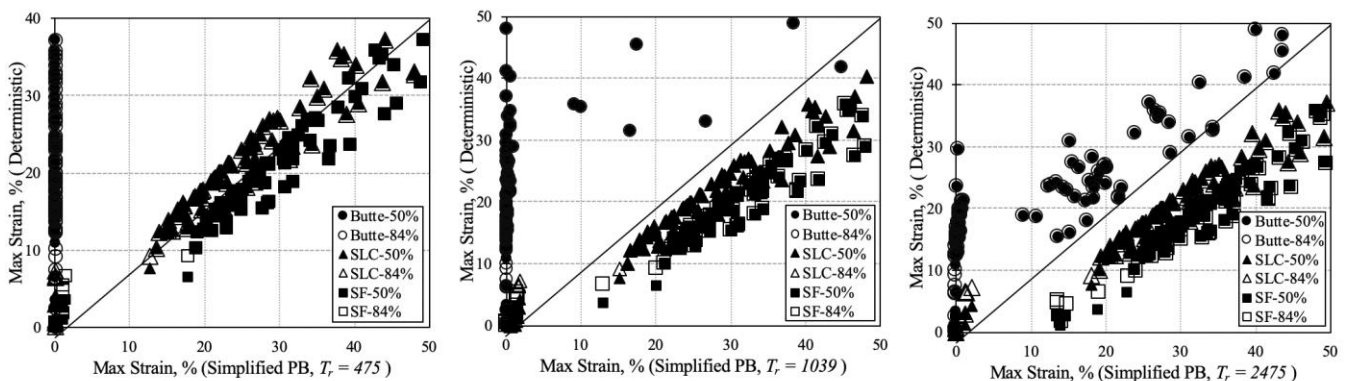


Figure 6-22. Comparison of deterministic and simplified performance-based maximum strains using the Boulanger and Idriss (2014) model.

6.12 Summary

This study analyzed several hazards: liquefaction triggering, post-liquefaction settlement, and lateral spread. The deterministic methods generally predicted significantly more earthquake induced hazard than probabilistic methods in Butte—an area of low seismicity. The deterministic results also generally showed more earthquake induced hazards than the probabilistic results at high return periods in Salt Lake City—an area of medium seismicity. In San Francisco—an area of high seismicity—the deterministic methods predicted slightly lower hazards than the probabilistic method, particularly at higher return periods. These results suggest that the deterministic results could be used as an upper-bound in areas of high seismicity, but in areas of low seismicity, the deterministic analysis could be optional. Engineers performing analyses in areas of medium to high seismicity could choose to use a deterministic analysis as a “reality check” against the simplified performance-based results. If both deterministic and performance-based methods are considered, the *lower of the deterministic and the probabilistic results* should govern the design.

This rule may seem counter-intuitive, but the idea is not completely foreign—when developing a spectral acceleration design envelope, seismic building code (e.g., IBC 2012) permits that the lower of the deterministic and probabilistic accelerations be used in design. Likewise, in a liquefaction hazard analysis, the lower value should govern. If the deterministic value is lower than the performance-based value, the combination of multiple seismic sources in the performance-based analysis may suggest greater liquefaction hazard than would be caused by a single earthquake event. Therefore, the deterministic analysis provides a type of “reality check” against the performance-based analysis, and the deterministic results should be accepted. If the performance-based value is lower than the deterministic value, the nearby governing fault may have a significantly low likelihood of rupturing within the design life of the structure. In this case, the deterministic results could be considered too extreme (especially for some projects which do not need to be designed to withstand such large events). Therefore, the performance-based results should be accepted as a representation of the more *likely* liquefaction hazard.

7.0 CONCLUSIONS

7.1 Summary

The purpose of the research performed was to provide the benefit of the full performance-based probabilistic earthquake hazard analysis using CPT data, without requiring special software, training, and experience. To accomplish this goal, simplified models of liquefaction triggering, lateral spread displacements, and post-liquefaction settlement were developed that reasonably approximate the results of full performance-based analyses. This final report volume for Phase 2 addresses Tasks 5 through 10 of the pooled fund study TPF-5(338) research contract. The Phase 1 final report volume was published separately and addressed Tasks 1 through 4 of the study, including development of a performance-based earthquake engineering (PBEE) liquefaction hazard analysis procedure for the CPT and of an analysis tool, *CPTLiquefy*, to simplify extensive probabilistic calculations.

The objective of this Phase 2 final report volume was to introduce the original models used to determine earthquake hazards (i.e. liquefaction triggering, post-liquefaction settlement, and lateral spread displacement) and provide in-depth derivations that demonstrate the development of the simplified methods and validate the simplified models by performing a site-specific analysis for several different sites. For use with the simplified procedures, liquefaction reference parameter maps were developed for states involved in this study. Comparisons were also provided of the simplified, pseudo-probabilistic, and deterministic procedures to the full performance-based procedure.

To assist in implementing the simplified procedures, a tool was created to perform the simplified calculations, called *CPTLiq*. *CPTLiq* is available in spreadsheet format and provides an easily implemented procedure. A step-by-step process is provided in a user's manual additional to this report, and will assist in the use of the *CPTLiq* tool in those states for which liquefaction parameter maps have been developed.

7.2 Limitations and Challenges

During the production of this report, a bias caused by the use of the 2014 MSF was discovered. However, upon further research, it was decided that the use of the 2012 MSF would be better suited for the simplified procedure. It is also important to remember that the simplified Ku et al. (2012) model uses Boulanger and Idriss (2014) relationships to define values of $q_{req} > 165$.

In the computational tool *CPTLiquefy*, γ_{max} was capped at 51.2% (Zhang et al., 2012). Users of the simplified performance-based lateral spread procedure need to be aware that all the lateral spread correction equations are based on the assumption that γ_{max} does not exceed 51.2%. Modifications to the equations may be needed if a new maximum value has been re-set.

Users of the simplified performance-based methods should be aware that the simplified method is trying to estimate the results of a very complex procedure with a few correction equations; errors are inevitable. In addition, even though the cities and soil profiles that have been selected represent a diverse combination of seismicity and soil conditions, the correction equations may not perform as well for other locations and profiles that have not been tested.

REFERENCES

Liquefaction Triggering:

- Boulanger, R. W., and Idriss, I. M. (2012). Probabilistic standard penetration test-based liquefaction-triggering procedure. *J. Geotech. Geoenviron. Eng.*, 10.1061/(ASCE)GT.1943-5606.0000700, 1185–1195.
- Boulanger, R. W., and Idriss, I. M. (2014). CPT and SPT based liquefaction triggering procedures. *Rep. UCD/CGM-14/01*, Dept. of Civil and Environmental Engineering, Univ. of California–Davis, Davis, CA.
- Cetin, K. O., et al. (2004). Standard penetration test-based probabilistic and deterministic assessment of seismic soil liquefaction potential. *J. Geotech. Geoenviron. Eng.*, 10.1061/(ASCE)1090-0241(2004)130:12(1314), 1314–1340.
- Cornell, C.A., and Krawinkler, H. (2000). Progress and challenges in seismic performance assessment. *PEER News*, April, 1-3. Deierlein, G.G., Krawinkler, H., and Cornell, C.A. (2003). A framework for performance-based earthquake engineering, Proc., 2003 Pacific Conference on Earthquake Engineering.
- Franke, K. and Wright, A. (2013) An Alternative Performance-Based Liquefaction Initiation Procedure for the Standard Penetration Test. *Geo-Congress 2013*, 10.1061/9780784412787.086, 846-849.
- Franke, K., Wright, A., and Ekstrom, L. (2014b). Comparative Study between Two Performance-Based Liquefaction Triggering Models for the Standard Penetration Test. *J. Geotech. Geoenviron. Eng.*, 10.1061/(ASCE)GT.1943-5606.0001094, 04014010.
- Franke, K.W., Wright, A.D., and Hatch, C.K. (2014c). PBLiquefY: A new analysis tool for the performance-based evaluation of liquefaction triggering. Proceedings, 10th National Conference on Earthquake Engineering, Paper No. 87, EERI, Oakland, CA.
- Franke, K.W., Mayfield, R.T., and Wright, A.D. (2014d). Simplified uniform hazard analysis for bridges, *Transportation Research Record*, TRB, in press, Washington D.C.
- Idriss, I.M., and Boulanger, R.W. (2008). *Soil liquefaction during earthquakes*. Monograph MNO-12, Earthquake Engineering Research Institute, Oakland, CA 261 pp.
- Idriss, I. M., and Boulanger, R. W. (2010). SPT-based liquefaction triggering procedures. *Rep. UCD/CGM-10/02*, Dept. of Civil and Environmental Engineering, Univ. of California–Davis, Davis, CA.

- Kramer, S.L. (2008). Evaluation of liquefaction hazards in Washington State. WSDOT Report WA-RD 668.1, 152 pp.
- Kramer, S.K., Franke, K.W., Huang, Y.-M., and Baska, D. (2007). Performance-based evaluation of lateral spreading displacement. *Proceedings, 4th International Conference on Earthquake Geotechnical Engineering*, Paper No. 1208, Thessaloniki, Greece, June 2007.
- Ku, C.-S., Juang, C. H., Chang, C.-W., and Ching, J. (2012). “Probabilistic version of the Robertson and Wride method for liquefaction evaluation: development and application.” *Canadian Geotechnical Journal*, 49(1), 27-44.
- Mayfield, R. T., Kramer, S. L., and Huang, Y.-M. (2010). Simplified approximation procedure for performance-based evaluation of liquefaction potential. *J. Geotech. Geoenviron. Eng.*, 10.1061/(ASCE) GT.1943-5606.0000191, 140–150.
- Seed, H.B. (1979). Soil liquefaction and cyclic mobility evaluation for level ground during earthquakes. *J. Geotech. Eng. Div.*, 105(GT2), p. 201-255.
- Seed, H.B. and Idriss, I.M. (1971). Simplified procedure for evaluating soil liquefaction potential,” *J. Soil Mech. and Found. Div.*, 97(SM9), p. 1249-1273.
- Seed, H.B. and Idriss, I.M. (1982). *Ground Motions and Soil Liquefaction During Earthquakes*. EERI, Oakland, CA, 134 pp.
- Seed, H.B., Tokimatsu, K., Harder, L.F. Jr., and Chung, R. (1985). Influence of SPT procedures in soil liquefaction resistance evaluations, *J. Geotech. Eng.*, 111(12), p. 1425-1445.
- Stewart, J.P., Liu, A.H., and Choi, Y. (2003). Amplification factors for spectral acceleration in tectonically active regions. *Bull. Seismol. Soc. Am.*, 93(7): 332-352.
- Ulmer, K. J. (2015). “Development of a Simplified Performance-Based Procedure for Assessment of Liquefaction Triggering Using Liquefaction Loading Maps.” M.S. *Thesis, 2015, Brigham Young University, Provo, UT.*
- USGS. (2014). USGS Unified Hazard Tool <https://earthquake.usgs.gov/hazards/interactive/> (October 25, 2018).

Liquefaction Settlement and Lateral Spread:

- Boulanger, R., & Idriss, I. (2012). Probabilistic Standard-Penetration Test-Based Liquefaction-Triggering Procedure. *Journal of Geotechnical and Geoenvironmental Engineering*, 1185-1195.

- Bray, J. D., ASCE, F., & Travasarou, T. (2007, April). Simplified Procedure for Estimating Earthquake-Induced Deviatoric Slope Displacements. *Journal of Geotechnical and Geoenvironmental Engineering*, 381-392.
- Cetin, K. O., & al., e. (2009, March). Probabilistic Model for the Assessment of Cyclical Induced Reconsolidation (Volumetric) Settlements. *Journal of Geotechnical and Geoenvironmental Engineering*, 387-396.
- Cetin, K. O., Seed, R. B., Kiureghian, A. D., Tokimatsu, K., Harder Jr., L. F., Kayen, R. E., & Moss, R. E. (2004, December). Standard Penetration Test-Based Probabilistic and Deterministic Assessment of Seismic Soil Liquefaction Potential. *Journal of Geotechnical and Geoenvironmental Engineering*, 1314-1340.
- Franke, K., Mayfield, R., & and Wright, A. (2014d). Simplified uniform hazard analysis for bridges. *Transportation Research Record*. Washington D.C.
- Franke, K., Wright, A., & Hatch, C. (2014c). PBLiquefY: A new analysis tool for the performance-based evaluation of liquefaction triggering. *Proceedings, 10th National Conference on Earthquake Engineering*. Oakland, CA: EERI.
- Huang, Y.-M. (2008). *Performance-based design and evaluation for liquefaction-related seismic hazards*. Seattle, Washington: University of Washington.
- Idriss, I., & Boulanger, R. (2008). Soil liquefaction during earthquakes. *Monograph MNO-12* (p. 261 pp). Oakland, CA: Earthquake Engineering Research Institute.
- Ishihara, K., & Yoshimine, M. (1992). Evaluation of settlements in sand deposits following liquefaction during earthquakes. *Soils Found.*, 32, 173-188.
- Kramer, S. L. (2008). *Evaluation of liquefaction hazards in Washington State*. Seattle: WSDOT Report.
- Kramer, S. L. (2014). Performance-based design methodologies for geotechnical earthquake engineering. *Bull Earthquake Engineering*, 1049-1070.
- Mayfield, R. T., Kramer, S. L., & Huang, Y.-M. (2010, January). Simplified Approximation Procedure for Performance-Based Evaluation on Liquefaction Potential. *Journal of Geotechnical and Geoenvironmental Engineering*, 140-150.
- Rathje, E. M., & Saygili, G. (2009, March). Probabilistic Assessment of Earthquake-Induced Sliding Displacements of Natural Slopes. *Bulletin of the New Zealand Society of Earthquake Engineering*, 42(1), 18-27.

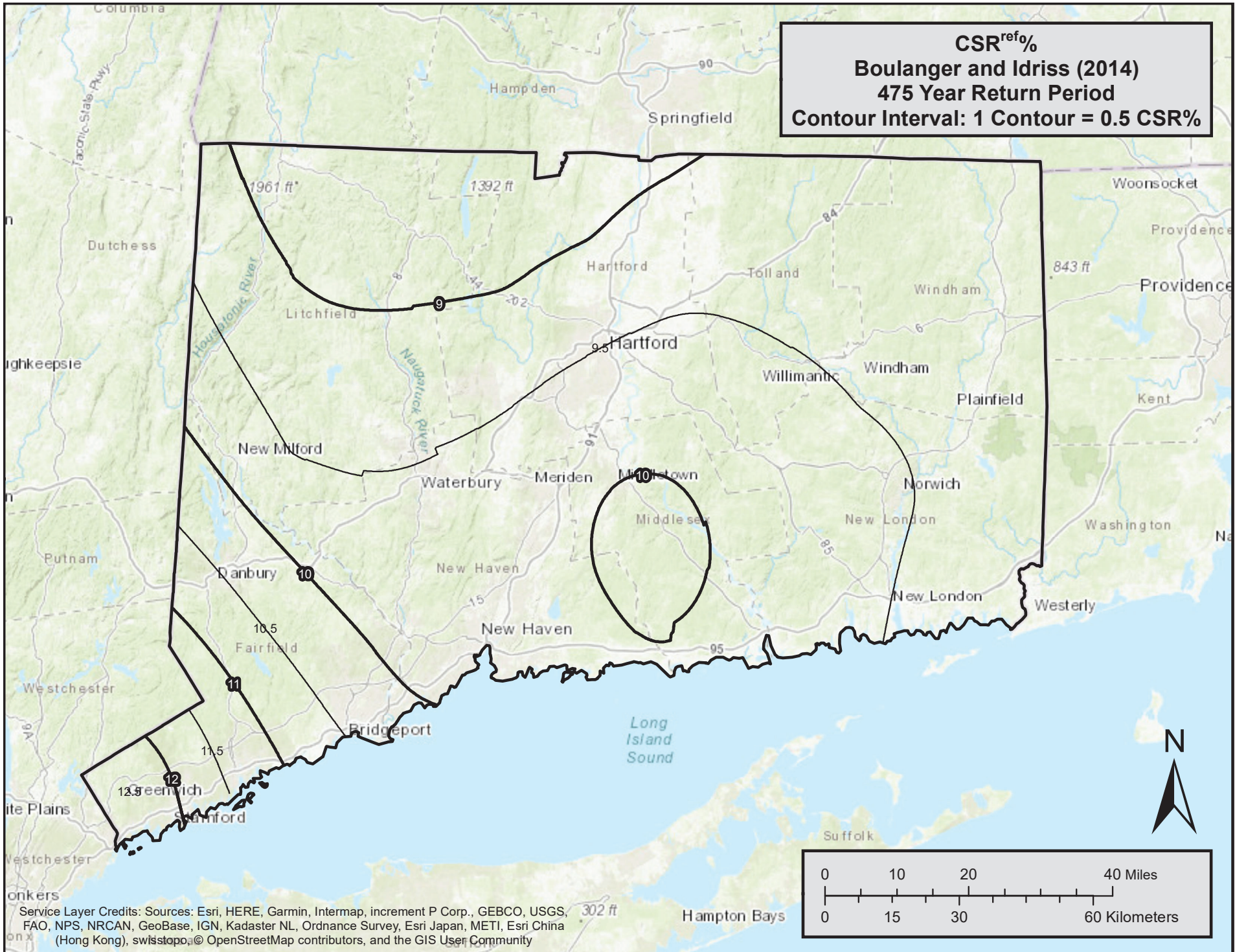
- Shamoto, Y., Zhang, J.-M., & Tokimatsu, K. (1998). New charts for predicting large residual post-liquefaction ground deformation. *Soil Dynamics and Earthquake Engineering*, 427-438.
- Tokimatsu, K., & Seed, B. H. (1987). Evaluation of settlements in sand due to earthquake shaking. *Journal of Geotechnical and Geoenvironmental Engineering*, 861-878.
- USGS. (2013, May 17). *2008 Interactive Deaggregations*. Retrieved June 2015, from Geologic Hazards Science Center: <http://geohazards.usgs.gov/deaggint/2008/>
- Wu, J., & Seed, R. B. (2004). Estimating liquefaction-induced ground settlement (case studies). *5th International Conf. on Case Histories in Geotechnical Engineering*.
- Youd, T., Hansen, C., & Bartlett, S. (2002). Revised multilinear regression equations for prediction of lateral spread displacement. *Journal of Geotechnical and Geoenvironmental Engineering*, 128(12), 1007-1017.

APPENDIX A: Liquefaction Reference Parameter Maps

For each of the four states participating in the study, the liquefaction reference parameter maps are presented on the following pages. The maps are organized by state in alphabetical order (Connecticut, Oregon, South Carolina, and Utah) and for three return periods in each of the following three sections:

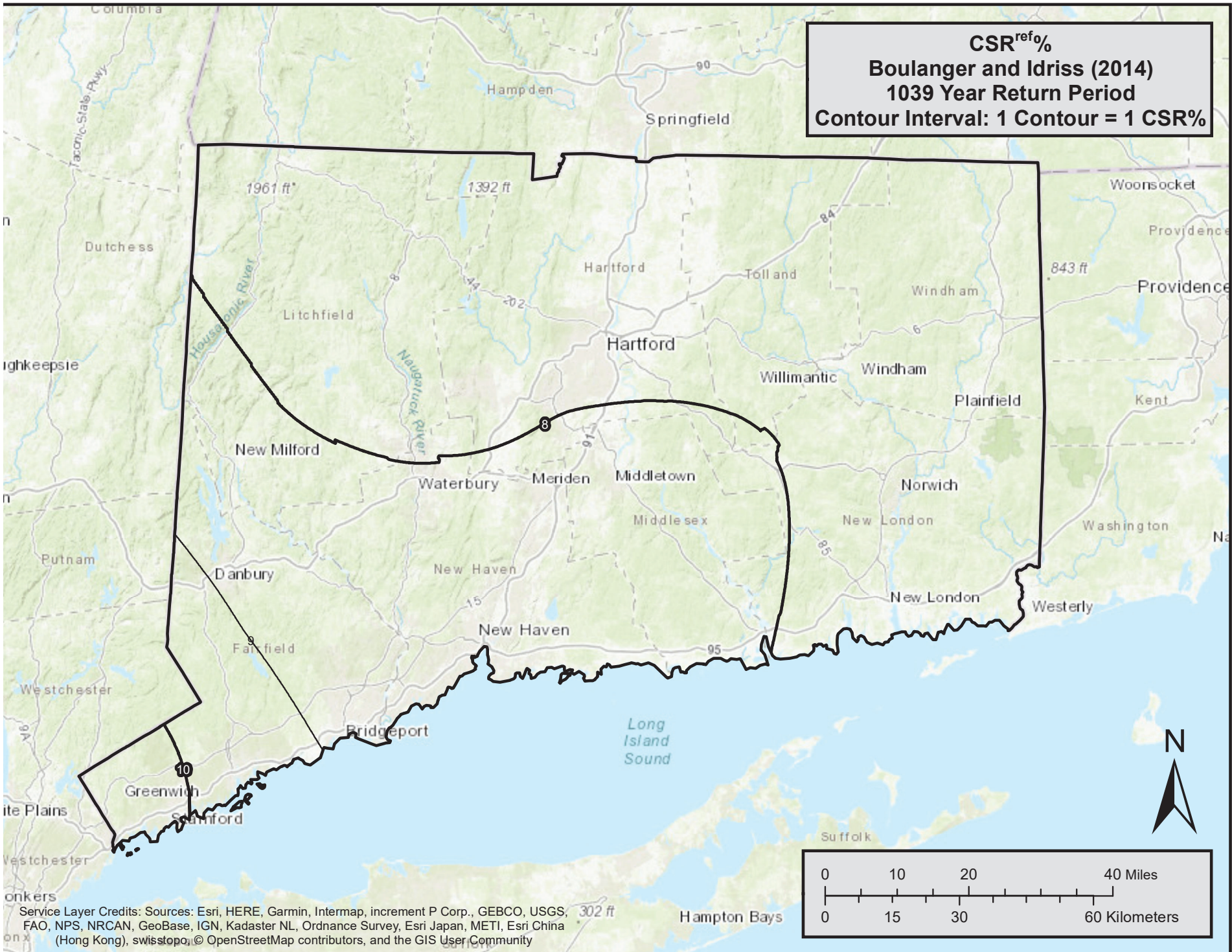
1. Liquefaction Triggering (reference CSR and q_{req})
 - a. Boulanger and Idriss (2014), CSR^{ref} (%)
 - b. Ku et al. (2012), q_{req}^{ref}
2. Settlement (reference vertical strain)
 - a. Boulanger and Idriss (2014), ε_v^{ref} (%)
 - b. Ku et al. (2012), ε_v^{ref} (%)
3. Lateral Spread (reference horizontal strain)
 - a. Boulanger and Idriss (2014), γ_{max}^{ref} (%)
 - b. Ku et al. (2012), γ_{max}^{ref} (%)

CSR^{ref}%
Boulangier and Idriss (2014)
475 Year Return Period
Contour Interval: 1 Contour = 0.5 CSR%

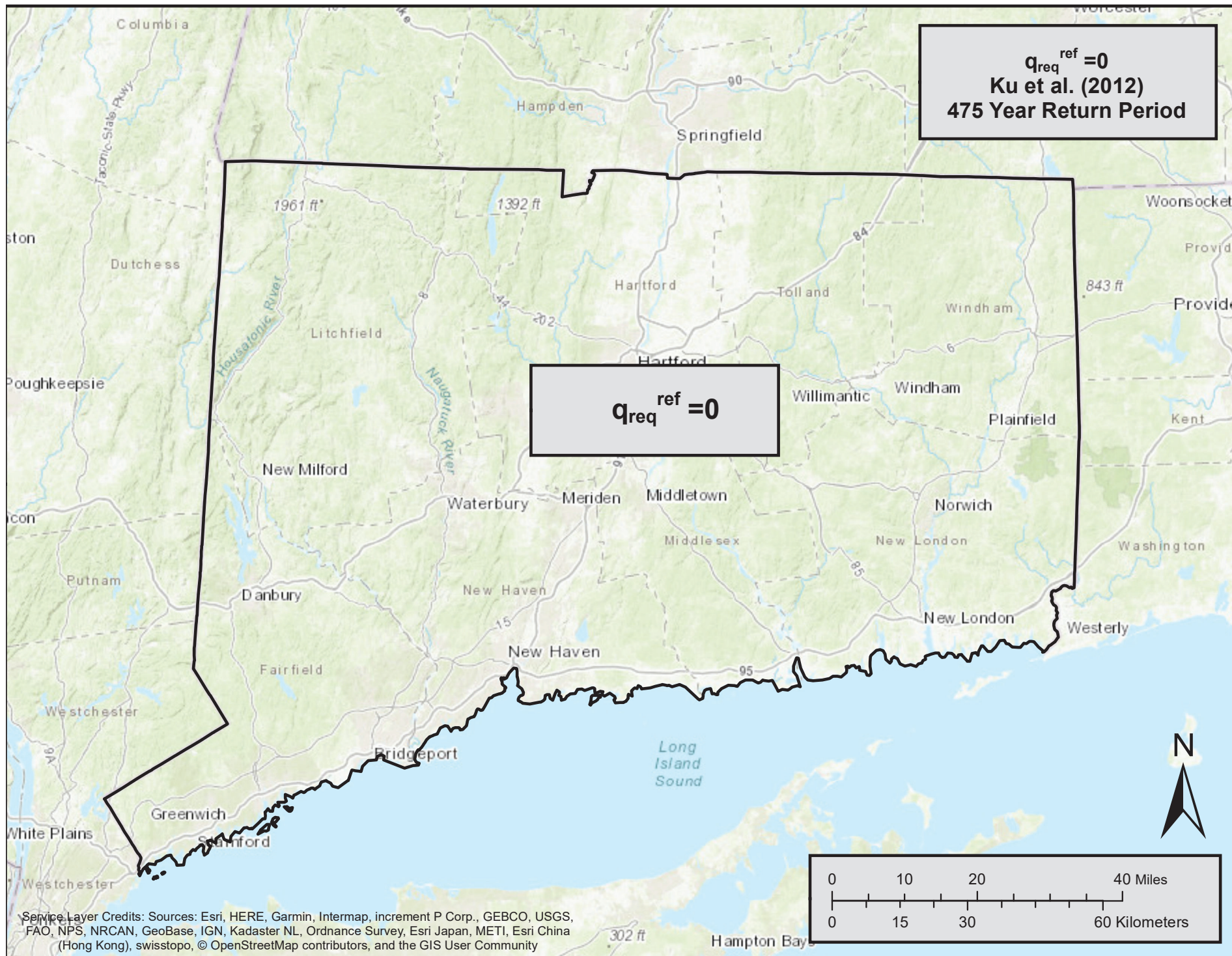


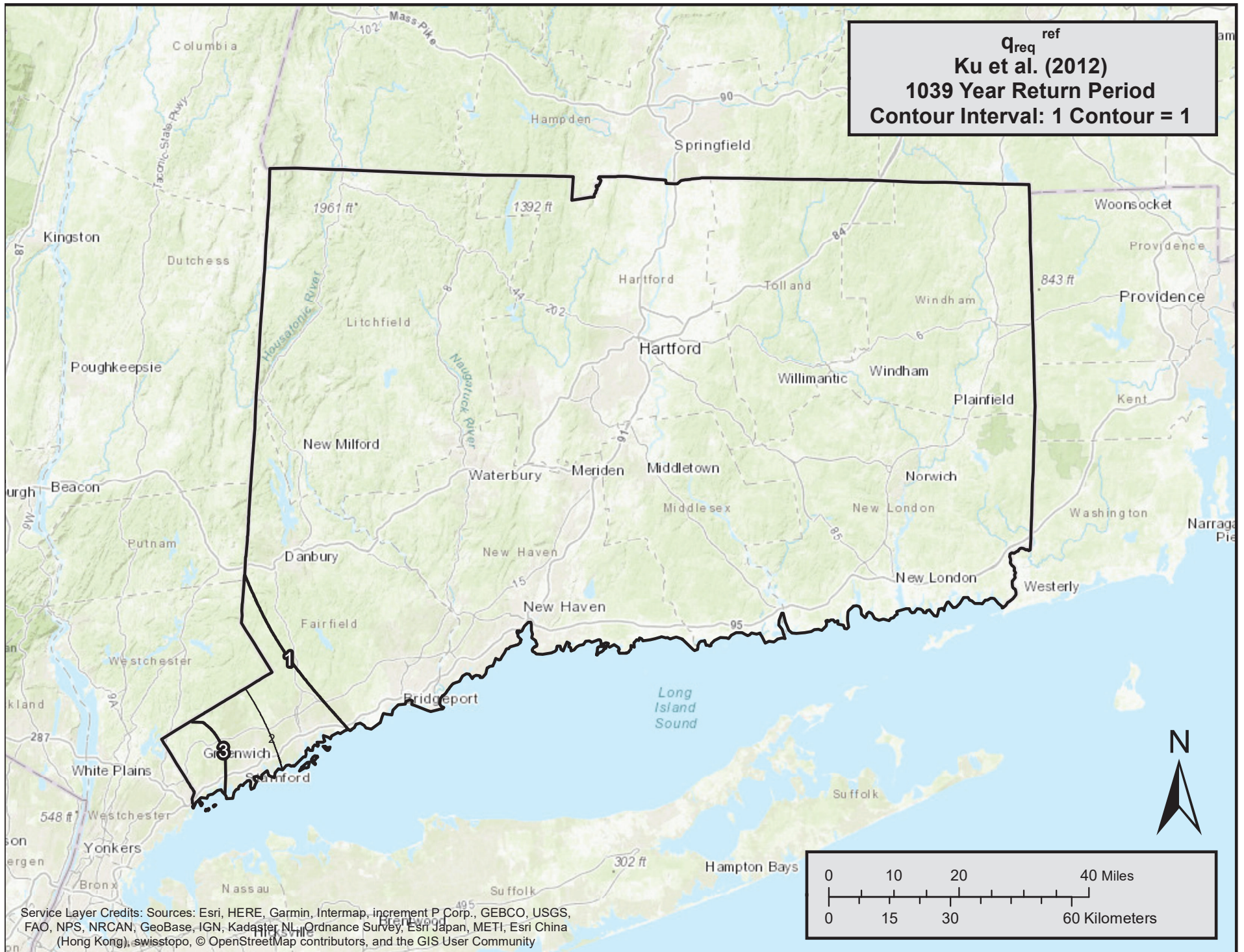
Service Layer Credits: Sources: Esri, HERE, Garmin, Intermap, increment P Corp., GEBCO, USGS, FAO, NPS, NRCAN, GeoBase, IGN, Kadaster NL, Ordnance Survey, Esri Japan, METI, Esri China (Hong Kong), swisstopo, © OpenStreetMap contributors, and the GIS User Community

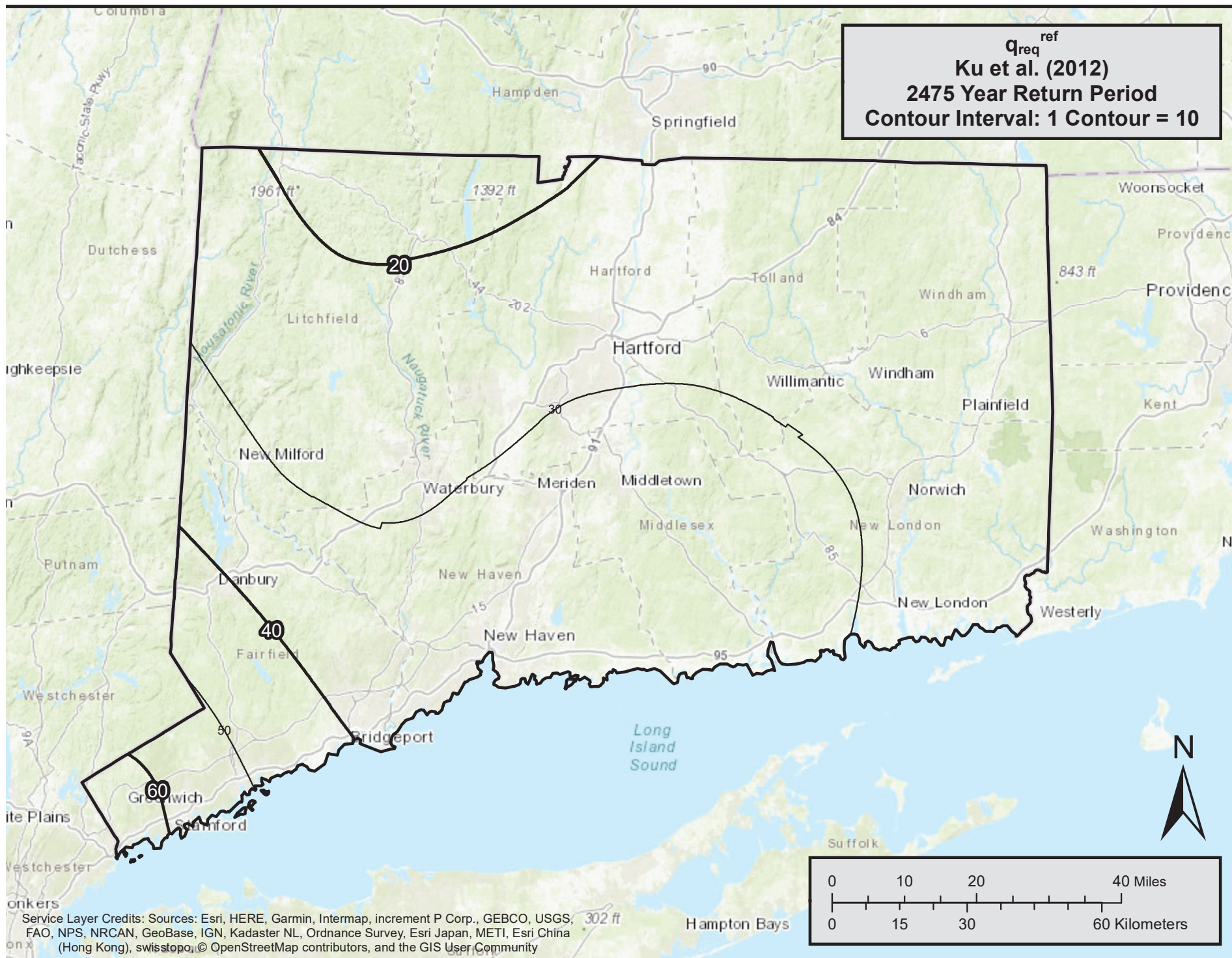
CSR^{ref}%
Boulanger and Idriss (2014)
1039 Year Return Period
Contour Interval: 1 Contour = 1 CSR%

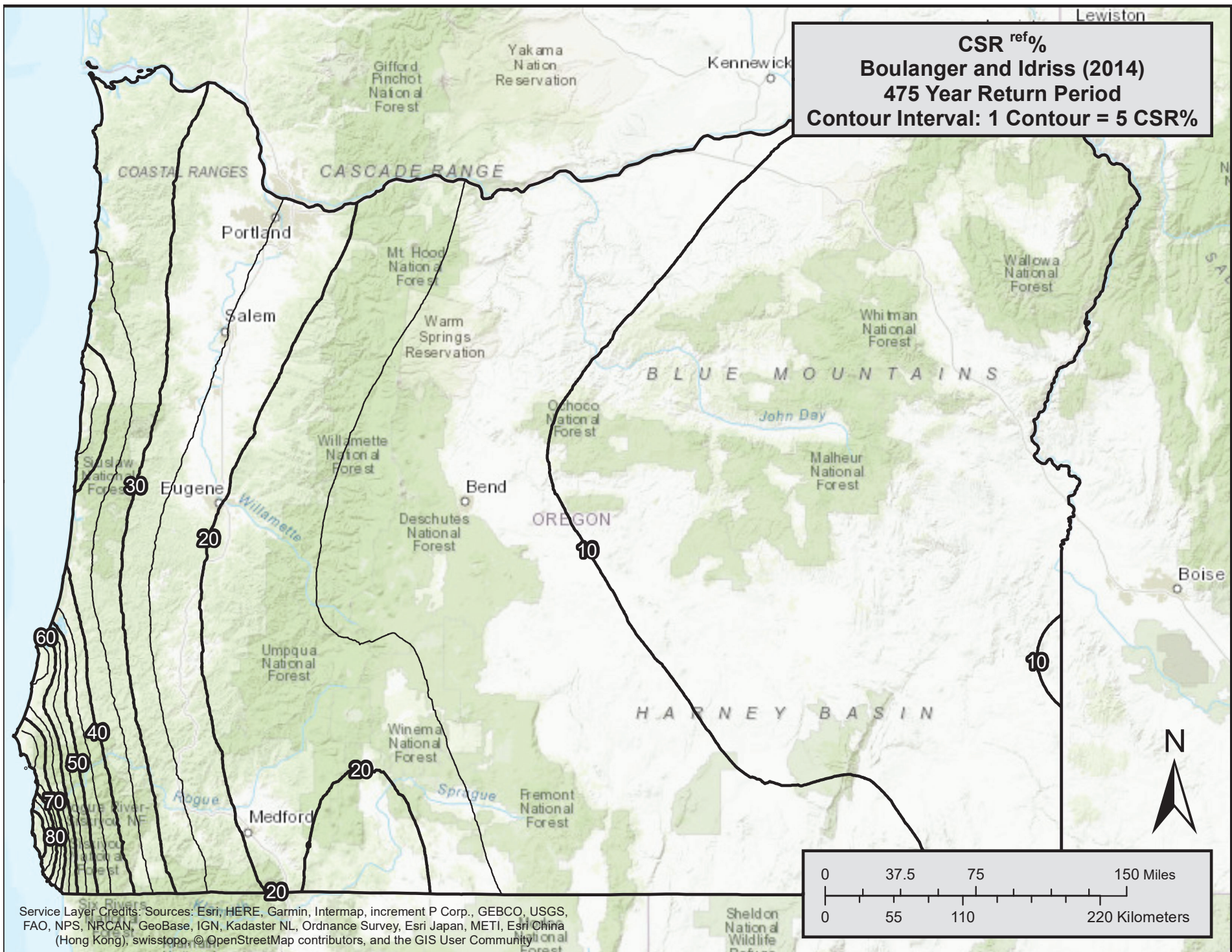


Service Layer Credits: Sources: Esri, HERE, Garmin, Intermap, increment P Corp., GEBCO, USGS, FAO, NPS, NRCAN, GeoBase, IGN, Kadaster NL, Ordnance Survey, Esri Japan, METI, Esri China (Hong Kong), swisstopo, © OpenStreetMap contributors, and the GIS User Community



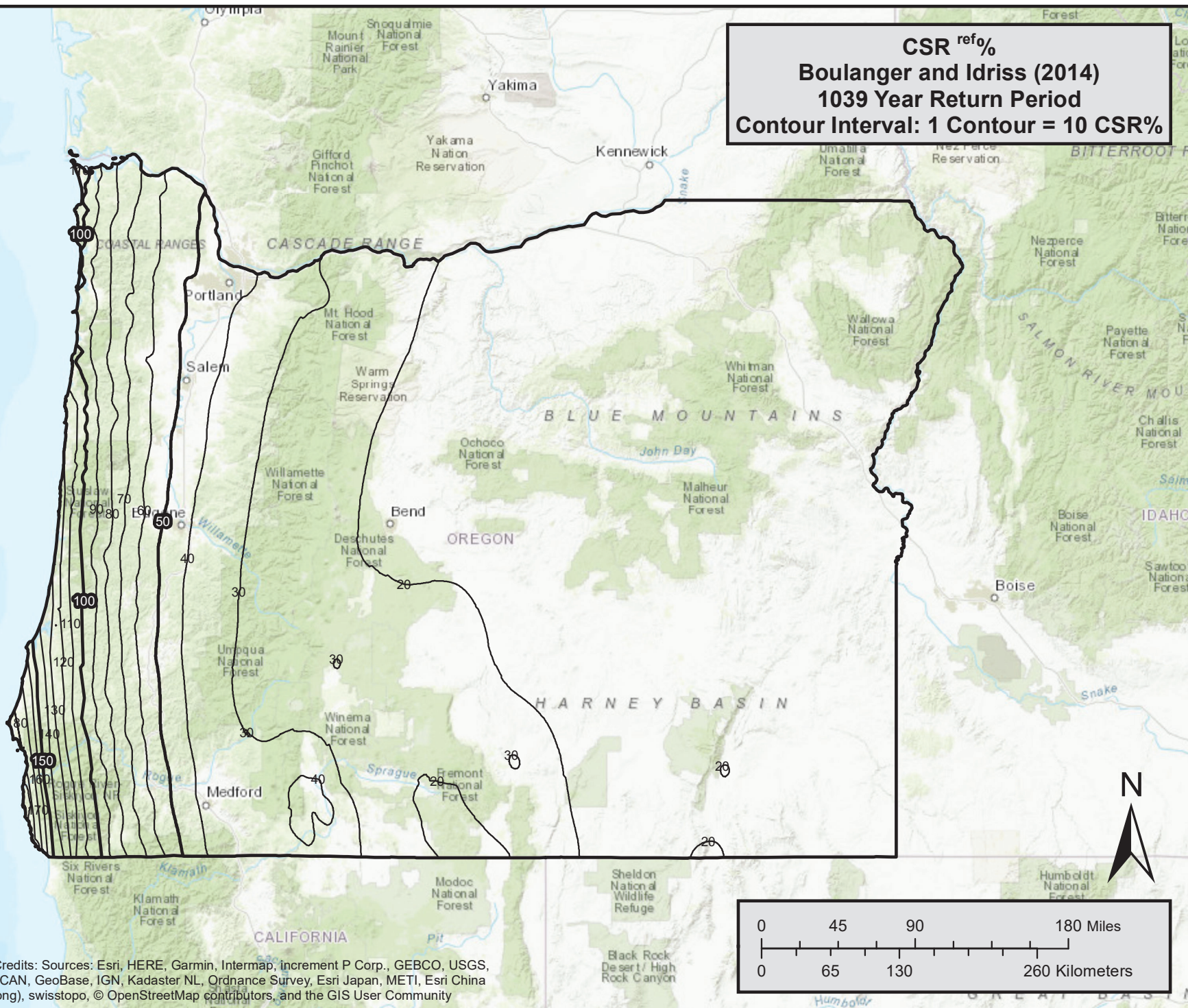






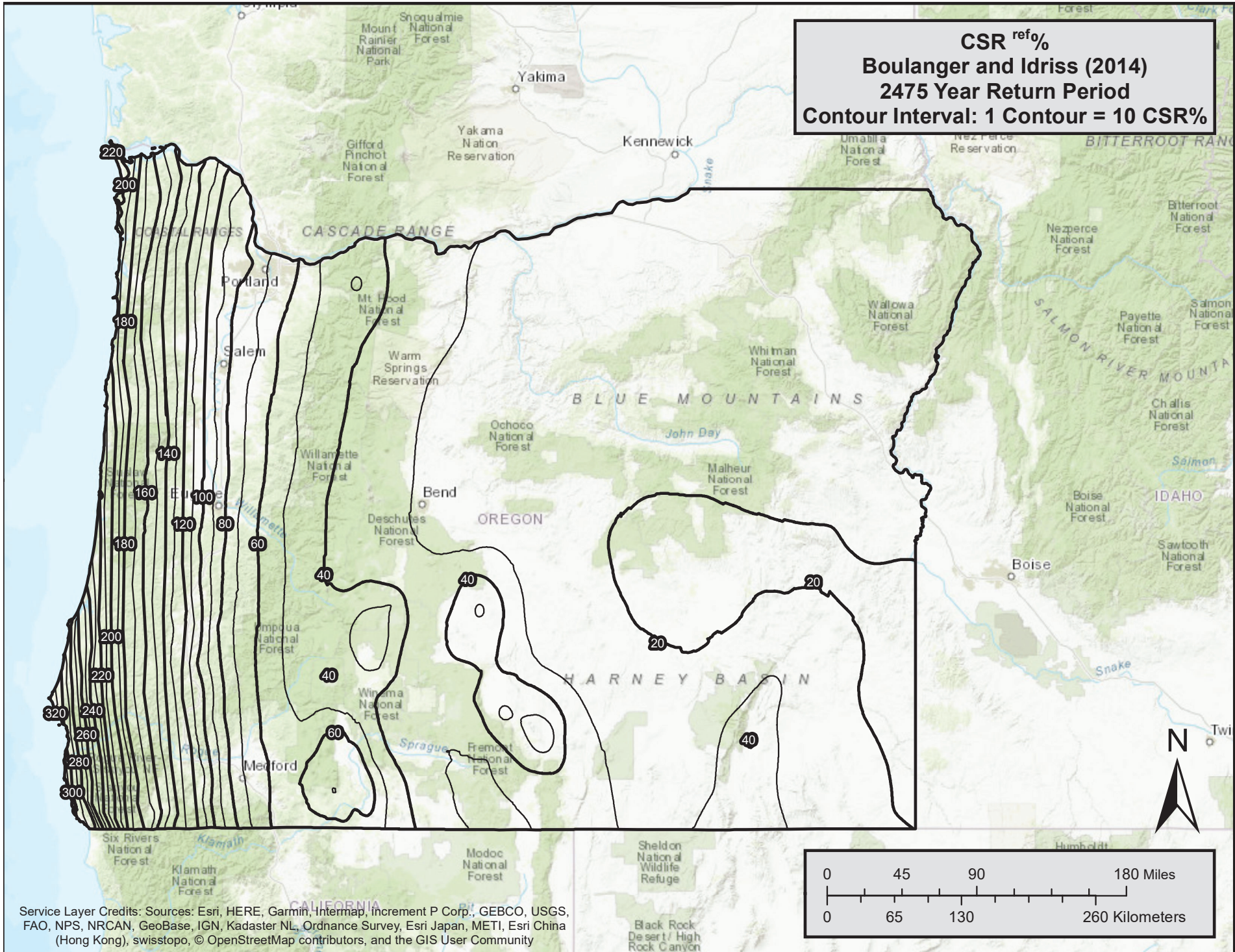
Service Layer Credits: Sources: Esri, HERE, Garmin, Intermap, increment P Corp., GEBCO, USGS, FAO, NPS, NRCAN, GeoBase, IGN, Kadaster NL, Ordnance Survey, Esri Japan, METI, Esri China (Hong Kong), swisstopo, © OpenStreetMap contributors, and the GIS User Community

CSR^{ref}%
Boulanger and Idriss (2014)
1039 Year Return Period
Contour Interval: 1 Contour = 10 CSR%

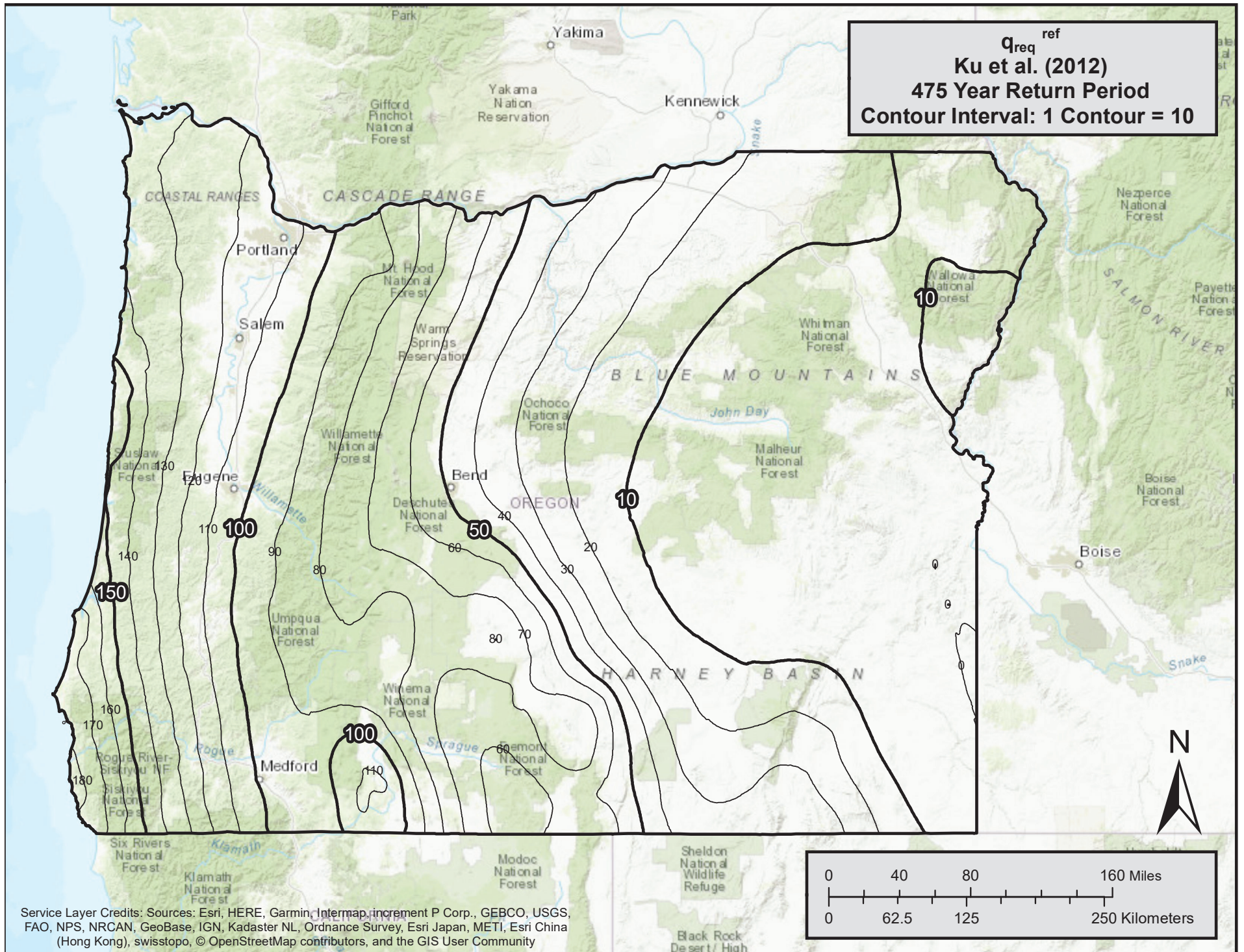


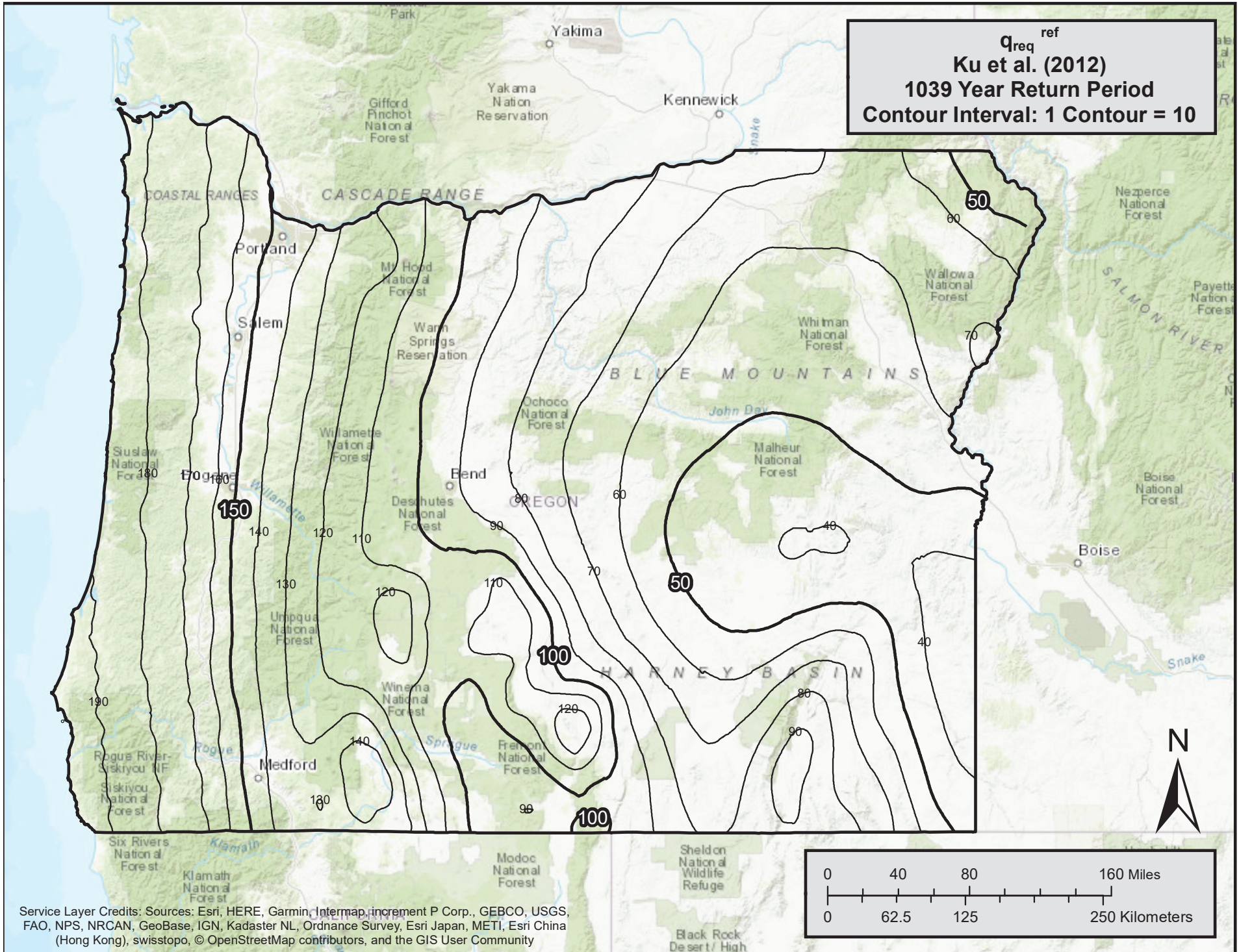
Service Layer Credits: Sources: Esri, HERE, Garmin, Intermap, increment P Corp., GEBCO, USGS, FAO, NPS, NRCAN, GeoBase, IGN, Kadaster NL, Ordnance Survey, Esri Japan, METI, Esri China (Hong Kong), swisstopo, © OpenStreetMap contributors, and the GIS User Community

CSR^{ref}%
Boulanger and Idriss (2014)
2475 Year Return Period
Contour Interval: 1 Contour = 10 CSR%

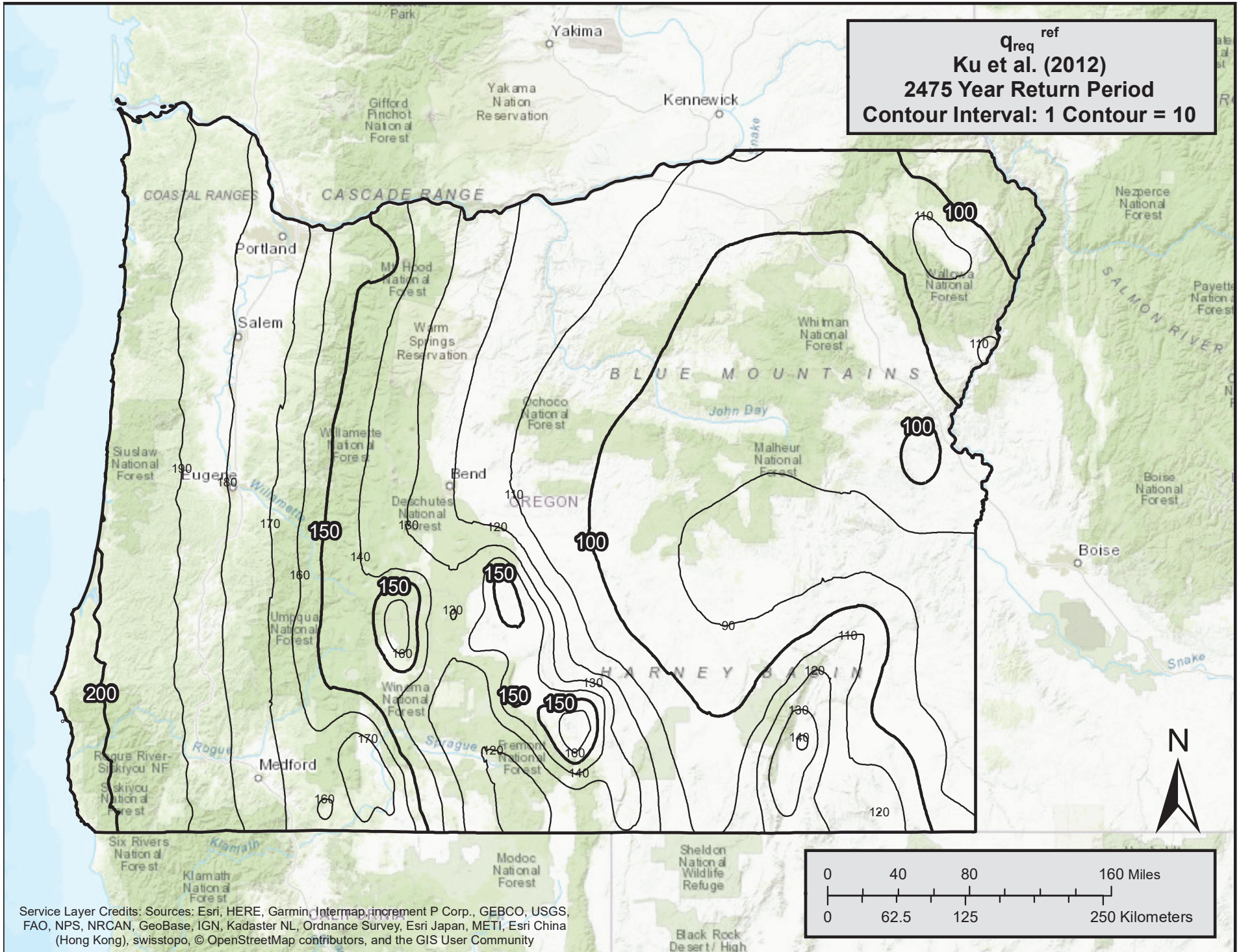


Service Layer Credits: Sources: Esri, HERE, Garmin, Intermap, increment P Corp., GEBCO, USGS, FAO, NPS, NRCAN, GeoBase, IGN, Kadaster NL, Ordnance Survey, Esri Japan, METI, Esri China (Hong Kong), swisstopo, © OpenStreetMap contributors, and the GIS User Community

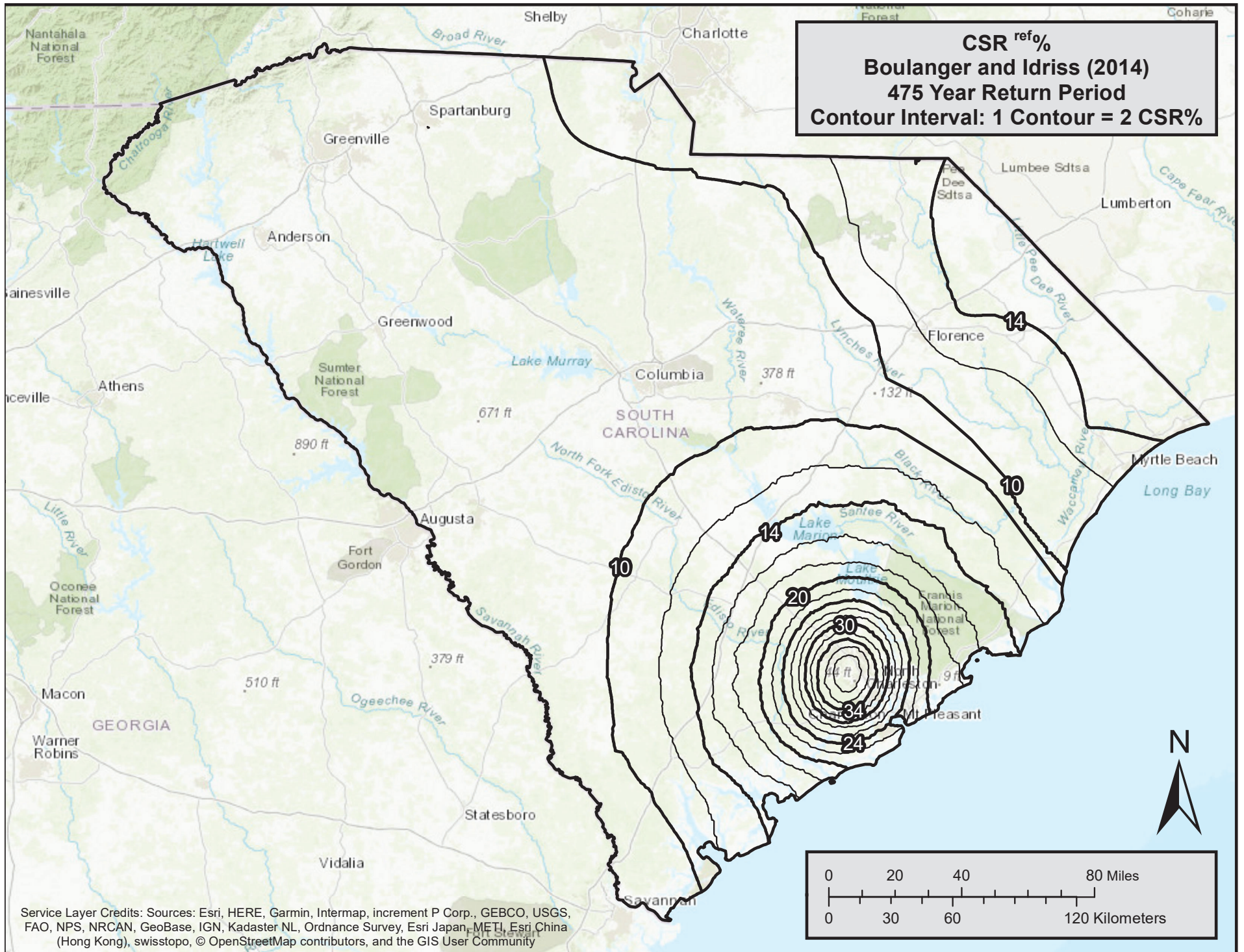


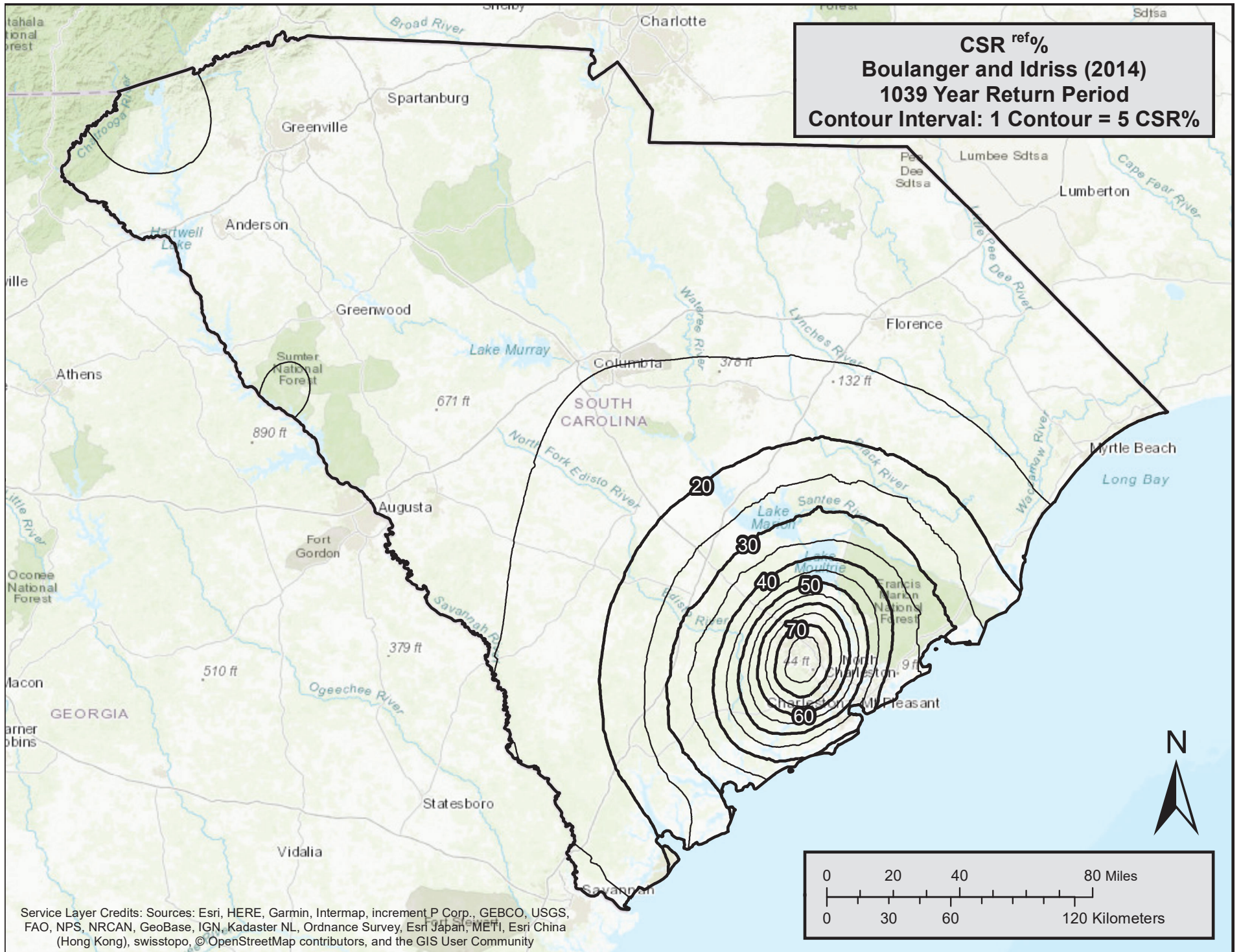


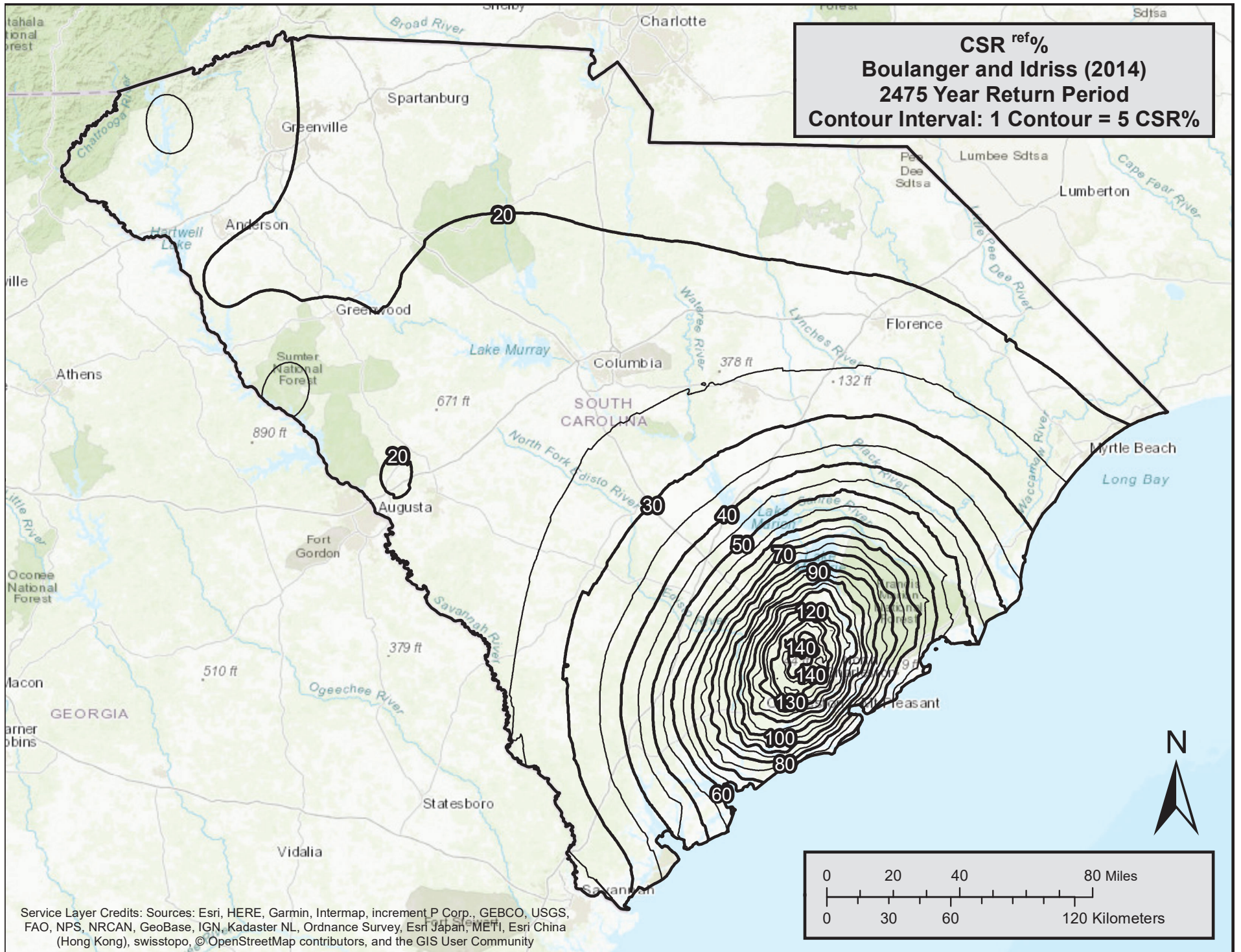
Service Layer Credits: Sources: Esri, HERE, Garmin, Intermap, increment P Corp., GEBCO, USGS, FAO, NPS, NRCAN, GeoBase, IGN, Kadaster NL, Ordnance Survey, Esri Japan, METI, Esri China (Hong Kong), swisstopo, © OpenStreetMap contributors, and the GIS User Community



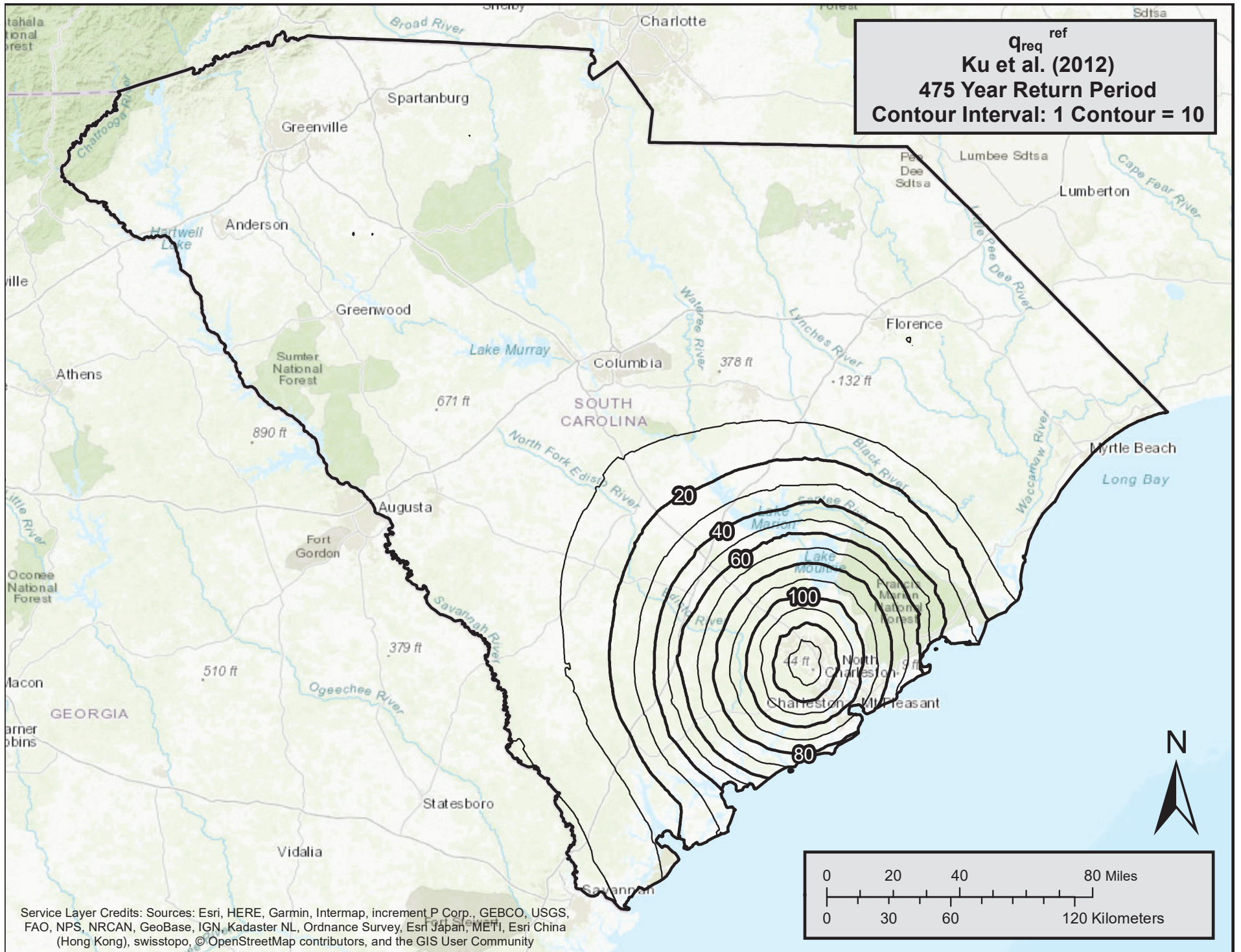
Service Layer Credits: Sources: Esri, HERE, Garmin, Intermap, increment P Corp., GEBCO, USGS, FAO, NPS, NRCAN, GeoBase, IGN, Kadaster NL, Ordnance Survey, Esri Japan, METI, Esri China (Hong Kong), swisstopo, © OpenStreetMap contributors, and the GIS User Community

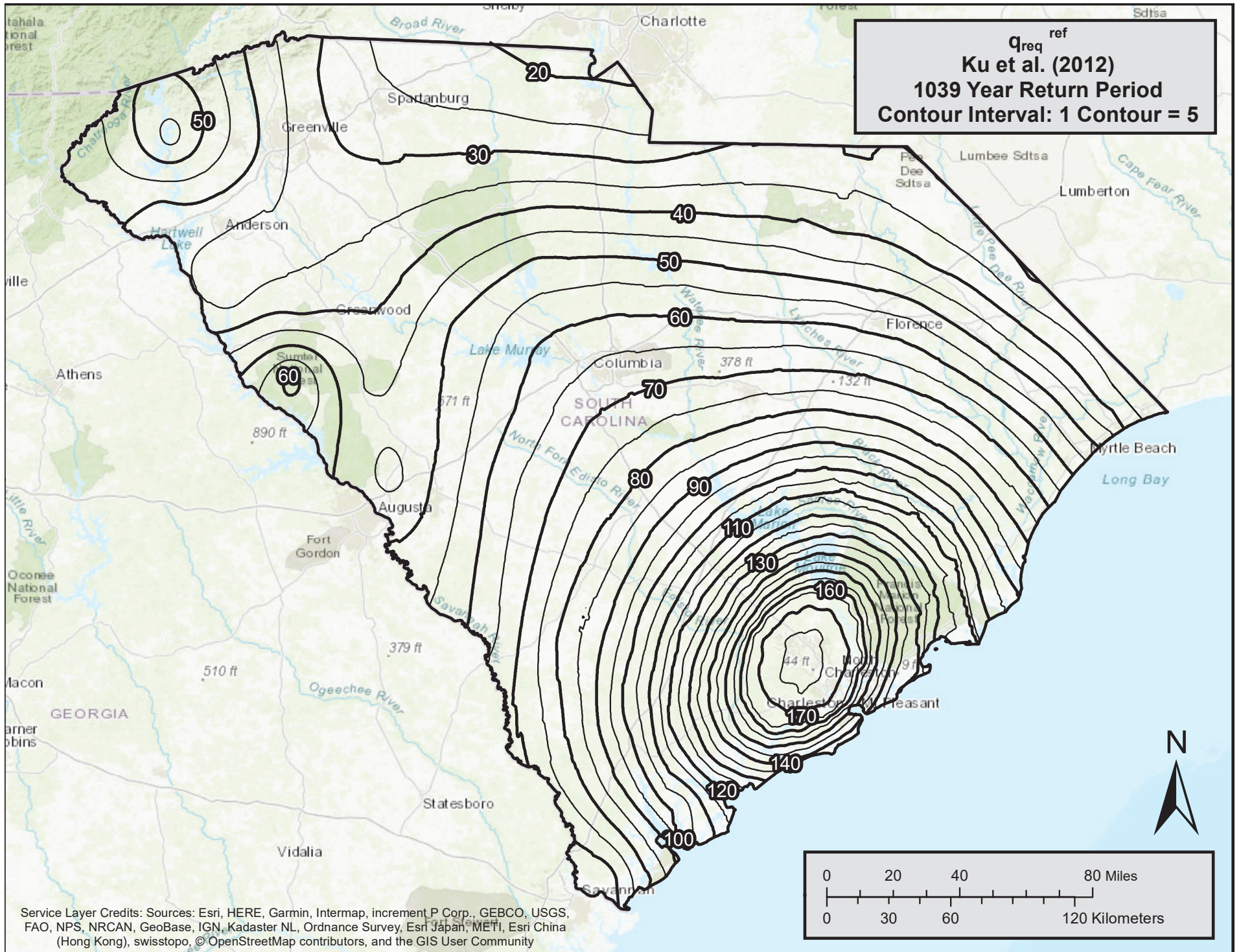


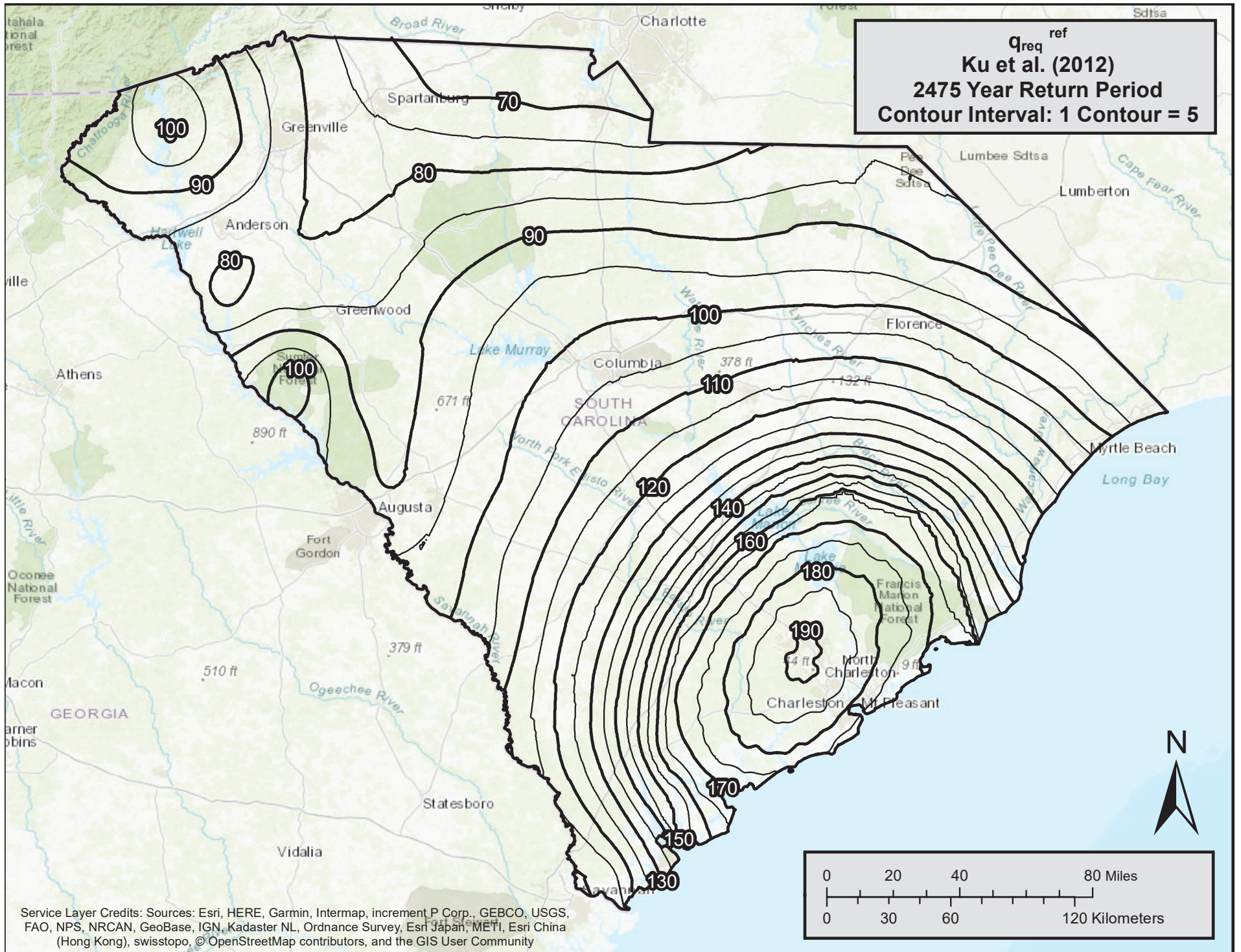




Service Layer Credits: Sources: Esri, HERE, Garmin, Intermap, increment P Corp., GEBCO, USGS, FAO, NPS, NRCAN, GeoBase, IGN, Kadaster NL, Ordnance Survey, Esri Japan, METI, Esri China (Hong Kong), swisstopo, © OpenStreetMap contributors, and the GIS User Community

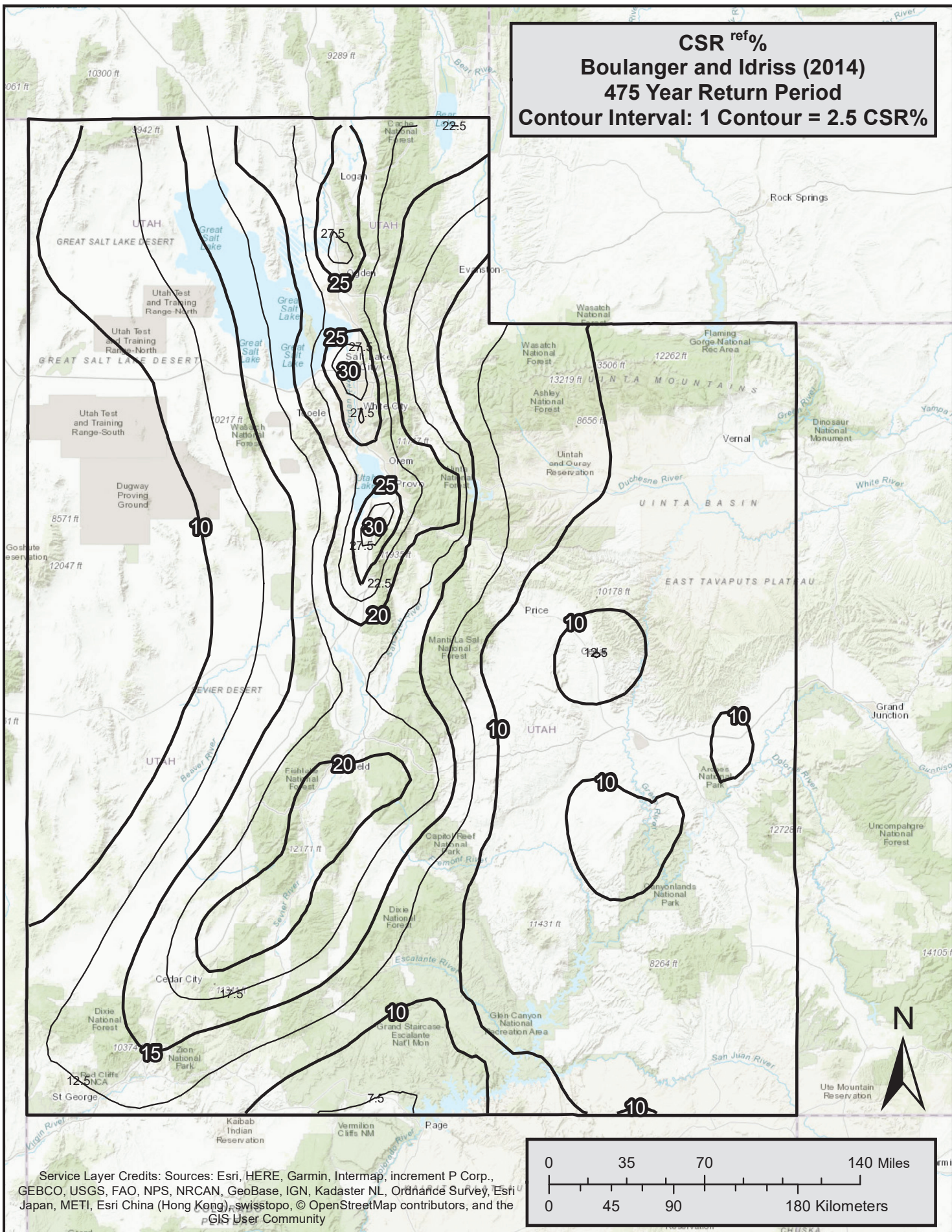






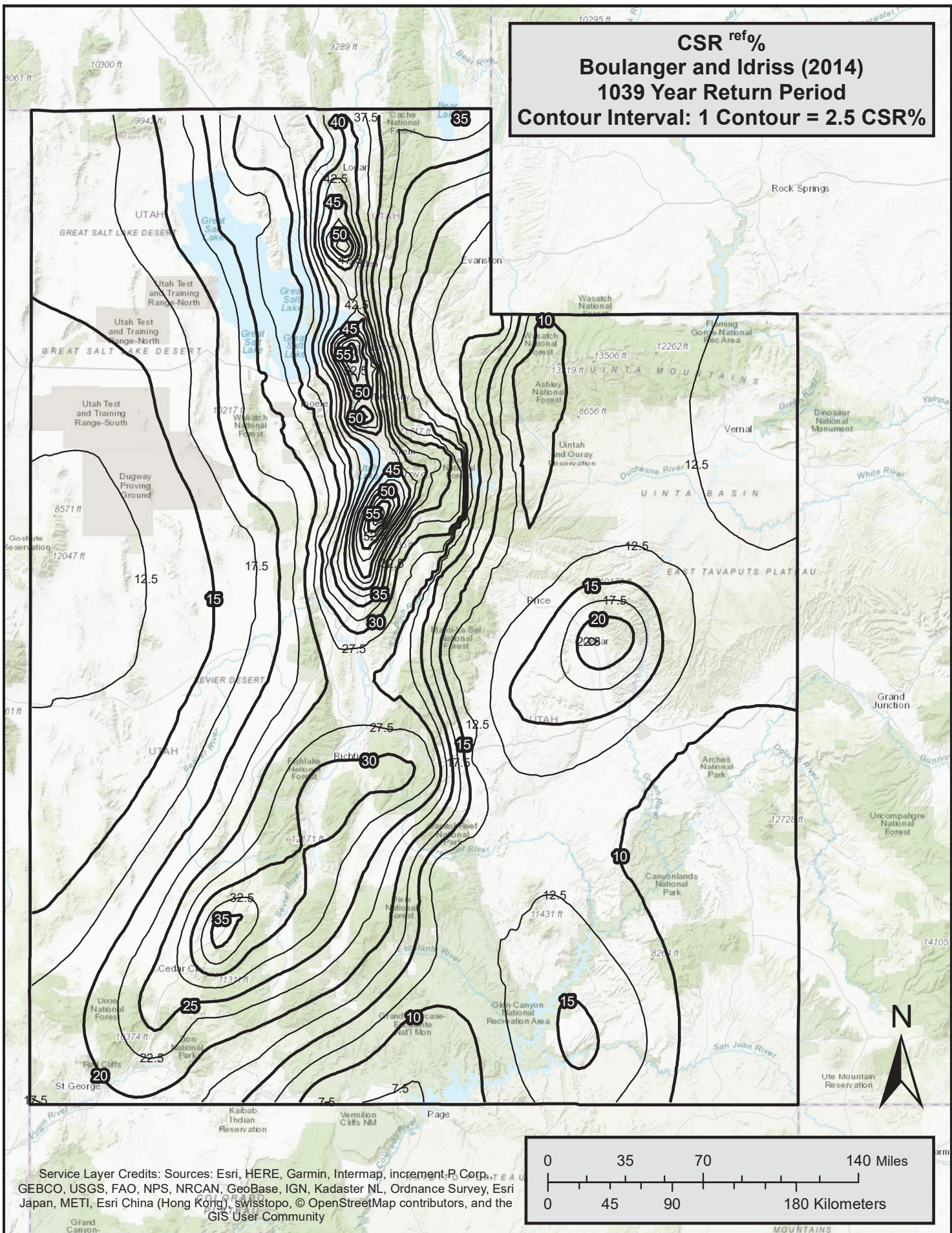
Service Layer Credits: Sources: Esri, HERE, Garmin, Intermap, increment P Corp., GEBCO, USGS, FAO, NPS, NRCAN, GeoBase, IGN, Kadaster NL, Ordnance Survey, Esri Japan, METI, Esri China (Hong Kong), swisstopo, © OpenStreetMap contributors, and the GIS User Community

CSR^{ref%}
Boulanger and Idriss (2014)
475 Year Return Period
Contour Interval: 1 Contour = 2.5 CSR%



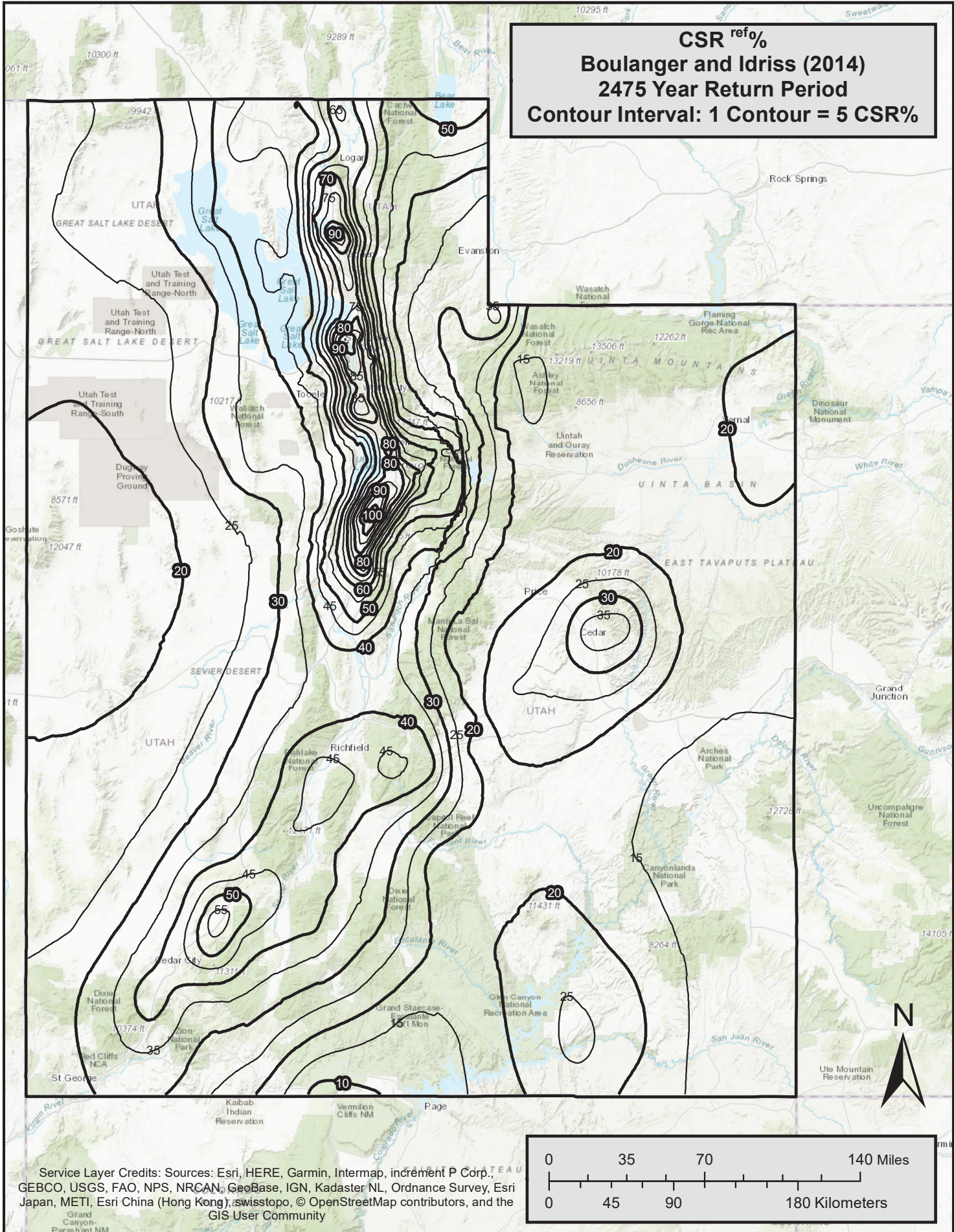
Service Layer Credits: Sources: Esri, HERE, Garmin, Intermap, increment P Corp., GEBCO, USGS, FAO, NPS, NRCAN, GeoBase, IGN, Kadaster NL, Ordnance Survey, Esri Japan, METI, Esri China (Hong Kong), swisstopo, © OpenStreetMap contributors, and the GIS User Community

CSR^{ref%}
Boulanger and Idriss (2014)
1039 Year Return Period
Contour Interval: 1 Contour = 2.5 CSR%

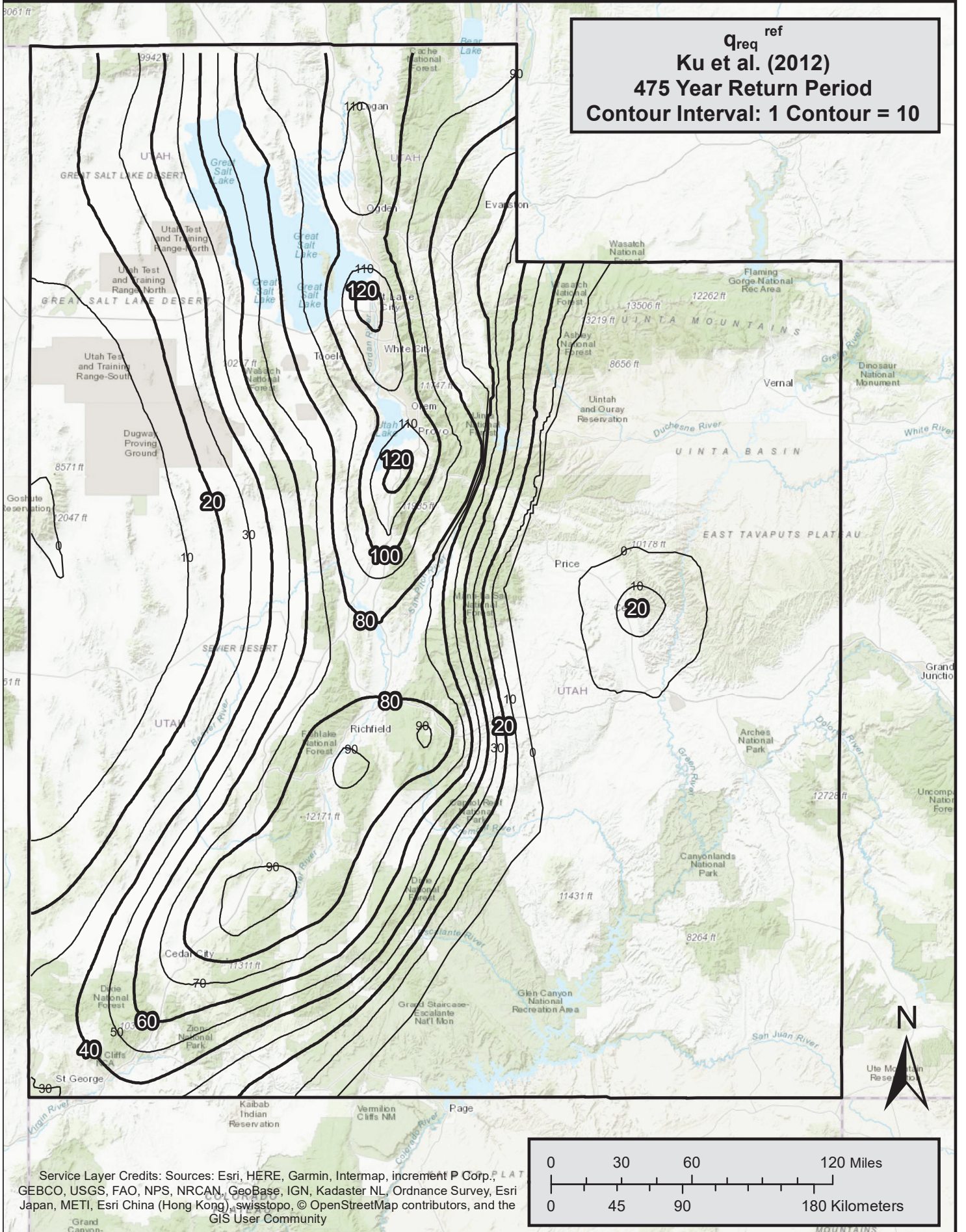


Service Layer Credits: Sources: Esri, HERE, Garmin, Intermap, increment P Corp., GEBCO, USGS, FAO, NPS, NRCAN, GeoBase, IGN, Kadaster NL, Ordnance Survey, Esri Japan, METI, Esri China (Hong Kong), swisstopo, © OpenStreetMap contributors, and the GIS User Community

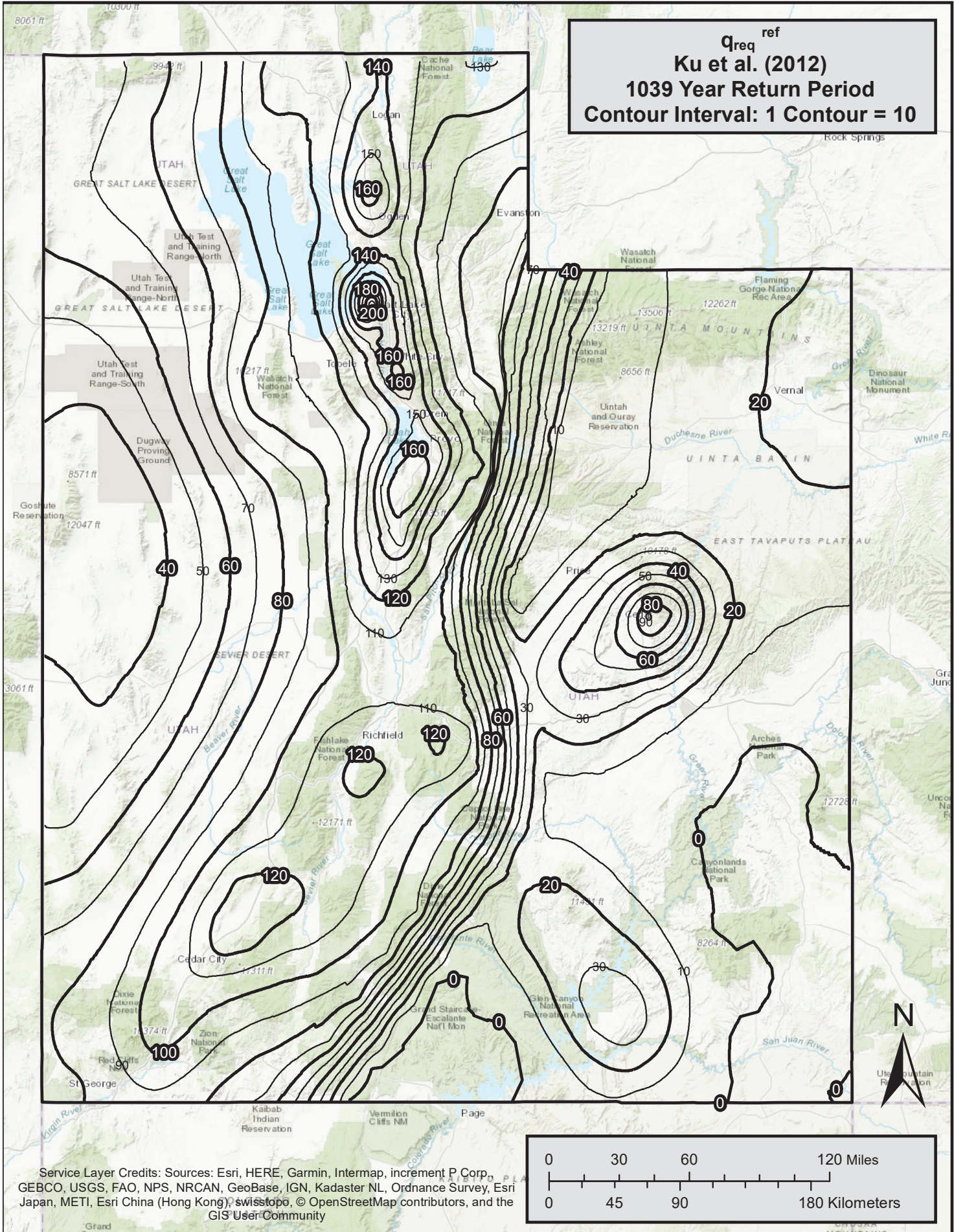
CSR^{ref%}
Boulanger and Idriss (2014)
2475 Year Return Period
Contour Interval: 1 Contour = 5 CSR%



Service Layer Credits: Sources: Esri, HERE, Garmin, Intermap, increment P Corp., GEBCO, USGS, FAO, NPS, NRCAN, GeoBase, IGN, Kadaster NL, Ordnance Survey, Esri Japan, METI, Esri China (Hong Kong), swisstopo, © OpenStreetMap contributors, and the GIS User Community

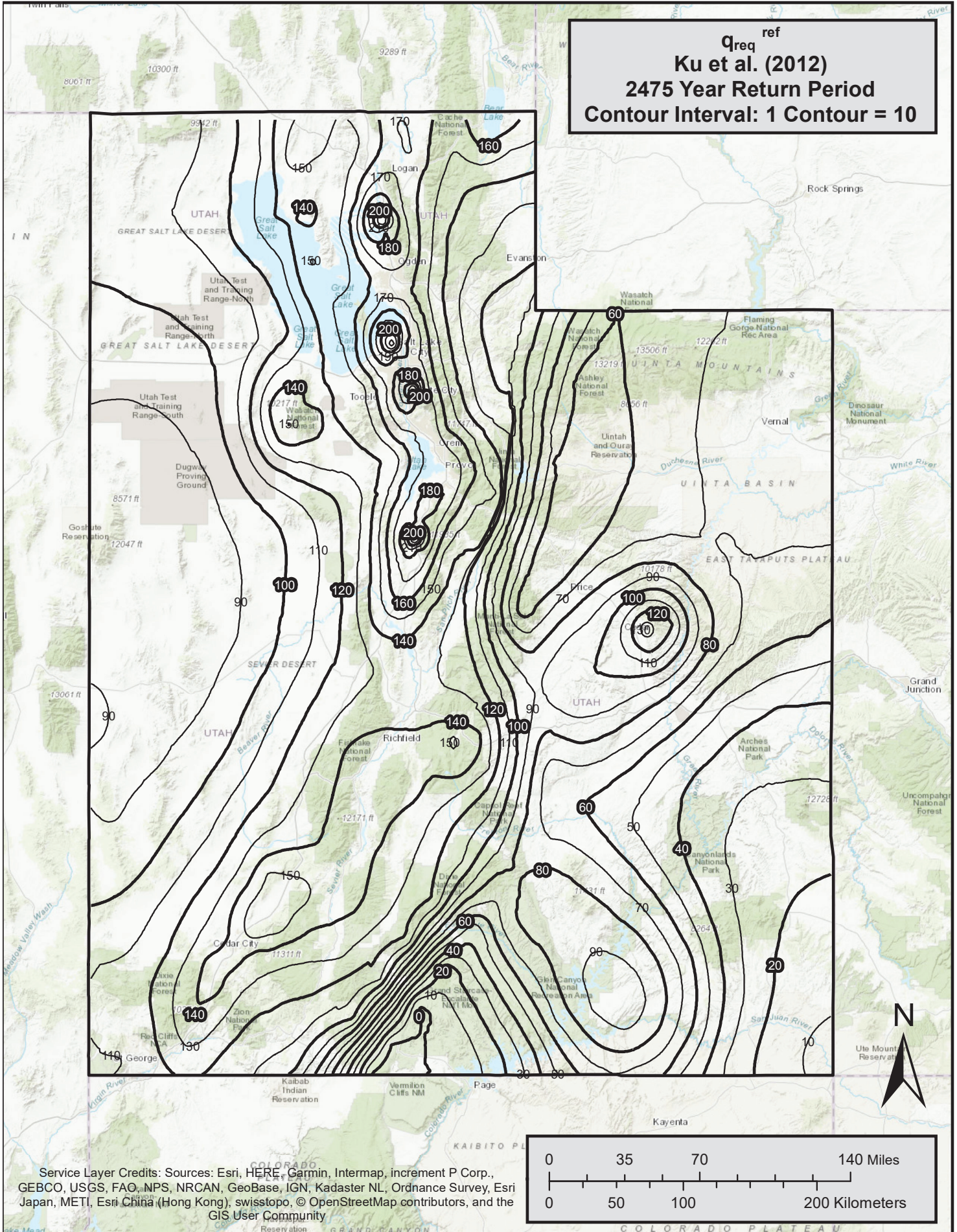


Q_{req}^{ref}
Ku et al. (2012)
1039 Year Return Period
Contour Interval: 1 Contour = 10

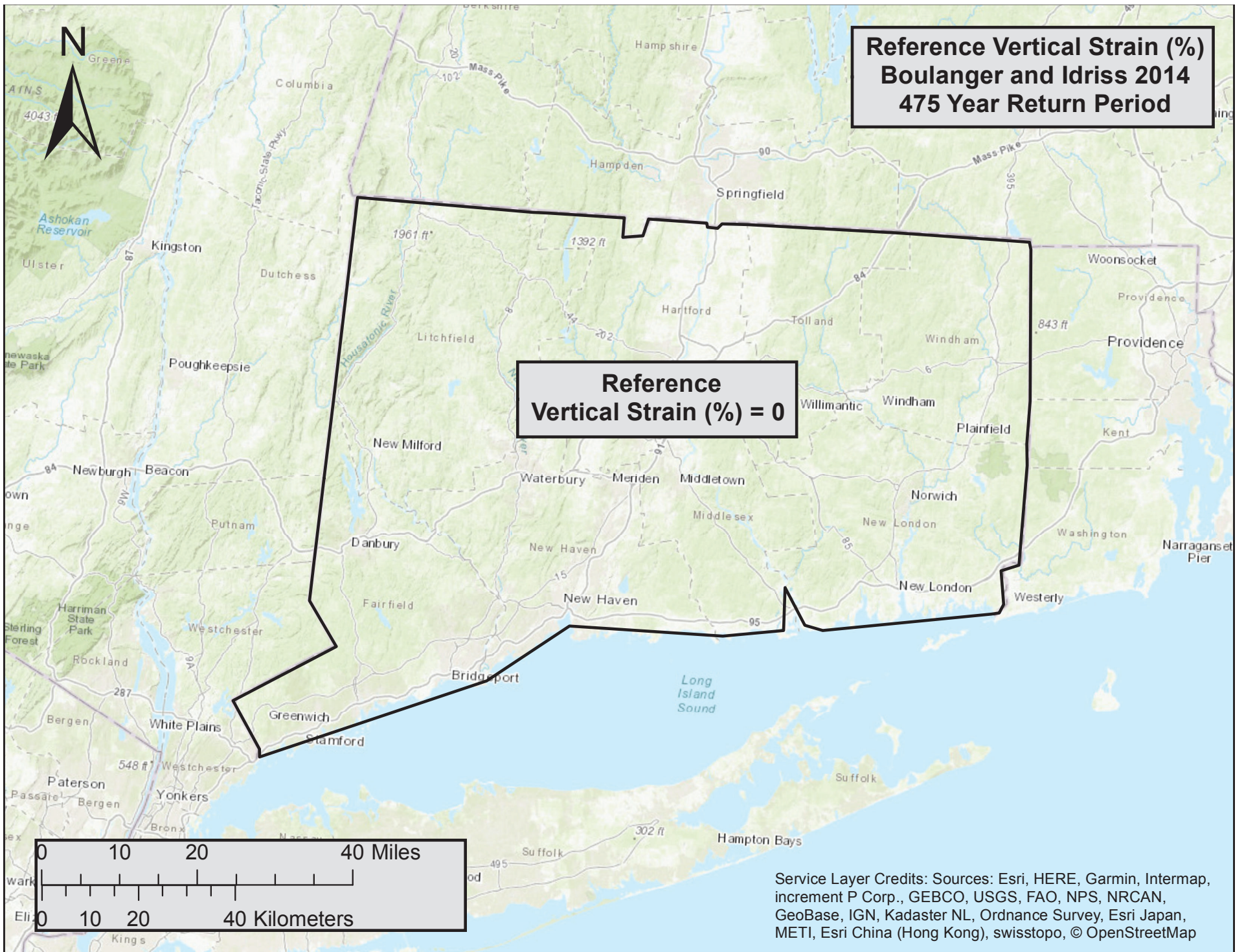


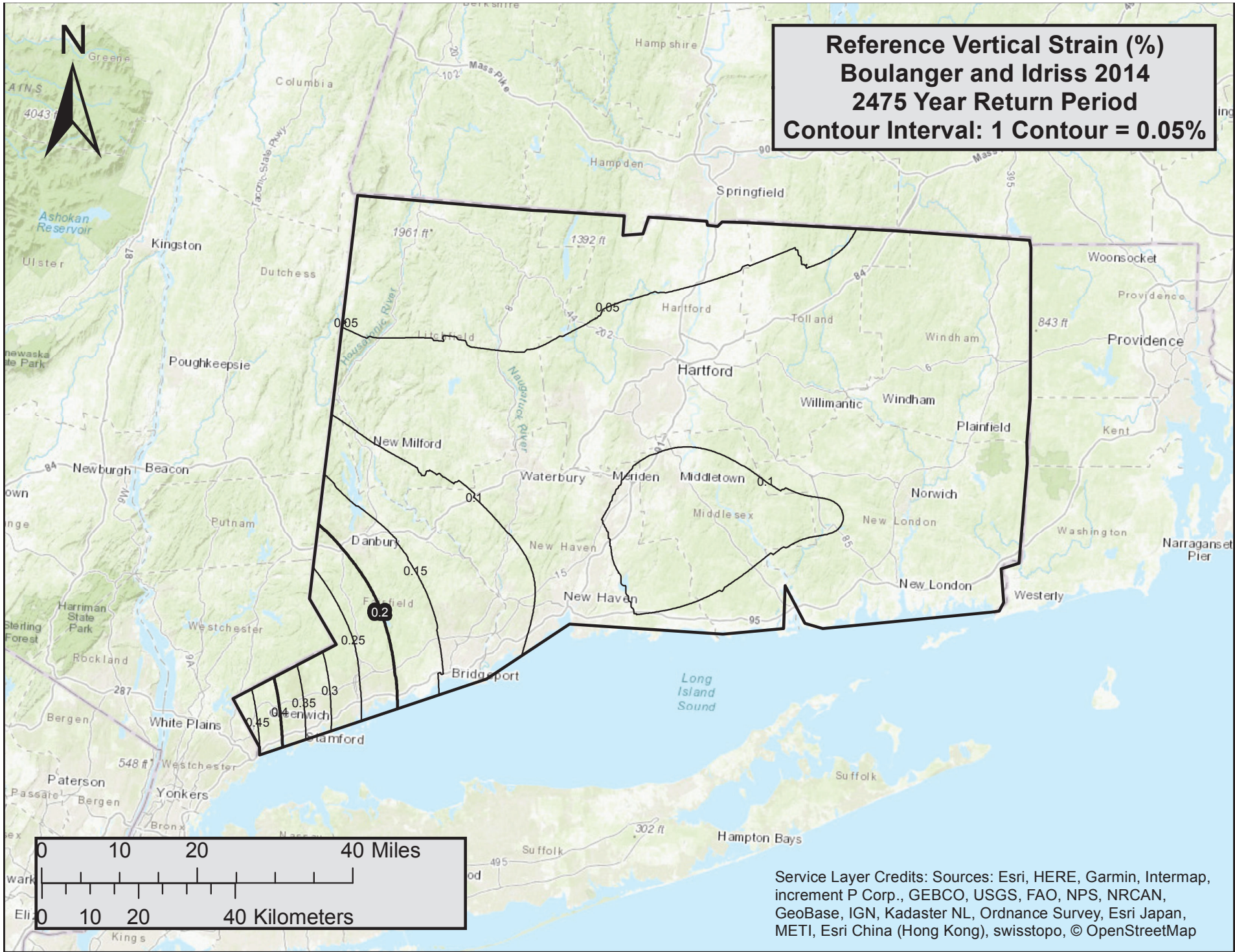
Service Layer Credits: Sources: Esri, HERE, Garmin, Intermap, increment P Corp.,
 GEBCO, USGS, FAO, NPS, NRCAN, GeoBase, IGN, Kadaster NL, Ordnance Survey, Esri
 Japan, METI, Esri China (Hong Kong), swisstopo, © OpenStreetMap contributors, and the
 GIS User Community

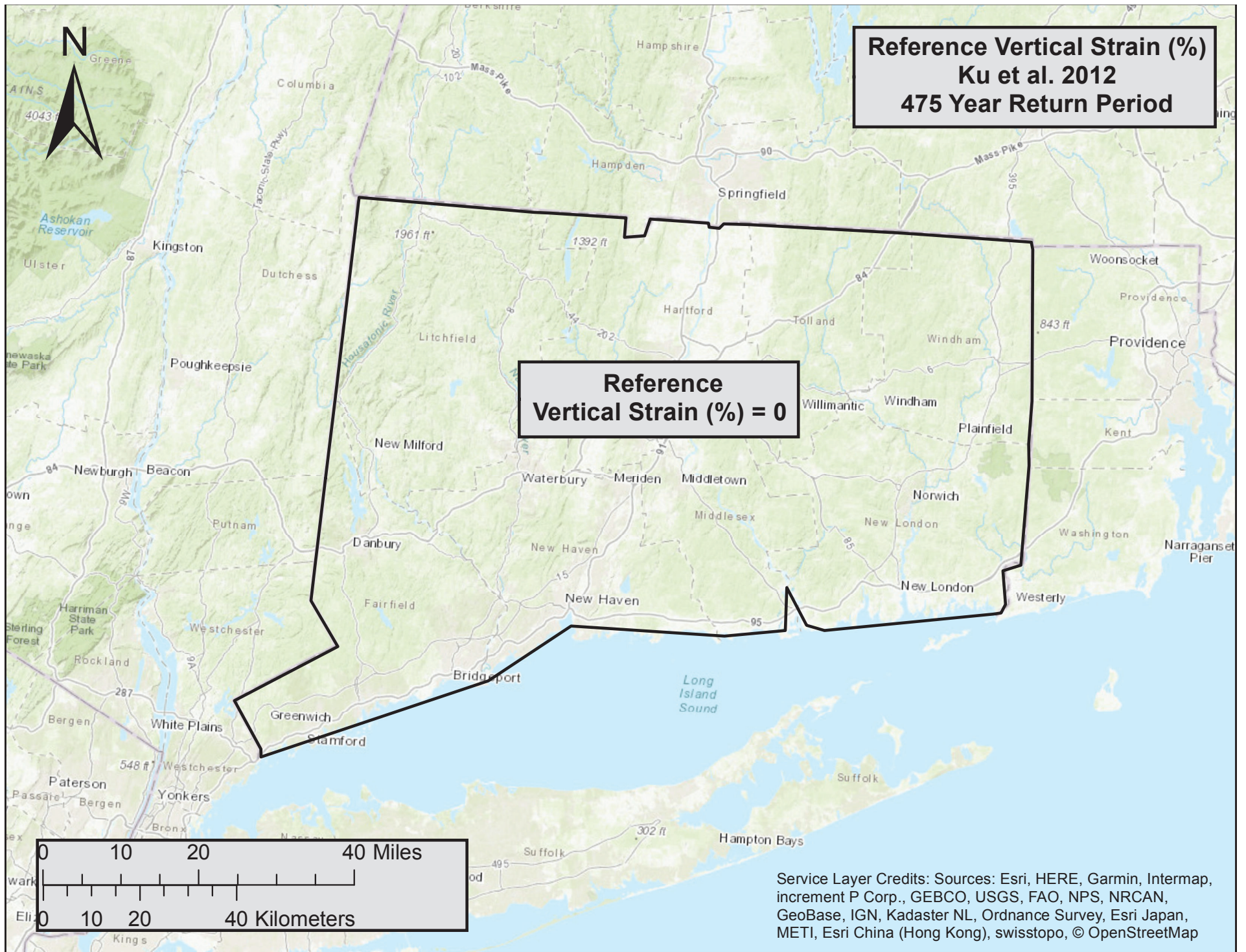
Q_{req}^{ref}
Ku et al. (2012)
2475 Year Return Period
Contour Interval: 1 Contour = 10

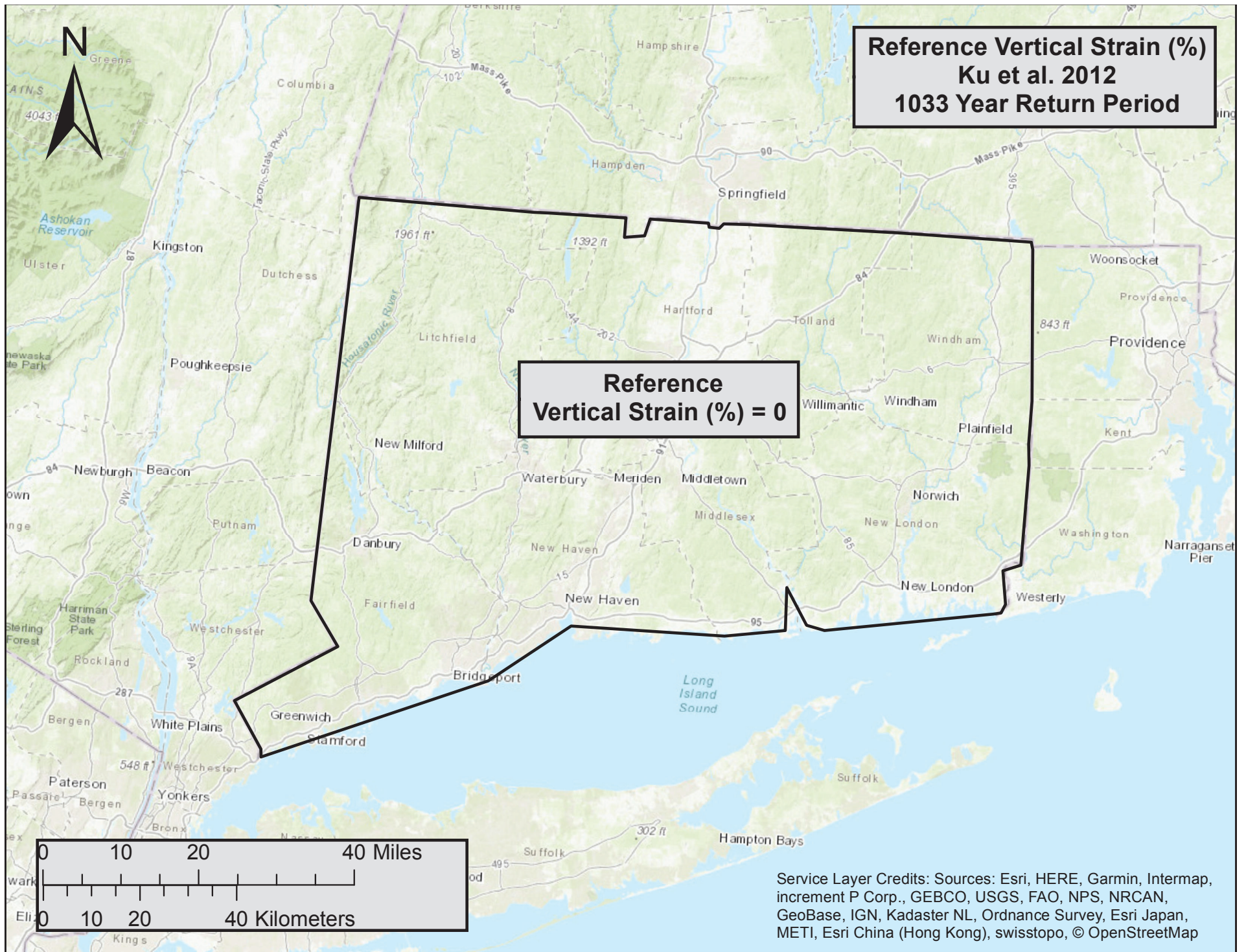


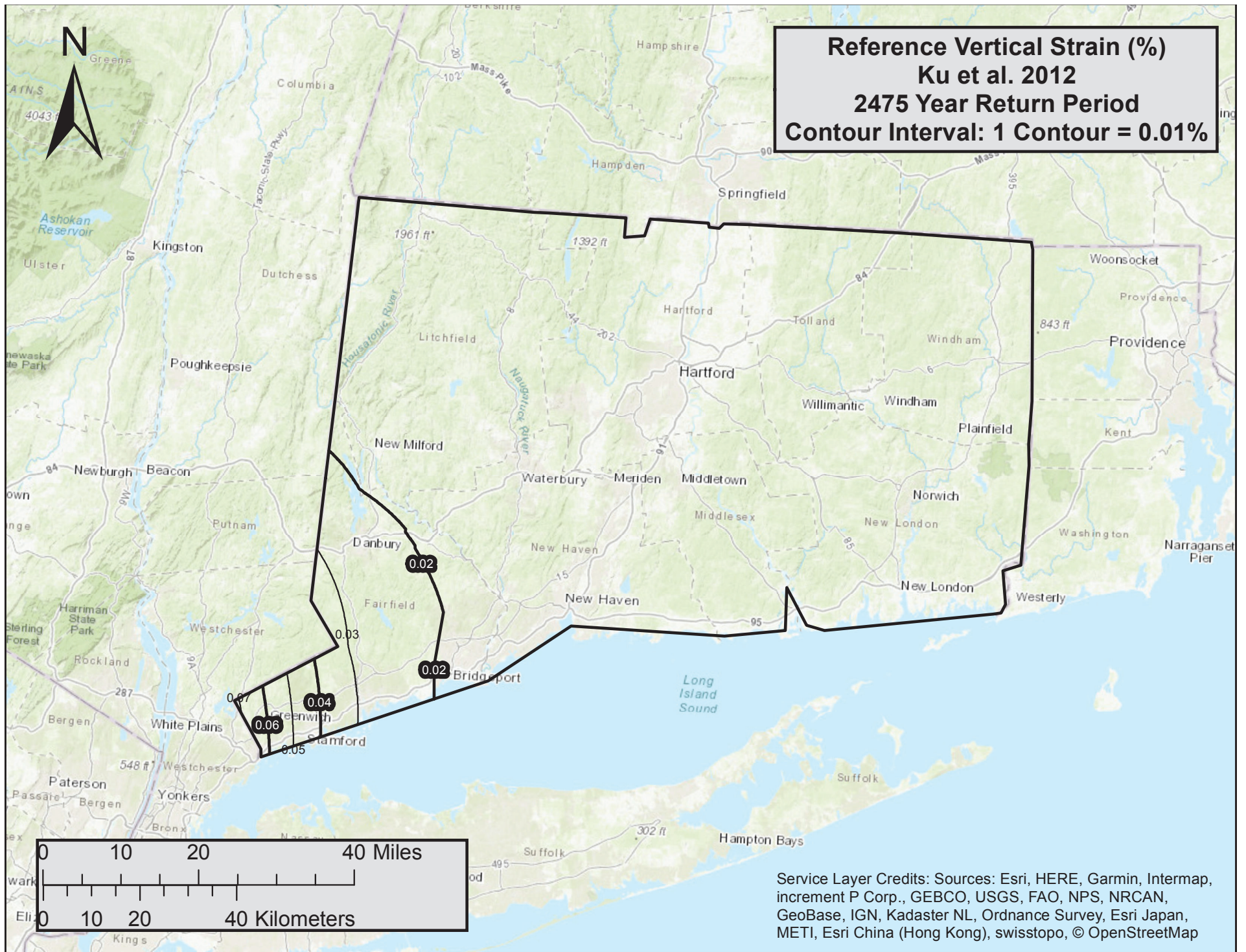
Service Layer Credits: Sources: Esri, HERE, Garmin, Intermap, increment P Corp., GEBCO, USGS, FAO, NPS, NRCAN, GeoBase, IGN, Kadaster NL, Ordnance Survey, Esri Japan, METI, Esri China (Hong Kong), swisstopo, © OpenStreetMap contributors, and the GIS User Community





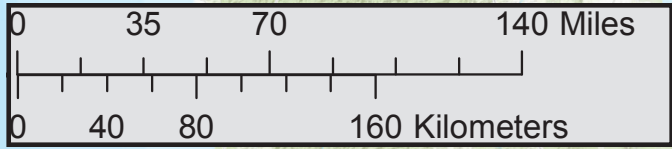
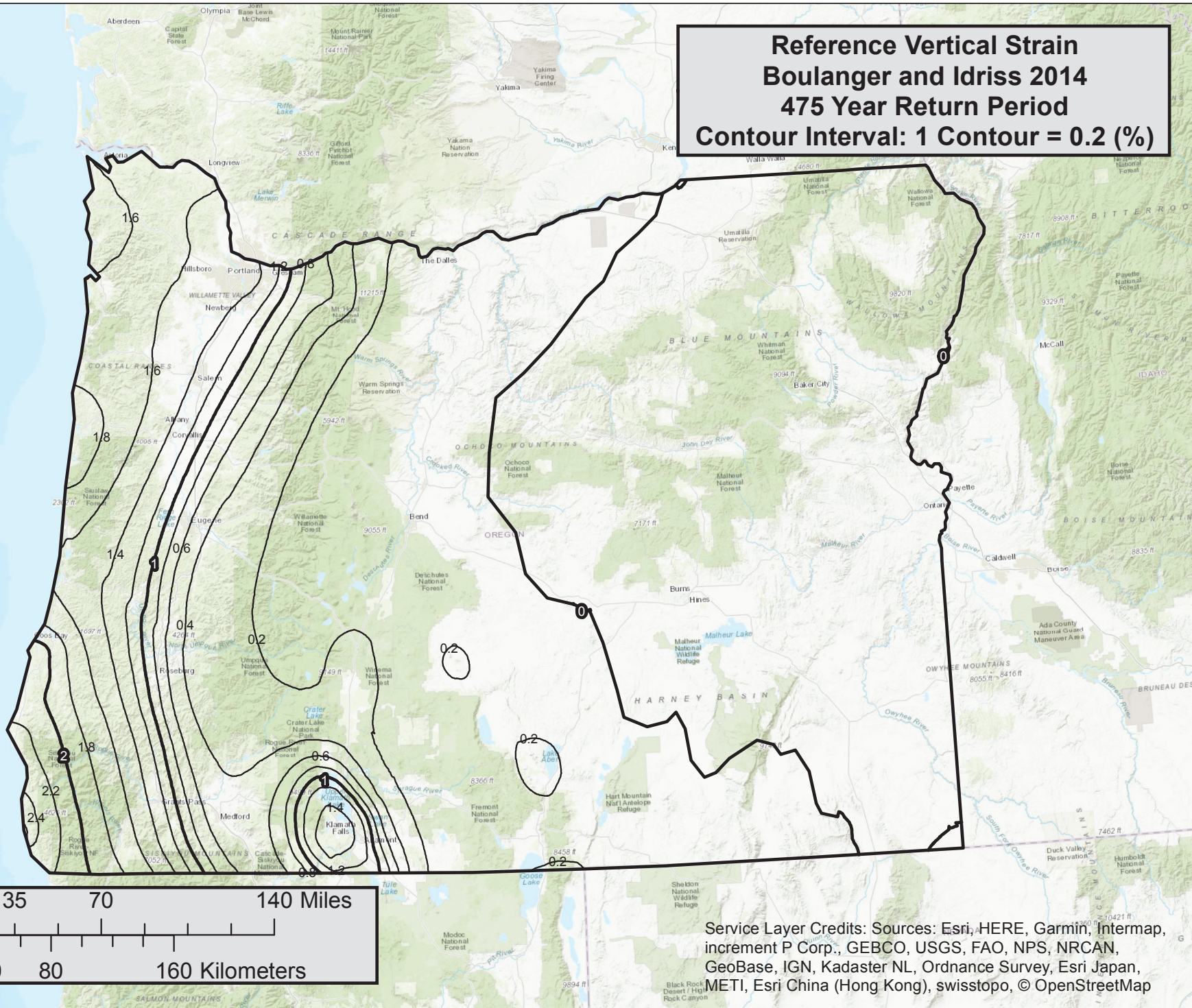








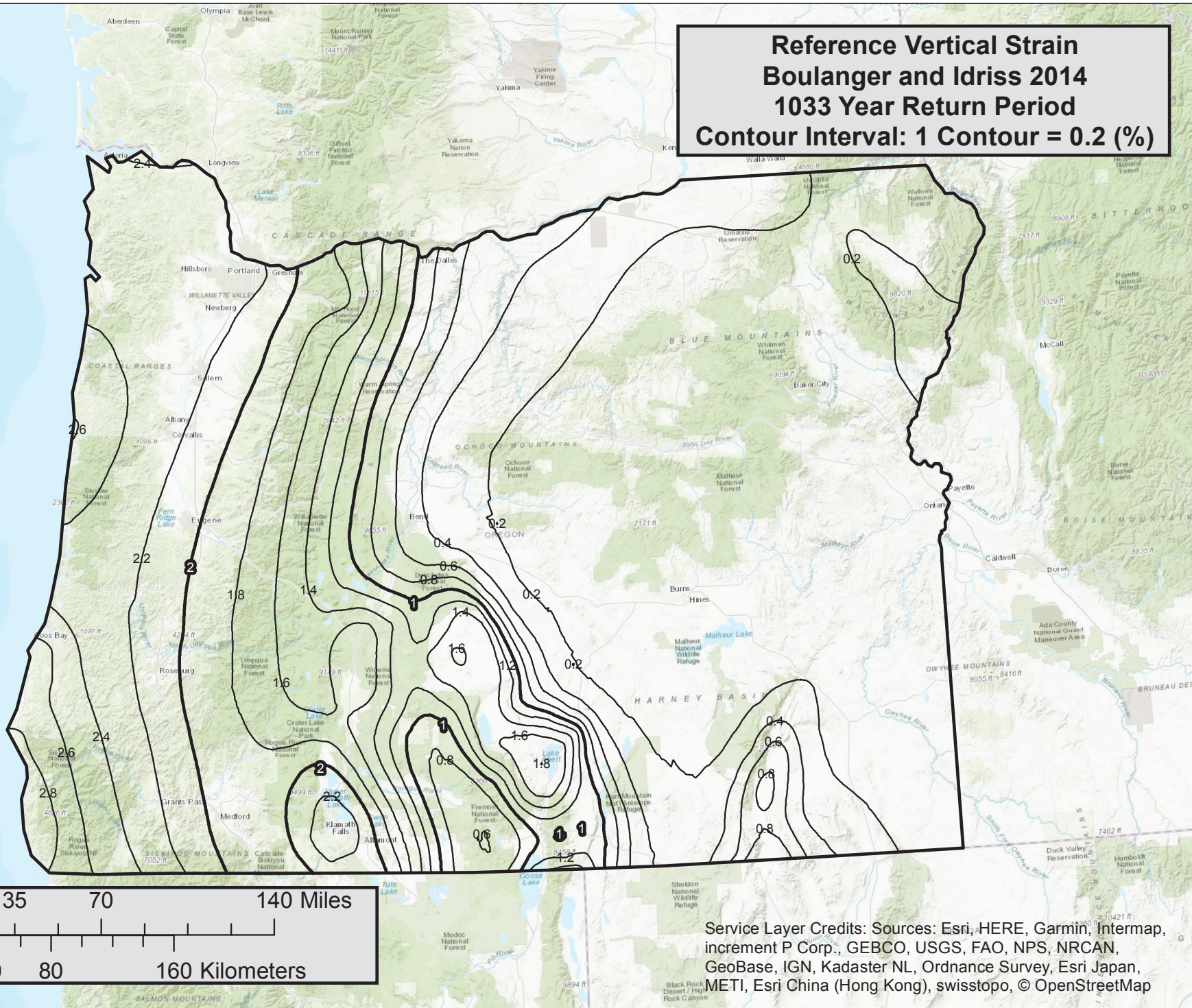
**Reference Vertical Strain
Boulanger and Idriss 2014
475 Year Return Period
Contour Interval: 1 Contour = 0.2 (%)**



Service Layer Credits: Sources: Esri, HERE, Garmin, Intermap, increment P Corp., GEBCO, USGS, FAO, NPS, NRCAN, GeoBase, IGN, Kadaster NL, Ordnance Survey, Esri Japan, METI, Esri China (Hong Kong), swisstopo, © OpenStreetMap



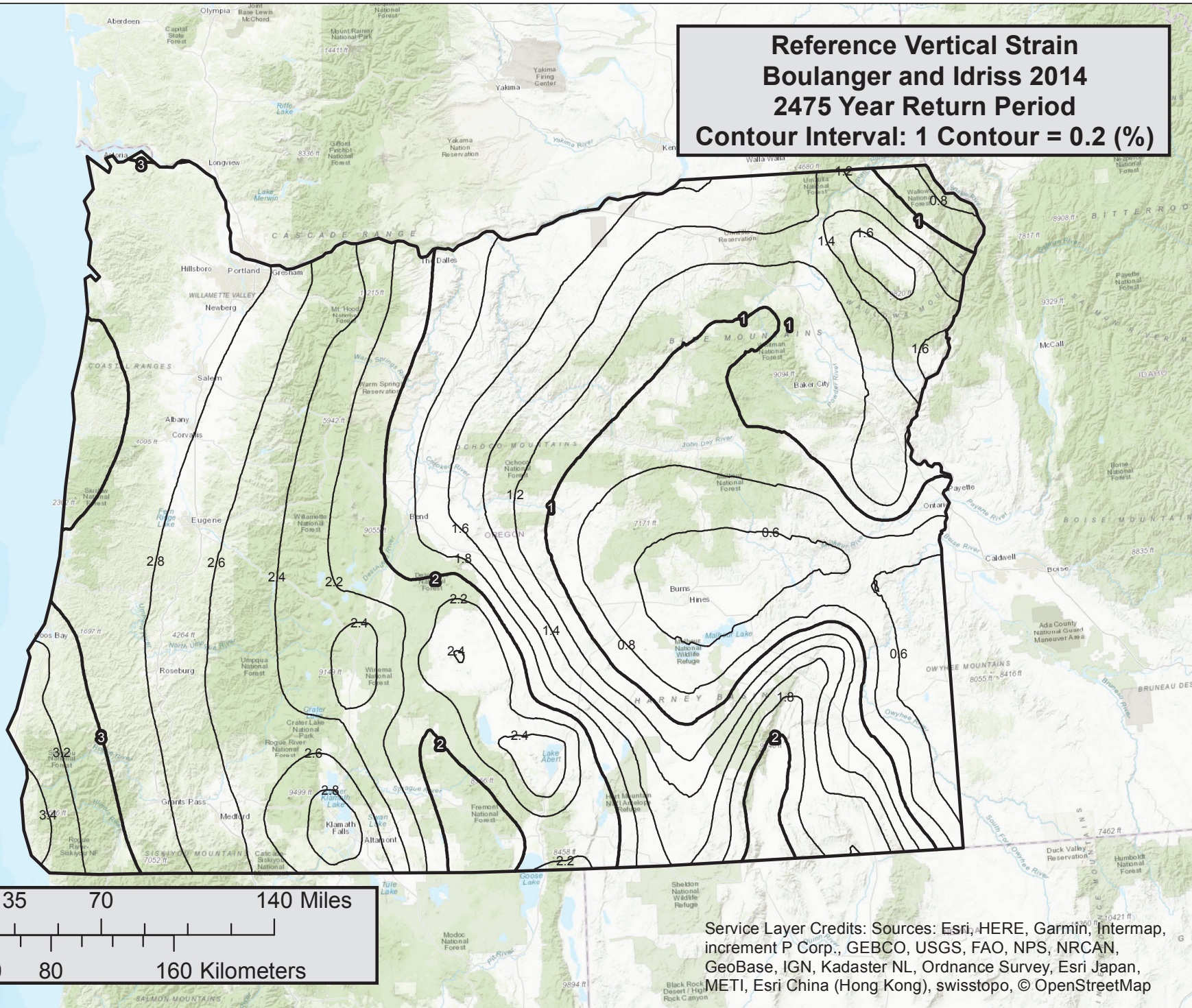
**Reference Vertical Strain
Boulanger and Idriss 2014
1033 Year Return Period
Contour Interval: 1 Contour = 0.2 (%)**



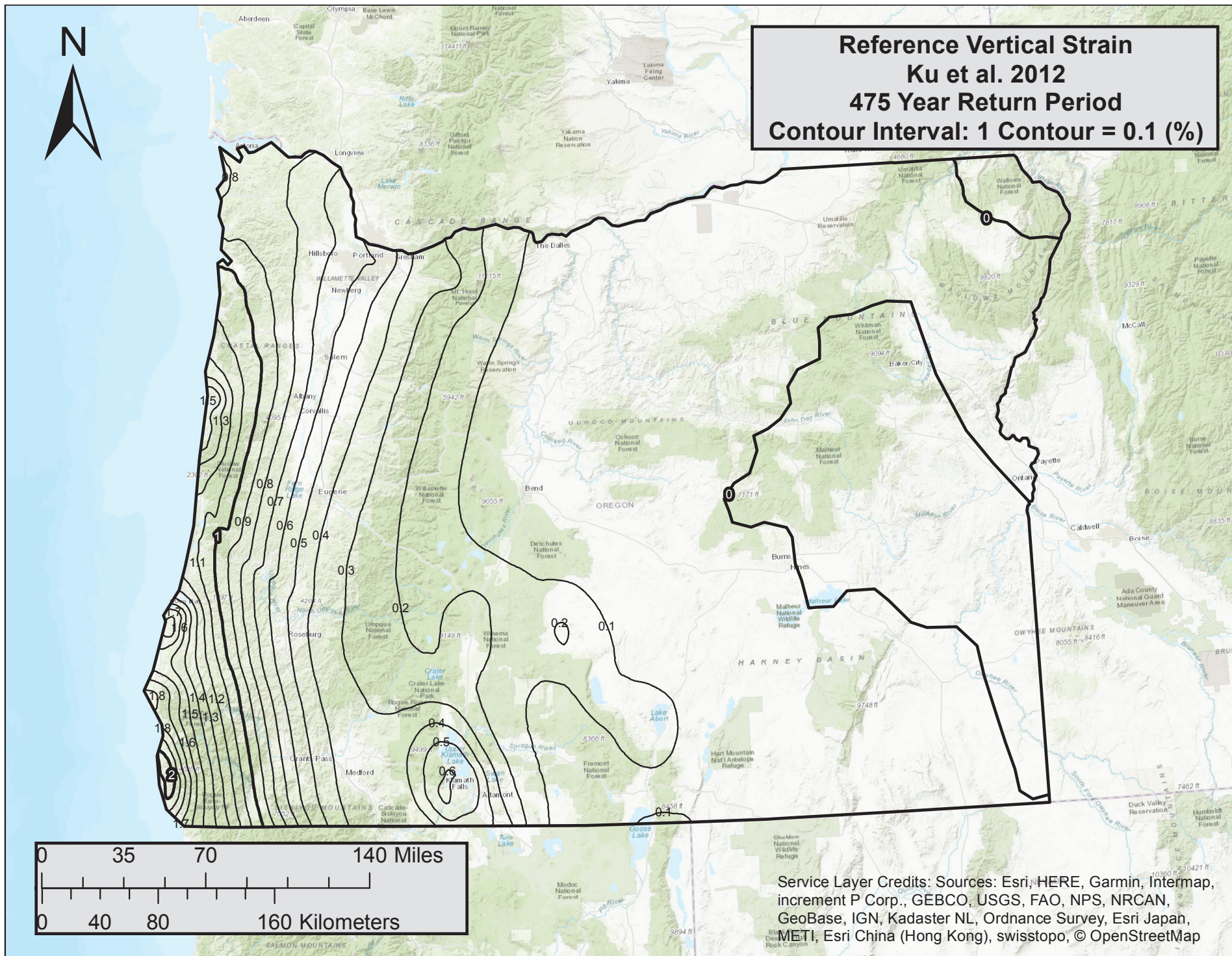
Service Layer Credits: Sources: Esri, HERE, Garmin, Intermap, increment P Corp., GEBCO, USGS, FAO, NPS, NRCAN, GeoBase, IGN, Kadaster NL, Ordnance Survey, Esri Japan, METI, Esri China (Hong Kong), swisstopo, © OpenStreetMap

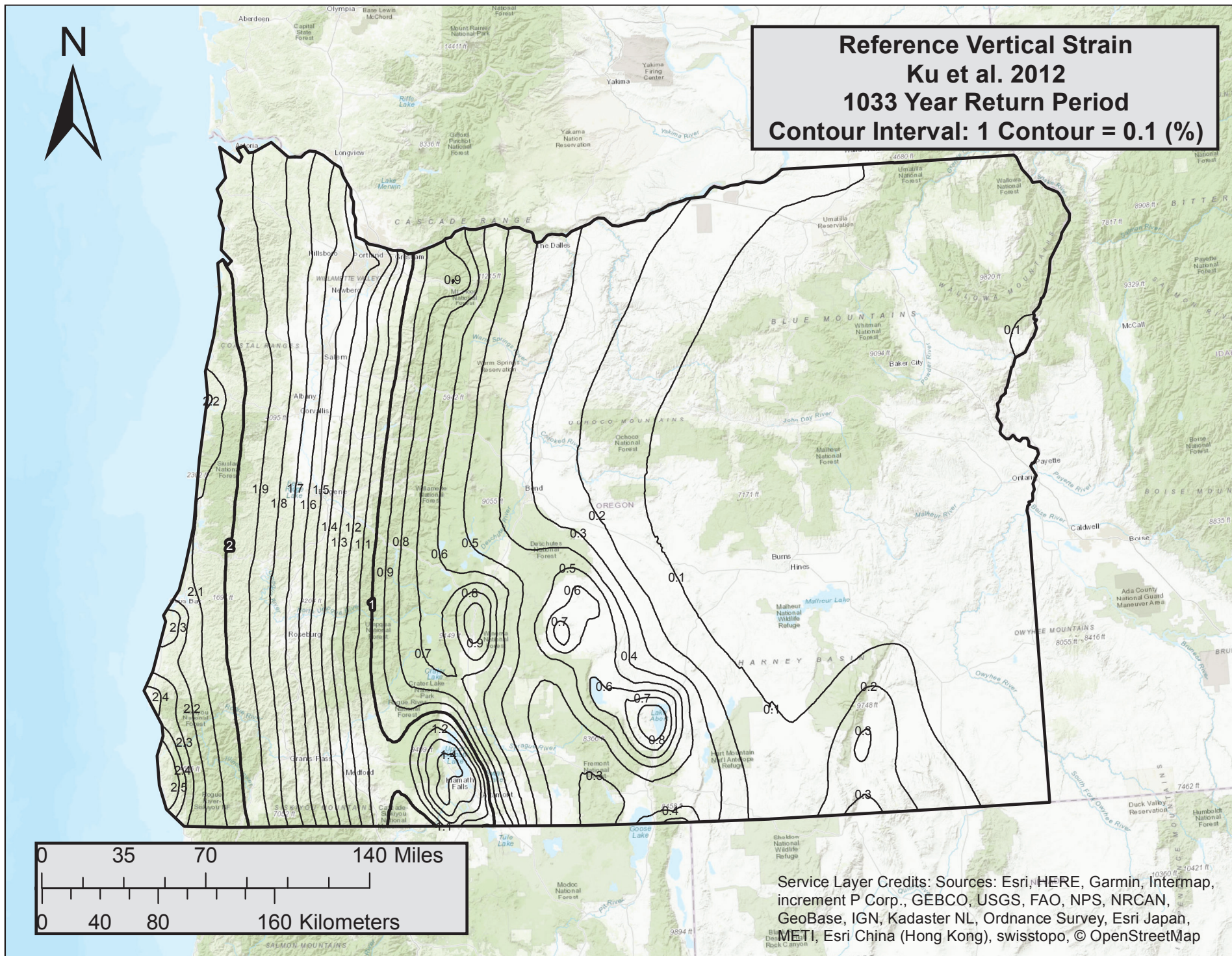


**Reference Vertical Strain
Boulanger and Idriss 2014
2475 Year Return Period
Contour Interval: 1 Contour = 0.2 (%)**

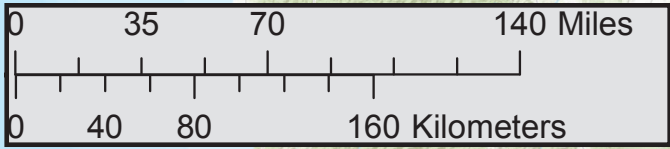


Service Layer Credits: Sources: Esri, HERE, Garmin, Intermap, increment P Corp., GEBCO, USGS, FAO, NPS, NRCAN, GeoBase, IGN, Kadaster NL, Ordnance Survey, Esri Japan, METI, Esri China (Hong Kong), swisstopo, © OpenStreetMap

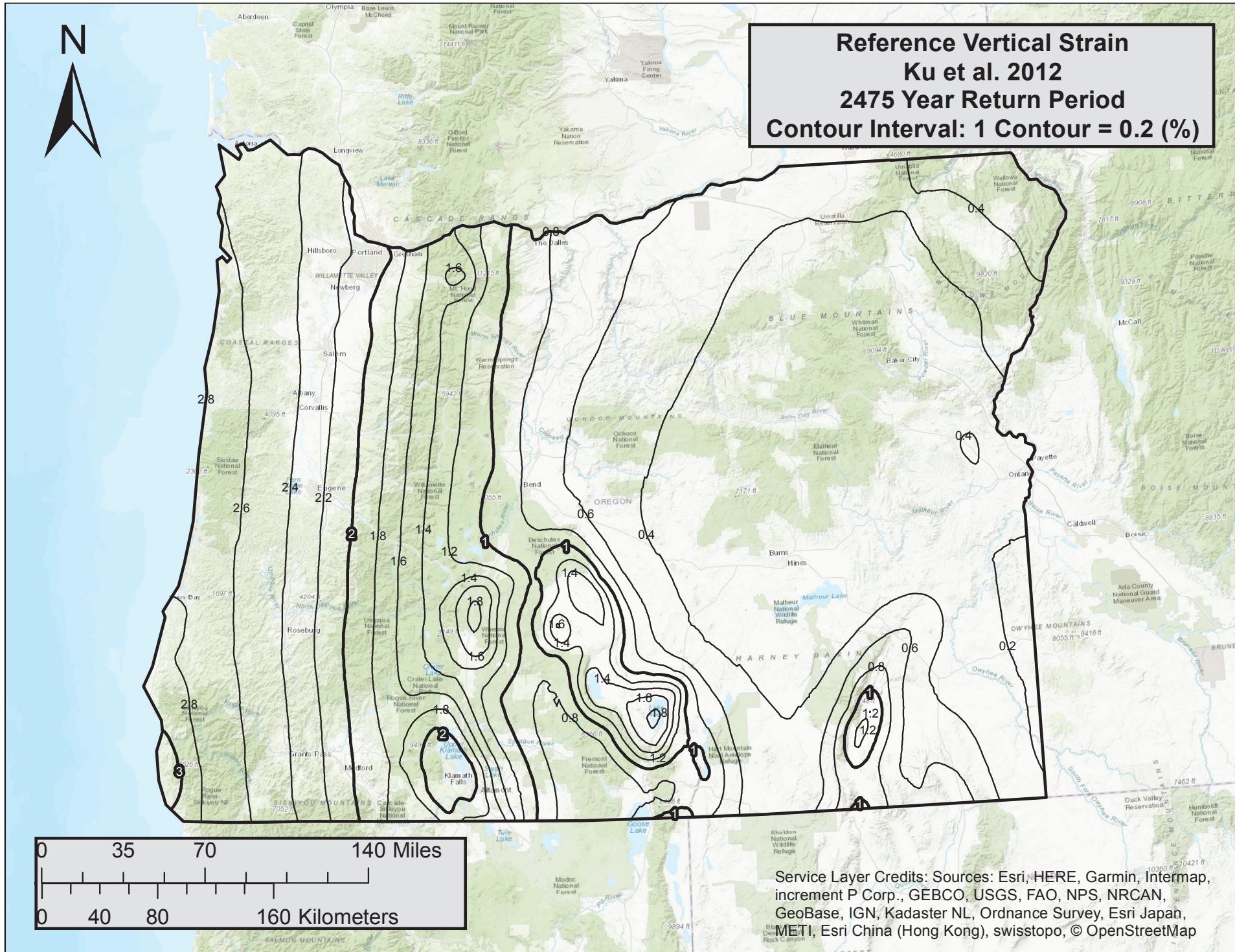




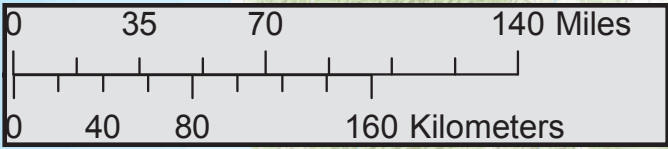
Reference Vertical Strain
Ku et al. 2012
1033 Year Return Period
Contour Interval: 1 Contour = 0.1 (%)



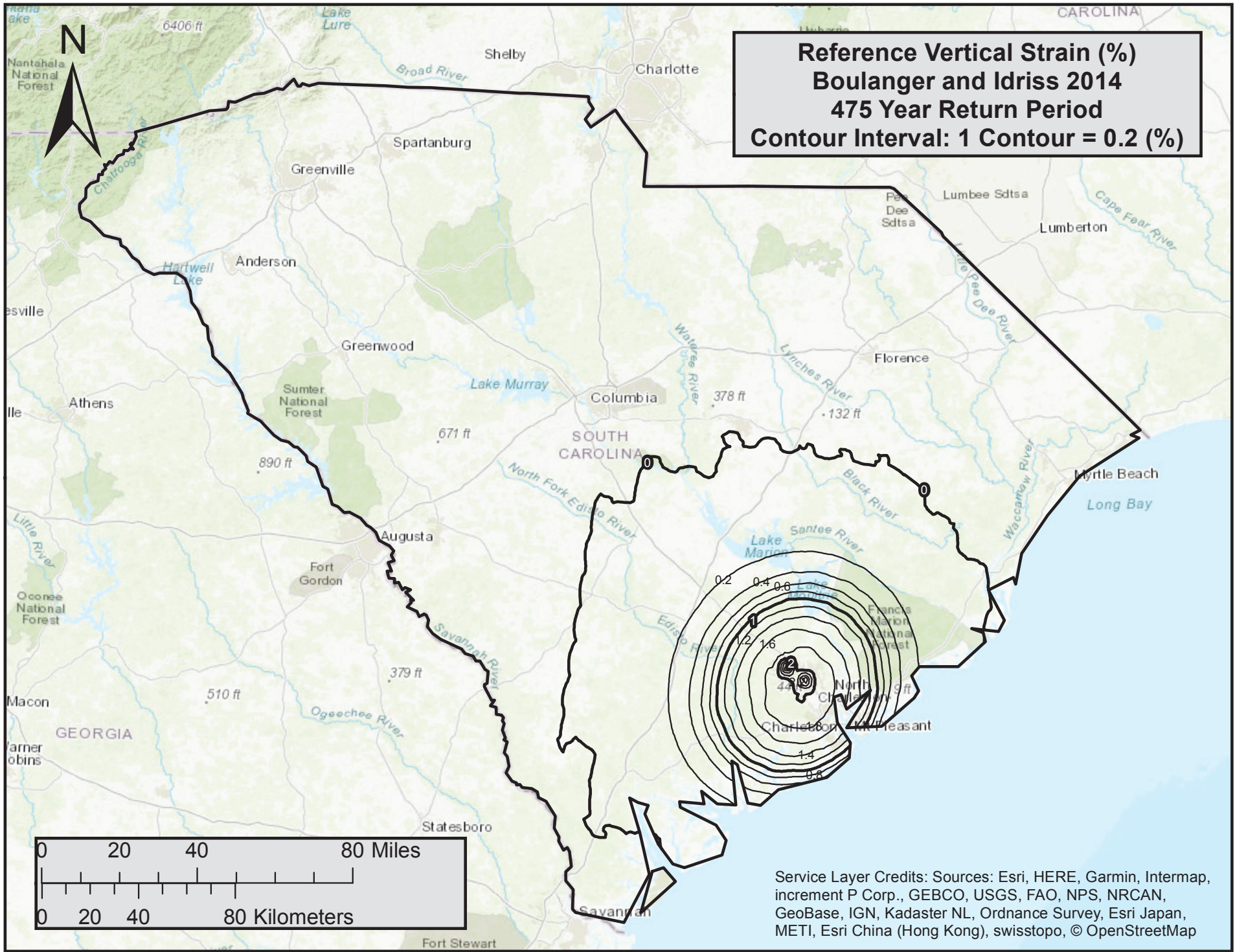
Service Layer Credits: Sources: Esri, HERE, Garmin, Intermap, increment P Corp., GEBCO, USGS, FAO, NPS, NRCAN, GeoBase, IGN, Kadaster NL, Ordnance Survey, Esri Japan, METI, Esri China (Hong Kong), swisstopo, © OpenStreetMap

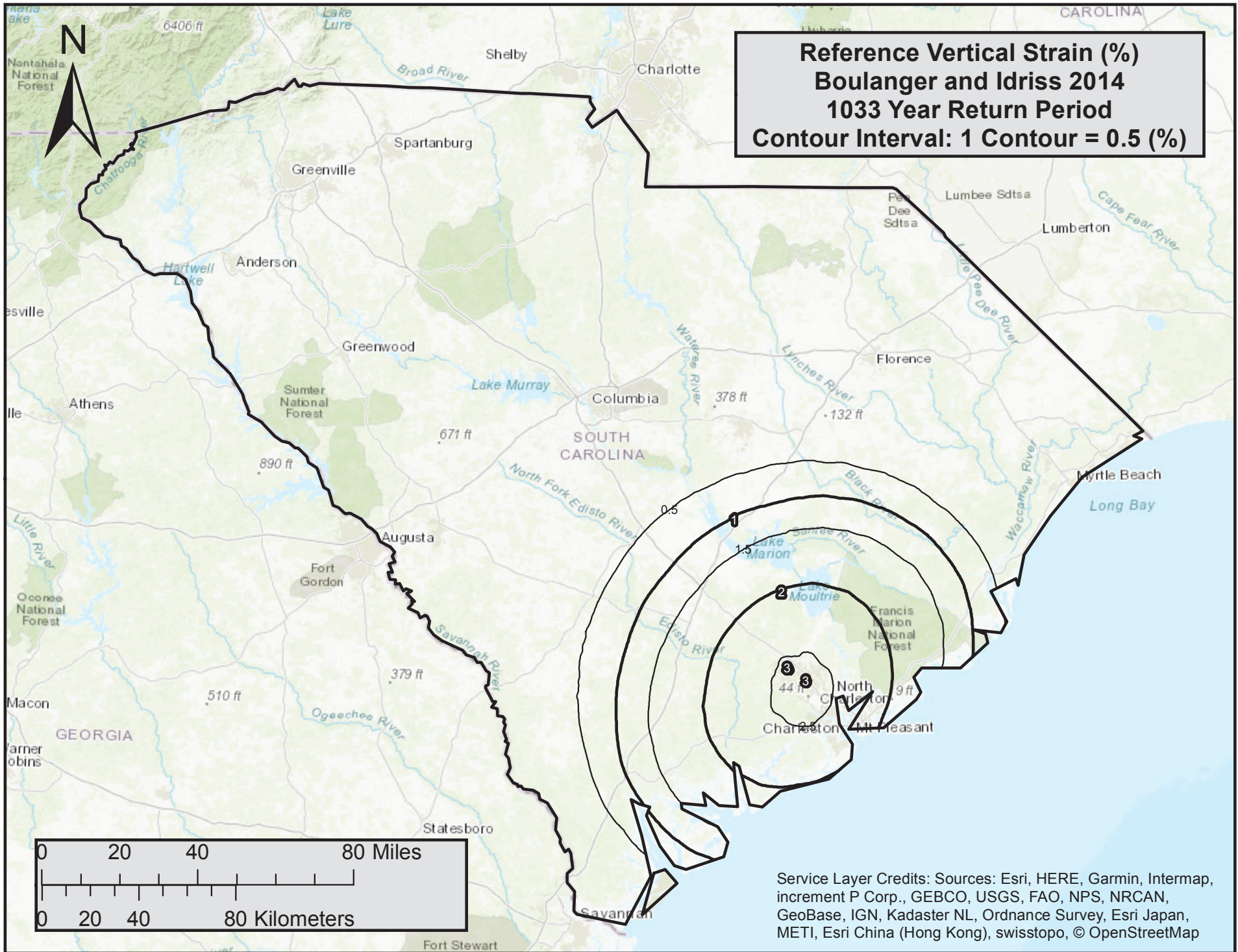


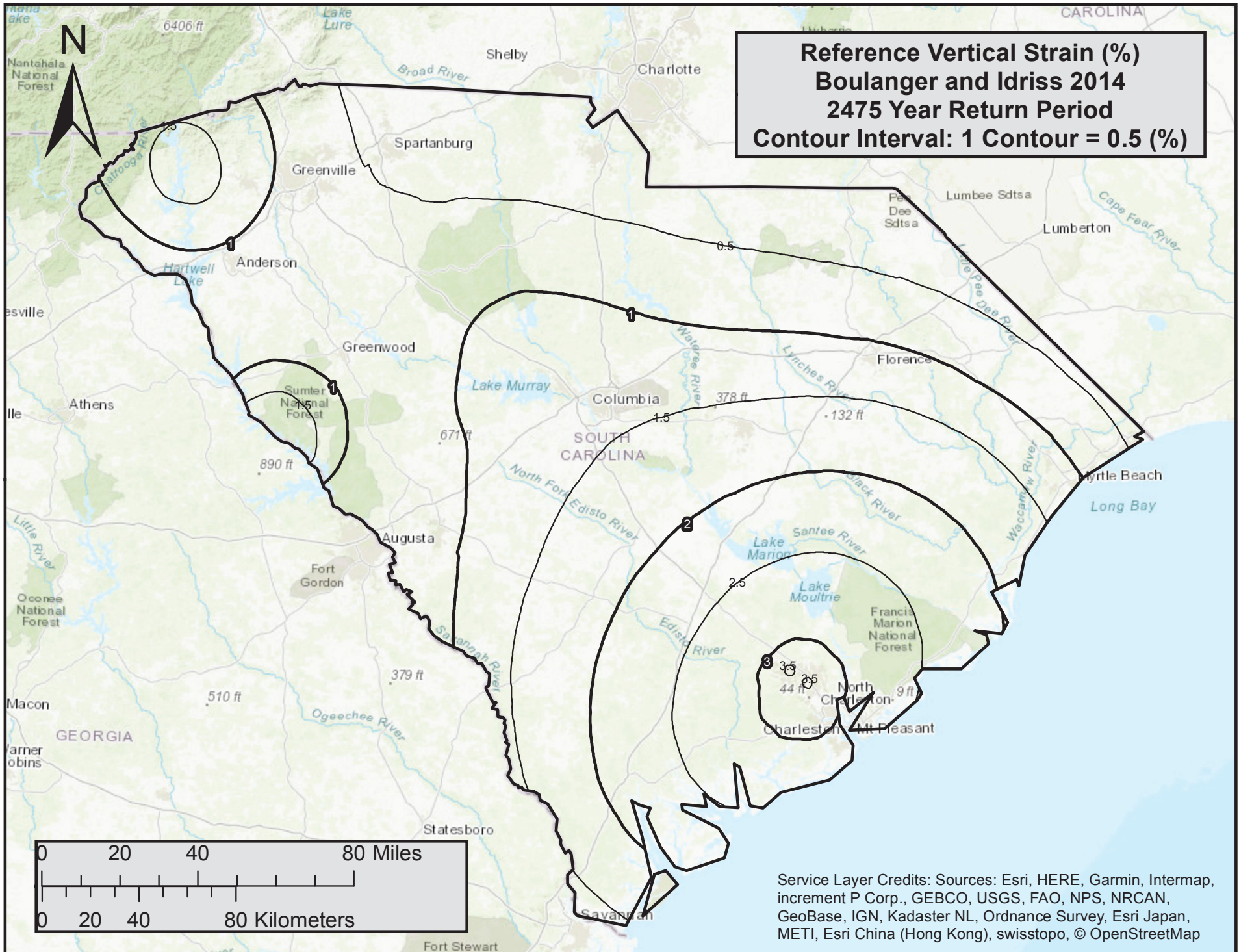
Reference Vertical Strain
Ku et al. 2012
2475 Year Return Period
Contour Interval: 1 Contour = 0.2 (%)

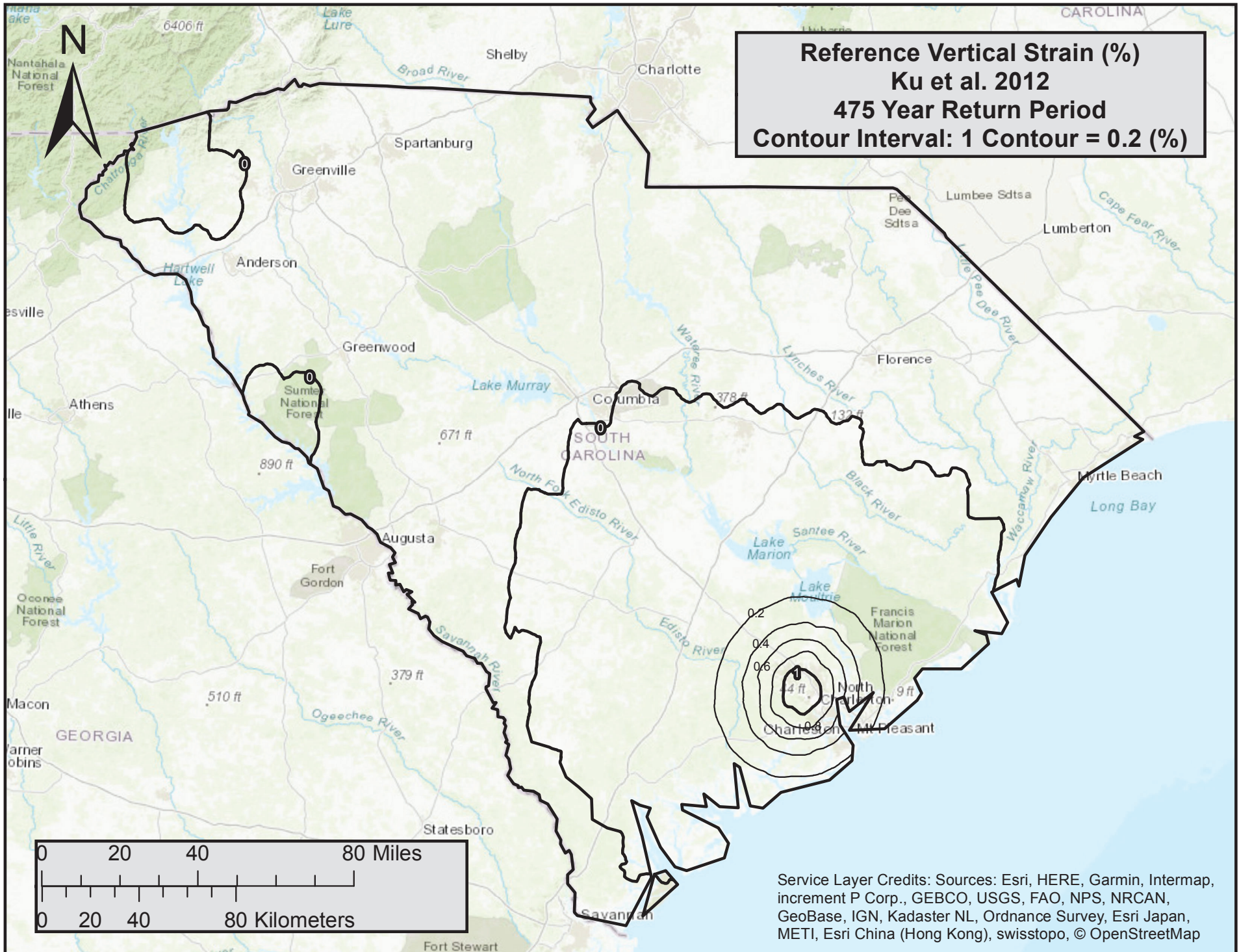


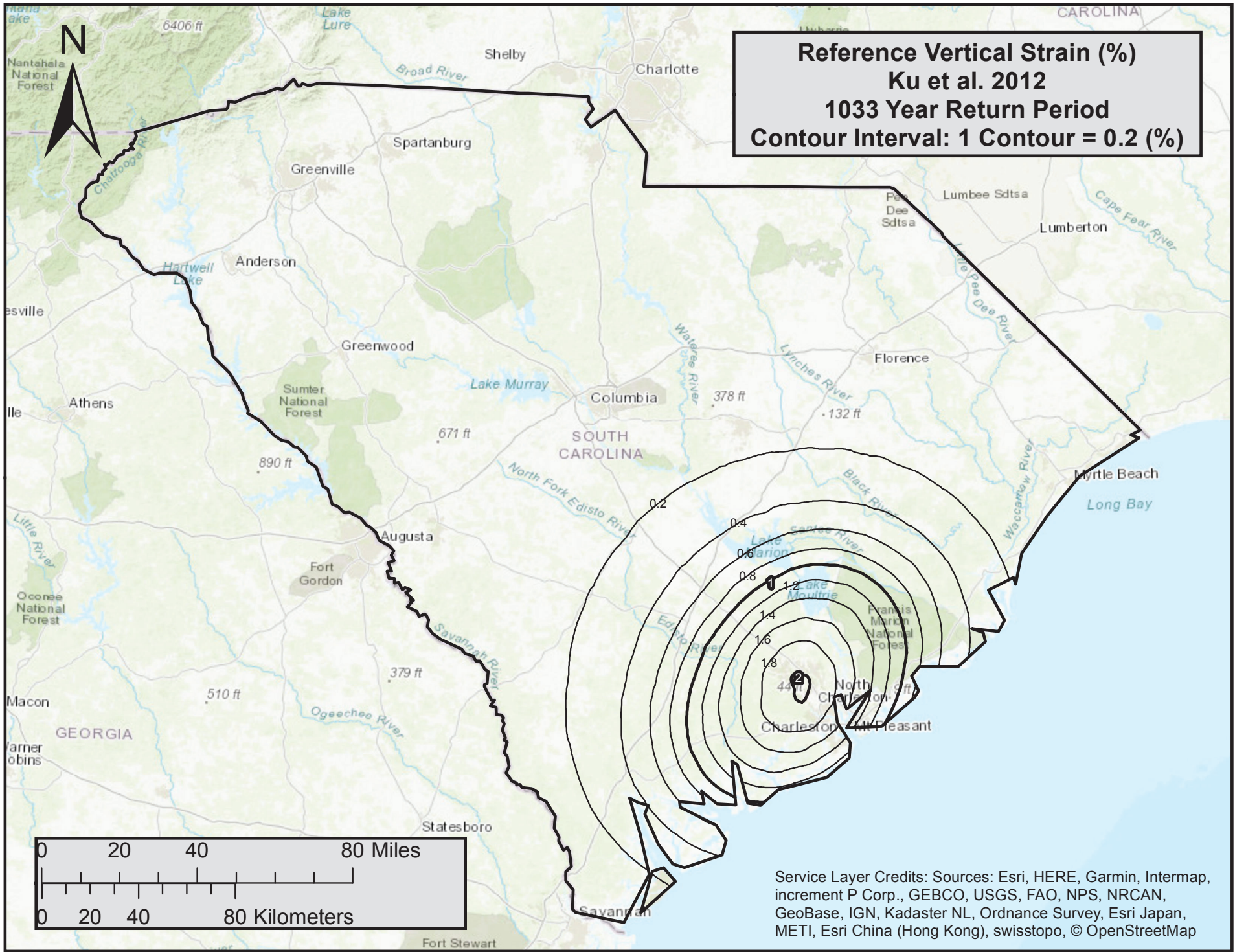
Service Layer Credits: Sources: Esri, HERE, Garmin, Intermap, increment P Corp., GEBCO, USGS, FAO, NPS, NRCAN, GeoBase, IGN, Kadaster NL, Ordnance Survey, Esri Japan, METI, Esri China (Hong Kong), swisstopo, © OpenStreetMap

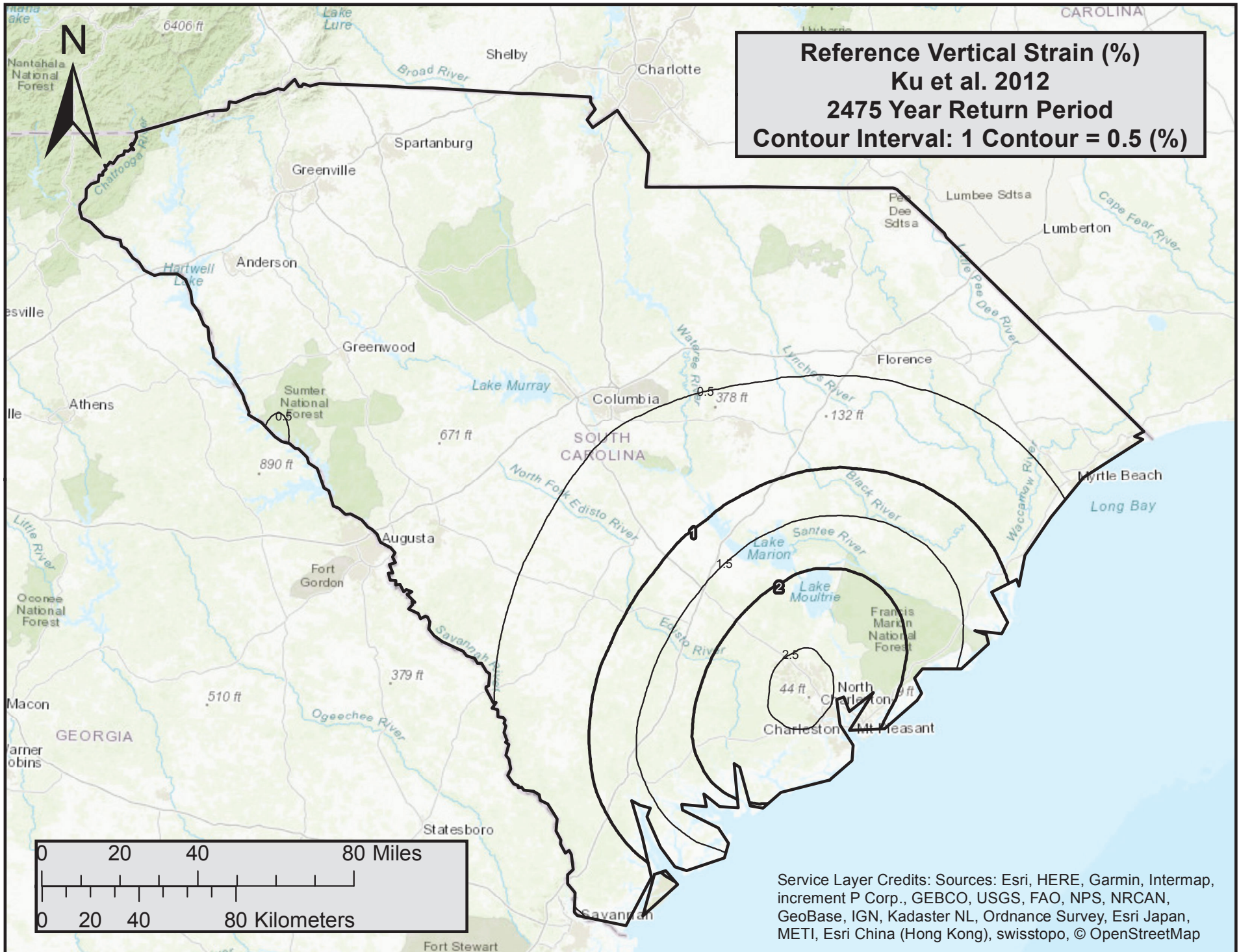


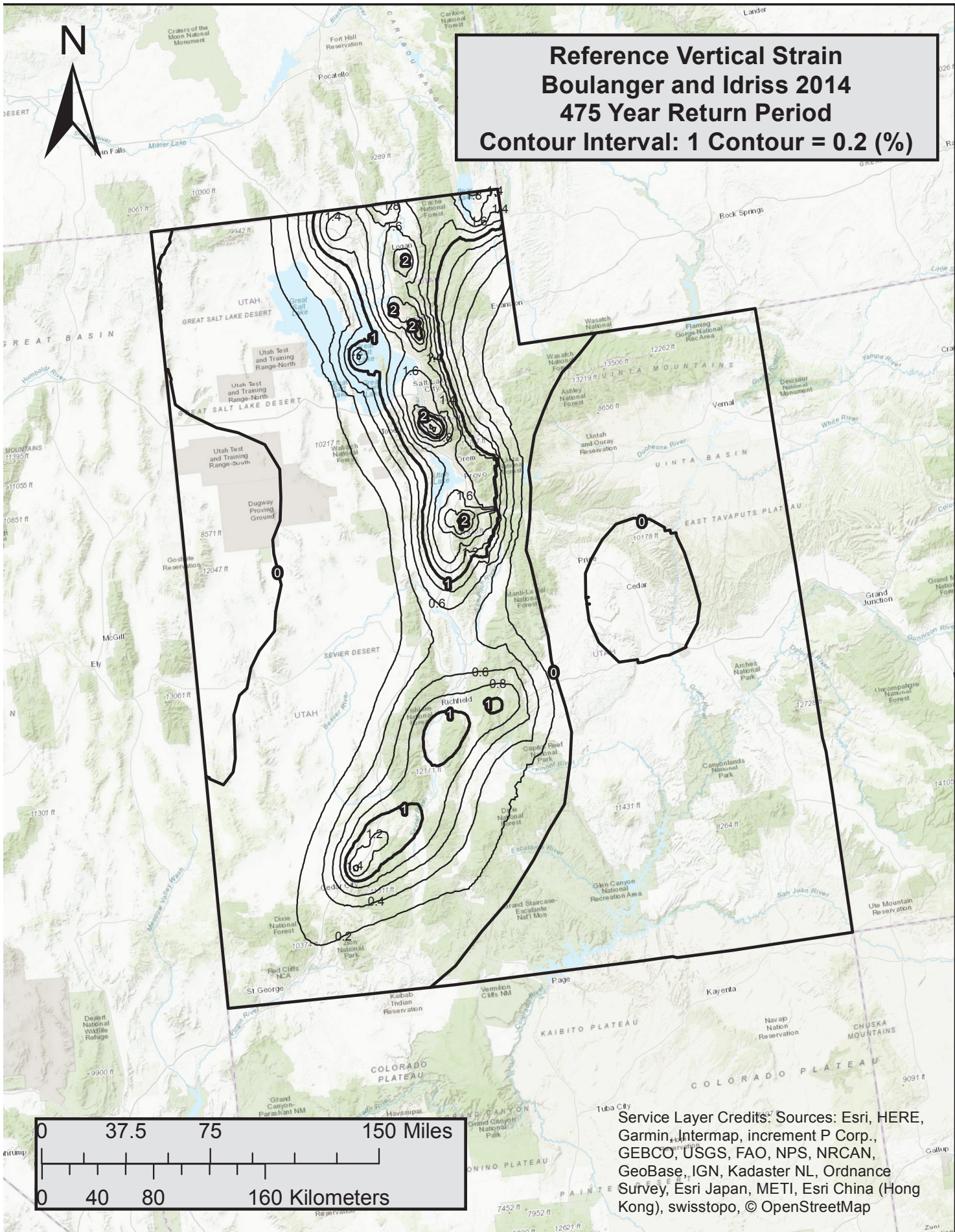




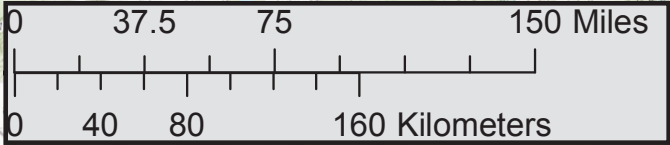






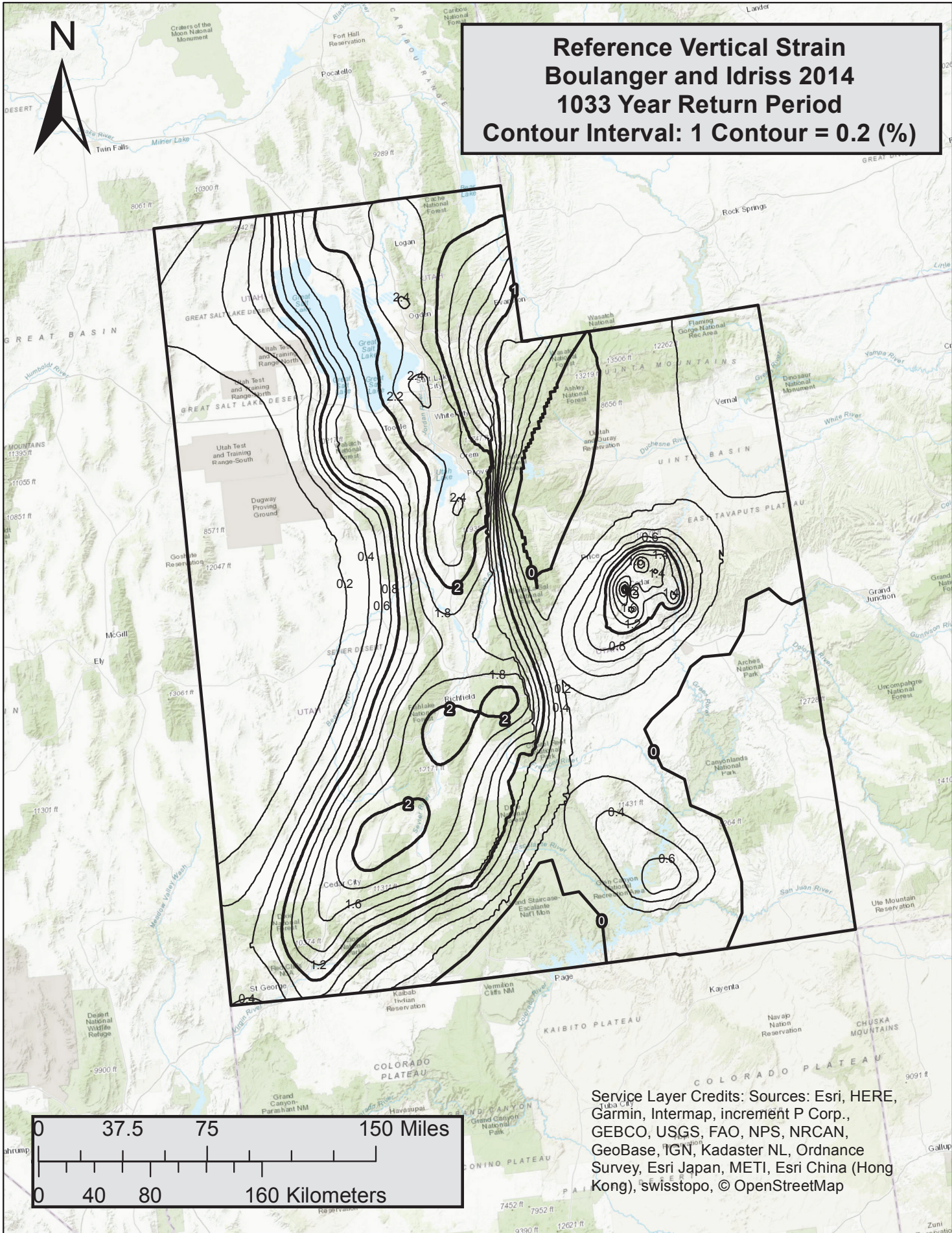


**Reference Vertical Strain
Boulanger and Idriss 2014
475 Year Return Period
Contour Interval: 1 Contour = 0.2 (%)**



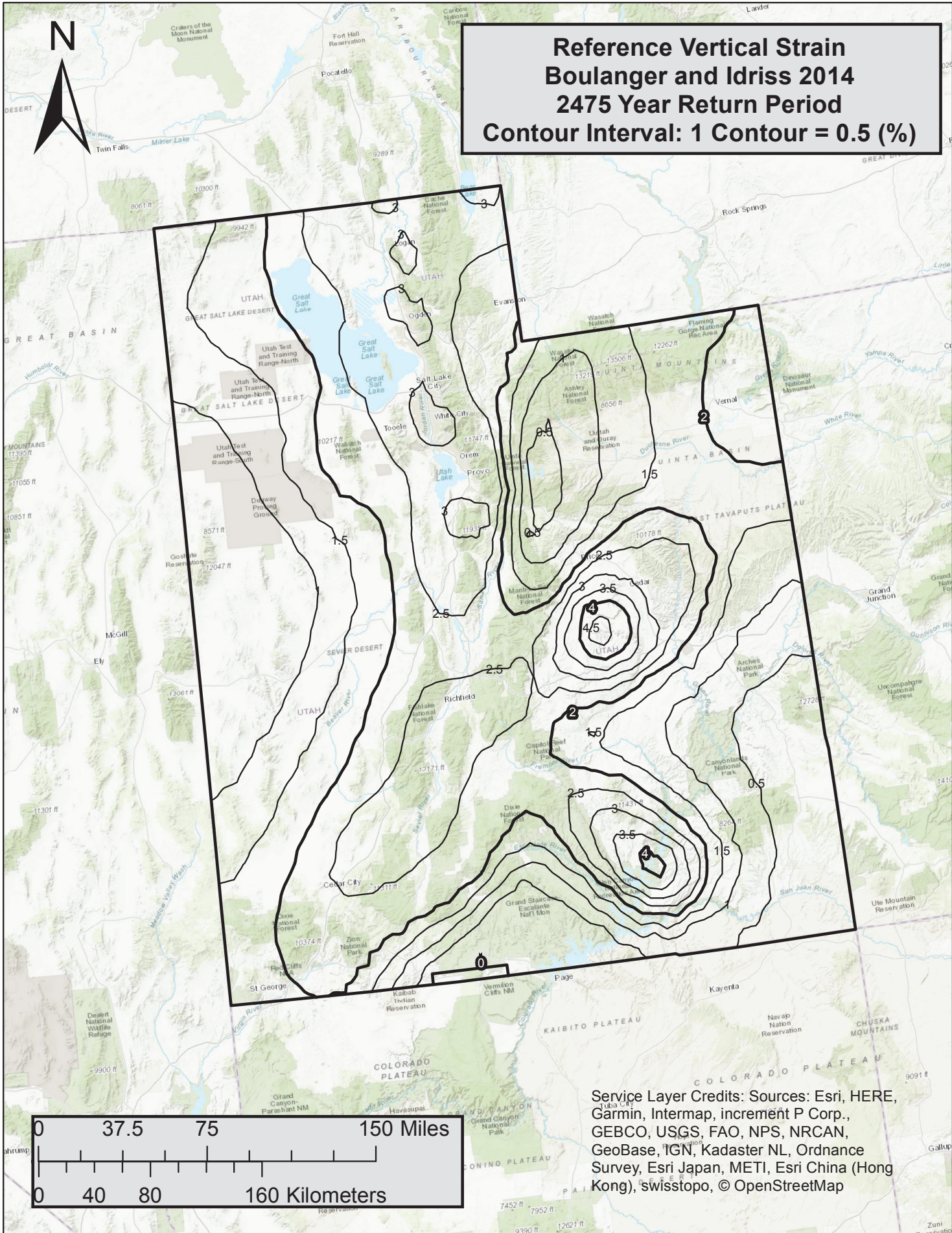
Service Layer Credits: Sources: Esri, HERE, Garmin, Intermap, increment P Corp., GEBCO, USGS, FAO, NPS, NRCAN, GeoBase, IGN, Kadaster NL, Ordnance Survey, Esri Japan, METI, Esri China (Hong Kong), swisstopo, © OpenStreetMap

**Reference Vertical Strain
Boulanger and Idriss 2014
1033 Year Return Period
Contour Interval: 1 Contour = 0.2 (%)**

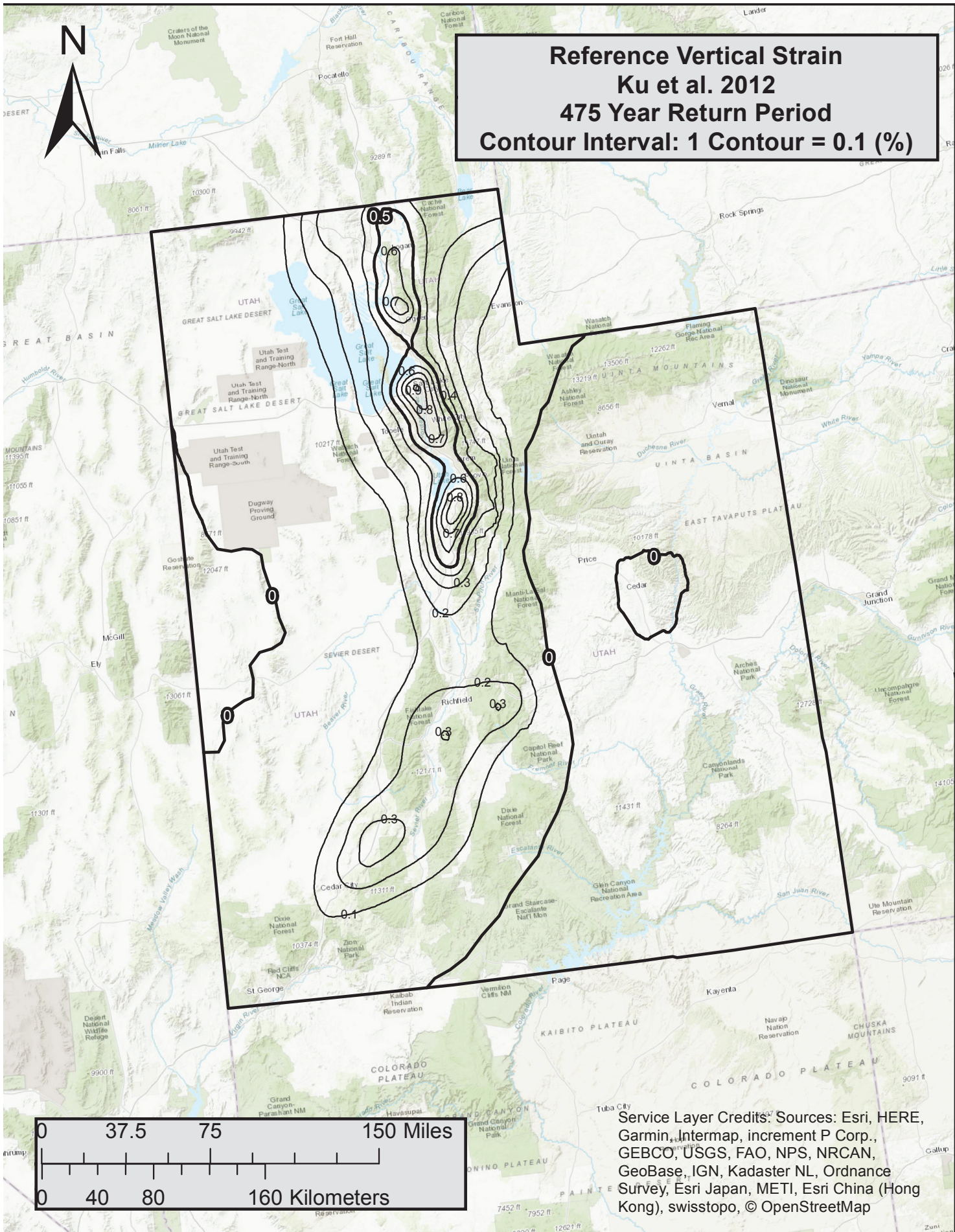


Service Layer Credits: Sources: Esri, HERE, Garmin, Intermap, increment P Corp., GEBCO, USGS, FAO, NPS, NRCAN, GeoBase, IGN, Kadaster NL, Ordnance Survey, Esri Japan, METI, Esri China (Hong Kong), swisstopo, © OpenStreetMap

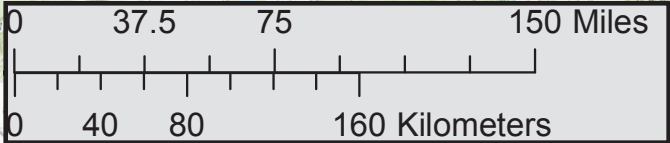
**Reference Vertical Strain
Boulanger and Idriss 2014
2475 Year Return Period
Contour Interval: 1 Contour = 0.5 (%)**



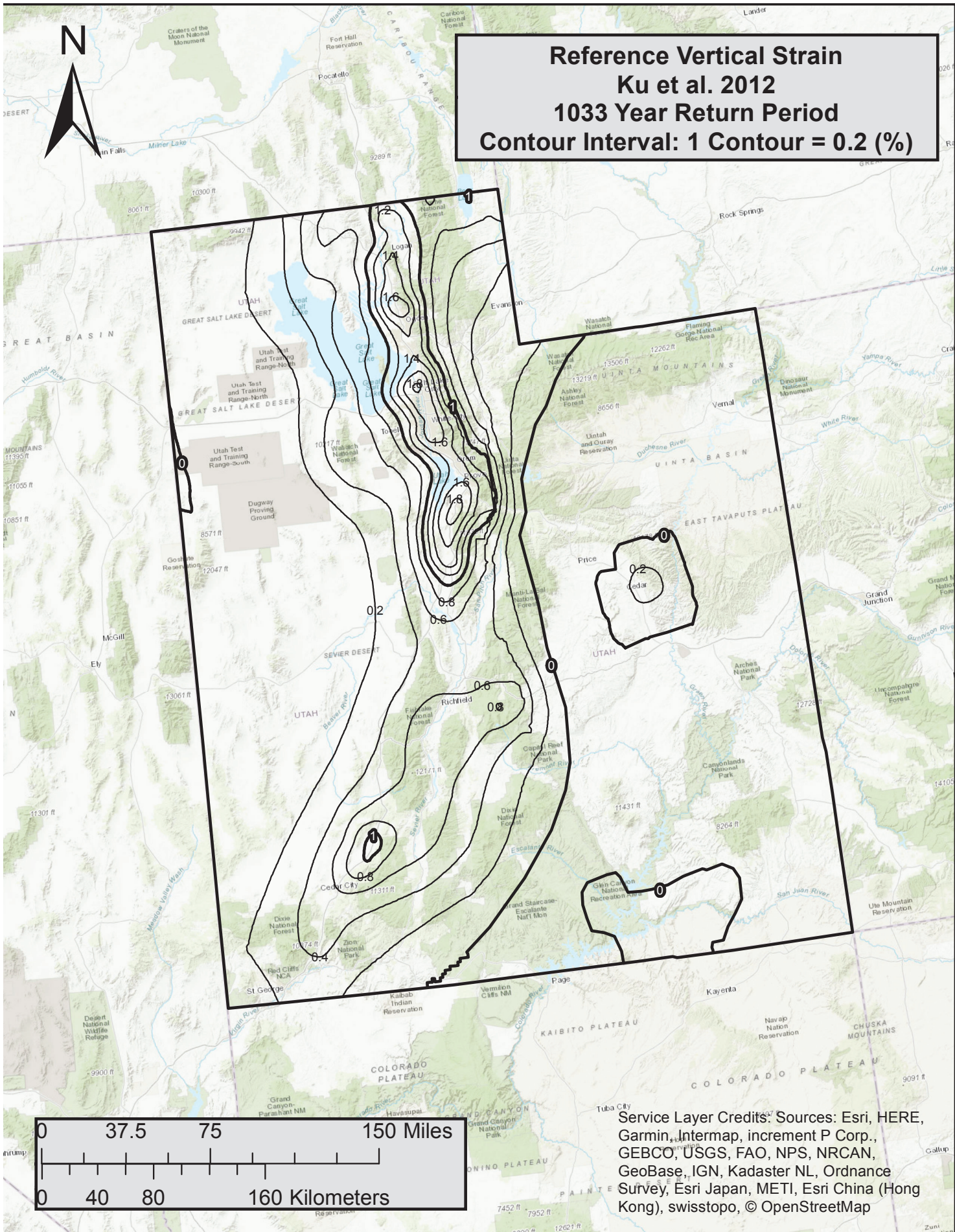
Service Layer Credits: Sources: Esri, HERE, Garmin, Intermap, increment P Corp., GEBCO, USGS, FAO, NPS, NRCAN, GeoBase, IGN, Kadaster NL, Ordnance Survey, Esri Japan, METI, Esri China (Hong Kong), swisstopo, © OpenStreetMap



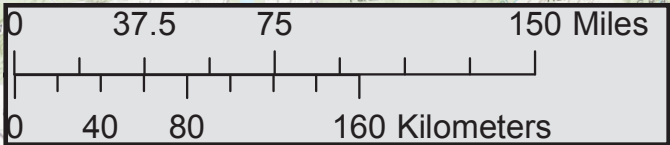
Reference Vertical Strain
Ku et al. 2012
475 Year Return Period
Contour Interval: 1 Contour = 0.1 (%)



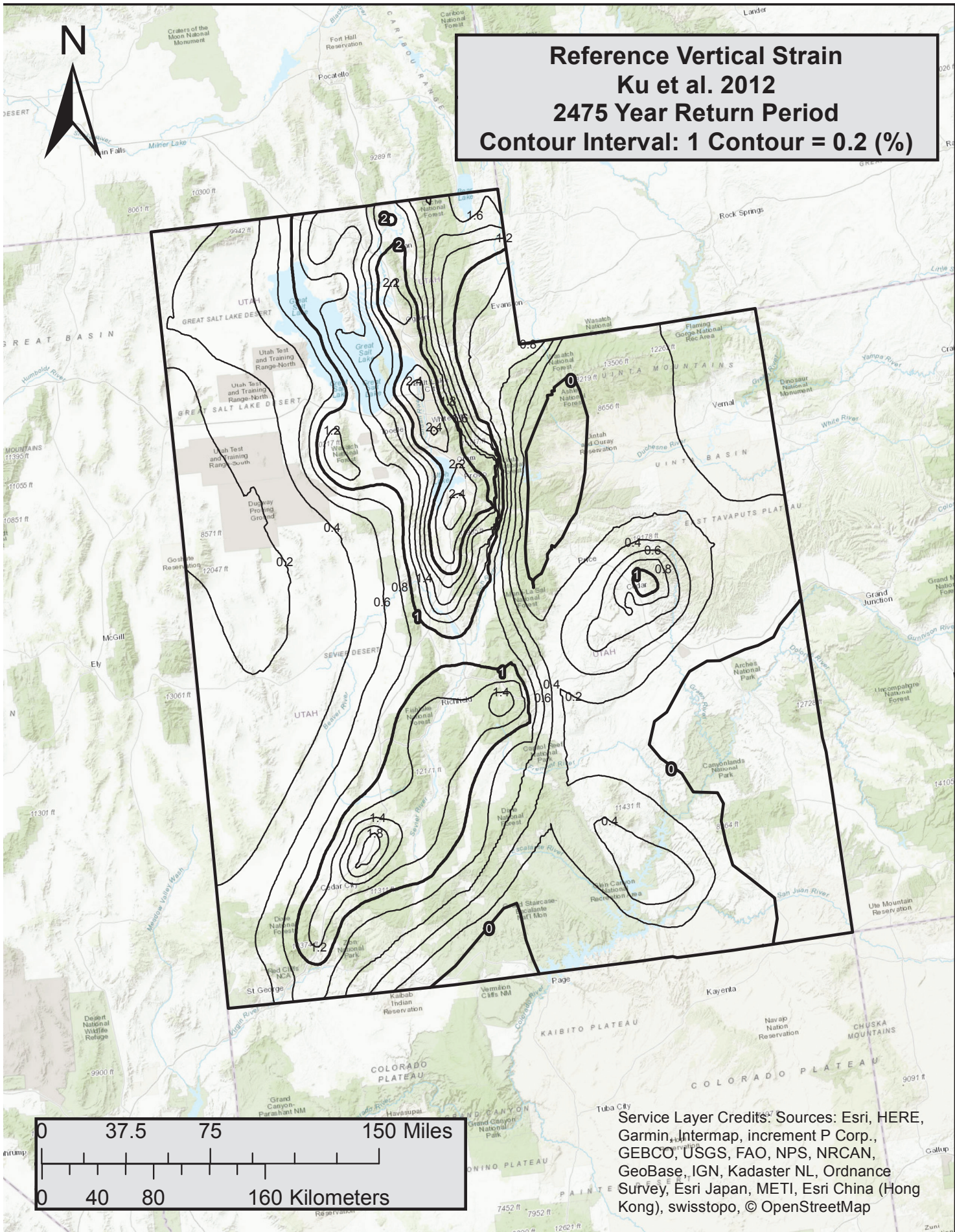
Service Layer Credits: Sources: Esri, HERE, Garmin, Intermap, increment P Corp., GEBCO, USGS, FAO, NPS, NRCAN, GeoBase, IGN, Kadaster NL, Ordnance Survey, Esri Japan, METI, Esri China (Hong Kong), swisstopo, © OpenStreetMap



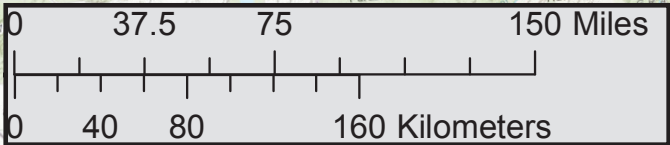
Reference Vertical Strain
Ku et al. 2012
1033 Year Return Period
Contour Interval: 1 Contour = 0.2 (%)



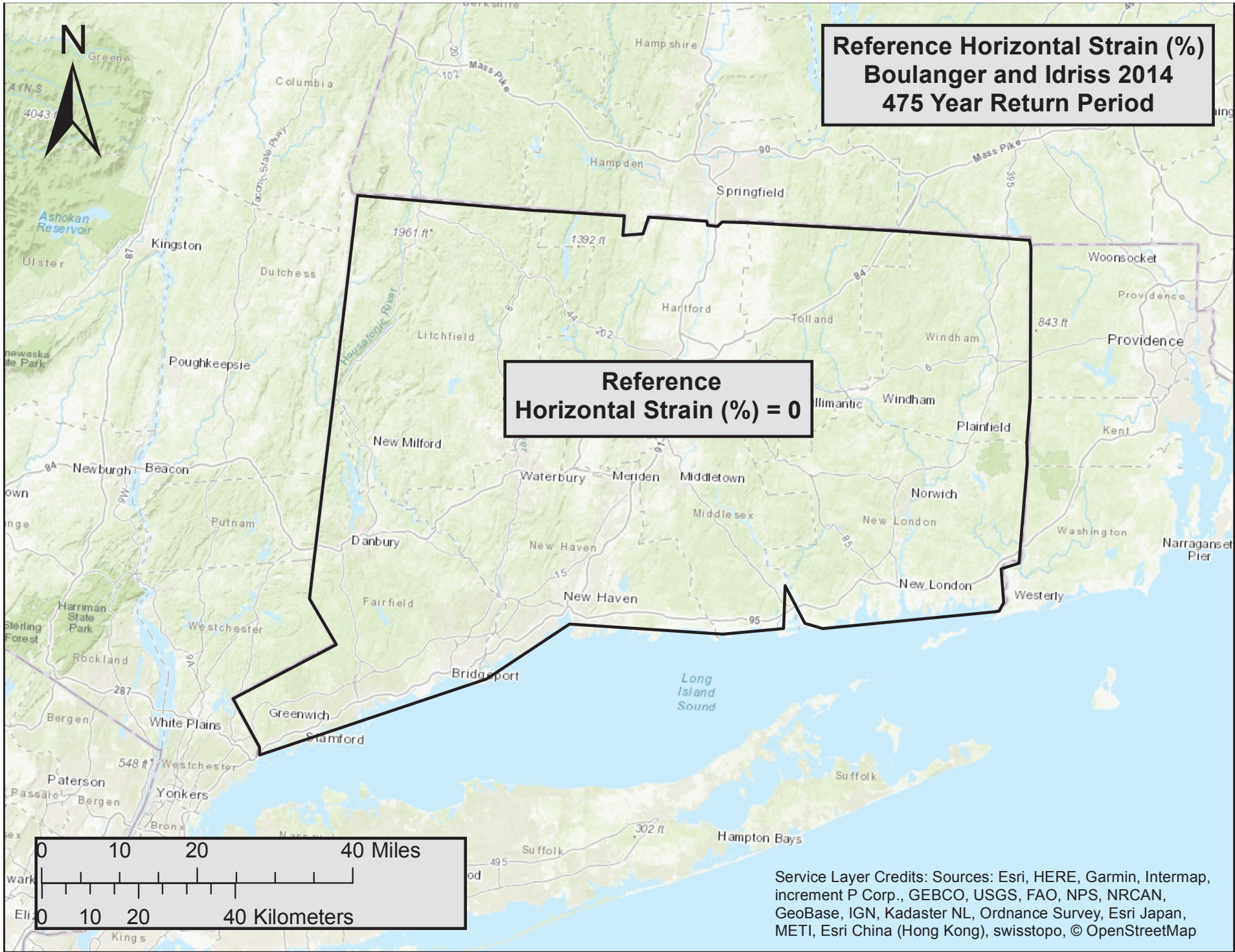
Service Layer Credits: Sources: Esri, HERE, Garmin, Intermap, increment P Corp., GEBCO, USGS, FAO, NPS, NRCAN, GeoBase, IGN, Kadaster NL, Ordnance Survey, Esri Japan, METI, Esri China (Hong Kong), swisstopo, © OpenStreetMap

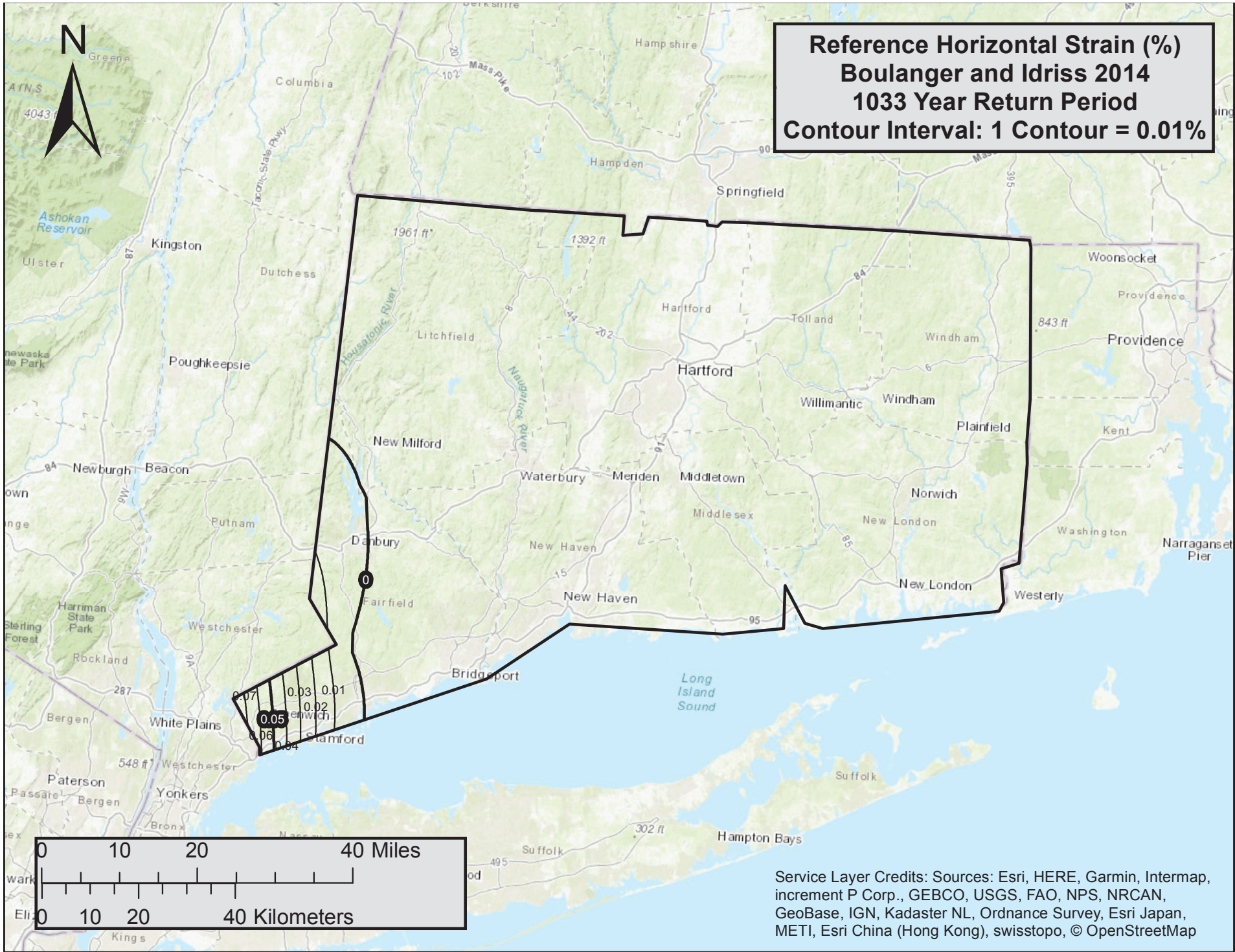


Reference Vertical Strain
Ku et al. 2012
2475 Year Return Period
Contour Interval: 1 Contour = 0.2 (%)

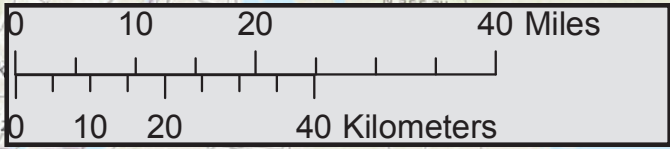


Service Layer Credits: Sources: Esri, HERE, Garmin, Intermap, increment P Corp., GEBCO, USGS, FAO, NPS, NRCAN, GeoBase, IGN, Kadaster NL, Ordnance Survey, Esri Japan, METI, Esri China (Hong Kong), swisstopo, © OpenStreetMap

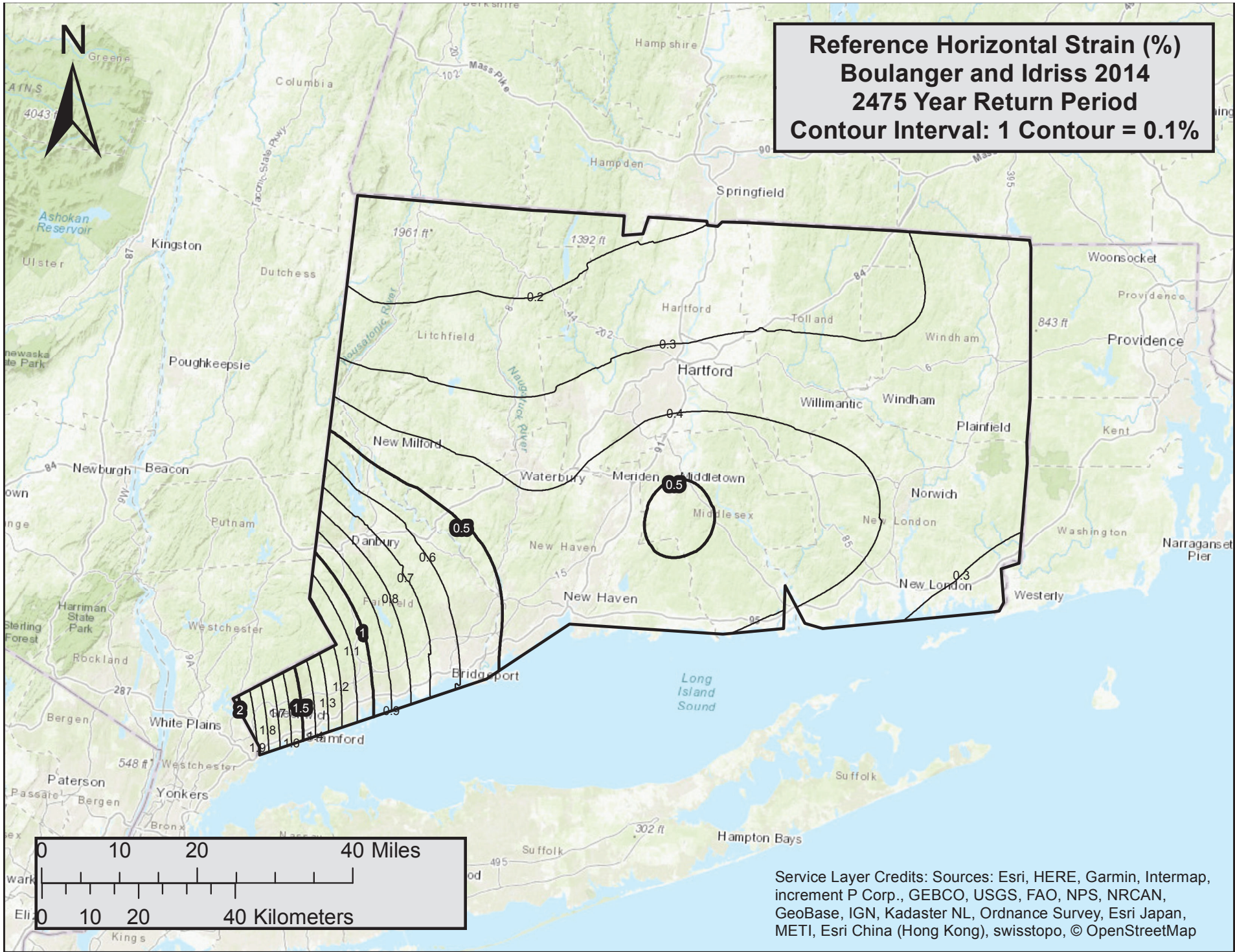


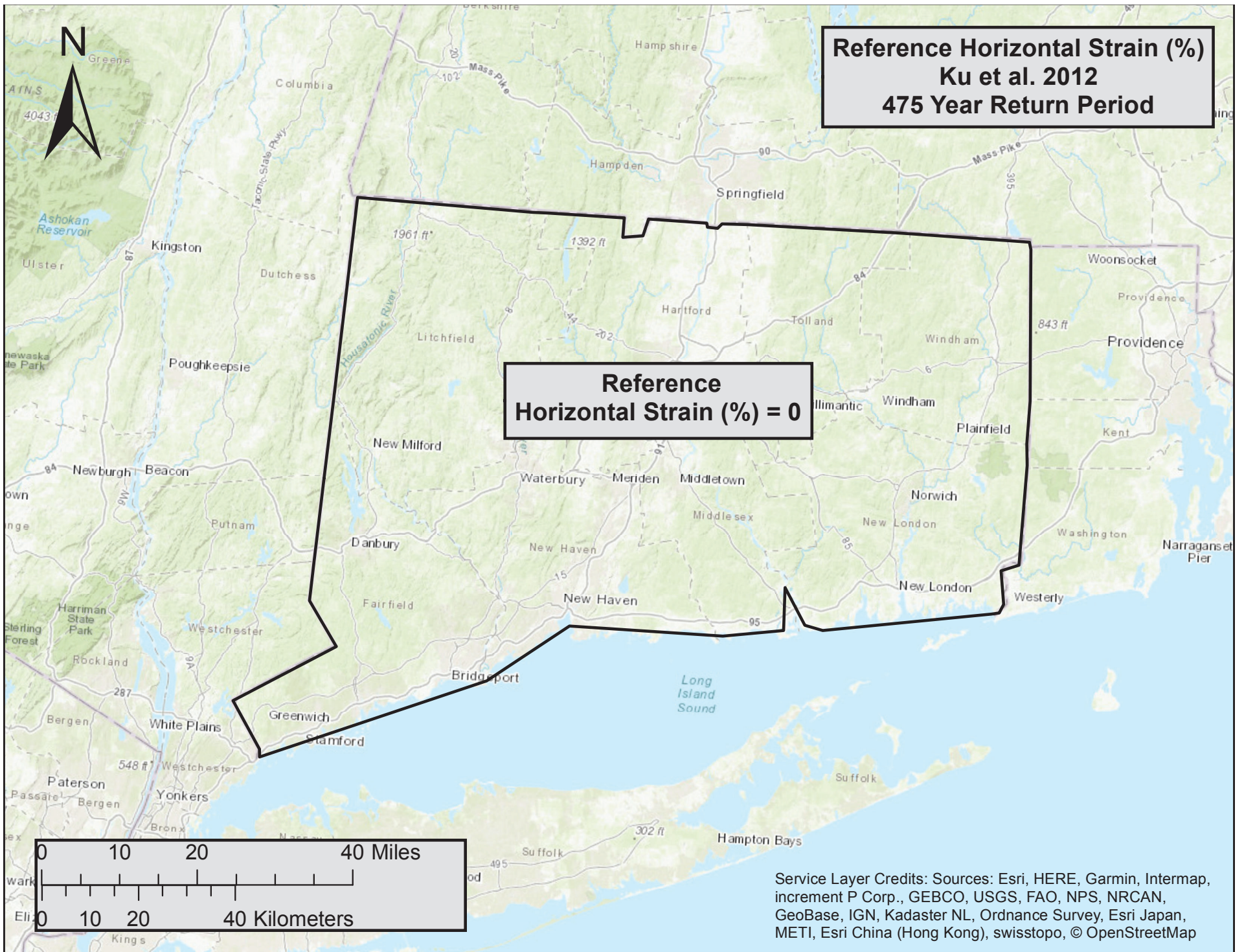


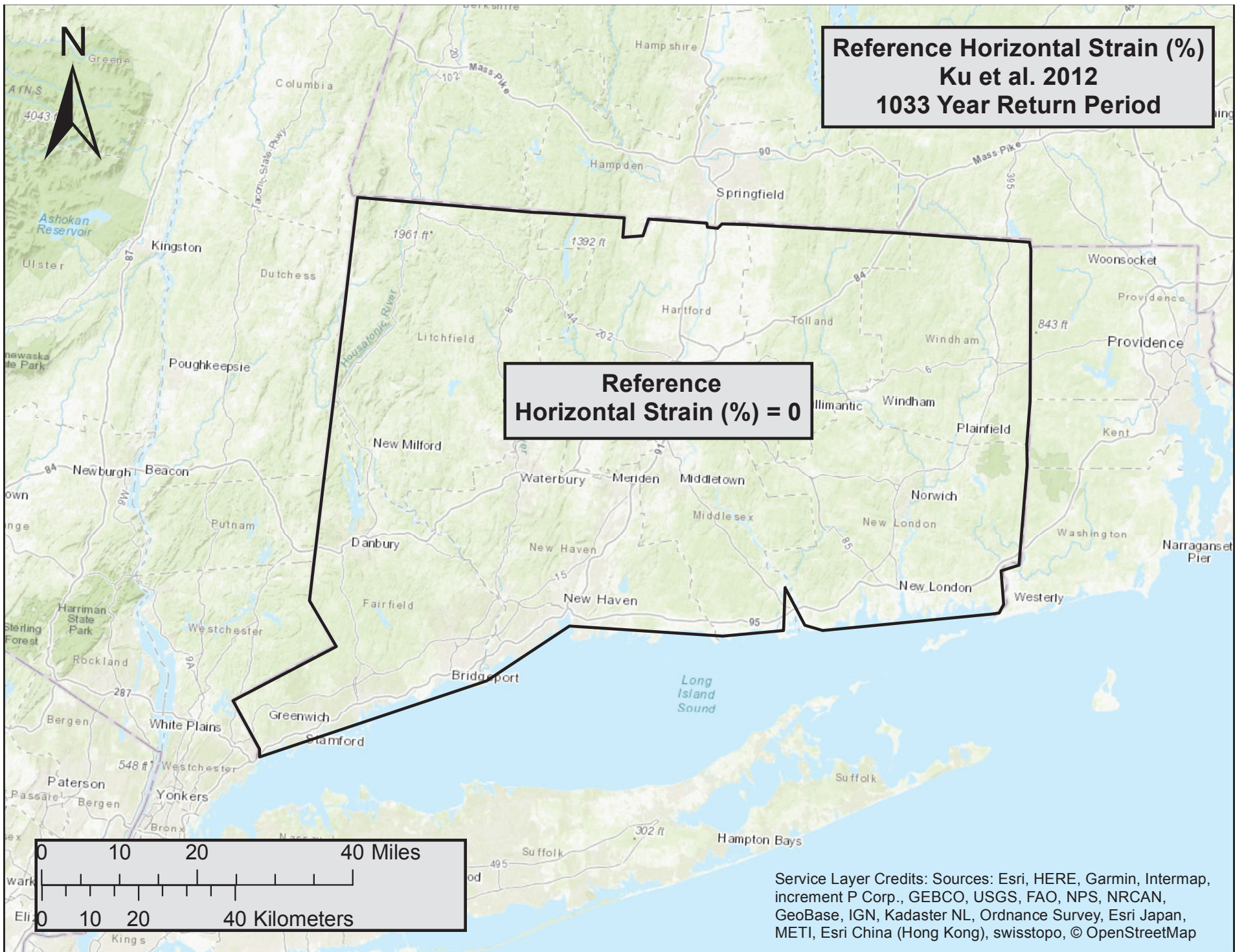
Reference Horizontal Strain (%)
Boulanger and Idriss 2014
1033 Year Return Period
Contour Interval: 1 Contour = 0.01%

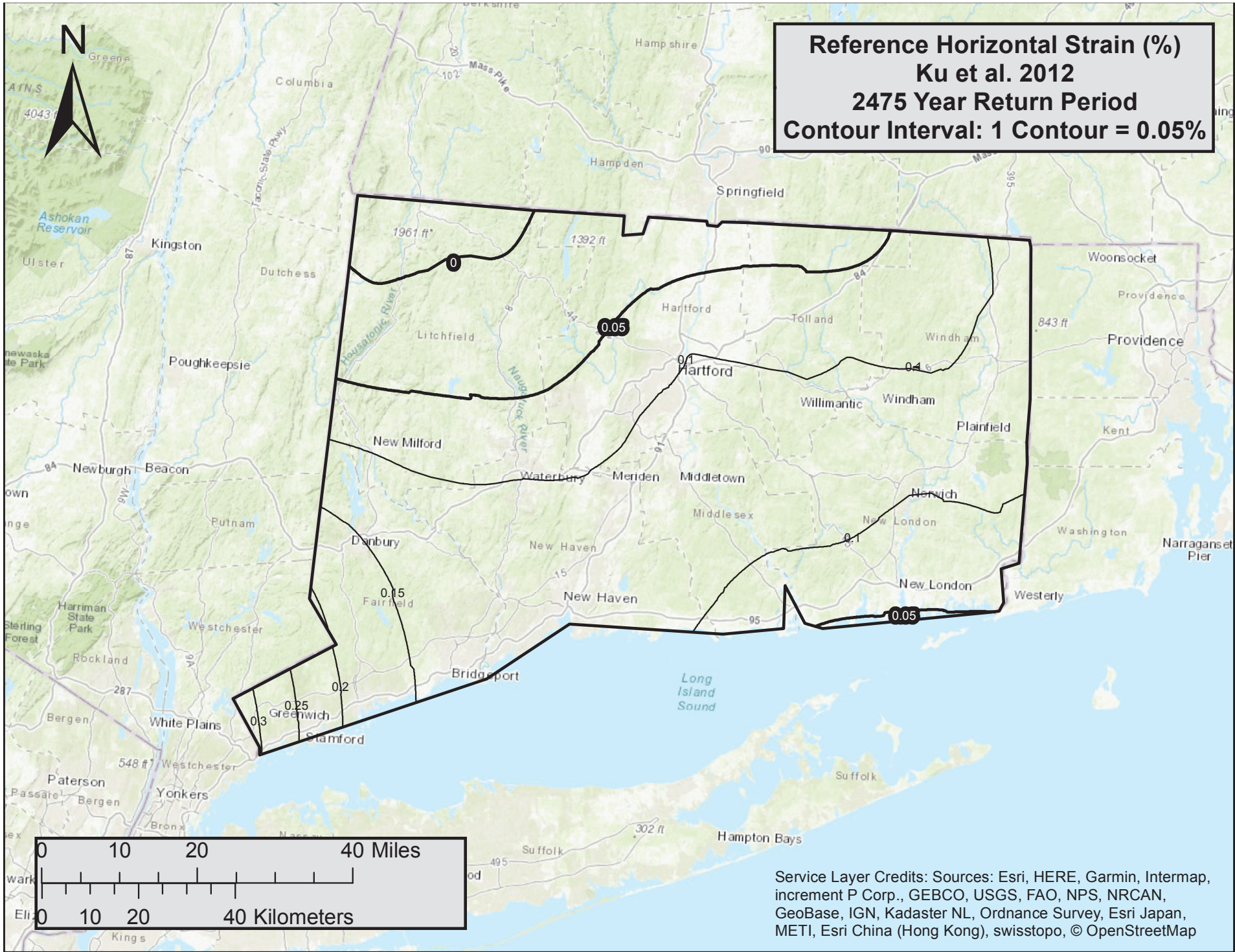


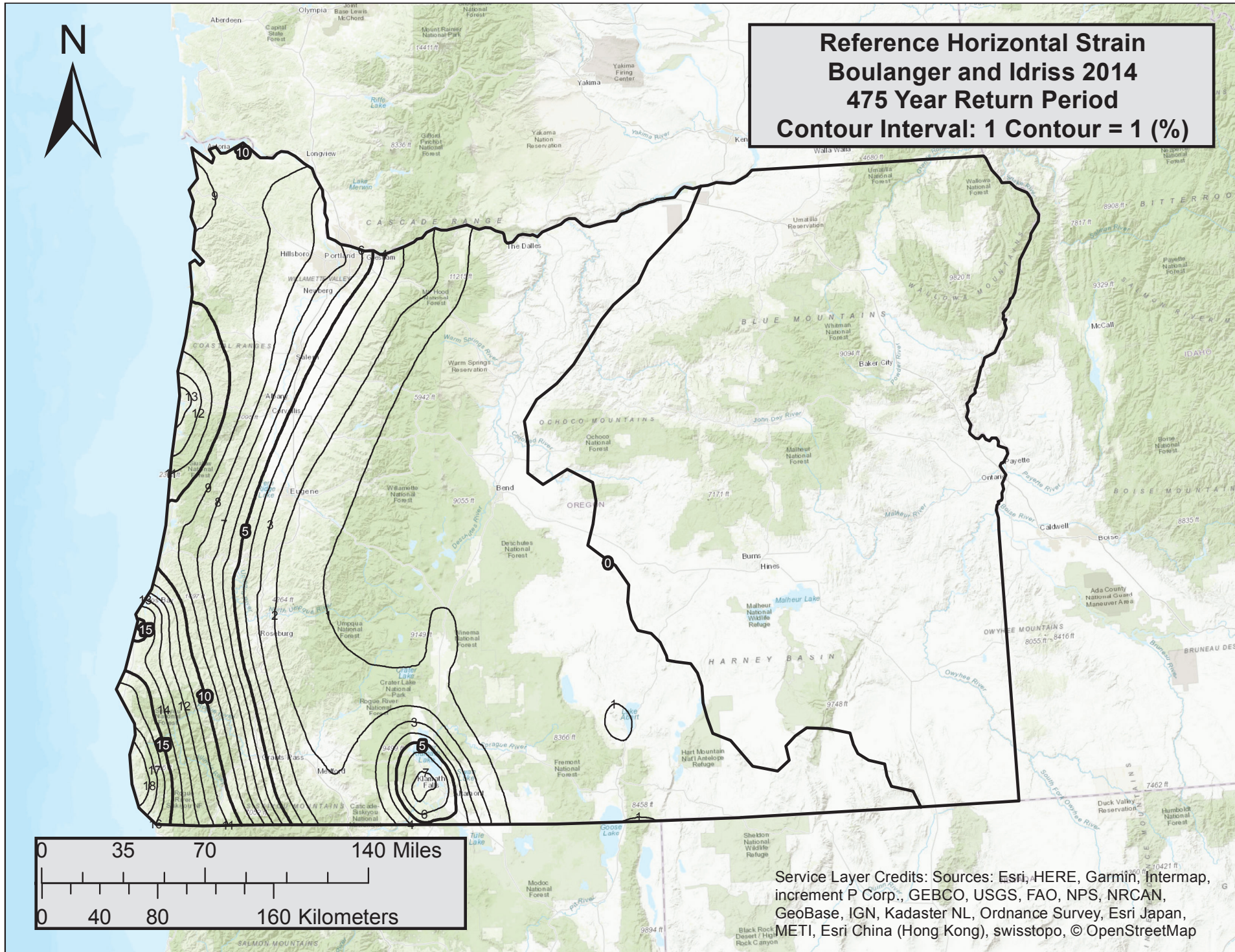
Service Layer Credits: Sources: Esri, HERE, Garmin, Intermap, increment P Corp., GEBCO, USGS, FAO, NPS, NRCAN, GeoBase, IGN, Kadaster NL, Ordnance Survey, Esri Japan, METI, Esri China (Hong Kong), swisstopo, © OpenStreetMap

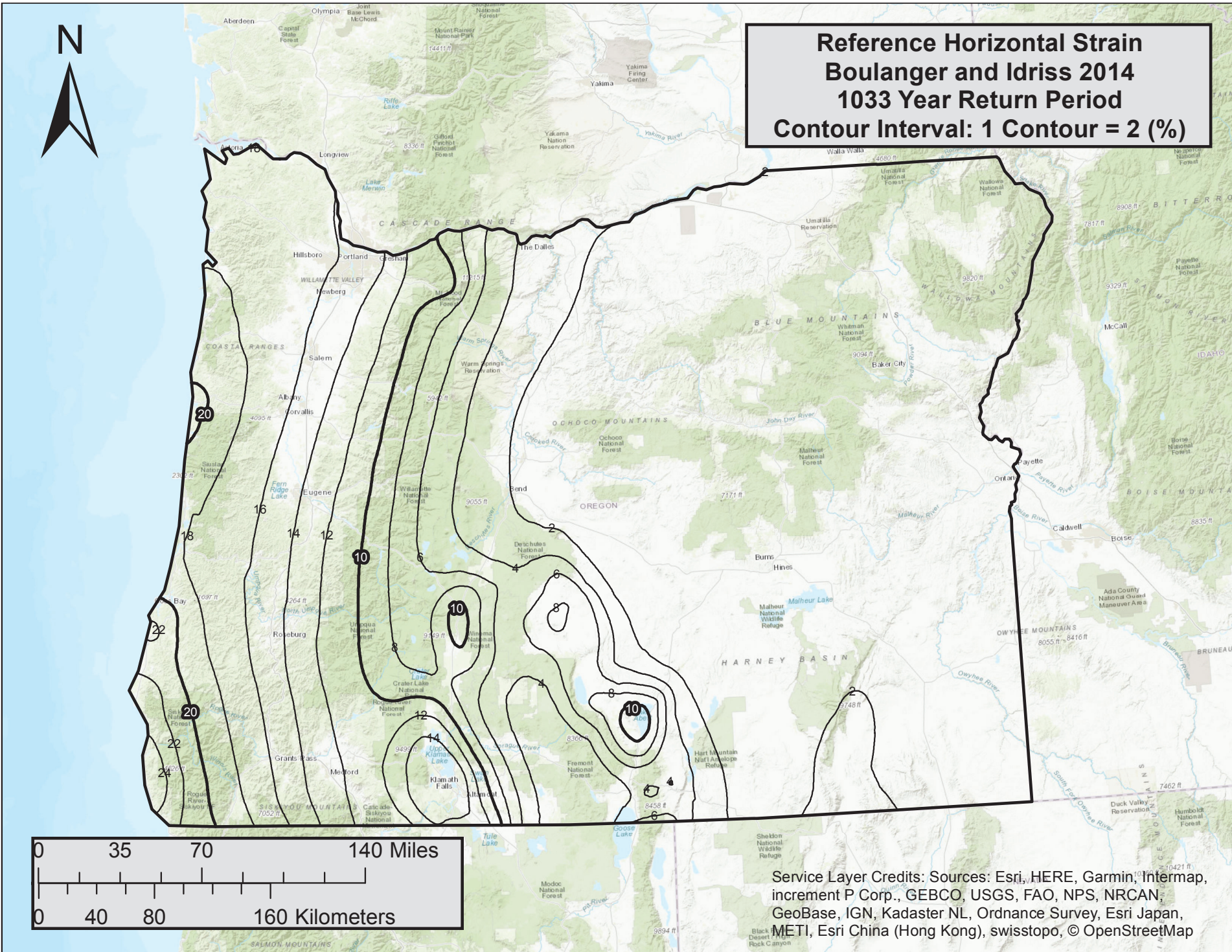




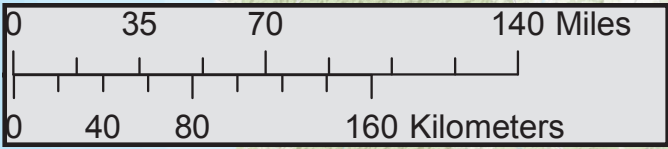




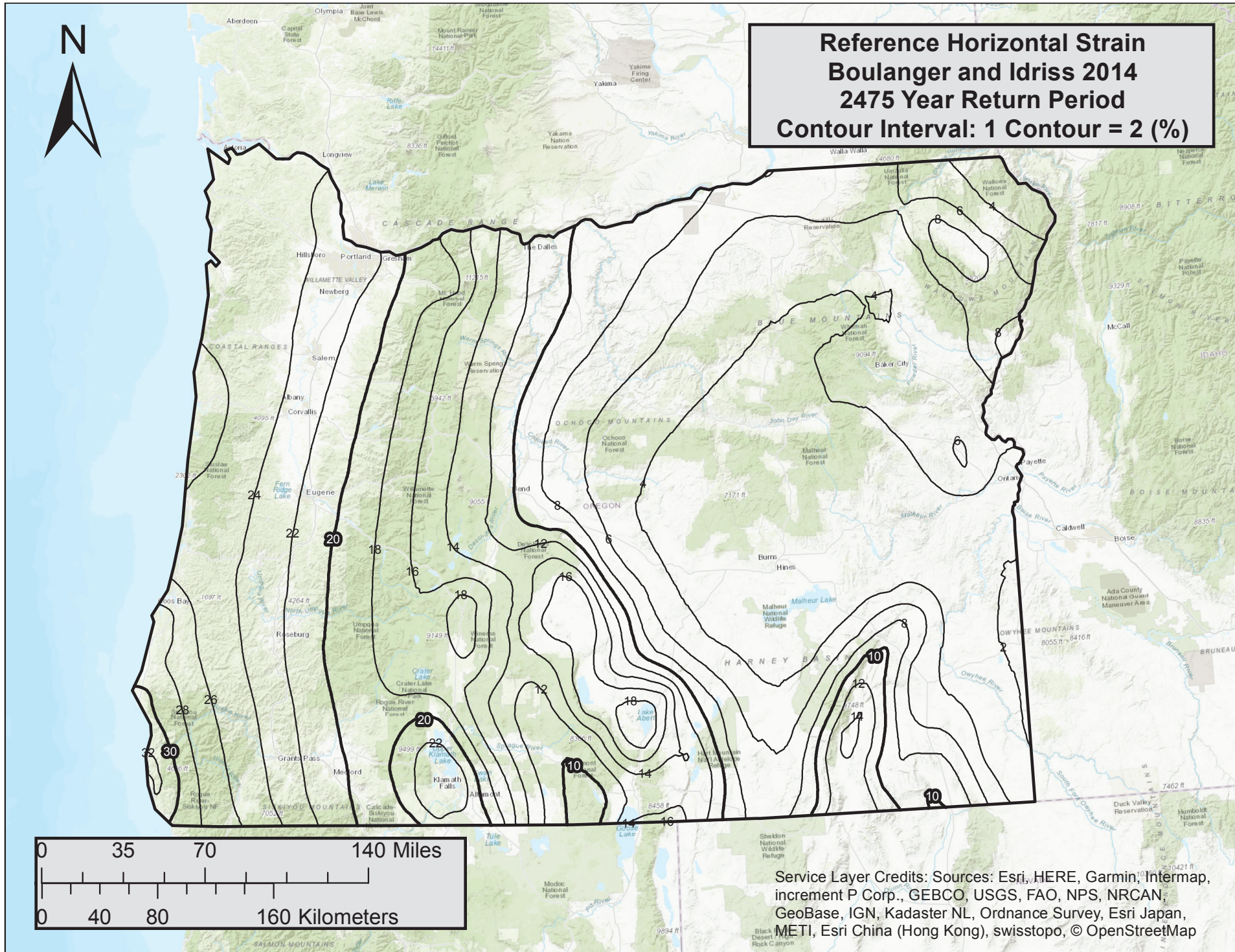




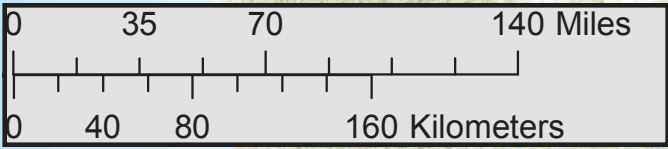
**Reference Horizontal Strain
Boulanger and Idriss 2014
1033 Year Return Period
Contour Interval: 1 Contour = 2 (%)**



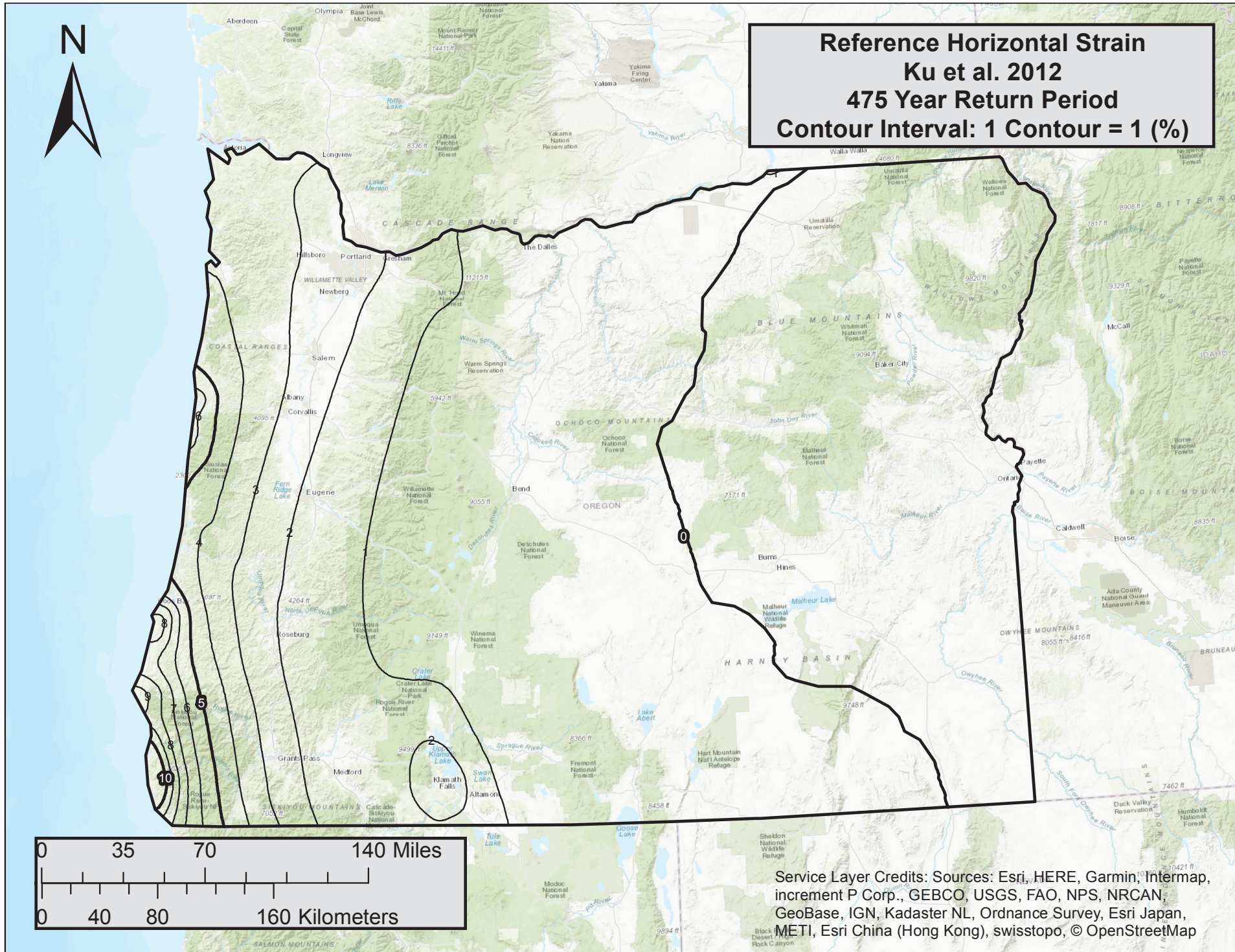
Service Layer Credits: Sources: Esri, HERE, Garmin, Intermap, increment P Corp., GEBCO, USGS, FAO, NPS, NRCAN, GeoBase, IGN, Kadaster NL, Ordnance Survey, Esri Japan, METI, Esri China (Hong Kong), swisstopo, © OpenStreetMap



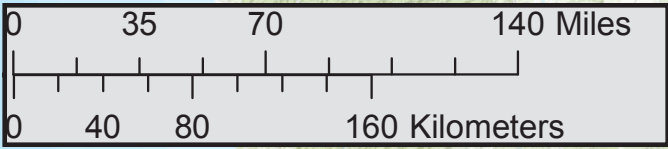
**Reference Horizontal Strain
Boulanger and Idriss 2014
2475 Year Return Period
Contour Interval: 1 Contour = 2 (%)**



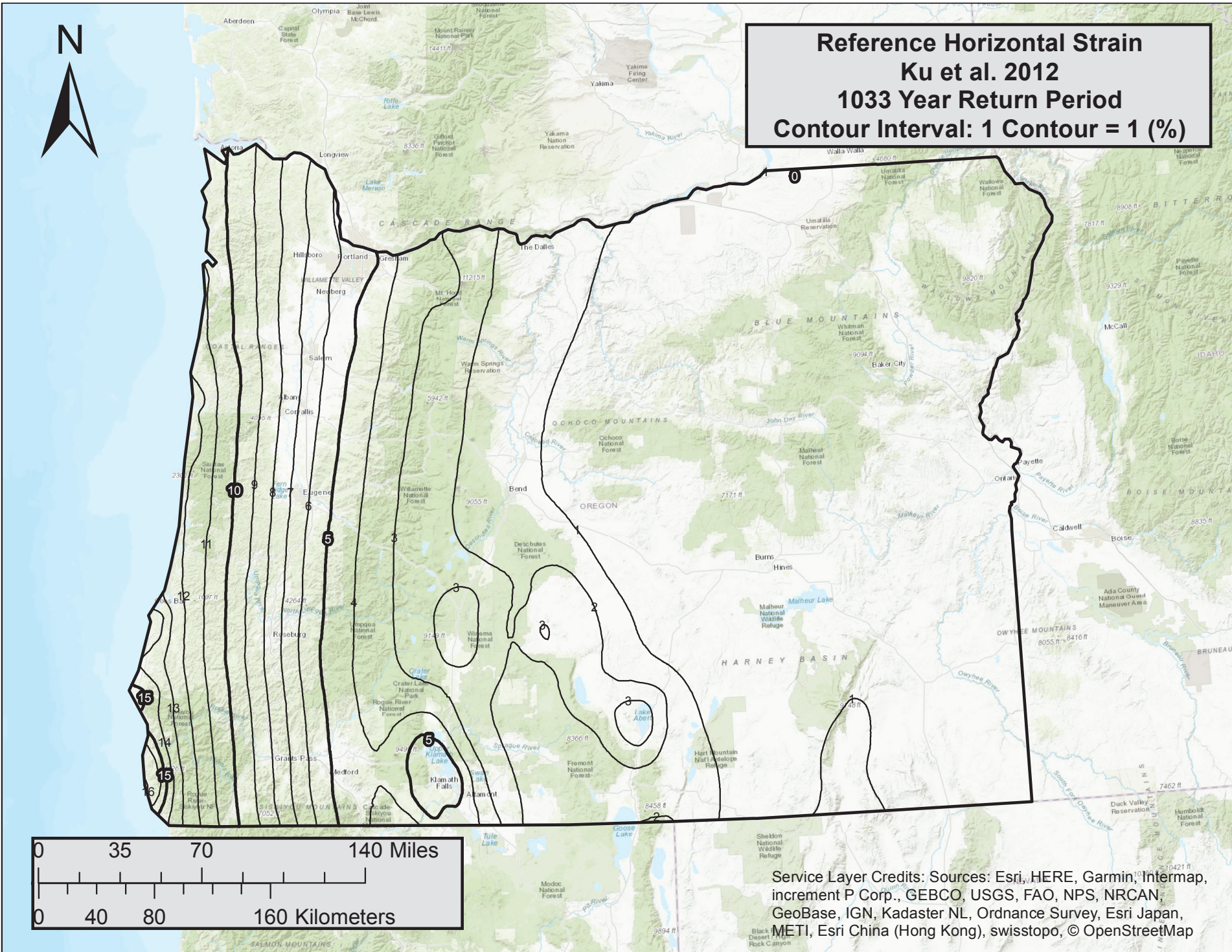
Service Layer Credits: Sources: Esri, HERE, Garmin, Intermap, increment P Corp., GEBCO, USGS, FAO, NPS, NRCAN, GeoBase, IGN, Kadaster NL, Ordnance Survey, Esri Japan, METI, Esri China (Hong Kong), swisstopo, © OpenStreetMap



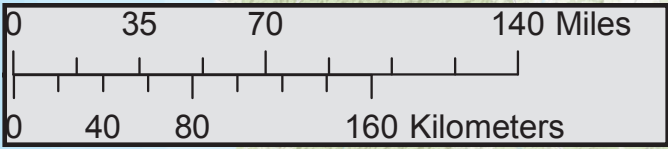
Reference Horizontal Strain
Ku et al. 2012
475 Year Return Period
Contour Interval: 1 Contour = 1 (%)



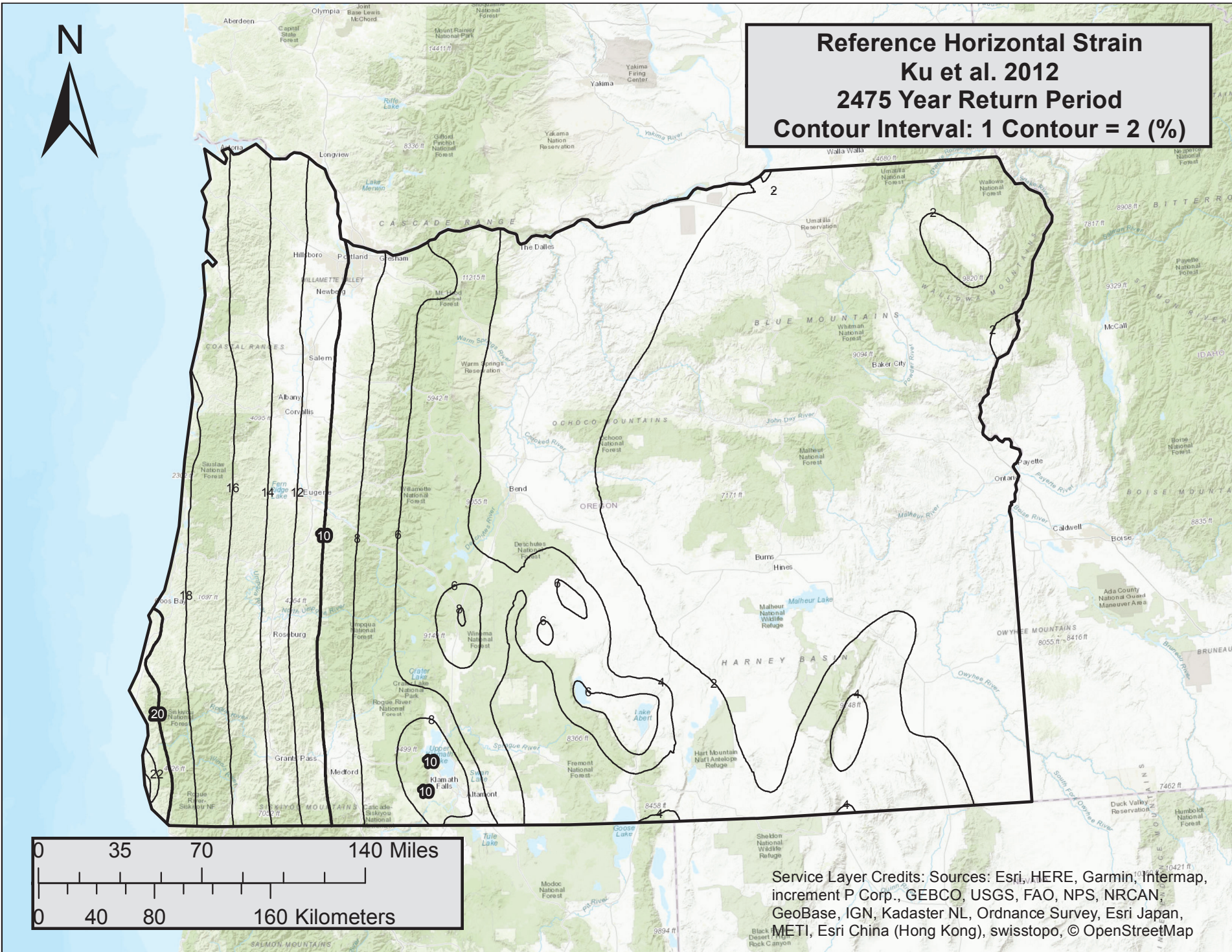
Service Layer Credits: Sources: Esri, HERE, Garmin, Intermap, increment P Corp., GEBCO, USGS, FAO, NPS, NRCAN, GeoBase, IGN, Kadaster NL, Ordnance Survey, Esri Japan, METI, Esri China (Hong Kong), swisstopo, © OpenStreetMap



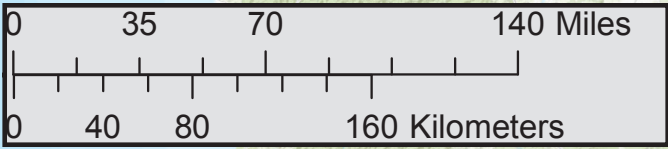
Reference Horizontal Strain
Ku et al. 2012
1033 Year Return Period
Contour Interval: 1 Contour = 1 (%)



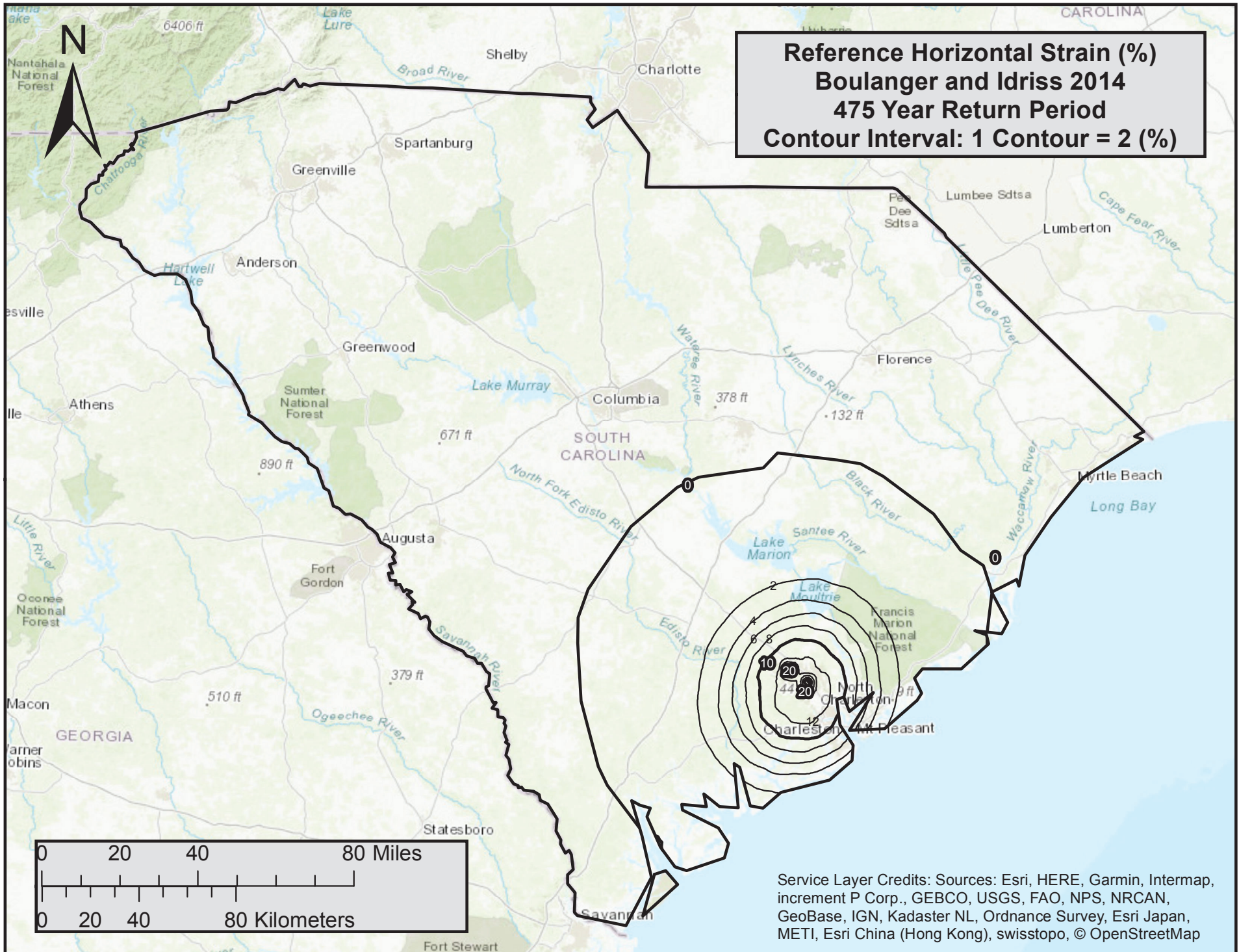
Service Layer Credits: Sources: Esri, HERE, Garmin, Intermap, increment P Corp., GEBCO, USGS, FAO, NPS, NRCAN, GeoBase, IGN, Kadaster NL, Ordnance Survey, Esri Japan, METI, Esri China (Hong Kong), swisstopo, © OpenStreetMap

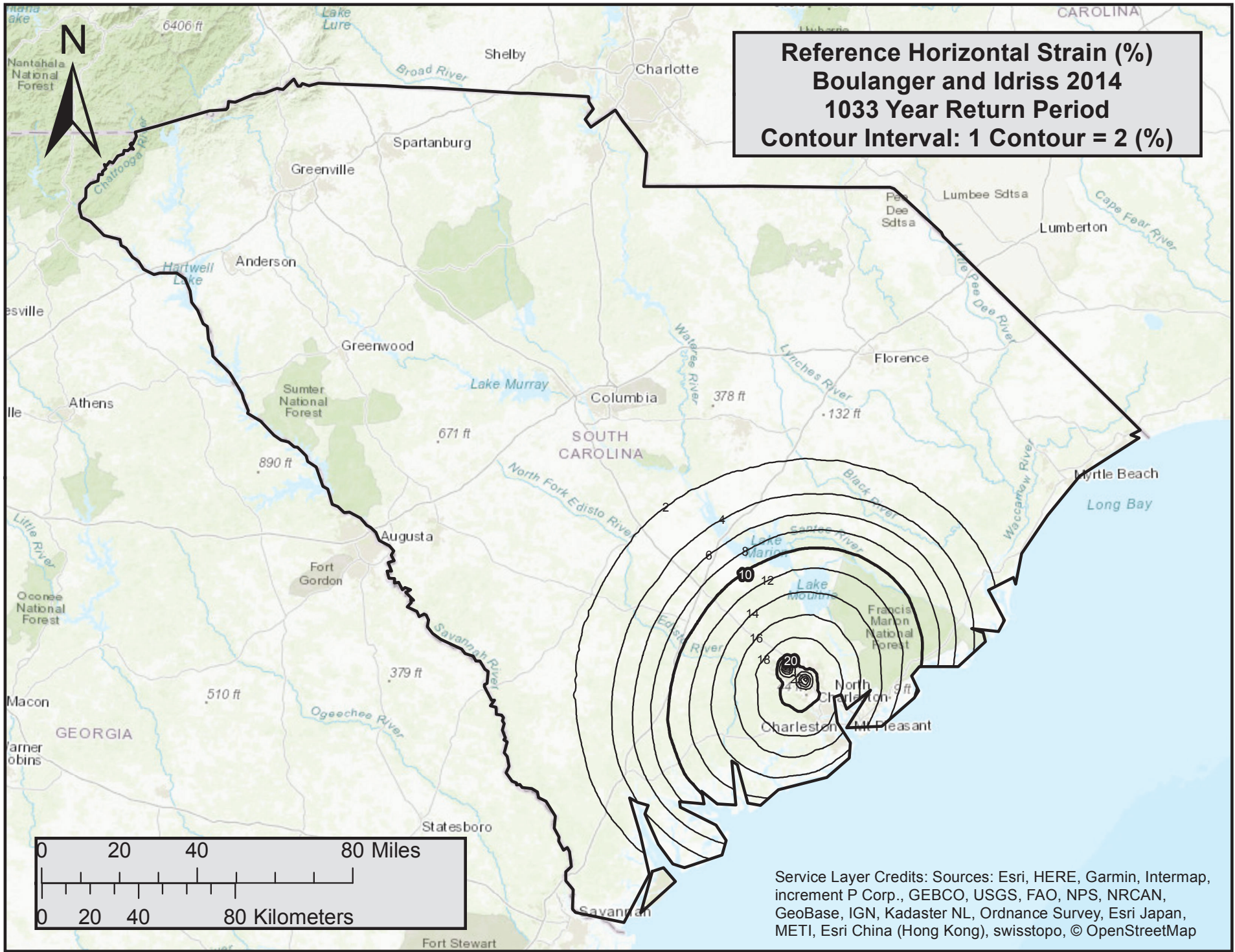


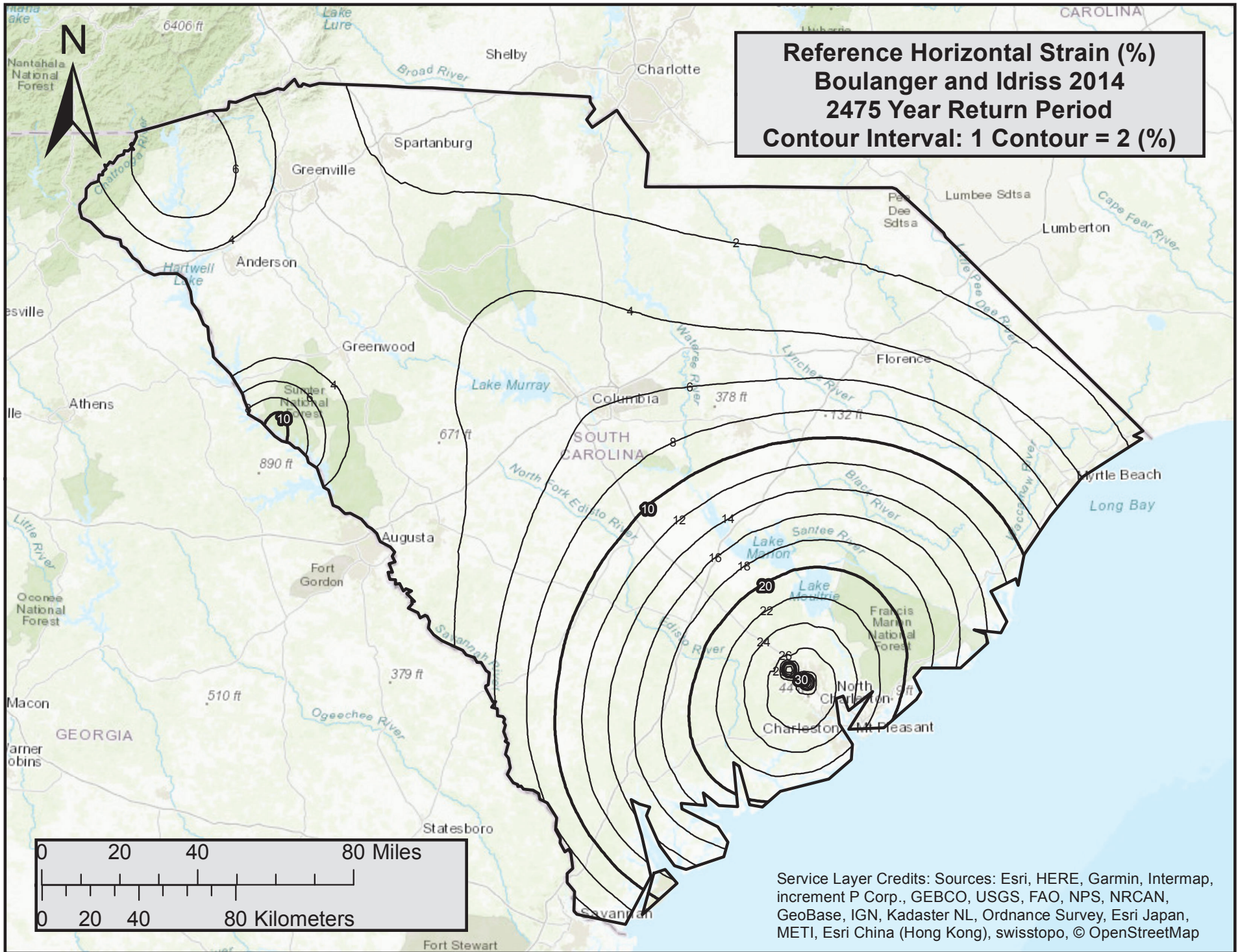
Reference Horizontal Strain
Ku et al. 2012
2475 Year Return Period
Contour Interval: 1 Contour = 2 (%)

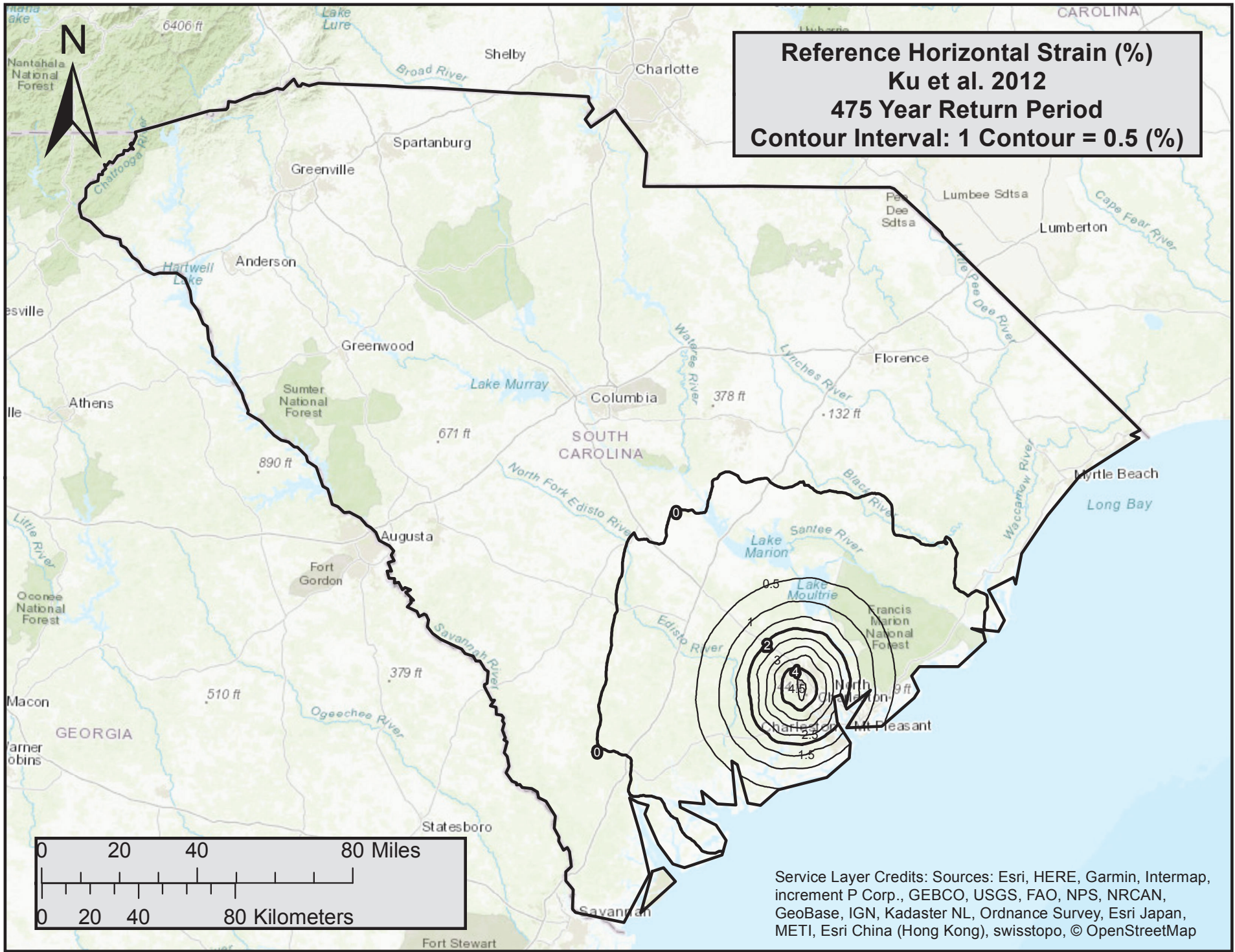


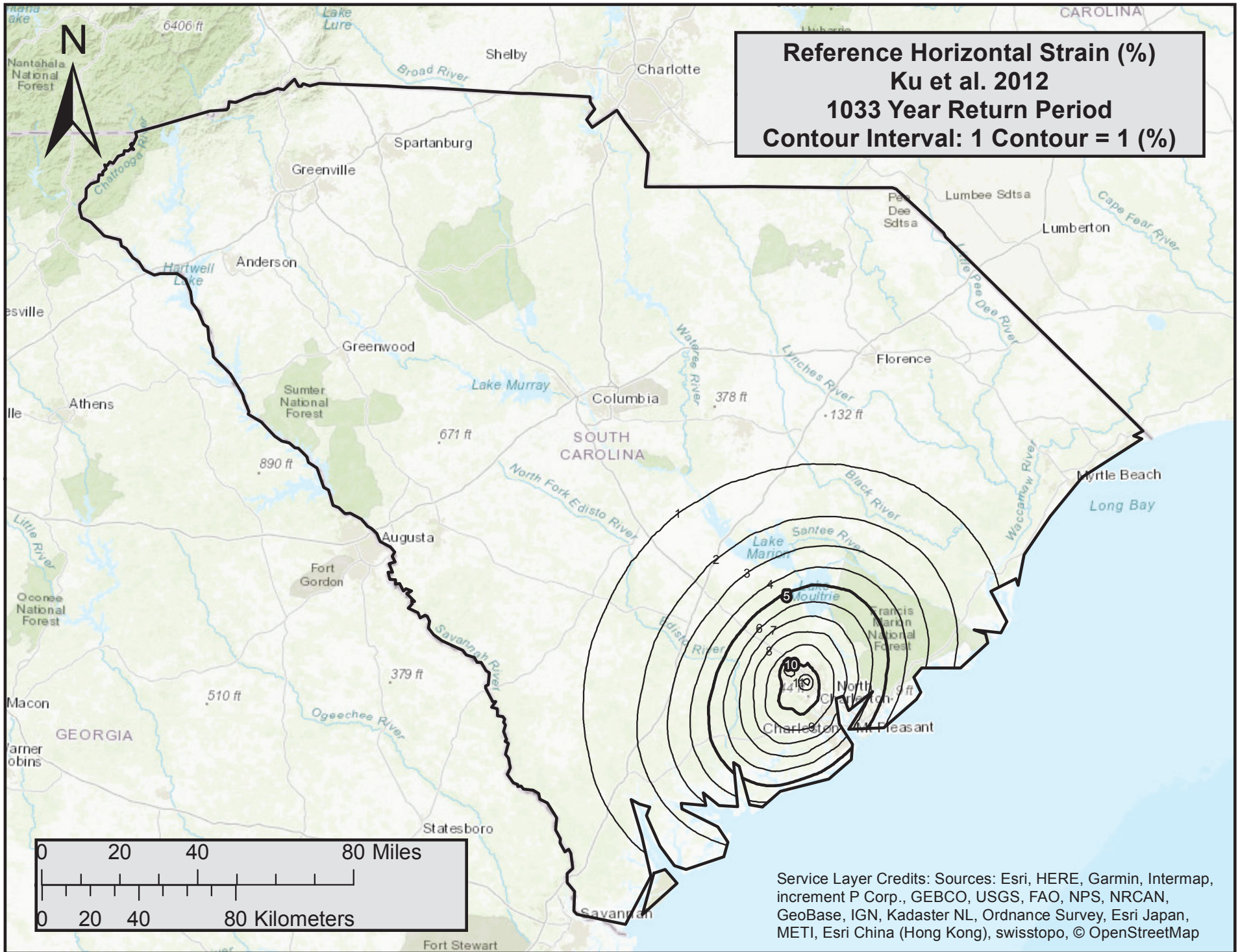
Service Layer Credits: Sources: Esri, HERE, Garmin, Intermap, increment P Corp., GEBCO, USGS, FAO, NPS, NRCAN, GeoBase, IGN, Kadaster NL, Ordnance Survey, Esri Japan, METI, Esri China (Hong Kong), swisstopo, © OpenStreetMap

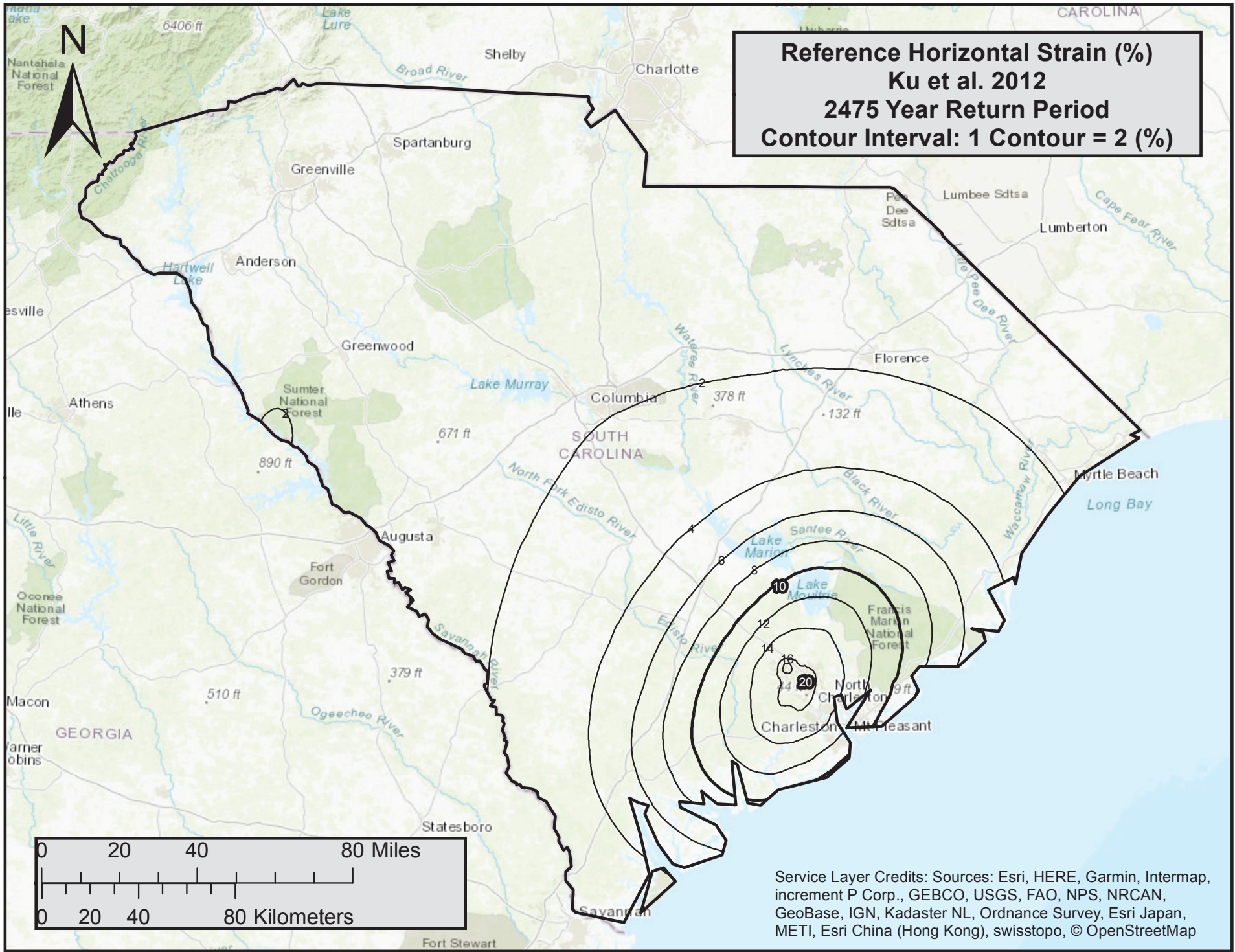


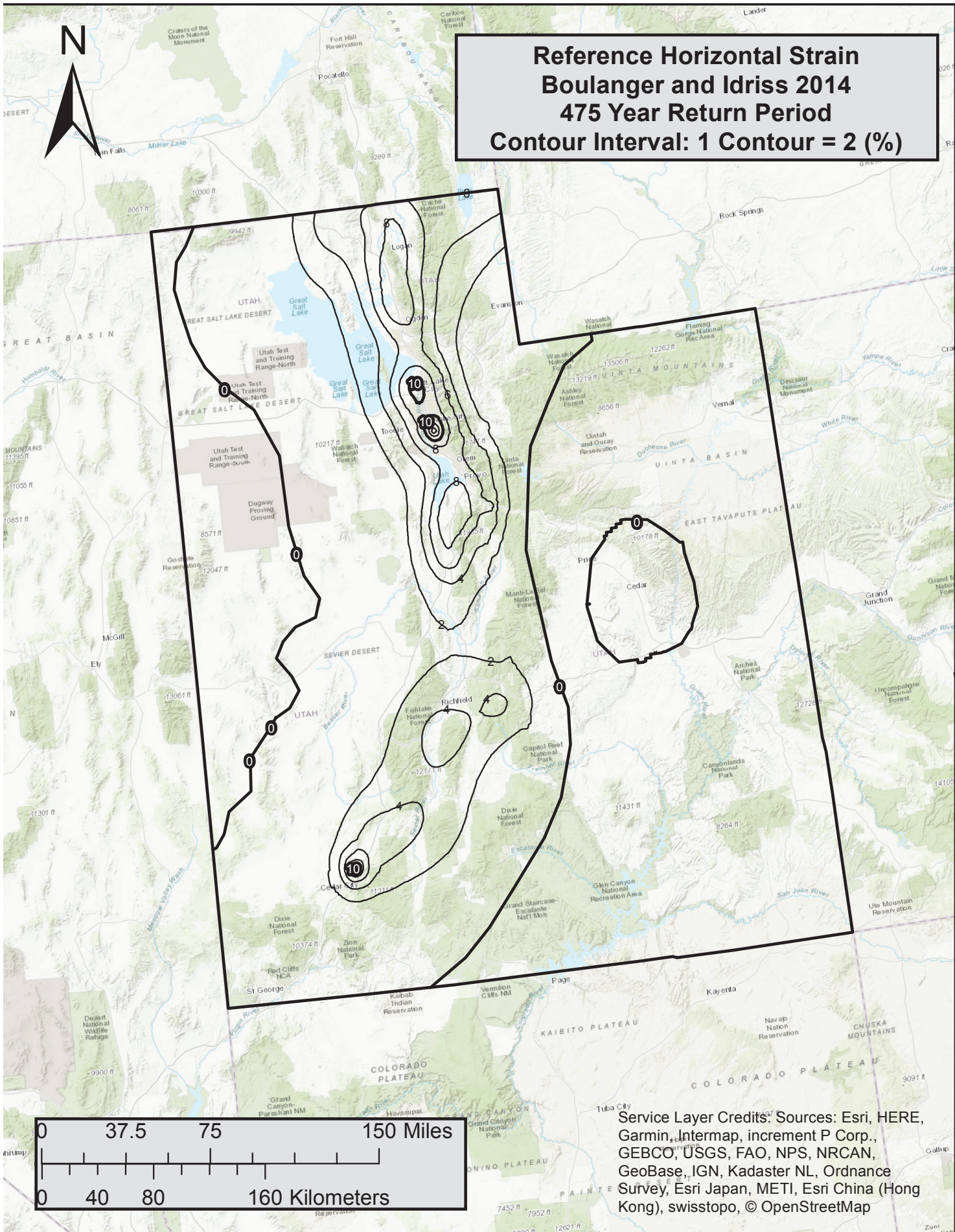




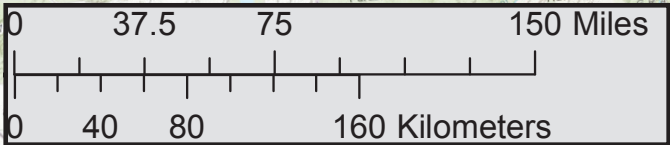




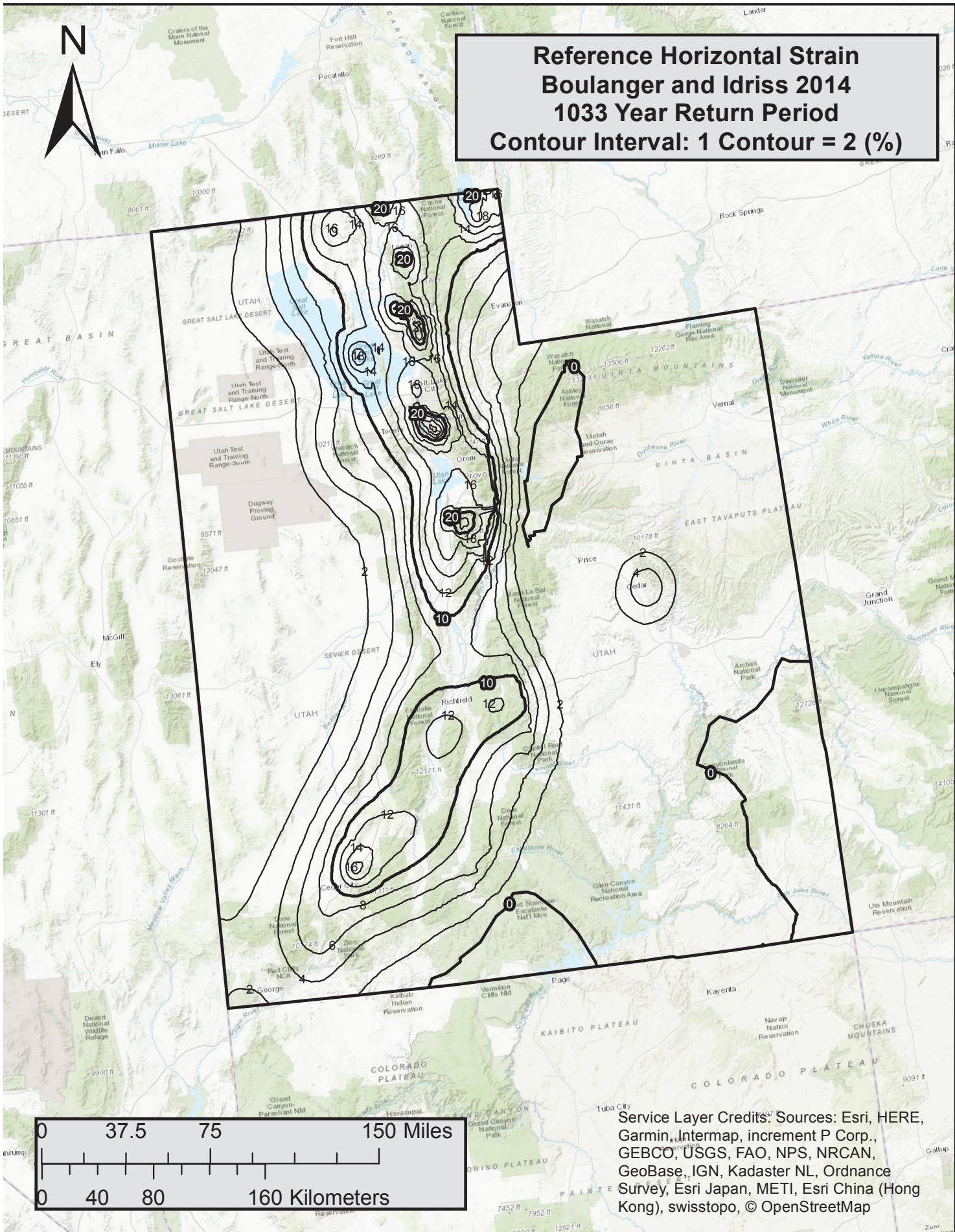


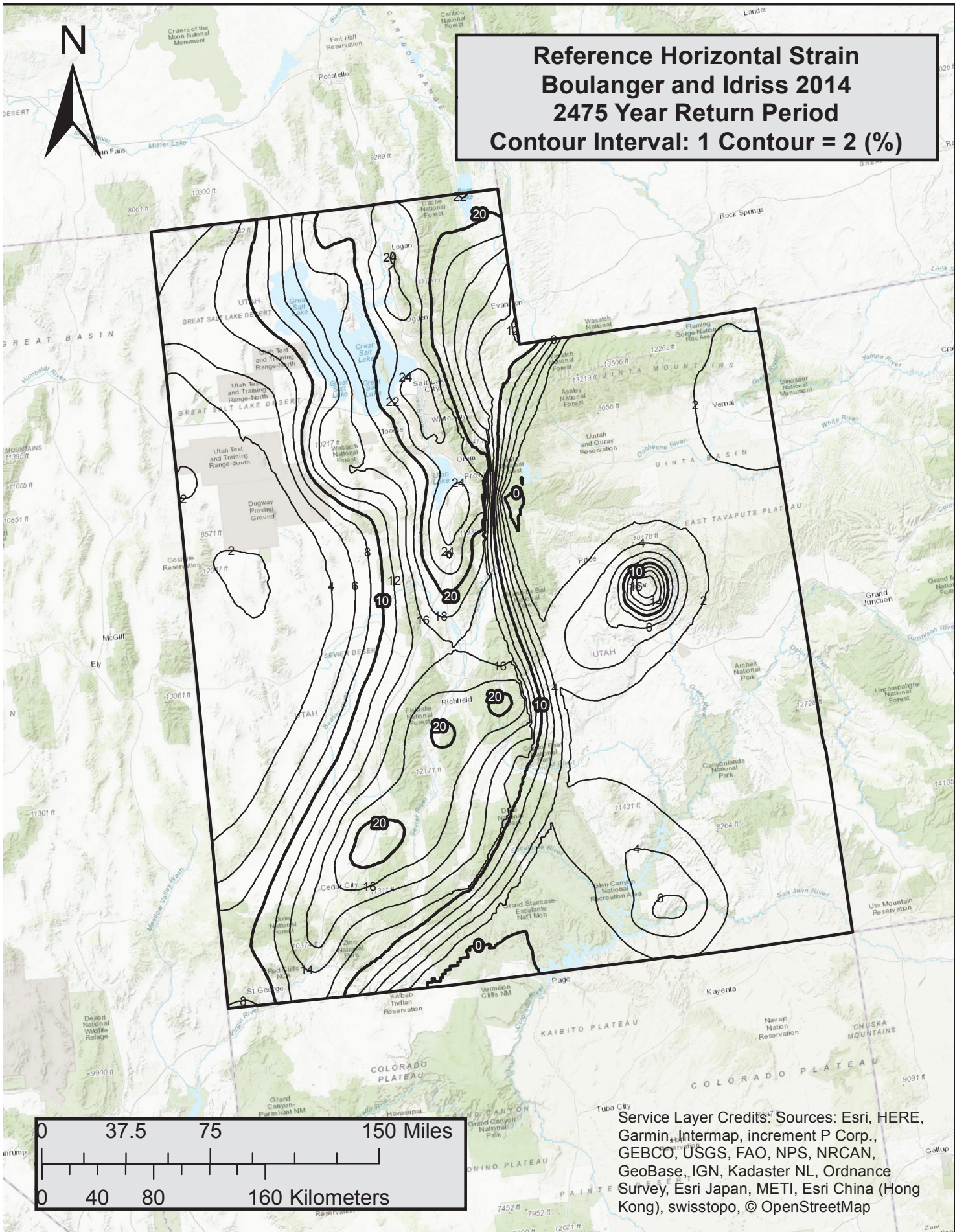


**Reference Horizontal Strain
Boulanger and Idriss 2014
475 Year Return Period
Contour Interval: 1 Contour = 2 (%)**

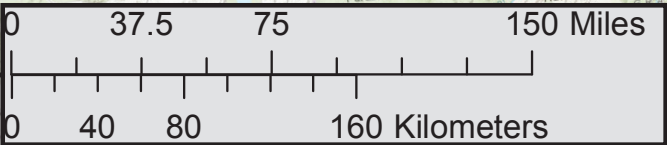


Service Layer Credits: Sources: Esri, HERE, Garmin, Intermap, increment P Corp., GEBCO, USGS, FAO, NPS, NRCAN, GeoBase, IGN, Kadaster NL, Ordnance Survey, Esri Japan, METI, Esri China (Hong Kong), swisstopo, © OpenStreetMap

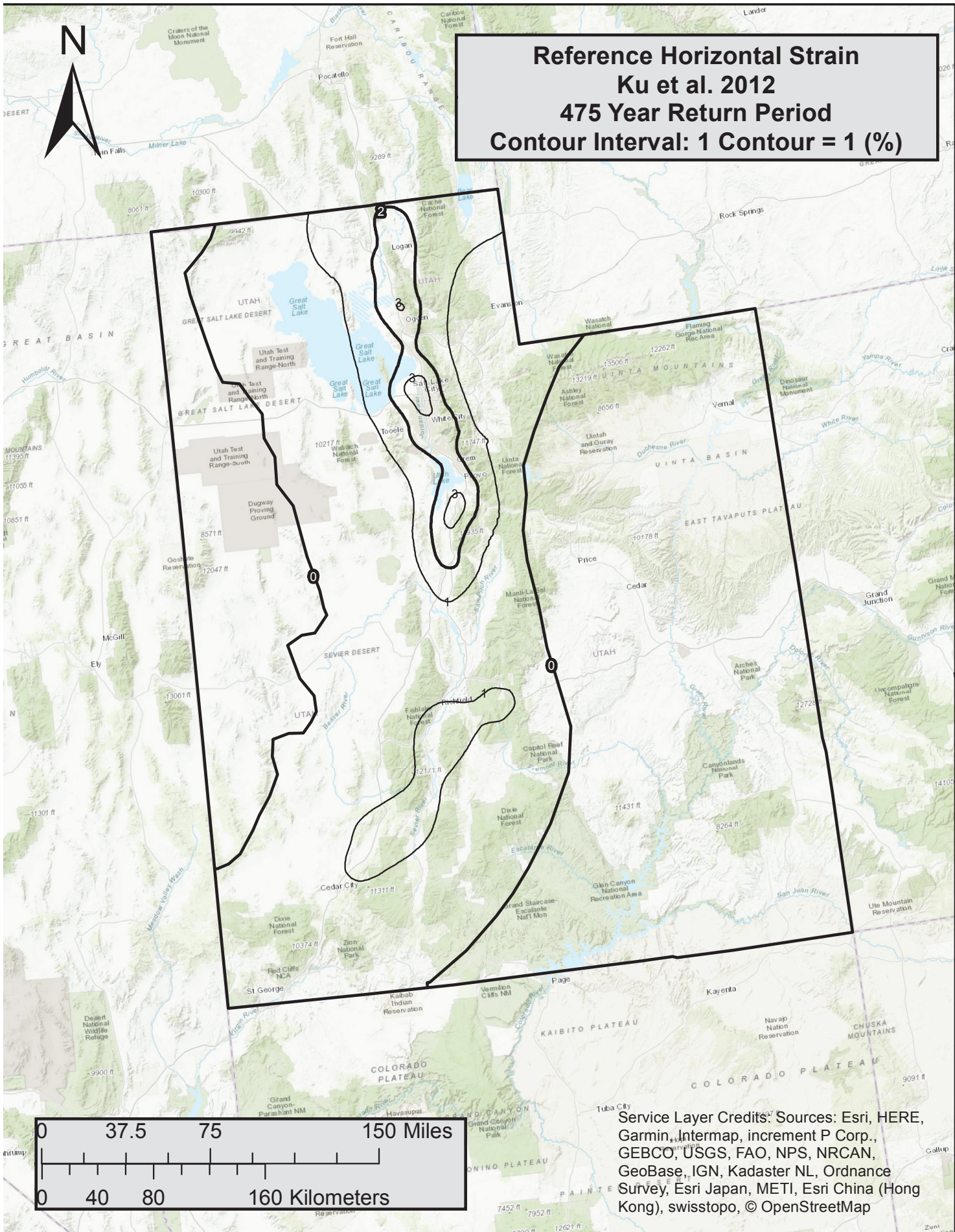




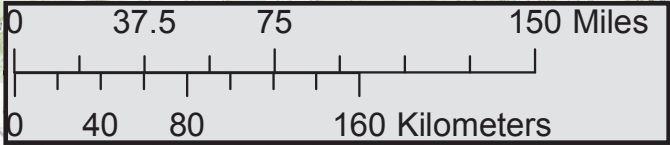
**Reference Horizontal Strain
Boulanger and Idriss 2014
2475 Year Return Period
Contour Interval: 1 Contour = 2 (%)**



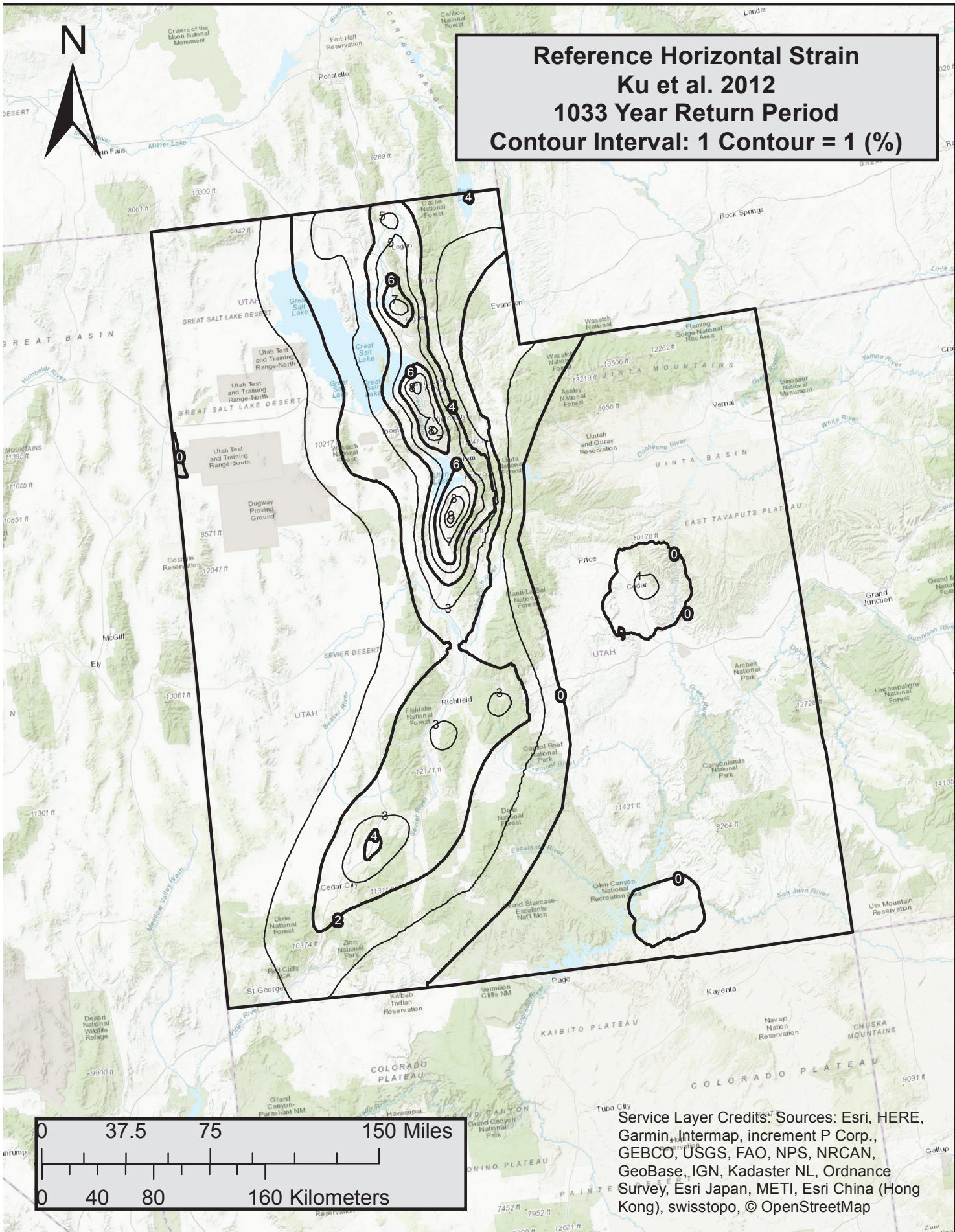
Service Layer Credits: Sources: Esri, HERE, Garmin, Intermap, increment P Corp., GEBCO, USGS, FAO, NPS, NRCAN, GeoBase, IGN, Kadaster NL, Ordnance Survey, Esri Japan, METI, Esri China (Hong Kong), swisstopo, © OpenStreetMap



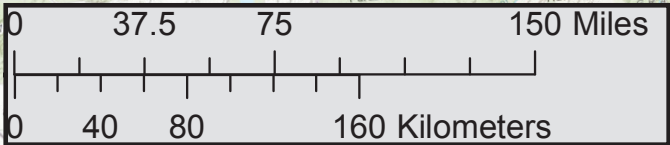
Reference Horizontal Strain
Ku et al. 2012
475 Year Return Period
Contour Interval: 1 Contour = 1 (%)



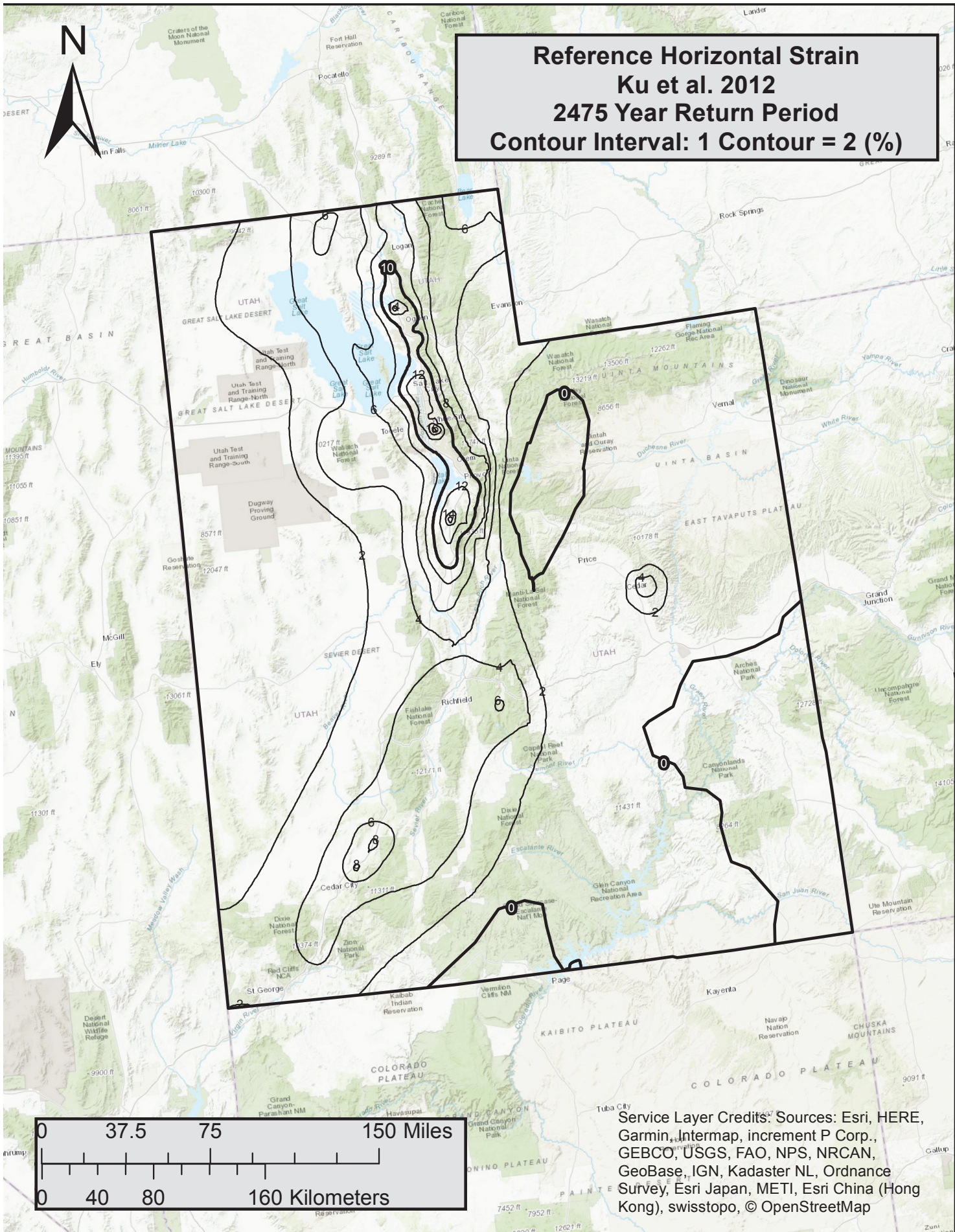
Service Layer Credits: Sources: Esri, HERE, Garmin, Intermap, increment P Corp., GEBCO, USGS, FAO, NPS, NRCAN, GeoBase, IGN, Kadaster NL, Ordnance Survey, Esri Japan, METI, Esri China (Hong Kong), swisstopo, © OpenStreetMap



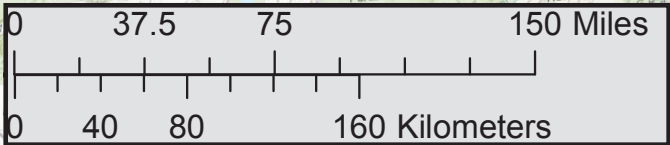
Reference Horizontal Strain
Ku et al. 2012
1033 Year Return Period
Contour Interval: 1 Contour = 1 (%)



Service Layer Credits: Sources: Esri, HERE, Garmin, Intermap, increment P Corp., GEBCO, USGS, FAO, NPS, NRCAN, GeoBase, IGN, Kadaster NL, Ordnance Survey, Esri Japan, METI, Esri China (Hong Kong), swisstopo, © OpenStreetMap



Reference Horizontal Strain
Ku et al. 2012
2475 Year Return Period
Contour Interval: 1 Contour = 2 (%)



Service Layer Credits: Sources: Esri, HERE, Garmin, Intermap, increment P Corp., GEBCO, USGS, FAO, NPS, NRCAN, GeoBase, IGN, Kadaster NL, Ordnance Survey, Esri Japan, METI, Esri China (Hong Kong), swisstopo, © OpenStreetMap